Development of "Open-Short Circuit" Dimensionless Figure-of-Merit (ZT) Measurement Technique for Investigation of Thermoelements and Segmented Thermoelectric Structures

A thesis submitted to Cardiff University in the candidature for the degree of Doctor of Philosophy

By

Nadhrah Md Yatim, BSc. (Hons), MSc.

Institute of Energy
School of Engineering
Cardiff University

May 2012

Abstract

The thermoelectric dimensionless figure-of-merit, ZT, which consists of the Seebeck coefficient, α, electrical resistivity, ρ and thermal conductivity, λ, is an important parameter that characterizes the energy conversion performance of thermoelectric materials and devices. Larger ZT indicates higher performance of thermoelectric device. Current techniques for determining ZT involve measurements of α, ρ and λ individually or ZT directly, but all techniques are carried out under a small temperature difference (ΔT). In reality, a thermoelectric device generally operates under a much larger ΔT and with an electrical current flowing through the thermoelectric materials. Clearly, ZT values are conventionally evaluated under a condition which differs significantly from the real operating conditions of thermoelectric devices.

Recently, a novel principle for ZT measurement has been proposed, which has the capability of measuring ZT values under a large ΔT and with an electrical current flowing through the samples. The main objective of the research embodied in this thesis is to investigate experimentally the feasibility of the proposed technique and subsequently to develop a laboratory measurement system for thermoelectric materials research. The feasibility of the proposed technique was investigated initially using thermoelectric modules. The results show a reasonable agreement with conventional techniques when it is used to measure ZT under a small ΔT. Furthermore, the investigation reveals that ZT obtained under a large ΔT differ significantly from those obtained under a small ΔT. This confirms the unique capability of the proposed technique.

The implementation of this technique for measuring the ZT of thermoelectric materials has proved to be very challenging due to the low electrical resistance (< 0.01 Ω) of the material samples. Following an in-depth experimental and theoretical investigation, a new design with a modified operating principle was proposed and carried out. The measurement system based on this new design was successfully developed, which has the capability of measuring single materials with different dimensions and under a larger ΔT. The performance of this system was investigated using a standard Bi_2Te_3 sample as the reference for calibration. The results show that the system has a repeatability of <10% and an accuracy of 13-32%. Investigation on single materials and segmented structures showed that there were noticeable differences between a small and a large ΔT, which can be attributed to the Thomson effect and changes in $\rho\lambda$ values. This finding contributes to an improved understanding and new knowledge of thermoelectric behaviour under a large temperature difference. The measurement technique developed in this work will provide a useful tool for investigation and for the optimization of advanced thermoelectric structures.

DECLARATION AND STATEMENTS

DECLARATION

This work has not previously been accepted in substance for any degree and is not concurrently submitted in candidature for any degree.

Signed……...(Nadhrah Md Yatim) Date…….

STATEMENT 1

This thesis is being submitted in partial fulfilment of the requirements for the degree of Doctor of Philosophy (PhD).

Signed …….(Nadhrah Md Yatim) Date…….

STATEMENT 2

This thesis is the result of my own independent work/investigation, except where otherwise stated. Other sources are acknowledged by explicit references.

Signed …….(Nadhrah Md Yatim) Date…….

STATEMENT 3

I hereby give consent for my thesis, if accepted, to be available for photocopying and for inter-library loan, and for the title and summary to be made available to outside organisations.

Signed ……(Nadhrah Md Yatim) Date……..

ACKNOWLEDGEMENTS

First and foremost I am thankful to Allah SWT for providing me strength, patience and determination to go on and complete this thesis.

My sincerest gratitude to my supervisor, Dr Gao Min who has supported me throughout my thesis with his supervision and knowledge. His invaluable guidance, constructive criticisms, insightful thinking as well as his enthusiasm in research has inspiring during my study. I also would like to express gratitude to the late Prof Mike Rowe for his assistance during my early day of enrolment at Cardiff University.

Special thanks go to all the technicians involved; Mr Steve Mead, Mr Alan Griffith, Mr Howard, Mr Bob and Mr Paul Farrugia for their assistance in construction of my apparatus, members of thermoelectric group at Cardiff University for their friendship and making my study life a memorable one. I would also like to convey thanks to Malaysian Government especially Ministry of Higher Education (MOHE) and Islamic Science University of Malaysia for providing the financial support.

My deepest appreciation goes to my beloved husband, M. Azlan for his constant care, love, supports and always standing beside me during happy and sad moments and to my sons M. Zakwan, M. Zaim and M. Zameer who have suffered the most during my absence in their most needed times. My acknowledgment also to my parents and in-laws for their understanding, persistent love, good wishes and support throughout my studies. This thesis is simply impossible without them.

Lastly, I offer my regards and gratitude to all of those who supported me in any aspect during the completion of the thesis.

CONTENTS

CHAPTER 5: DESIGN AND CONSTRUCTION OF LARGE TEMPERATURE DIFFERENCE (LΔT) FACILITY FOR SINGLE THERMOELEMENT MEASUREMENT

CHAPTER 6: RESULTS AND DISCUSSIONS

CHAPTER 7: CONCLUSIONS AND FURTHER WORK

LIST OF SYMBOLS

A	Cross sectional area
C_p	*Specific heat*
C'_p	*Heat capacity per volume*
D	*Density*
I_c	Close circuit voltage
I_s	Short circuit current
K	Thermal conductance
L	*Distance*
$L\Delta T$	Large temperature difference
P_o	Power output
Q	Rate of heat flow
$\vec{Q}$	Heat Flux
Q_h	*Rate of h*eat flow at hot side
R_i	Internal resistance
R_T	Total resistance
$S\Delta T$	Small temperature difference
T_m	Modified mean temperature
T_{mean}	Mean temperature
V_c	Close circuit voltage
V_o	Open circuit voltage
V_R	Resistive voltage
V_S	Seebeck voltage
V_T	*Voltage drop across the sample*
ZT	Dimensionless figure-of-merit
ZT_c	Dimensionless figure-of-merit obtain using conventional method
ZT_m	Modified dimensionless figure-of-merit
ZT_w	Dimensionless figure-of-merit with correction factor
ZT_{wo}	Dimensionless figure-of-merit without correction factor
α	Seebeck coefficient
α_{eff}	Effective Seebeck coefficient
α'	Thermal diffusivity
β	Thomson coefficient
η	TEG efficiency
κ	*Ratio of thermal wave amplitude*
λ	Thermal conductivity
π	Peltier coefficient
ρ	Electrical resistivity
σ	Electrical conductivity
φ	*Thermal wave phase difference*

ϕ	TEC Coefficient of Performance
ω	*Angular frequency*
ΔT	Temperature difference
ΔT_c	Close circuit temperature difference
ΔT_o	Open circuit temperature difference
ΔT_s	Short circuit temperature difference
∇T	Temperature gradient

LIST OF FIGURES

LIST OF TABLES

CHAPTER 1

Introduction

1.1 History of Thermoelectrics

A thermoelectric phenomenon is a science related to the production of electrical potential from temperature difference or the production of temperature difference from electrical potential. These phenomena are due to three reversible thermoelectric effects, namely the Seebeck effect (1821), the Peltier effect (1834) and the Thomson effect (1851).

Even though Anatychuk [1] claims that thermoelectricity was first discovered by Volta, the thermoelectricity era only begin in 1821 after Thomas Johann Seebeck discovered the deflection of a compass needle if placed near the closed-loop circuit made of two dissimilar metals with the junction maintained at a different temperature [2]. Unaware of an electric current at the time, Seebeck erroneously assumed that this was a thermomagnetic effect. Two years later Orstead [3] determined that the metals in Seebeck's experiments were reacting to the temperatures, producing an electric voltage that in turn created a magnetic field that moved the needle.

Developments in thermoelectricity continued with the finding of French scientist Jean Charles Anthanase Peltier in 1834 who observed the opposite effect by passing a current through a series of conductors. Unfortunately, Peltier

did not relate his discovery to the one made by Seebeck 12 years earlier. Until a couple of years later in 1838, Lenz concluded that the direction of the current flow determined whether heat was absorbed or generated at the junctions. The third thermoelectric effect, known as the Thomson effect, was predicted by William Thomson (Lord Kelvin) in 1851, where a homogeneous conductor will either absorb or reject heat resulting from the flow of an electrical current in the presence of a temperature gradient.

Further developments in thermoelectricity continued when in 1909 and 1911, Rayleigh and Altenkirch [4] showed that good thermoelectric materials should possess a large Seebeck coefficient, high electrical conductivity and low thermal conductivity. A high electrical conductivity is necessary to minimize Joule heating, whilst a low thermal conductivity helps to retain heat at the junctions and maintain a large temperature gradient. These three properties were later embodied in the so-called figure-of-merit, Z. Since Z varies with temperature, a more useful parameter known as dimensionless figure-of-merit, ZT is usually used. The dimensionless figure-of-merit is defined as:

$$ZT = \frac{\alpha^2\sigma}{\lambda}T = \frac{\alpha^2\sigma}{(\lambda_l + \lambda_e)}T \quad \dots\dots (1.1)$$

where α is the Seebeck coefficient, σ is the electrical conductivity and λ is thermal conductivity. The ZT is derived from the performance of thermoelectric cooler as shown in Appendix 1. The thermal conductivity of a thermoelectric

material is the sum of a lattice component, λ_l and an electronic component, λ_e , which represent phonon and charge carrier transport respectively.

1.2 Thermoelectric materials

Since the discovery of thermoelectricity there has not been much development in thermoelectric applications due to poor materials' performance. Initial researches were focused on metals and metal alloys that have high electrical conductivity. But it was found that the Seeback coefficient in metals was low (<40 μV/K). In addition, thermal and electrical conductivities are related by the Weidemann-Franz-Lorenz' law results in an increase in the thermal conductivity if the electrical conductivity is increased. During the 1930's thermoelectric research went through a resurgence of interest with the discovery of semiconductor materials, in which the Seebeck coefficient greater than 100 μV/K was obtained [4]. Since then, many new approaches to improve ZT have been proposed as a result of progress in solid state physics [5].

Three well-established thermoelectric materials are bismuth telluride (Bi_2Te_3), lead telluride (PbTe) and silicon germanium (SiGe). Over the past 50 years, significant improvements have been made in developing high ZT materials. Due to the strong dependency of thermoelectric properties on temperature, the practical operating temperature of a particular material is generally limited [6,7] as depicted in Figure 1.1. Bi_2Te_3 offered peak ZT at room temperature and was found to be suitable for operation at a temperature ranges

between 300-500 K, PbTe is suitable for operation at an intermediate temperature range (600-900 K) and SiGe at high temperature range (1000-1300 K). In order to compete with the commercial power generation and refrigeration techniques currently being used and to fulfil the requirements of large-scale industrial application, ZT larger than 3 are desirable. Consequently, many efforts have been made to improve thermoelectric efficiency during the past decades. The first and most notable approach is to search for a new thermoelectric material with improved properties. The second approach is to optimize the current system and the third approach involves finding cheap materials or manufacturing processes to reduce the cost of thermoelectric devices.

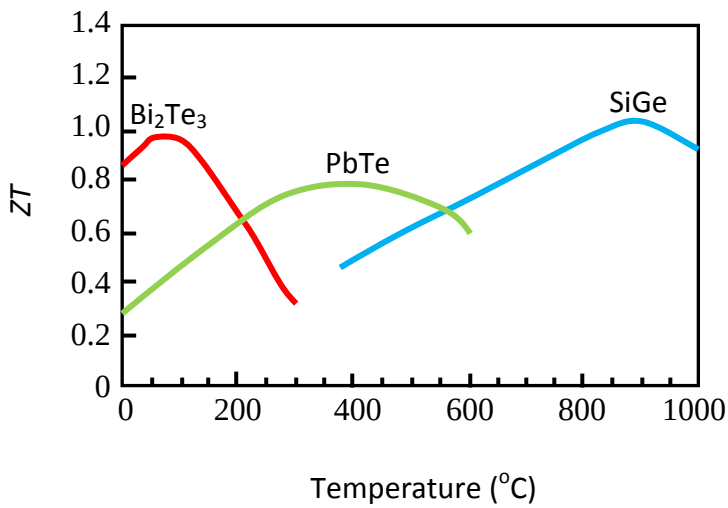

Figure 1.1: Dimensionless figure-of-merit as a function of temperature for n-type Bi_2Te_3, PbTe and SiGe showing peaks at different temperature range [7].

In 1993 Hicks and Dresselhaus [8] proposed an approach to increase thermoelectric performance by nanostructure engineering. Nanostructure materials could exploit reduced dimensionality to increase the power factor ($\alpha^2\sigma$) by increased electronic mobility and density of state near the Fermi level. In addition, thermal conductivity could be reduced with an increase in boundary scattering if the semiconductor size was smaller than the phonon wavelength but larger than the electrons or holes wavelength, without adversely affecting its electrical transport [9]. Since then, a number of experiments have been carried out on 2D, 1D and 0D systems. For example, Harman et al. [10] shows that PbTe/PbTeSe quantum dot superlattice structures could yield a $ZT\sim$0.8 at $T\sim$300 K and $ZT\sim$2 at T~550 K whereas Venkatasubramaniam [11] shows that Bi_2Te_3 and Sb_2Te_3 thin-film superlattice structures have ZT~2.4 at room temperature.

In 1995 [12] Slack proposed a concept referred to as the phonon-glass electron–single crystal (PGEC). According to this concept, good thermoelectric materials should have electrical properties that could conduct electricity like a crystalline solid and have thermal properties to maintain heat like a glass. This can be achieved by the placement of atoms in the large voids of the material structure, thus greatly reducing the total thermal conductivity of the materials and consequently increasing ZT. Since then, several classes of complex materials have been intensively investigated, such as skutterudite [13,15], clathrate [14,15] and half-Heusler alloys [16,17] systems.

Recently, a new class of thermoelectric materials has been developed based on metal oxides such as $SrTiO_3$, Na_2CoO_4, $CaMnO_3$, $(ZnO)(In_2O_3)$, ZnO and $CuAlO_2$ [18]. They have attracted increased attention due to their thermal and chemical stability in air at high temperature, oxidation resistance, reduced toxicity, easy manufacture and low cost [19-23]. However, the general problems reported with oxide thermoelectrics were related to weak mechanical strength and high contact resistance at interfaces of oxides and electrodes. Despite all the new thermoelectric materials that have been investigated, the Bi_2Te_3 compound and its alloys are still the best materials at room temperature.

1.3 Thermoelectric measurements

Thermoelectric properties are evaluated based on three parameters: the Seebeck coefficient, α, electrical resistivity, ρ and thermal conductivity, λ. A good thermoelectric material must have a large Seebeck coefficient, low electrical resistivity and low thermal conductivity. These requirements are summarized in the definition of the dimensionless figure-of-merit, ZT described by equation (1.1).

In order to determine ZT, thermoelectric measurement usually involves measurements of all three thermoelectric properties. Many methods techniques have been reported to measure these properties but the most popular methods to measure the Seebeck coefficient, electrical resistivity and thermal conductivity are using the hot probe, 4-probe and laser flash techniques respectively.

Alternatively, ZT can be measured directly using the Harman method. More technique and a detailed description of thermoelectric measurements will be presented in Chapter 2.

1.4 Thermoelectric Applications

Two major applications of the thermoelectric effects for energy conversion are power generation based on the Seebeck effect and refrigeration based on Peltier effect. Even though the efficiency of thermoelectric materials is relatively low (<15%) compared with conventional power-generation and refrigeration systems, thermoelectric devices offer several other advantages over conventional technologies, such as the absence of moving parts, high reliability, a reduction of maintenance and an increase in system life (more than 100,000 hour life under steady state operation [24]). The absence of a working fluid avoids hazard due to environmentally dangerous leakages, there is no noise or vibration and they can function in environments that are too severe, too sensitive or too small for conventional refrigeration.

In the past four decades thermoelectric generators have been used by NASA in more than 40 spacecrafts, mostly for planetary exploration missions powered by Radioisotope Thermoelectric Generators (RTGs) [25-27]. The application of thermoelectric generators for specific purposes have been used in a military such as for battery replacement in the field and for powering lightweight portable battery chargers [28]; in medical applications such as

cardiac pacemakers and defibrillators [29]; in industrial applications for corrosion control (imposed current cathodic protection); in oil pipelines and sea buoys [30] and for commercial products such as wrist-watches [31]. Potential applications of utilizing industrial waste heat have also been investigated. These include waste heat recovery from processing plants of combustible solid waste [32-33], automobile exhaust and engine heat [34], gas-fired dehydrator boiler [35] and underwater wellhead [36].

Applications of thermoelectric refrigerators are generally limited to niche areas where reliability is more important than efficiency. For example, thermoelectric devices have been used in localized cooling of computer chips, optoelectronics, environmental sensors, laser diodes, infrared detectors, and electronic devices as well as for recreational refrigerators such as portable picnic coolers and recreational vehicle refrigerators [2, 37-38].

1.5 Thermoelectric Effects

1.5.1 Seebeck effect

The Seebeck effect involves the generation of electromotive force (emf) voltage in a device that consists of two different materials in the presence of a temperature gradient, as shown in Figure 1.2. It is the basis for temperature measurement and thermoelectric power generation. The Seebeck coefficient, α, is defined as the open circuit voltage produced in a circuit of two distributed

conductors joined together and with a temperature difference of 1 degree Kelvin applied across the two junctions,

$$\alpha_{ab} = \lim_{\Delta T \to 0} \frac{\Delta V_{ab}}{\Delta T} \dots \dots (1.2)$$

where α_{ab} is the relative Seebeck coefficient in volts per degree temperature difference (V/K) or more often in $(\mu V/K)$, ΔV_{ab} is an open circuit voltage produced in a circuit of two dissimilar conductors with a temperature difference, ΔT , across the two junctions.

The Seebeck coefficient could be positive or negative corresponding to a p-type and n-type material respectively. When heat is applied at one of the junctions, the majority charge carriers in the material (electrons or holes) have higher energies and velocities than charge carriers at the cold end. As a result the charge carriers diffuse from the hot side to the cold side, leaving behind their oppositely charged carriers at the hot side. This creates a thermoelectric voltage. At the same time this voltage develops an opposing electric field. When in equilibrium, an equal amount of charge carriers drift back to the hot side to prevent further charge diffusion. The Seebeck coefficient is positive when the direction of the electric current is the same as the direction of the thermal current.

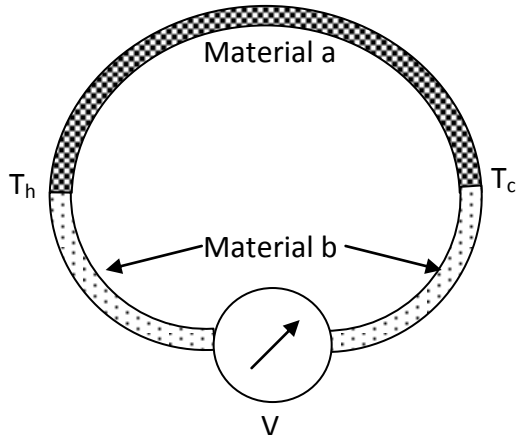

Figure 1.2: The Seebeck effect in an opened circuit consists of two dissimilar semiconductors. The temperature difference between the two junctions creates the potential difference shown at voltmeter [39].

1.5.2 Peltier effect

The Peltier effect is an opposite of the Seebeck effect, where the temperature gradient across a device of two different materials is generated in the presence of an electrical current as illustrated in Figure 1.3. Electric current that flows around the circuit will result in heat absorption at one junction and heat rejection at another junction. Heat absorption or rejection at the two junctions will be reversed if the electric current changes direction. This effect is the basis of thermoelectric refrigeration or heating.

When electric potential is established in a circuit, electrons or holes will be induced to cross the junctions. Because of the different Fermi level of the two materials, this process will be accompanied with heat absorption at a junction

due to the fact that electrons and holes need to gain energy to jump from one material to another. At another junction electrons or holes will release energy as they travel from a high Fermi level material to a lower Fermi level material.

The amount of energy absorbed or rejected at a junction depends on the amount of current supplied. The Peltier coefficient, π, is a measure amount of heat, Q , absorbed or rejected at the junction of two different materials when one coulomb of charge flows across the junction. This could be written as;

$$\pi_{ab} = \frac{Q}{I} \ (at\ \Delta T = 0) \ldots\ldots (1.3)$$

where π_{ab} is the relative Peltier coefficient of material a to b which has a unit of Watt/A or in Volts. The Peltier coefficient can be positive or negative depending on the direction of the electrical current and thermal current. If the electrical current flows in the opposite direction to that of thermal current, the Peltier coefficient is negative. If the electrical current flows in the same direction as the thermal current, the Peltier coefficient is positive. In other words, n-type material will have a negative Peltier coefficient and p-type will have a positive Peltier coefficient.

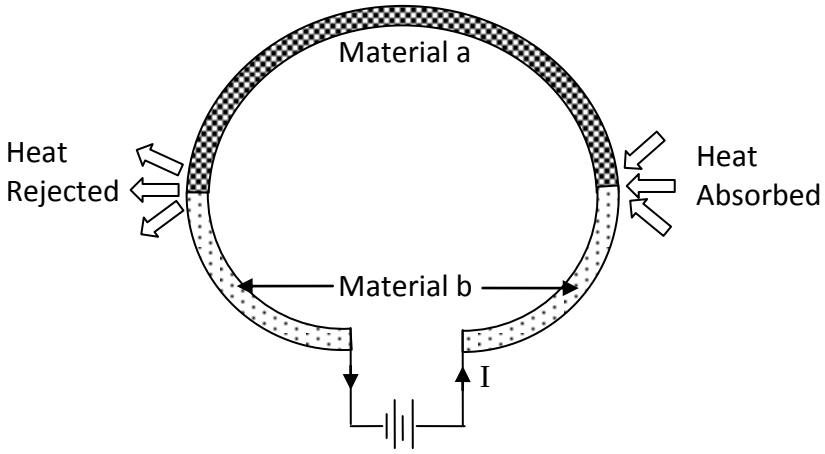

Figure 1.3: The Peltier effect in a closed circuit of two dissimilar semiconductors. As the current flows through the loop, heat is liberated from one junction and absorbed at the opposite.

1.5.3 Thomson effect

The Thomson effect describes the rate of heat generated or absorbed in a single current-carrying conductor subjected to a temperature gradient. Unlike the Peltier effect, where heat absorption or rejection occurs at the junction, the Thomson effect occurs along single material. The Thomson coefficient, β, is a measure of the rate of heat absorbed or rejected, Q, per unit current, I and temperature difference, ΔT. It can be written as;

$$\beta = \lim_{\Delta T \to 0} \frac{Q}{I\Delta T} \dots\dots (1.4)$$

The unit for the Thomson coefficient is V/K. The Thomson coefficient can be positive, negative or of zero value. The Thomson coefficient shows a positive

value for metals such as zinc and copper, which have higher potential at the hotter end and lower potential at the cooler end. When the positive charge carrier moves from the hotter end to the cooler end, it is moving from a high to a low potential, so there is a release of energy as it give up the excess energy to the surroundings, as illustrated in Figure 1.4. On the other hand, metals such as iron, cobalt and bismuth, which have lower potential at the hotter end and higher potential at the cooler end, increase their energy at the expense of their surroundings by absorbed heat as the negative charge carrier transfer from low potential to high potential as it moves from the hotter to the cooler end.

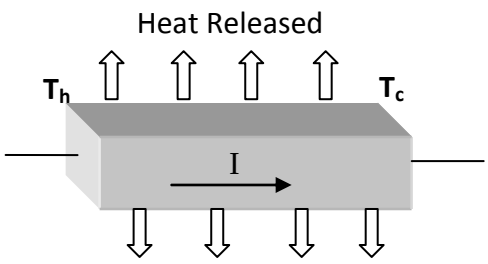

Figure 1.4: Thomson Effect of single semiconductor. Heat will be absorbed or rejected as the current flows through the conductor depending on the direction of current.

1.5.4 Kelvin Relationship

The Kelvin relationship was derived from the first and second laws of thermodynamics by Lord Kelvin that bears his name. It can be shown that:

$$\pi = \alpha T \ldots\ldots (1.5)$$

$$\beta = \frac{d\alpha}{dT} T \ldots\ldots (1.6)$$

where α, π and β are the Seebeck, Peltier and Thomson coefficients respectively and T is an absolute temperature. These relationships are important as they show the correlation between the three thermoelectric properties.

1.6 Background to the Present Research

The dimensionless figure-of-merit, ZT, as mentioned previously, is an important parameter used in the determination of thermoelectric performance. Conventionally, ZT was obtained indirectly through separate measurements of individual thermoelectric properties or directly through the Harman method. The direct method has the advantage of rapid execution, a smaller amount of sample handling and identical chemical and physical condition during measurement. However, the direct method based on the Harman method is associated with relatively large error. Therefore, individual measurements of α, ρ and λ are usually employed in practice.

In this study, an alternative technique of direct ZT measurement is investigated. The technique was derived in 2001 from the idea of different ΔT

produced during open and short circuit while under constant heat flows [40]. Initial investigation was carried out a year later by Kontastinov [41].

A unique characteristic embodied in this novel technique is its capability to measure ZT under operational conditions, in particular ZT can be measured under condition of a large temperature difference with the influence of the Thomson effect. To date, all conventional ZT measurement technique can only be undertaken under condition of a small temperature difference and neglecting the influence of the Thomson effect. Successful implementation of this technique will open a new dimension for the ZT assessment of segmented and functionally graded materials which is not possible using conventional method and is for the first time to be measured directly. Consequently, more accurate evaluation of conversion efficiency can be derived. In addition, this technique could facilitate the study of the effects that are negligible under small temperature difference. Interestingly, this technique is not limited to ZT measurements only but all thermoelectric properties (Seebeck coefficient, electrical and thermal conductivity) can also be determined in the same measurement. The usefulness of this technique is that it can be applied to single materials as well as to module devices. However, implementation to single materials is more challenging and difficult due to its very small resistance.

1.7 Aim and Objectives

The proposed novel technique for direct ZT measurement has the unique capability of measuring ZT under large temperature difference and involves a closed-circuit. This is a capability that none of current thermoelectric measurement techniques can offer. If this proposed technique can be successfully established, it will not only provide a new way to determine ZT but, more importantly, it will enable investigating the influence of the Thomson effect and offer the capability to determine the ZT of segmented thermoelectric materials for the first time.

The aim of this project is to develop this novel ZT measurement technique. It is noted that the conditions required by this technique are relatively easier to satisfy using a thermoelectric module because of its large internal resistance (up to a few ohms). The strategy is to investigate the "proof of principle" using a thermoelectric module. Once it is proved feasible, the investigation will progress to develop a measurement facility that is suitable for measuring a single piece thermoelectric materials which has a much smaller internal resistance around 0.01 ohm. To achieve this challenging goal, a number of key objectives have been identified as follows:

1. To design and construct a simplified measurement system for investigating the "proof of principle" using a thermoelectric module as a testing sample.

2. To identify key challenges and to seek the solutions that will enable successful implementation of this technique for thermoelectric materials with a dimension of around $3\text{mm}\times3\text{mm}\times8\text{mm}$.
3. To design and construct a prototype of ZT measurement systems, followed by investigating its suitability for thermoelectric materials measurement, as well as repeatability and accuracy.
4. To apply this technique to investigate the thermoelectric properties of uniform materials and segmented materials in particular, under large temperature differences.

CHAPTER 2

Literature Review

2.1 Introduction

To increase the competitiveness of thermoelectric applications, most of the research has been devoted to improving the thermoelectric conversion efficiency. Thermoelectric efficiency increased by increasing the thermoelectric materials' figure-of-merit [25]. Thus, dimensionless figure-of-merit is one of the important parameters that influence device performance. Clearly, thermoelectric measurements that allow analysis of the device efficiency become important. This involves measurements of all the thermoelectric properties. In this chapter, a brief introduction on the operating principles of thermoelectric generators and refrigerators will be given, followed by a focused review on the present measurement techniques for thermoelectric figure-of-merit.

2.2 Thermoelectric Generator and Refrigerator

Two main applications of thermoelectric effects are in power generation and refrigeration. The basic structures of thermoelectric devices consist of a number of p-type and n-type semiconductor thermoelectric elements connected electrically in series and thermally in parallel [42]. Figure 2.1 shows the basic structure of a thermoelectric generator (TEG) and a thermoelectric cooler (TEC).

Conducting strips, usually made of copper, are used to connect p and n-type thermoelectric elements.

In the TEG device, heat supplied at one side of the materials increased the kinetic energy of the charge carriers in both legs. The presence of a thermal energy difference leads to diffusion of carriers from the hot end to the cold end as shown in Figure 2.1 (a). The accumulation of charge carriers at the cold end results in an electric field opposing this, creating current flows around the loop.

The operation of a TEC can be viewed as a reversed process to that of a TEG. When a voltage is applied such that the positive terminal is connected to n-type and the negative terminal connected to p-type thermoelements, a current will flow through the device from n-type to p-type as shown in the Figure 2.1 (b). In the n-type leg, the current is carried by the diffusion of electrons in the opposite direction of the current flow while in the p-type leg the current is carried by the diffusion of holes in the same direction as the current flow. Both charge carriers carry thermal energy away as they move so the upper junction will become cold while the bottom junction becomes hot. Though the current is flowing through them in series, the thermal energy is being pumped away from the cold side to the hot in parallel.

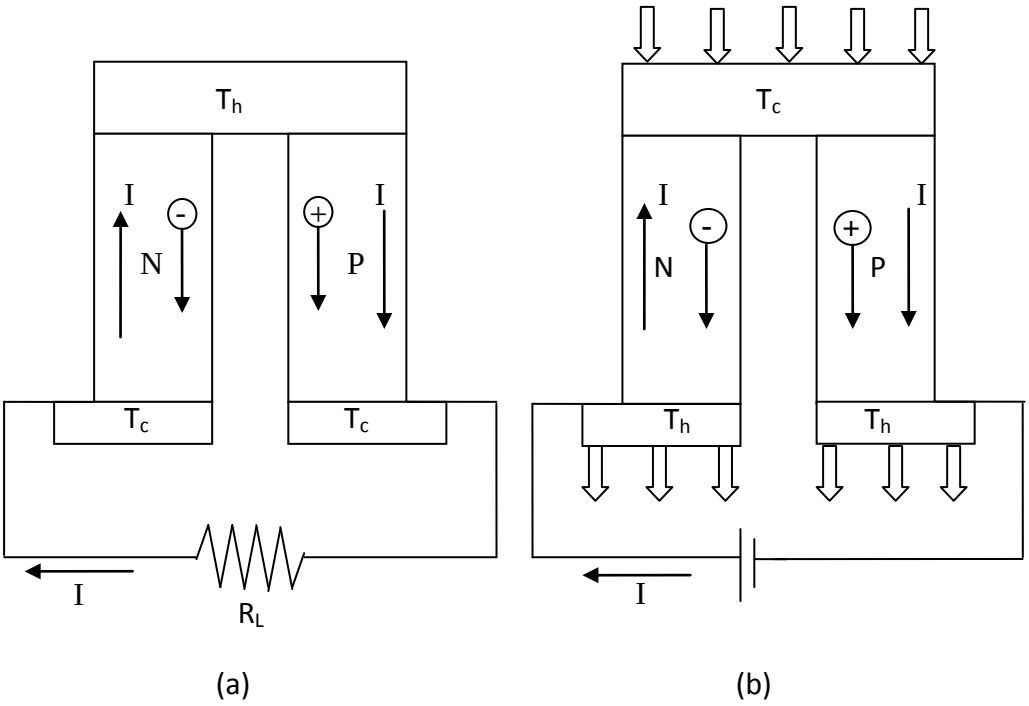

Figure 2.1: Schematic diagram of the basic structure of (a) thermoelectric power generation (TEG) and (b) thermoelectric refrigeration (TEC).

2.3 Importance of ZT Measurement

The efficiency, η, of a thermoelectric generator is determined from the amount of electric power produce, P_o (Watt) divided by the rate of heat flow being absorbed, Q_{in} (Watt), at the hot side;

$$\eta = \frac{P_o}{Q_{in}} \dots\dots (2.1)$$

The electrical power delivered at the load can be given as;

$$P_o = I^2 R_L \dots\dots (2.2)$$

where I is electric current and R_L is load resistance.

Under a steady state condition, four phenomena contribute to energy flow as a result of a current flows in the circuit; 1) heat flow through the thermoelectric material due to heat conduction under the temperature difference, 2) the absorbed heat at the hot side junction due to the Peltier effect, 3) the heat produced due to electrical resistance of material, known as Joule heating and 4) heat produced along thermoelement due to the Thomson effect. On the assumption that half of the Joule heating goes to the hot side and half to the cold side of the module [43] and if the contribution of the Thomson effect could be neglected [44], the equation that governs the heat flow at the hot side can be written as;

$$Q_h = \alpha I T_h - \frac{1}{2} I^2 R + K\Delta T \ldots\ldots (2.3)$$

where α is total Seebeck coefficient, K is total thermal conductance and R is the total resistance. Using equation (2.2) and (2.3), it can be shown that the maximum efficiency of the thermoelectric generator is given by [45,46];

$$\eta_{max} = \left(\frac{T_h - T_c}{T_h}\right) \frac{\sqrt{(1 + Z\bar{T})} - 1}{\sqrt{(1 + Z\bar{T})} + \left({T_c}/{T_h}\right)} \ldots\ldots (2.4)$$

where $\bar{T} = \left(\frac{T_h + T_c}{2}\right)$ is the mean temperature and $Z = \frac{\alpha^2}{\rho\lambda}$ is the figure-of-merit, which depends on the properties of the thermoelectric materials.

A similar approach could be used to derive the coefficient of performance, ϕ, of a thermoelectric refrigerator. The coefficient of performance

is defined as the ratio of heat absorbed, Q_c, at the cold end to the electrical power consumed, P_{in}. The amount of heat absorption at the cold end of a thermoelectric refrigerator can be written as;

$$Q_c = \alpha I T_c - \frac{1}{2} I^2 R - K\Delta T \ldots\ldots (2.5)$$

Note that the heat conduction has different signage in equation (2.5) compared with equation (2.3), which indicates that the temperatures T_h and T_c are opposite.

Electrical power supplied to the system is given by [44];

$$P_{in} = I^2 R + \alpha I \Delta T \ldots\ldots (2.6)$$

Using equations (2.5) and (2.6), it can be shown that the maximum coefficient of performance is [44,45];

$$\phi_{max} = \left(\frac{T_c}{T_h - T_c}\right) \frac{\sqrt{1 + Z\bar{T}} - \left({T_h}/{T_c}\right)}{\sqrt{1 + Z\bar{T}} + 1} \ldots\ldots (2.7)$$

It can be seen clearly, from equations (2.4) and (2.7), that the conversion efficiency and the coefficient of performance of a thermoelectric device depends on the temperature difference across the thermoelectric device, the average temperature of operation and the transport properties of the materials embodied in ZT. In order to increase the conversion efficiency for given operating conditions (i.e ΔT and $\bar{T}$), it is desirable to employ high ZT thermoelectric materials.

2.4 ZT Measurement – Indirect Approach

There are two approaches to the measurement of dimensionless figure-of-merit; indirect or direct. In the indirect approach, all thermoelectric properties, namely α, ρ and λ are measured individually and the ZT can be calculated using equation (1.1). A direct approach determines ZT directly from measurement (e.g the Harman method). Discussed below are some of the measurement techniques used to determine ZT indirectly by measuring α, ρ and λ individually.

2.4.1 Seebeck Coefficient Measurement

The Seebeck coefficient is defined as the ratio of potential difference, ΔV, to a temperature difference, ΔT. It is crucial to determine α with high accuracy as it is a squared dependence in the mathematical expression of Z. Even though in principle the measurement is simple, the measurement becomes complicated by the absence of standards [47]. Schematic arrangement of α measurement is shown in Figure 2.2, which shows the commonly used 2-point and 4-point probes and the recently improved uniaxial 4-probe [48]. In general, two pairs of thermocouple probe serves as temperature and voltage measurement. Thermocouple across the sample measure temperature difference between these two points while voltage produced at the same position can be measured using one of the thermocouple legs as the probe. The measured relative Seebeck

coefficient (see equation 1.2) can be determined using two basic techniques, namely, the differential and integral method.

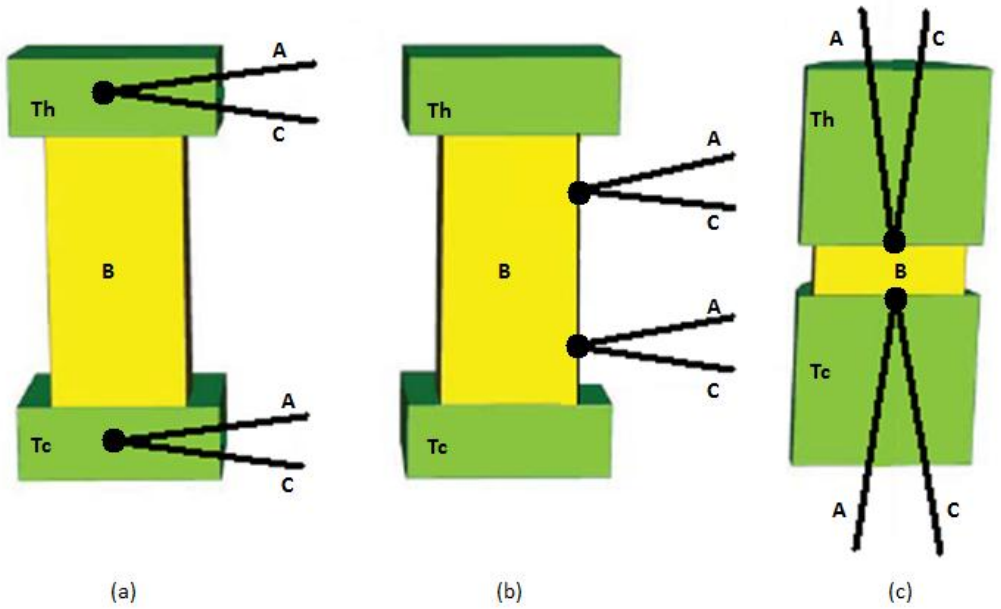

Figure 2.2: Schematic arrangement of relative Seebeck coefficient measurements based on (a) 2-point, (b) 4-point and (c) uniaxial 4-point where A, C indicates thermocouples and B indicates a sample [48].

2.4.1.1 Differential Method

This is the most popular method in thermoelectrics. The techniques based on this method involve establishing a small temperature difference across the sample throughout temperature range. Various types of apparatus based on the differential method have been previously described [49-53]. Among those, hot probe is one of the well known instruments use for thermoelectric

measurement. A small source of heat from the hot probe applied at one end of the sample producing a temperature difference typically of 5-15 K across the sample and is maintained under steady state at mean temperature of interest. The absolute Seebeck coefficient of the sample to be examined, α_b , can then be calculated providing the absolute Seebeck coefficient of the reference material, α_a , is known (by referring to Figure 2.2), which gives,

$$\alpha_b = \alpha_{ab} - \alpha_a \ldots\ldots (2.8)$$

where α_{ab} is Seebeck coefficient of sample b relative to reference sample a.

More accurate results is obtained from the slope of a multiple data points of a Seebeck voltage-temperature difference plot, rather than determined from a single point measurement. This feature helped to eliminate offset errors as shown in Figure 2.3 (a). Significant efforts also have been made to improve the accuracy, rapidity and reproducibility of α measurements [49-53]. Besides the steady state technique, the AC techniques [54-55] and quasi-steady state [56-57] were also developed to improve accuracy and rapidity. Accuracy and rapidity could be improved by neglect resistive voltage and steady state measurement as in DC measurement.

Seebeck measurements at high temperature, which is critical for a thermoelectric generator, imposes more challenges due to the lack of standardized guidelines for measurement procedures [47], poor apparatus design and an inadequate measurement technique [58] that could lead to irreproducibility and inconsistency. A number of recent papers have reported

some attempts that may improve high temperature measurement. These include: Burkov et al [59], Zhou et al [60], Iwanaga et al [48] and Poonambalam et al [61]. In Iwanaga et al's work, a uniaxial 4-point geometry (Figure 2.2 (c)) was used that offered direct contact between the thermocouples and the sample surface.

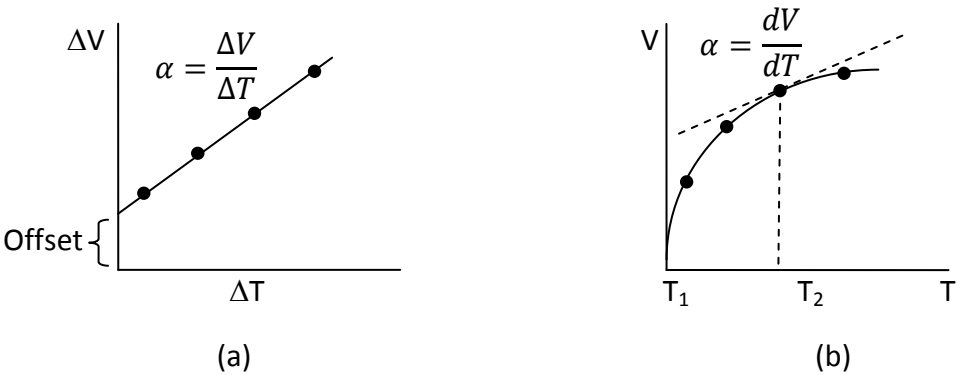

Figure 2.3: Graphical illustrations of (a) the differential and (b) the integral Seebeck coefficient measurement techniques [58].

He claims that the design enables larger forces to be exerted by thermocouples onto the sample surface, thus minimizing the contribution of thermal and electrical contact resistance. Measurement was made between room temperature and up to 1200 K using a differential steady state method with an accuracy of 5-10%. Burkov et al develop an apparatus to measure bulk

and thin film sample from 100 K to 1300 K using differential method with accuracy of 4-10% while Poonambalam et al developed an apparatus capable of measuring α of bar or rod shaped samples using a quasi-steady state condition over a temperature span of 300-1000 K with an uncertainty within 1-2 $\mu V / K$.

2.4.1.2 Integral Method

Another technique used to measure α is the integral method, also known as large ΔT method. In contra with differential method which use small temperature difference (usually <10 K), integral method imposes large temperature difference across the sample (>15 K). It is often used to measure α of long metal wire samples, metallic ribbons, semimetals, and some semi-degenerate semiconductors but not widely employed for thermoelectric materials. The general experimental setup usually involves holding one end of the sample at a fixed temperature (generally 0°C) and the other end is varied throughout the temperature range of interest (can be several hundred degrees hotter than the cold side). Because of the non-linear temperature dependence of the Seebeck coefficient over a large ΔT range, an integral evaluation is appropriate and can be written as;

$$V_{ab} = \int_{T_c}^{T_h} \alpha_{ab} \Delta T \ldots\ldots (2.9)$$

Using a suitable fitting method applied to the entire data set $V_{ab}(T_h, T_c)$, the Seebeck coefficient at a selected temperature point can be obtained from

the slope of the Seebeck voltage versus temperature, at that particular point of the curve as shown in Figure 2.3 (b). The integral method offers several advantages over the differential method due to its capabilities to include inhomogeneity or anisotropy of the sample [62] and to simulate more closely the operation of an actual thermoelement in a device [47]. However, the accumulation of enough points is needed and careful selection of fitting method must be employed. Various curve fitting techniques were discussed by Wood et al [62]. Satisfactory fitting is more difficult to obtain due to the difficulty of maintaining T_c isothermal throughout the large ΔT at high temperatures which may requires additional corrections [58].

Even though differential and integral method measurements using different approach, both of these measurements are derived from the same fundamental. This has been demonstrated by Wood et al [62]. The measured α of short rod-shaped samples of several thermoelectric materials using integral method up to 1000°C showed good agreement with differential method. The same results obtained for differential and integral method. However it is limited to analysis of metal, semimetal and degenerate semiconductor only while measurement on nondegenerate semiconductor and insulator give contrasting results [63].

2.4.2 Electrical Resistivity Measurement

Electrical resistivity measurement requires the determination of electrical resistance, R, length, L and uniform cross sectional area, A, of the examined sample based on the equation $\rho = RA/L$. While the length and the cross sectional area can be measured directly, the resistance of the sample may be determined from Ohm's law, $V = IR$. Well-established methods for measuring ρ are the 2-probe, 4-probe and Van der Pauw methods. However, only the 2-probe and 4-probe methods will be discussed below.

2.4.2.1 The 2-probe method

In the 2-probe method, the same probe of the current flow is used to measures a voltage drop, V_T, across the sample as current flows through the sample. The resistivity is calculated by;

$$\rho = \frac{V_T A}{IL} \ldots\ldots (2.10)$$

The above equation assumes that the current passes uniformly through the sample. Therefore, the accuracy of measurement depends on the distribution of the current within the sample. This method requires good contact with the sample. In order to achieve good contact, soldering or insert compliant material, such as indium foil for lower temperatures or graphite felt for higher temperatures is usually used between the ends of the semiconductor thermoelectric sample and the current electrodes.

The drawback of this method is that the resistance obtained includes the contact resistance at the junctions. A further complication can come from the fact that contact resistance may vary with temperature. Typically, in the case of metals, the contact resistance is far smaller than the resistance of the sample, and can thus be ignored. However, when one is measuring semiconductors (e.g. thermoelectric materials) the contact resistance can be significant and the results obtained are subject to a significant error in the measured sample resistance. Besides, in order to obtain a reasonable voltage drop across the sample, a significant current density is required. As a result, a temperature gradient can be established across the sample due to the Peltier effect. An AC current can be employed in order to eliminate this error.

2.4.2.2 The 4-probe method

This method is more suitable for the measurement of semiconductors including thermoelectric materials. In this technique, two outer probes are used to inject a fixed current into the sample, while two inner probes measure the voltage produced. Using separate probes for current and voltage eliminate the electrical contact resistance due to negligible current passed through the voltage probes. Moreover, if the voltage probes are placed close together and far from the current probes, uniform current flows between the voltage probes can be achieved. For example, in 1973, Rayden et al showed that the voltage probe should be inset by at least the width of the sample [64]. One example of a 4-

probe resistivity apparatus which covers a temperature range of 300-1300 K is shown in Figure 2.4 has an estimated error of 1% [60].

For a disk-shaped sample, a linear 4-probe method is commonly used as shown in Figure 2.5. The four probes were arranged in line, with equal spacing, s, between the probes. Here the current probes represent a dipole source, which establishes a field distribution inside the sample.

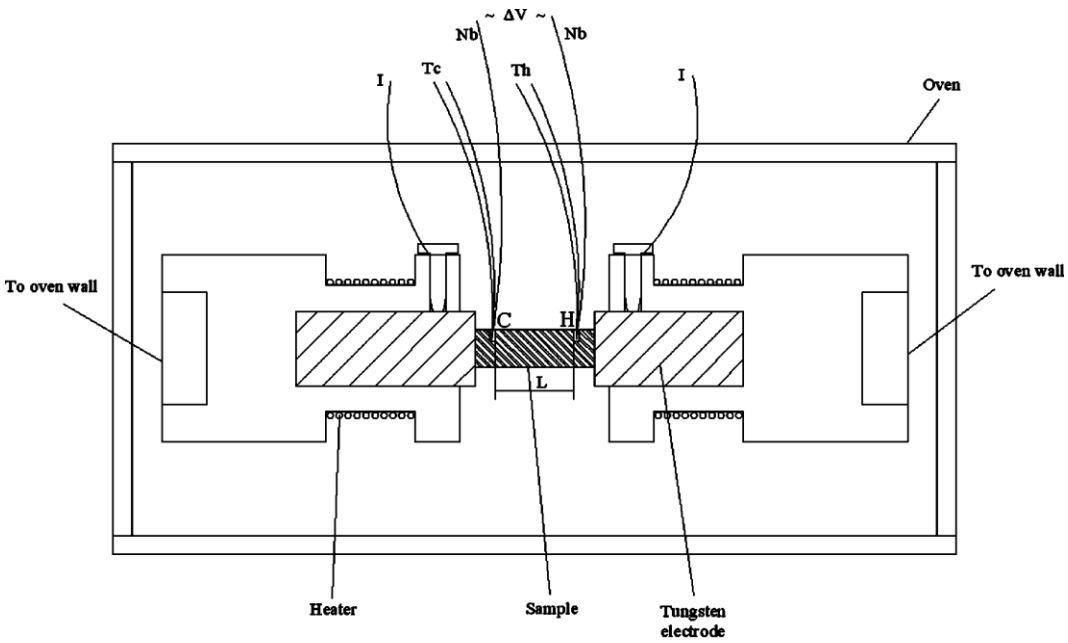

Figure 2.4: Schematic diagram of high temperature α and ρ measurement apparatus using the 4-probe method [60].

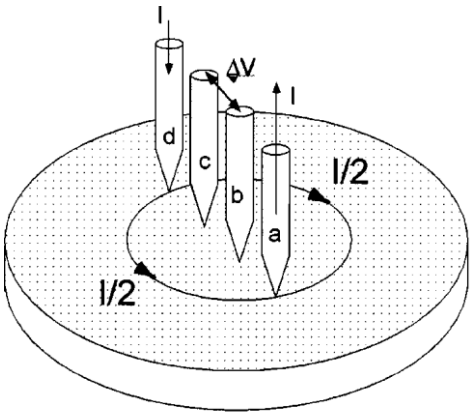

Figure 2.5: Linear 4-probe arrangement [65].

By solving the potential difference between the two inner probes under various boundary conditions (set by the sample size and thickness), it have been shown that the resistivity of a semi-infinite sample with thickness, t, larger than the probe spacing, s, $(t \geq s)$, can be calculated from;

$$\rho = 2\pi s \left(\frac{V}{I}\right) \ldots \ldots (2.11)$$

In the case of thin samples (i.e $t \leq s$),

$$\rho = \frac{\pi t}{\ln 2}\left(\frac{V}{I}\right) \ldots \ldots (2.12)$$

However, the calculated potential distributions above are based on a single dipole source without considering the edge effects. In general, correction factors are needed, which depend on the size and thickness of the sample as well as the position of the electrodes with respect to the boundary of the sample

[65]. For example, the resistivity of a disk-shaped sample with correction factors can be expressed as;

$$\rho = t \cdot CF_d \cdot CF_t \cdot \left(\frac{V}{I}\right) \dots \dots (2.13)$$

where t is the thickness of sample, V is the measured voltage, I is the current supplied, CF_d is the correction factor based on the ratio of diameter and probe spacing and CF_t is the correction based on the ratio of thickness and probe spacing. Further information regarding the correction factors for different sample geometries and positions can be found in Ref [66]. The linear 4-probe technique offers advantages which include speed and ease of application, and it can be employed for thin-film or disc samples. The use of point contact current probes eliminates the need for soldered connections. In addition, the standard corrections are readily available. However, the disadvantage of this technique is the difficulty to adapt to measurements above ambient temperatures [47].

Resistivity measurements using described methods above usually are carried out using direct current. This often requires averaging the voltages in both forward and reverse current direction in order to minimize the effects of Seebeck voltages [61,64]. However, voltage arises from asymmetry in the mounting of the sample and a non-homogenous sample cannot be removed by using this method.

Another approach to overcome errors due to the temperature gradients in thermoelements was proposed by Goldsmid [64] by measuring voltage drop

immediately after the current is applied. This can be achieved using AC current or chopped DC current. It can minimize the influence of the Seebeck voltage contribution arising from the Peltier effect. Since the Seebeck voltage takes time to develop in a bulk sample, reversing the current in a shorter time than that needed for the Seebeck voltage to build up can effectively minimize the influence of the Seebeck effect. The AC current technique has been implemented by Zhou [60] (Figure 2.4) above room temperature. On the other hand, the chopped DC current has been implemented in an apparatus developed by Dauphinee et al [64] and Rowe et al [67]. This technique has the advantages of AC current while maintaining simplicity as in DC current.

Recently, Nishida claims that the most dependable method to separate electrical resistance voltage from Seebeck voltage is to use a high-speed and high resolution DC measurement technique. From his experimental results measured under vacuum condition, a plateau region on the voltage versus time plot was observed with the duration of 1.1-1.3 s just after turning the current on and off. This plateau region reflects negligibly small Peltier pumping before it flows into the region between the voltage probes after 1.3 s. The measurement error increased with an increase in current. Therefore if the voltage can be detect within a duration of the plateau region by ensure a sufficient distance between the current and voltage probes, electrical resistivity of the sample can be determined accurately regardless the driving current being DC, AC or chopped DC [68].

2.4.3 Thermal Conductivity Measurement

Thermal conductivity, λ, is the most difficult measurement among the three parameters due to the fact that heat loss is inevitable. This is worse with thermoelectric materials because of their low thermal conductivity and small sample size. Thus a challenge in designing thermal conductivity apparatus is to minimize these losses. Thermal conductivity measurement requires the determination of temperature gradient, ∇T, developed across the sample corresponding to heat flux, $\vec{Q}$. This is according to the relationship:

$$\vec{Q} = -\lambda \nabla T \ldots\ldots (2.14)$$

There are several methods for the measurement of λ but in general it may be divided into two categories, the steady state method and the dynamics method. In the steady state method, measurement was made only after equilibrium had been reached. This type of measurement requires a lengthy process but can achieve a high accuracy. On the other hand, the dynamics method requires measurement of the thermal gradient as a function of time. The dynamics method results are not so affected by heat losses. However, this type of method usually gives thermal diffusivity value instead of thermal conductivity. It is preferable for its rapidity and wide temperature range. Discussed below are examples of the techniques for each type of the methods describe above. These include axial, radial, comparative techniques (steady state methods) and Amstrong and laser flash techniques (dynamics methods).

2.4.3.1 Steady State method

One of the steady state methods to measure thermal conductivity is that of using an axial heat flow as shown schematically in Figure 2.6. A sample with a cross sectional area, A, is connected to a heat sink at a reference temperature, T_0, while another end is attached to a heater that has a temperature, T_h. Assuming that the temperature is uniform and the heat losses are negligible, heat supplied from the heater, Q, is conducted along a uniform cross sectional area, A, with the distance between two thermometers of L.

The thermal conductivity of the sample can be calculated by;

$$\lambda(T) = \frac{Q}{A}\frac{L}{\Delta T} \dots\dots (2.15)$$

where $\Delta T = T_h - T_o$ is the temperature difference between the thermometers. The difficulty of this measurement is associated with the heat flux measurement. Heat flux can be measured directly (referred to as an absolute method, for example, by measuring the electrical power going into the heater) or indirectly (for example, by comparison with a reference material), referred to as the comparative method. Thermal conductivity can be measured accurately above room temperature for example the one reported by Goldsmid whose successfully measured λ of Bi_2Te_3 from 100-300 K with error not exceeding 3% [64]. However, prevention of heat loss is extremely difficult for measurements above room temperature. At high temperature, insulation around the sample, installation of a radiation shield and guard may become ineffective.

This problem can be minimized by using the radial heat flow method as shown in Figure 2.7. The temperature difference developed at different radii was measured as the heat generated in the centre along the axis of a cylindrical sample. λ can be computed from the formula below,

$$\lambda = \frac{Q \cdot ln\left({r_2}/{r_1}\right)}{2\pi L \cdot \Delta T} \ldots\ldots (2.16)$$

where r_1 and r_2 are the radial positions of the inner and outer thermocouples respectively, ΔT is the measured temperature difference, Q is heat energy input and L is the sample length. This method is, in principle, suitable for measurement of thermoelectric materials. However, a problem is associated with sample size. As a sample becomes smaller, positioning thermocouples at certain radii imposes a challenge [70].

In comparative methods, the idea is to pass a heat flux through a known sample and an unknown sample and to compare the respective thermal gradients, which will be inversely proportional to their thermal conductivities. Most commonly, the unknown sample is sandwiched between two known samples (the references), to take into consideration the minor heat losses that are very difficult to eliminate.

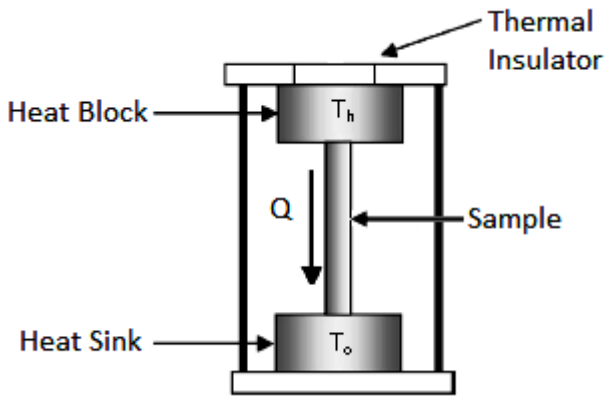

Figure 2.6: Absolute axial flow measurement of thermal conductivity above room temperature [69].

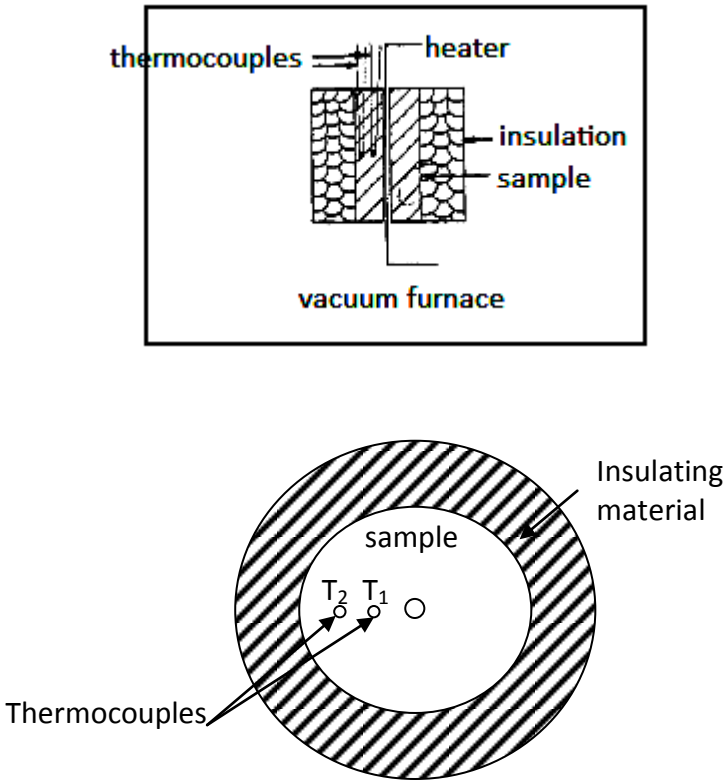

Figure 2.7: Schematic diagram of radial flow measurement technique for measuring of thermal conductivity [70].

An example of schematic diagram of comparative method is shown in Figure 2.8. The thermal conductivity of the unknown sample can be calculated from;

$$\frac{Q}{A} = \lambda_s \frac{\Delta T_s}{L} = \lambda_R \frac{\Delta T_1 + \Delta T_2}{2} \frac{1}{L} \dots \dots (2.17)$$

where λ_s and λ_R is thermal conductivity of the unknown sample and the references respectively, ΔT_s , ΔT_1 and ΔT_2 are temperature difference across sample, across top reference material and across bottom reference materials respectively, and L is distance across it. The greatest drawback of this method is the lack of reproducible reference materials that have a similar thermal conductivity to the test samples [64].

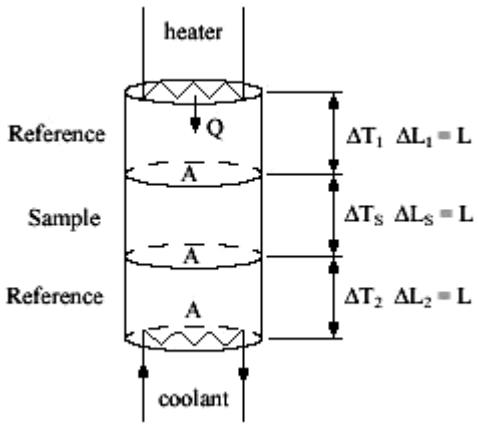

Figure 2.8: Schematic diagram of the comparative method for measuring thermal conductivity [71].

2.4.3.2 The dynamic method

Dynamic methods do not require the lengthy period of time that is needed to reach equilibrium in a steady state method. The theory is based on the fact that temperature distribution varies with time. These techniques generally involve the measurement of thermal diffusivity, α', rather than thermal conductivity, λ, as in the steady state method. For homogenous material, α' is related to λ by;

$$\lambda = \alpha' D C_p$$

$$= \alpha' C_p' \ldots\ldots (2.18)$$

where D is the density, C_p is the specific heat and C_p' is the heat capacity per unit volume. Clearly, separate determinations of the specific heat and density are necessary to obtain thermal conductivities. Dynamics methods may be divided into two categories: periodic and transitory temperature methods.

(i) The Angstrom Method

The Angstrom method is an example of a dynamics periodic method. When a thermal wave propagates in a medium, the amplitude and phase at any point depend on the properties of the medium and the frequency of the wave. In this method, the changes in amplitude and phase of the temperature wave are observed as it passes down a long thin rod. This is done by heating one end of a sample using a periodic heat source which has a period of $2\pi/\omega$ while another end is free to radiate to the ambient temperature. The amplitude of the

sinusoidal temperature wave with an angular frequency, ω, decays exponentially towards the other end. Thus, comparison of the amplitude and phase at two points along the sample enables the thermal diffusivity to be determined. Taking into account the heat losses from the surfaces, the ratio of the amplitude of the thermal wave at two points, κ, separate by the distance, L, with phase difference, φ, is calculated by [64];

$$\alpha' = \frac{\omega L^2}{2\varphi \ln \kappa} \dots \dots (2.19)$$

For accurate measurement, typically used sample has dimension of 300-500mm long and a diameter of 3-9mm [72] which is not suitable for thermoelectric materials. However, Abeles et al [73] managed to measure a shorter Ge sample with dimension of 7.6×7.6mm^2 and 51mm long using higher frequency up to temperatures of 800°C. A much shorter sample was reported successfully measured by Lopez et al [74] using BiSbTe sample of 3.5mm long. The measurement use a slight modification to the Angstorm method initiated from Tomokiyo and Okada's. Because the sample was short, the temperature of the sample continued to rise indefinitely and to prevent this, the sample was attached to a periodic heater, mounted on a thermal resistor that was directly attached to a heat sink as illustrated in Figure 2.9.

(ii) The Laser Flash Method

The laser flash method is an example of the dynamic transitory method and the most popular method for measuring thermal conductivity of solids. In this method, the front face of a thermally insulated sample (usually, a small disk) is subjected to a very short pulse of heat came from a laser, electron beam or xenon flash lamp with irradiation times ≤ 1msec. The resulting temperature rise on the back surface of the sample is usually recorded by an oscilloscope or high speed chart recorder.

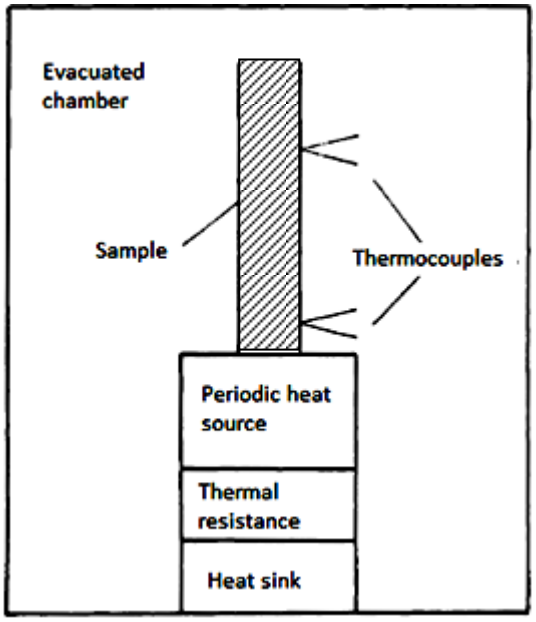

Figure 2.9: Schematic diagram of a modified Angstrom method for small size samples [73].

If there is no heat loss, the characteristic rising profile of the temperature as a function of time is shown by the curve A in Figure 2.10 while curves B and C shows the actual results of measurements with increasing heat losses.

The thermal diffusivity is calculated using;

$$\alpha' = 0.1388\frac{L^2}{t_{1/2}} \ldots\ldots (2.20)$$

where L is sample thickness and $t_{1/2}$ the time taken for the back surface temperature reach half its maximum value. The reproducibility of thermal diffusivity measurement at room temperature is reported to be ±2% [67]. The errors can be attributed to deviation from ideal assumptions of an adiabatic sample and instantaneous pulse heating. Correction factors have been introduced to account for deviation due to heat losses, finite pulse duration, non-uniform pulse heating and non-homogeneous structures.

2.5 ZT Measurement – The Direct Approach

Thermoelectric figure-of-merit can be determined directly using a method described by T.C. Harman in 1958 [75]. The theory is based on the ZT association with the co-existence of the Seebeck voltage and the resistive voltage across the sample when a small direct current is passed through the sample. This will cause a temperature gradient due to the Peltier effect being generated at the junction at a rate of αIT .

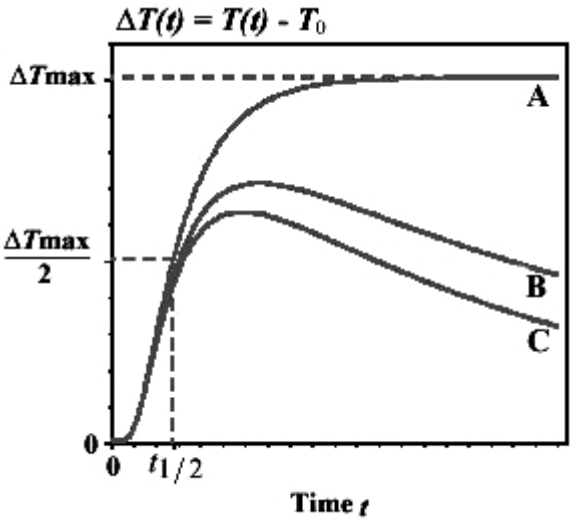

Figure 2.10: Typical curves of the rear surface temperature history for various experiments conditions. Curve A shows an ideal temperature profile without heat loss and curves B and C show the temperature profile with heat losses at a different rate.

The Peltier heat flow from one end to another will be accompanied by heat conduction in the opposite direction, at a rate of $\frac{\lambda A}{L}\Delta T$. Assuming no heat loss from the sample and contact resistance is negligible, Peltier heat is in balances with heat transported across the sample when the system reaches a steady state,

$$\alpha IT = \frac{\lambda A}{L}\Delta T \ldots\ldots (2.21)$$

where α and λ are the Seebeck coefficient and thermal conductivity, L is the sample length, I is the current flow in the circuit, T is the ambient temperature

and A is cross sectional area of the sample. The Joule and Thomson heat can be neglected because of the small current applied. The Seebeck coefficient, α, and electrical resistivity, ρ, are defined as,

$$\alpha = \frac{V_s}{\Delta T} \dots\dots (2.22)$$

$$\rho = \frac{RA}{L} = \frac{V_R A}{IL} \dots\dots (2.23)$$

where V_s is the Seebeck voltage, V_R is the electrical resistive voltage under isothermal condition, A is the cross sectional area, L is the sample length and ΔT is the temperature difference across the sample.

The thermal conductivity, λ , is derived based on equations (2.21) and (2.22) as,

$$\lambda = \frac{\alpha ITL}{A\Delta T}$$

$$= \frac{V_s}{\Delta T^2}\frac{ITL}{A} \dots\dots (2.24)$$

When the current flows, temperature difference develop across the sample produce a voltage where the total voltage, V_T , produce under adiabatic condition is given by,

$$V_T = V_s + V_R \dots\dots (2.25)$$

From definition of $ZT = {\alpha^2 T}/{\rho\lambda}$ and by substituting equations (2.22)-(2.24) above, dimensionless figure-of-merit becomes,

$$ZT = \frac{V_s}{V_R}$$

$$= \frac{V_T}{V_R} - 1 \ldots \ldots (2.26)$$

Clearly, simplifications used in the Harman method by neglecting radiation and convection heat losses from the sample surfaces as well as conduction heat loss from current and voltage wires introduce errors. To include these influences, Harman later derived an equation with correction factors [64] and this was later confirmed by Bowley et al [76]. He showed that the correction of radiation heat loss of bismuth telluride sample at room temperature is less than 1% using different sizes of homogenous and isotropic samples. Correction for Harman method which includes heat loss from wire and voltage probes also has been reported by Abrutin et al [77].

Using another approach, Penn [78] replaced the voltage probe at the end of the sample to the sample itself by a distance at least as large as the largest cross sectional dimension. The voltage-time plot showed the same behaviour observed except that after an instantaneous rise, voltage remain constant (plateau) for a short time before then rising slowly and asymptotically to a final value. The same plateau was also observed when the current was off. These characteristics enabled accurate determination of both the electrical resistivity and Seebeck voltages without requires separate measurement of the Seebeck coefficient.

There are few ways to measure ZT using the Harman method. In the original/classical Harman method, ZT is obtained indirectly from determination

of electrical resistive voltage, V_R , from measurements of V_T and V_S using small direct current. V_T is obtain after steady state is achieved meanwhile V_S is obtain from separate measurement using the same equipment. The fact that the total voltage, V_T and the Seebeck voltage, V_S, are measured under the same equipment, make the measurement more convenient and hence minimize instrumental error.

In the modified Harman method, ZT is obtained directly by measuring voltage produced by supplying direct and alternating current across the sample. The ZT is given by,

$$ZT = \frac{V_{DC}}{V_{AC}} - 1 \ldots\ldots (2.27)$$

where V_{DC} and V_{AC} represent the voltage values obtained by the DC and AC method respectively. When a constant direct current (DC) is applied, the voltage produced consists of the resistive voltage, V_R and the Seebeck voltage, V_S. When alternating current (AC) is applied, the changes in current polarity will subsequently change the resistive voltage direction, V_R , but not the Seebeck voltage component, V_S . As the result, both voltages can be separated. The main drawbacks of this method are due to the fact that its accuracy depends on the frequency of alternating current [79] and parasitic heat losses such as radiation heat to the environment especially at high temperature which can alter the result substantially [80]. Research also has been reported to improve accuracy of the Harman method as reported in [81-83]. Practically, measurements are made

using a forward and reverse direct current in order to eliminate the disbalance of the zero bias and the effect of the thermoelectric voltage. The ZT parameter was calculated using $ZT = \frac{V_f - V_r}{2V_{AC}} - 1$, from the results of measured voltages, V_{AC} , V_f, and V_r using alternating, forward, and reverse currents respectively [79]. This method is the basis of commercial portable Z-meter equipment as shown in Figure 2.11. The meter is capable of measuring Z , R_{AC} and $\Delta T_{\max}$ of single and 2-stage TEC modules [84-86].

Another method of determining ZT based on the Harman method was proposed by Buist [87] in 1992 known as the transient method. This method is made based on determination of Seebeck voltage, V_s , that is slightly different from the original Harman method based on determination of the electrical resistive component, V_R. When current is applied as shown in Figure 2.12 (a), the voltage raises instantaneously to the resistive voltage value, V_R and then increase asymptotically to the steady state voltage, V_T , as in Figure 2.12 (b). When the current is off, the voltage drops instantaneously to Seebeck voltage, V_s , before decay exponentially to zero. By utilizing of high speed analog-to-digital converter with high resolving power [79], the transient method improves ZT accuracy and reproducibility [87].

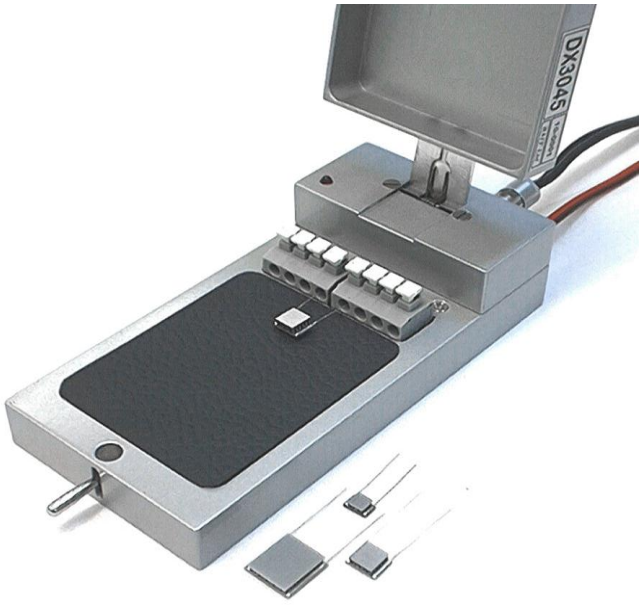

Figure 2.11: A typical commercial Z-meter [84].

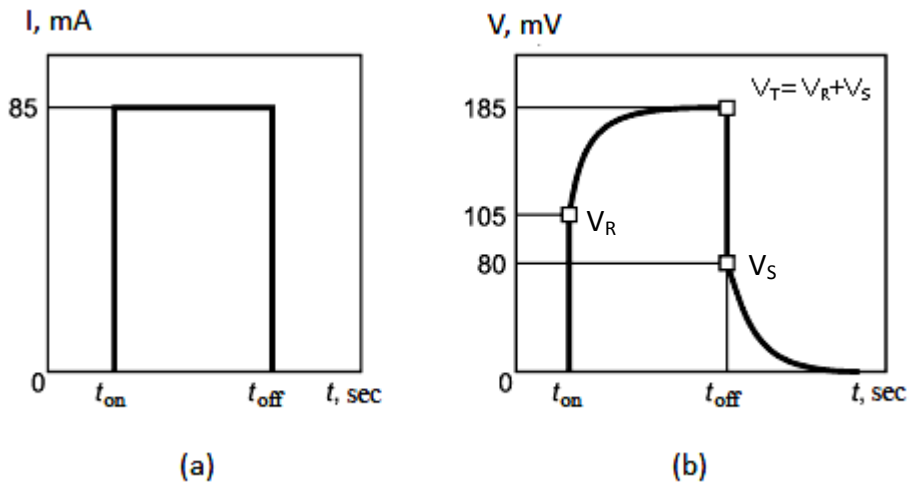

Figure 2.12: Illustration of the transient Harman method (a) rectangular current pulse which flows through the sample and (b) corresponding voltage characteristic used to calculate the ZT [79].

Although many techniques has been discussed above, in general the Harman technique is limited to only thermocouple, module or cascade/multistage modules [88]. The measurement successfully demonstrated near or below room temperature due to negligible heat loss. However, the Harman method is not suitable for inhomogeneous samples (e.g., segmented, functionally-graded or irregular shaped) due to different temperature drops in individual segments and measurement on higher temperature as required in TEG applications. Few studies have been made on measurement above room temperature using this method such as reported in [89-91]. For example, Fujimoto et al [90] observed that, by using the transient method, the measurement of ZT from room temperature to 573 K using n-type Bi_2Te_3 samples showed a very good agreement with other measurement techniques. However, studies by Jacquot et al [91] theoretically show that application of Harman method at much higher temperatures (~1000 K) could not easily be implemented due to the strong influence of sample thickness and contact resistance.

2.6 Large Temperature Difference Measurements

All ZT measurements described above derived from small ΔT measurement throughout temperature range except integral method of Seebeck coefficient measurements. However, in reality, thermoelectric devices operate under larger temperature differences than that is allowed in ZT measurement.

Neglecting thermoelectric properties dependence with temperature in ZT calculation would introduce significant errors. This is especially true for TEG in waste heat recovery applications where a larger temperature range is involved in order to improve its efficiency. Practically, this can be realized by the development of functionally graded materials (FGM), segmented and cascaded structures. Unfortunately, it is not possible to measure the ZT of these structures using conventional methods due to the different temperatures that are produced along the device. Conventional ZT was estimated from modelling and computational calculation. Although there are few papers reporting on the practical instrumentation of large ΔT measurement, the aim of the methods concentrated on the measurement of power output performance and the efficiency of the TEG.

One of the earliest attempts was proposed by Y. S. Kang et al [92] in 1997. He developed an apparatus that was capable of measuring samples with dimensions of 10-20 mm diameter and 5-30 mm length up to temperature 1073 K. The measurement was focused on thermoelectric power output performance which was determined from the measurement of current and voltage produced. The two samples measured were FGM (n-type Bi_2Te_3, PbTe, SiGe) and segmented (p-type Bi_2Te_3, PbTe) thermoelectric leg. Both measurements observed lower power output produced compared with a calculation using measured resistance. A year later, Y. S. Kang et al [93] made a comparison between a segmented and FGM sample (n-type Bi_2Te_3, PbTe, SiGe) and observed higher power output

achieved by segmented sample under the same temperature difference. This is due to the lower contact resistance in the segmented sample. Although Y. S. Kang et al managed to measure the power output of the TEG under large ΔT, the resistance of the sample was obtained under a small temperature difference by supplied small current (~15 mA) to prevent the Peltier effect.

In 1998 and 1999, another apparatus for large temperature difference measurement was reported by E. Muller et al [94, 95]. By contrast to Y. S. Kang works, the efficiency, Seebeck coefficient, electrical resistance and thermal conductance of $FeSi_2$ sample were measured with the hot side temperature up to 873 K while maintaining the cold side at near room temperature. A tunable low resistance load, based on a switch relay was constructed to reduce overall load resistance. Thermal conductance was obtained from the average sample heat flow and the sample interface temperature while sample resistance is obtained by voltage measurement with varied load resistance. The internal resistance of the $FeSi_2$ series measured were almost double compared to the material while the efficiency measured was lower than the material [94]. On the other hand, resistance in the FGM $FeSi_2$ was higher than expected while the homogeneous $FeSi_2$ sample was in good agreement with the standard sample [95].

More recent research has been reported by A. Muto et al [96] in 2009 which employs an effective properties approach to model a TEG leg. An effective dimensionless figure-of-merit, ZT under large ΔT can be represented similarly to

the definition of ZT under small ΔT provided that all effective thermoelectric properties are used during calculation, $Z\bar{T} = \frac{\alpha^2{}_{eff}}{\rho_{eff}\lambda_{eff}}\bar{T}$. Seebeck coefficient was measured using integral method, electrical resistance was measured using 4-wire AC method and the heat conduction was measured from heat flows, Q_H, to the sample. ZT can then be calculated by measuring all these three parameter and represented as $ZT = \frac{V^2{}_S}{\Delta T R \dot{Q}_H}\bar{T}$. Effective thermoelectric properties were compared with intrinsic thermoelectric properties that were derived from effective properties derivative, which shows ZT calculated from intrinsic properties drop more rapidly with increasing temperature than ZT_{eff}.

2.7 Conclusion

In summary, both direct and indirect ZT measurement methods have their advantages and disadvantages. In general, the Harman method is subject to a higher degree of uncertainty compared with individual measurements. Despite this, the Harman method may be an option for its simplicity. Moreover, the fact that direct measurement is applied to the same sample prevents ambiguity caused when different measurements are taken on different samples, such as crystallography direction and variation of properties as function of time. Nevertheless, direct measurement is generally faster than combining measurements of α, ρ and λ on separate measurement systems.

Both direct and indirect techniques were used under condition of a small temperature difference. For example, α measurement typically measures

between 5-10 K temperature difference, ρ under isothermal conditions, λ at various temperature differences (usually small) depending upon the technique employed and the Harman method is invariably used under condition of a small temperature difference. In practice, the operational temperature differences typical for thermoelectric devices are much larger than that usually employed in ZT measurements. Although there are few papers that describe measurement under large temperature difference, only Muto et al [96] report the measurement of ZT. However, ZT reported is determined by measuring all thermoelectric properties individually. This is a completely different approach from that used in this study, which measures ZT directly under operating conditions. It allows study on the effects that only exist under condition of a large temperature difference (e.g the Thomson effect).

CHAPTER 3

Theoretical Background of Open-Short Circuit Technique

3.1 Introduction

In chapter 2 we already discussed the importance of the figure-of-merit, Z, in determination of the thermoelectric performance and techniques to measure ZT. Indirect method of ZT measurement requires different shape, size, temperature, and operating conditions for each measurement system. This will introduce significant error which becomes more complex for samples that are non-homogeneous and of differing crystallography. Furthermore, lot of samples are needed to evaluate the same thermoelectric material which will increase the cost of sample production as well as the maintenance of the equipment. Moreover, it will also increase time consumption due to need for more measurement. To overcome these problems, direct method using Harman technique is preferable which offer easiest and fastest way to obtain ZT. The disadvantage of this method is that it introduces a bigger error (~20%) compared to individual measurement method (~10%) [97]. Its application is limited at lower temperatures and non-segmented and non-FGM structures. Both direct and indirect techniques in the current method measure ZT under a small temperature difference throughout the temperature range. In this chapter,

theoretical background of new technique capable to measure ZT directly and under operating temperature is discussed.

3.2 Dimensionless Figure-of-Merit, ZT

The figure-of-merit, Z, was made of thermoelectric properties of the Seebeck coefficient, electrical resistivity and thermal conductivity. Z is usually multiplied by the mean temperature, $\bar{T} = \frac{(T_h+T_c)}{2}$ to give the so-called dimensionless figure-of-merit, ZT, used widely in literature. It should be noted that the validity of efficiency, η , and coefficient of performance, ϕ , formulation from equations (2.4) and (2.7) is only relevant for ZT obtain under small temperature difference. This is due to the fact that the heat balance equations used in derivation are based on the assumption that Seebeck coefficient is independent of temperature thus no Thomson effect is included [44, 45]. In general, electrical resistivity involves measurement under isothermal conditions to prevent the Peltier effect. The Seebeck coefficient is usually measured under condition of a small temperature difference of around 5-10K while thermal conductivity is measured at various temperature differences (usually small) depending upon the technique employed. The most common variations of the Harman technique also limit the measurement to a small temperature difference. In reality, thermoelectric devices operate at a much higher temperature difference than that employed for ZT measurement. Clearly, significant errors can exist due to neglecting the effects that only become

significant under a large temperature difference [98]. In the absence of ZT measurement under a large temperature difference, its conversion efficiency is currently estimated using the average value of many ZT measurements under small temperature differences over the temperature range [98].

3.3 Background of the Open-Short Circuit Technique

The new technique used in this research was proposed theoretically in 2001 by Gao Min [97]. After that, an initial study has been made by Konstantinos [99] to measure the ZT of a thermoelectric module, which will be explained more in Chapter 4. The new technique proposed offer several advantages which will be beneficial to thermoelectric measurement. Initial study suggests that this method offers easy and rapid measurements due to its capability to measure ZT directly. More importantly this technique allows ZT measurement under a large temperature difference and current flowing. The success of ZT measurement under large temperature difference will determine the performance of the thermoelectric material under real operating conditions. It has also proved to be beneficial for the measurement of more complex structures such as segmented or functionally graded material which are designed for operating under condition of a larger temperature difference.

3.4 Principle of the Open-Short Circuit Technique

The basic schematic diagram of the arrangement for ZT measurement is shown in Figure 3.1. Thermoelectric material (sample) under evaluation is sandwiched between a heater and a heat sink. The sample is connected to terminals A and B which can be opened or short circuited. Figure 3.2 shows an equivalent circuit, where the thermoelectric sample can be represented as a thermoelectric battery with an internal resistance, R_i. When heat from the heater is supplied to flow through the sample, a temperature difference will be produced between the hot junction, T_h and the cold junction, T_c.

Under open circuit conditions $(R_L = \infty)$, the Seebeck voltage, V_o, generated across the thermoelectric material due to the difference in temperature, ΔT_o, at the hot and cold junctions can be expressed as,

$$V_o = \bar{\alpha}\Delta T_o \quad \dots\dots (3.1)$$

with $\bar{\alpha} = \frac{\alpha_h + \alpha_c}{2}$ is the mean Seebeck coefficient over the thermoelectric sample where α_h and α_c are the Seebeck coefficients for the hot and cold end, respectively. Assuming the measurement is done in an adiabatic condition where all the heat from the hot junction is transferred to the cold junction by conduction, the total rate of heat flow can be written following Fourier's law as,

$$Q_o = \lambda \frac{A}{l}(T_h - T_c)$$

$$= K\Delta T_o \dots\dots (3.2)$$

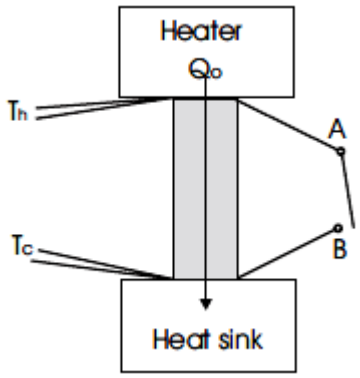

Figure 3.1: Schematic diagram of the open-short circuit technique for ZT measurement [97].

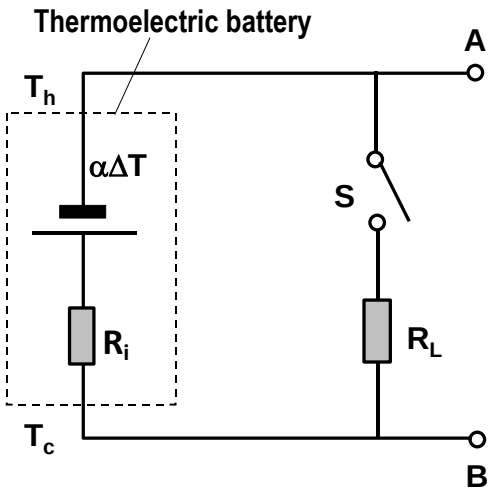

Figure 3.2: Equivalent circuit for thermoelectric battery [101].

where K is thermal conductance of the thermoelectric sample at that particular temperature and ΔT_o is the open circuit temperature difference.

When terminals A and B are in short circuited $(R_L = 0)$, the temperature difference across the specimen will change from ΔT_o to ΔT_s, corresponding to the temperature difference during the short circuit while current flowing into it. Figure 3.3 (a) shows the expected schematic change in the temperature difference across the specimen when the circuit is switched from open circuit to short circuit, while the corresponding change in the Seebeck voltage is displayed in Figure 3.3 (b). The voltage produced can be written as,

$$\bar{\alpha}\Delta T_s = I_s R_i \ldots\ldots (3.3)$$

Because of the current flow, the total heat flow through the sample is not only from the heat conduction from the heater but also from heat absorbed due to the Peltier effect at the hot junction, T_h , as well as a contribution from the Joule heating which is given by,

$$Q_s = \bar{\alpha} I_s T_h - \frac{1}{2} I_s^2 R_i + K\Delta T_s \ldots\ldots (3.4)$$

where I_s is short circuit current, R_i is the internal resistance of the thermoelectric sample, T_h is temperature at hot end and ΔT_s is the difference in temperature across the sample when A and B are short circuited. Note that for equation (3.4) to be valid, constant thermal and electrical conductivities of the thermoelectric sample between T_h and T_c are required so that the Joule heat and Thomson heat affect both ends equally.

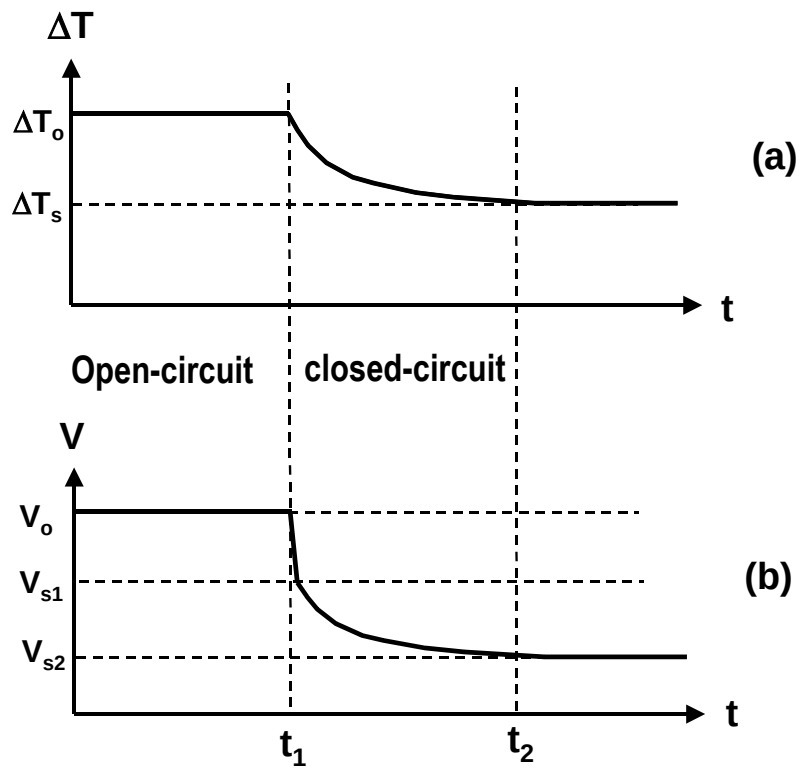

Figure 3.3: Schematic of transient processes in thermoelectric materials from open circuit to short circuit (a) Temperature difference; (b) Voltage across the specimen [98].

Consequently it is essential that the temperature difference between T_h and T_c achieves steady state before measurement is made. The four formulas above (equation 3.1-3.4) were the basis for the derivation of the formula for this novel technique as explained below. If the rate of heat input, Q_o, is kept constant during open and short circuit, the following relationship can be derived,

$$Q_o = Q_s$$

$$K\Delta T_o = \bar{\alpha} I_s T_h - \frac{1}{2} I_s^2 R_i + K\Delta T_s$$

$$\frac{\Delta T_o}{\Delta T_s} = \frac{\bar{\alpha} I_s T_h}{K\Delta T_s} - \frac{I_s^2 R_i}{2K\Delta T_s} + 1 \ldots\ldots (3.5)$$

By replacing $I_s = \frac{\bar{\alpha}\Delta T_s}{R_i}$ obtained from equation (3.3) into equation (3.5),

$$\frac{\Delta T_o}{\Delta T_s} = \frac{\bar{\alpha} T_h}{\mathrm{K}\Delta T_s}\left(\frac{\bar{\alpha}\Delta T_s}{R_i}\right) - \frac{R_i}{2K\Delta T_s}\left(\frac{\bar{\alpha}\Delta T_s}{R_i}\right)^2 + 1$$

$$= \frac{\bar{\alpha}^2}{KR_i} T_h - \frac{\bar{\alpha}^2}{KR_i}\left(\frac{\Delta T_s}{2}\right) + 1 \ldots\ldots (3.6)$$

Using definition $Z = \frac{\bar{\alpha}^2}{KR_i}$ into equation (3.6),

$$\frac{\Delta T_o}{\Delta T_s} = ZT_h - \frac{1}{2} Z\Delta T_s + 1$$

$$= Z\left(T_h - \frac{T_h - T_c}{2}\right) + 1$$

$$\therefore Z\bar{T} = \frac{\Delta T_o}{\Delta T_s} - 1 \ldots\ldots (3.7)$$

with $\overline{T} = \left(\frac{T_h + T_c}{2}\right)$ is the mean temperature of the short circuit. This is the first equation of this technique and will be referred to as the "*temperature measurement method*". The second equation can be derived by replacing $\Delta T_o = {V_o}/{\overline{\alpha}}$ from equation (3.1) and $\Delta T_s = {(I_s R_i)}/{\overline{\alpha}}$ from equation (3.3) into equation (3.7),

$$Z\overline{T} = \frac{V_o}{I_s R_i} - 1 \ldots\ldots (3.8)$$

The second equation will be referred to as the "*electrical measurement method"*. It is apparent that temperature measurement method introduces simplicity of instrumentation as it only requires the measurement of temperature difference between samples during open and short circuit conditions. However, theoretically the electrical measurement method which requires measurement of the Seebeck voltage during open circuit, the current flows and resistance of the sample during the short circuit can be achieved more accurately because current and voltage can be measured more accurately than temperature measurement.

Besides the advantages of measuring ZT directly, this novel technique also has the capability to determine all the thermoelectric properties using the same experimental setup. The Seebeck coefficient of the sample can be determined from the voltage generated at terminals A and B and the temperature difference during open-circuit by,

$$\alpha_s = \frac{V_o}{\Delta T_o} - \alpha_c \ldots\ldots (3.9)$$

where α_s and α_c are the absolute Seebeck coefficient of the sample and interconnector respectively. Interconnector usually made of metal such as copper was used due to negligible Seebeck coefficient compared with that of good thermoelectric materials (i.e. $\alpha_s > \alpha_c$).

The resistivity of the thermoelectric sample, $= {R_i A}/{l}$, can be obtained by determining the resistance of the sample using [42],

$$R_i = R_L \left(\frac{V_o}{V_{s1}} - 1 \right) \ldots\ldots (3.10)$$

where V_{s1} is the voltage taken at the moment immediately after terminals A and B are closed while the temperature difference across the specimen is still very close to the open circuit value, ΔT_o, as indicated in Figures 3.3 (a) and (b). Alternatively, by using equation (3.3) resistance can be calculate by,

$$R_i = \frac{\bar{\alpha} \Delta T_s}{I_s} \ldots\ldots (3.11)$$

Note that sample's resistance obtained from equations (3.10) and (3.11) is valid for any temperature difference. This is different compared with conventional resistance measurement methods that are usually performed under a small temperature difference to prevent the influence of the Peltier effect.

Once ZT, α and ρ are determined, thermal conductivity can easily be calculated from,

$$\lambda = \frac{\alpha^2}{Z\rho} \ldots\ldots (3.12)$$

Alternatively, by knowing the total heat flows into the sample, thermal conductivity may be estimated from the determination of module conductance during open circuit. From equation (3.2),

$$K = \frac{Q_o}{\Delta T_o} \ldots\ldots (3.13)$$

It is important to have an adiabatic condition to guarantee the success of the measurement.

3.5 Non short-circuited condition

Another advantage of this novel technique is that it is not limited to one size and dimension of thermoelectric material. Since a thermoelectric module has a bigger internal resistance, R_i, than that in a single thermoelement or thermocouples, it is much easier to obtain the short circuit condition. This is due to the bigger ratio between internal resistance, R_i, and resistance of the short circuit wire connection, R_L, used. However, with modification to the derivation of the equation (3.3) above, a smaller resistance of thermoelectric material such as in a single element or thermocouples can be measured. In this case, equation (3.3) can be expressed as,

$$\bar{\alpha}\Delta T_c = I_c(R_i + R_L) \ldots\ldots (3.14)$$

where ΔT_c and I_c refers to the temperature difference and the current produced under a closed circuit condition $(R_L \neq 0)$. This will lead to a modification in the

ZT equation, which can be derived by replacing I_s in equation (3.5) with I_c obtained from equation (3.14) above,

$$\frac{\Delta T_o}{\Delta T_c} = \frac{\bar{\alpha} T_h I_c}{K \Delta T_c} - \frac{I_c^2 R_i}{2K\Delta T_c} + 1$$

$$= \frac{\bar{\alpha} T_h}{K\Delta T_c}\left(\frac{\bar{\alpha}\Delta T_c}{R_i + R_L}\right) - \frac{R_i}{2K\Delta T_c}\left(\frac{\bar{\alpha}\Delta T_c}{R_i + R_L}\right)^2 + 1$$

$$= \frac{\bar{\alpha}^2}{K}\left(\frac{T_h}{R_i + R_L}\right) - \frac{\bar{\alpha}^2}{K}\left(\frac{R_i \Delta T_c}{2(R_i + R_L)^2}\right) + 1$$

$$= \frac{\bar{\alpha}^2}{K R_i}\left(\frac{R_i T_h}{R_i + R_L}\right) - \frac{\bar{\alpha}^2}{K R_i}\left(\frac{R_i^2 \Delta T_c}{2(R_i + R_L)^2}\right) + 1$$

$$= Z\left(\frac{R_i T_h}{R_i + R_L} - \left(\frac{R_i}{R_i + R_L}\right)^2 \frac{\Delta T_c}{2}\right) + 1$$

$$\therefore ZT_m = \frac{\Delta T_o}{\Delta T_c} - 1 \ldots\ldots (3.15)$$

with $T_m = \frac{R_i}{R_i + R_L}\left(T_h - \frac{R_i}{R_i + R_L}\frac{\Delta T_c}{2}\right)$ is the effective mean temperature. By defining $a = \frac{R_i + R_L}{R_i}$, T_m can be simplified as,

$$T_m = \frac{R_i}{R_i + R_L}\left(T_h - \frac{R_i}{R_i + R_L}\frac{\Delta T_c}{2}\right)$$

$$= \frac{1}{a}\left(T_h - \frac{\Delta T_c}{2a}\right)$$

$$= \frac{1}{a}\left(\frac{2aT_h - T_h + T_c}{2a}\right)$$

$$= \frac{(2a - 1)T_h + T_c}{2a^2} \ldots\ldots (3.16)$$

Note that the short circuit temperature difference, ΔT_s, has now been replaced with the closed circuit temperature difference, ΔT_c. According to the equation, temperature difference changes with the changing of external load, R_L. Provided that the dimensionless figure-of-merit of the thermoelectric material is constant over the temperature range, the changes of temperature difference can be plotted on a graph as shown in Figure 3.4. This has been proven [101] by adding the variable resistor as shown schematically in Figure 3.5. By keeping constant heat flows during the open circuit and the short circuit throughout R_L range, changes in ΔT_c obtained agree well with those calculated where,

$$\frac{\Delta T_o}{\Delta T_c} = ZT_m + 1$$

$$\Delta T_c = \frac{\Delta T_o}{ZT_m + 1}$$

$$= \frac{\Delta T_o}{Z\left[\frac{(2a-1)T_h + T_c}{2a^2}\right]} \quad \dots\dots (3.17)$$

As R_L increases, ΔT_c gets smaller. This means that it is getting harder to observe changes in temperature difference between open and closed circuit for a much smaller resistance sample. Consequently, a larger temperature difference is required.

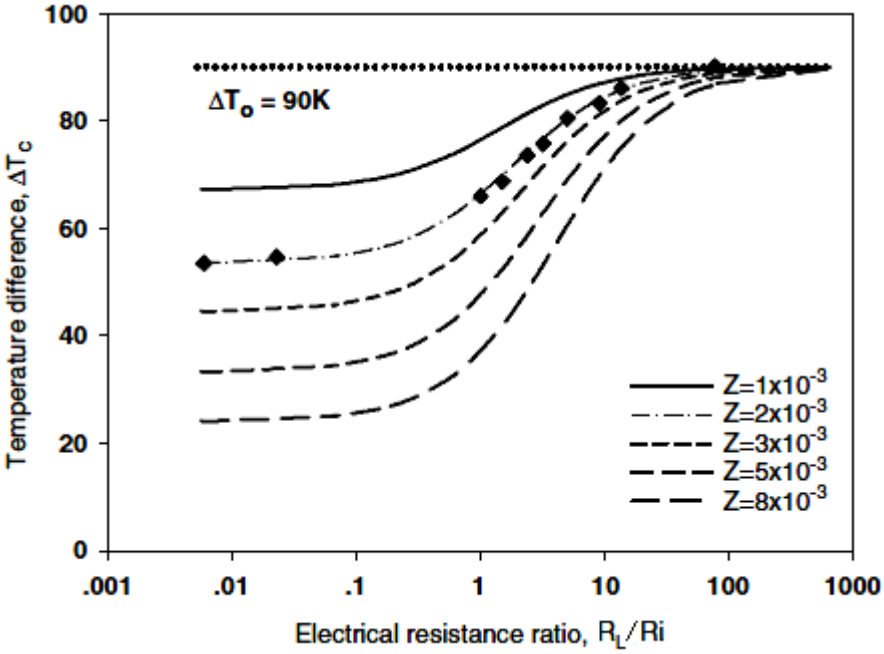

Figure 3.4: Temperature difference across the specimen during closed circuit, ΔT_c, as a function of the ratio of R_L / R_i for different values of thermoelectric figure-of-merit.

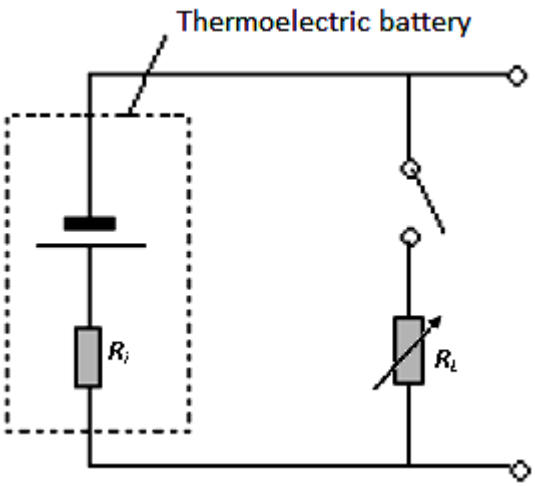

Figure 3.5: Schematic diagram of closed circuit temperature difference study with changes in load resistance.

By knowing the trend of ΔT_c changing with $\frac{R_L}{R_i}$, the short circuit temperature difference, ΔT_s , can be indirectly determined by extrapolating the $\Delta T_c - \frac{R_L}{R_i}$ curve to $R_L = 0$. In this case, an appropriate curve fitting based on equation (3.17) is necessary. On the other hand, a match of the experimental data with the theoretical derivation of the $\Delta T_c - \frac{R_L}{R_i}$ curve line will directly determine the Z value of the sample.

3.6 Large temperature difference measurement

The figure-of-merit defined by $\frac{\bar{\alpha}^2}{\rho\lambda}$ has been derived assuming thermoelectric properties of α, ρ and λ are independent of temperature. In reality, this is not the case. Consequently, the Thomson effect was neglected. This can be shown from definition of the Thomson coefficient, $\beta = T \cdot \frac{d\alpha}{dT}$ where if the Seebeck coefficient is constant (i.e. $\frac{d\alpha}{dT} = 0$), the Thomson coefficient is zero. By contrast, if the Seebeck coefficient is dependent on temperature, $\frac{d\alpha}{dT} \neq 0$, the effect become important as $\beta \neq 0$. To overcome this problem, an average Seebeck coefficient, $\bar{\alpha}$, over the required temperature range is used

and an average product of $\rho \cdot \lambda$ is taken rather than a separate parameter over temperature range [44] as shown below,

$$Z = \frac{\langle \alpha_p - \alpha_n \rangle^2}{\left(\langle \rho_p \lambda_p \rangle^{1/2} + \langle \rho_n \lambda_n \rangle^{1/2} \right)^2} \ldots\ldots (3.18)$$

where angular brackets indicate temperature-averaged quantities. However, Z defined in equation (3.18) would provide results within 10% of the true value [102] only if the temperature differences are small. It becomes progressively more inaccurate with increasing temperature difference.

For operation under a large temperature difference the Thomson effect could be taken into account by modifying the heat balance equation. For a thermoelectric generator, total heat flows from the hot side can be written as [100],

$$Q_h = \alpha_h I T_h - \frac{1}{2} I^2 R_i + K \Delta T - \frac{1}{2} \beta \Delta T I \ldots\ldots (3.19)$$

where β is the Thomson coefficient. A factor of ½ has been introduced into the last term in equation (3.19), following the simplification similar to the one used when dealing with the Joule heat. It is assumed that half of the Thomson heat flows to the hot end and half flows to cold end for a thermally insulated sample. Note that the Thomson heat is either released or absorbed depending on the materials, direction of the electrical current and temperature difference. Rearranging equation (3.19),

$$Q_h = \left(\alpha_h - \frac{\beta \Delta T}{2 T_h} \right) I T_h - \frac{1}{2} I^2 R_i + K \Delta T$$

$$= \alpha_e I T_h - \frac{1}{2} I^2 R_i + K\Delta T \ldots\ldots (3.20)$$

where $\alpha_e = \left(\alpha_h - \frac{\beta \Delta T}{2T_h}\right)$ is the effective Seebeck coefficient. By replacing an average Seebeck coefficient with an effective Seebeck coefficient, the modified figure-of-merit can be expressed as,

$$Z_m = \frac{\alpha_e^2}{\rho\lambda} = \frac{\left(\alpha_h - \frac{\beta\Delta T}{2T_h}\right)^2}{\rho\lambda} \ldots\ldots (3.21)$$

It can be seen that if ΔT is much smaller than T_h , the Thomson effect can be neglected. However, if ΔT becomes comparable with T_h, the contribution of the Thomson effect to the thermoelectric process can no longer be neglected. The same concept can be applied to a thermoelectric cooler as the charge carrier moves from the cold end to the hot end and the heat balance equation at the cold end can be written as,

$$Q_c = \alpha_c I T_c - \frac{1}{2} I^2 R_i - K\Delta T + \beta \Delta T I$$

$$= \left(\alpha_c + \frac{\beta\Delta T}{2T_c}\right) I T_c - \frac{1}{2} I^2 R_i - K\Delta T \ldots\ldots (3.22)$$

The Thomson effect could significantly influence the effective Seebeck coefficient under conditions of a large temperature difference. Theoretically, an increase in the effective Seebeck coefficient will increase the effective figure-of-merit while a reduction in the effective Seebeck coefficient will decrease the effective figure-of-merit.

3.7 Conclusion

A new technique based on open and short circuit provides an alternative for the direct measurement of the thermoelectric figure-of-merit. The technique offers measurement under a large temperature difference which indicates that ZT obtained using this technique provides a realistic evaluation under real operating conditions. Another unique criterion is that ZT derived from this technique shows a dependency with current flow through the material. By contrast, conventional ZT measurement defined by ${\alpha^2}/{(\rho\lambda)}$, is independent of measuring current. This gives the new technique the capability of measuring the realistic ZT of a segmented or a functionally gradient structure which was difficult using conventional methods. This is because small differences in current or temperature across the segmented sample can significantly affect the ZT value.

CHAPTER 4

"Proof of principle" of the Open-Short Circuit Technique

4.1 Introduction

Previously, Konstantinos [99] has investigated the feasibility of the open-short circuit technique by developing an apparatus to measure a thermoelectric module. He concluded that the ZT of a bismuth telluride thermoelectric module under large temperature difference measurement (ΔT) reduced significantly as compared to conventional measurement at the same mean temperature, a phenomenon that is not to be ascribed to experimental error. Even though Konstantinos did the initial measurement of the module under a large temperature difference, the results were arguable. Simplification adopted by assuming constant heat flux was provided during the measurement could introduce error to the measurement result. Moreover, there is no proof that the measurements are true as no comparison/benchmarking was made with conventional method.

The focus of this chapter is to study the feasibility of the proposed technique which includes measurement of the figure-of-merit obtained from the temperature measurement method and the electrical measurement method. To investigate how accurately ZT measurement was obtained from this apparatus and how well this technique agrees with conventional method. The results were

compared with the expected ZT calculated from thermoelectric properties. If small ΔT is applied to the sample, theoretically, results obtained are comparable with conventional method because thermoelectric properties are observed under a small ΔT. Upon confirming the results with the conventional method, study on the effect of real operating conditions to ZT can be investigated through comparison with a large ΔT measurement determined using the same technique.

4.2 Design and Construction

A thermoelectric module was selected for initial investigation because it was much easier to obtain a short circuit condition due to the larger internal resistance compared to the short circuit wire employed. As for the type of materials, bismuth telluride was the best option due to its high figure-of-merit at room temperature. The higher the figure-of-merit of the thermoelectric material, bigger temperature difference, voltage and current could be observed. Investigation was carried out using the previous apparatus with significant modification to improve measurement reliability. Two major issues needed to be addressed in order to make module measurements successful are discussed below.

As discussed in chapter 3, one important requirement for the new proposed technique was an equal rate of heat flow through the examined module during open and closed circuit conditions. The most crucial factor that

was not considered in previous measurements was to confirm that the heat flow to the module was constant. Technically this could be achieved by maintaining a constant power supply to the heater and minimizing the heat loss from the heater to the environment, so heat loss can be neglected. The usage of a thermoelectric module as a heater in the previous design may introduce more uncertainty into the experiment since the heat flux to the examined module was not solely coming from the electrical power supply but also from the heat absorbed at the cold side, T_c, of the module due to the Peltier effect. Although alternatively heat supplied from the heater module could be calculated from its thermoelectric properties, the fact that these properties were obtained under a small temperature difference introduced inaccuracy by not considering temperature dependency.

To overcome this problem, the thermoelectric module as a heater was replaced with a resistive heater. Heat flow to the module was monitored in two ways, directly and indirectly. In absolute measurement, heat flow can be calculated by directly measuring the electrical power supply to the heater. Even though this method allows the determination of heat flow to be made easier and quicker, the results obtained in this way can introduce significant error as heat loss take place from the other surface (the one that is not attached to the examined module) of the heater. Thus this method is only useful as an initial indicator. In order to monitor if the heat flux was constant or not, a known reference material was sandwiched between the heater and the examined

sample. Heat flow can be calculated from the temperature difference produced between two known points in the reference material with known thermal conductivity by using Fourier's Law;

$$\frac{Q}{A} = \vec{Q} = -\lambda \frac{dT}{dx} \dots\dots (4.1)$$

where Q is the rate of heat flow through the examined module, $\vec{Q}$ is the heat flux, A is the cross sectional area, ${dT}/{dx}$ is the temperature gradient produced between the two known points and λ is the thermal conductivity of the reference material.

Since the heater will be mounted on the reference material, a high thermal conductivity material is needed to minimize heat loss. Copper was chosen due to its high thermal conductivity (λ = 4 W/cmK), thus ensuring that all the supplied heat was transferred equally within the volume of the block almost instantly. The length of the copper designed as the reference material (addressed as the heat flow meter or copper block later) is determined by the quantity of heat flux it is expected to measure. Minimum heat flux was considered in the design because it will set the limit of heat flow meter design capability. Theoretically, to achieve minimum temperature difference of 10 K across the examined module, taking the examined sample's thickness as 0.171 cm and general Bi_2Te_3 thermal conductivity, λ, as 1.5×10^{-2} W/cmK, minimum rate of heat flow required can be calculated using equation (4.1),

$$Q_A = N\left(-\frac{\lambda A}{l}\Delta T\right)$$

$$= 2 \times 127 \times \frac{1.5 \times 10^{-2} \frac{W}{cmK} \times 0.14cm \times 0.14cm}{0.171cm} \times 10K$$

$$= 4.367W \ldots \ldots (4.2)$$

Assuming that the radial heat loss from the copper is negligible, the distance required between two thermocouples at the reference material can be calculated. Based on (i) the thermal conductivity of the copper (i.e., 4 W/cmK), (ii) the cross sectional area of the copper block of 4×4 cm^2 (i.e., the same as cross-sectional of examined module) and (iii) minimum temperature difference allowed which was set at 1 K was higher than the accuracy of the temperature meter, a minimum distance of 14.6 cm was required between thermocouples. The distance of 14.6 cm for the heat flow meter was too long and not practical for implementation. It may also introduce significant heat loss and inaccuracy in measurement.

There were two solutions being considered here. The first option was to change the reference material to one with much lower thermal conductivity such as stainless steel ($\lambda \approx 0.16$ W/cmK), brass ($\lambda \approx 1.09$ W/cmK) [103], or iron ($\lambda \approx 0.804$ W/cmK) [104]. The second option was to reduce the cross sectional area, A, of a reference material. The minimum distances required for stainless steel, brass and iron for minimum heat flux were 0.59 cm, 3.99 cm and 2.95 cm respectively. The minimum distance required for iron is reasonable for fabrication and implies a flow meter that is not too thin as in the case with stainless steel, which will prove to be unsuitable for insertion of thermocouples.

If copper is used, the cross sectional area has to be reduced to 1.5×1 cm^2. Using the same distance achievable for iron, the temperature differences may be calculated as;

$$\Delta T = \frac{Ql}{\lambda A} = \frac{4.367W \times 2.95cm}{4W/cmK \times 1.5cm \times 1cm}$$

$$= 2.26K \ldots\ldots (4.3)$$

The temperature difference achievable for copper with a reduced A was higher than the temperature difference achieved by iron for the same distance, l. This gave the advantage to copper since the bigger the temperature difference, the smaller the error will be. Moreover, radial heat loss will be minimized due to smaller surface area from which heat can escape.

Another important consideration that needed to be looked into was the minimum detectable changes in heat flux for which the heat flow meter was designed. According to Fourier's law, 10% changes in heat flux will induce 10% changes in temperature difference. By taking the minimum resolution of temperature measurement using an ordinary temperature meter 0.1 K, 10% changes in the heat flux for the above design induced changes of 0.2 K in the temperature difference, which was measureable. The design is capable of measuring changes in heat flux as small as 5%. By using more sophisticated instrumentation for temperature measurement with much smaller resolution, will increase the capability. For example, by using a PicoLog data logger with a resolution of 0.025 ^{o}C, will allow to detect heat flux changes up to 1.2%.

The only problem that arose with this design was the smaller contact surface with the examined module, which will introduce uneven heat distribution. Changing the examined module to a smaller size is not a solution because it will introduce other problems. The reduction in module resistance will make it harder to achieve the short circuit condition. To prevent this, the contact surface of the copper block was designed to have the same size as the examined module but became narrow as shown in Figure 4.1. By maintaining the size of copper block contact equal to the module surface size will ensures heat distributes uniformly over the entire 4×4 cm^2 cross sectional area. Optimization of the design was simulated using Patran software as shown in Figure 4.2. Thermal conductivity of copper, module, box container and wool insulation used in the simulation are 4.01 W/cmK, 0.015 W/cmK, 0.003 W/cmK and 0.0003 W/cmK respectively. Heat provided at hot side of the copper was 20 W while boundary condition of 300 K was defined for all side of the box container.

Optimization in Figure 4.2 helps to design the thickness of the bottom part of the copper block to allow constant heat flow before it enters the sample. The position of the thermocouple's holes can also be identified to prevent positioning them at points of accumulated heat flux. In this setup, constant heat flow can be confirmed by monitoring non changes in temperature differences produced at the heat flow meter during open and short circuit states.

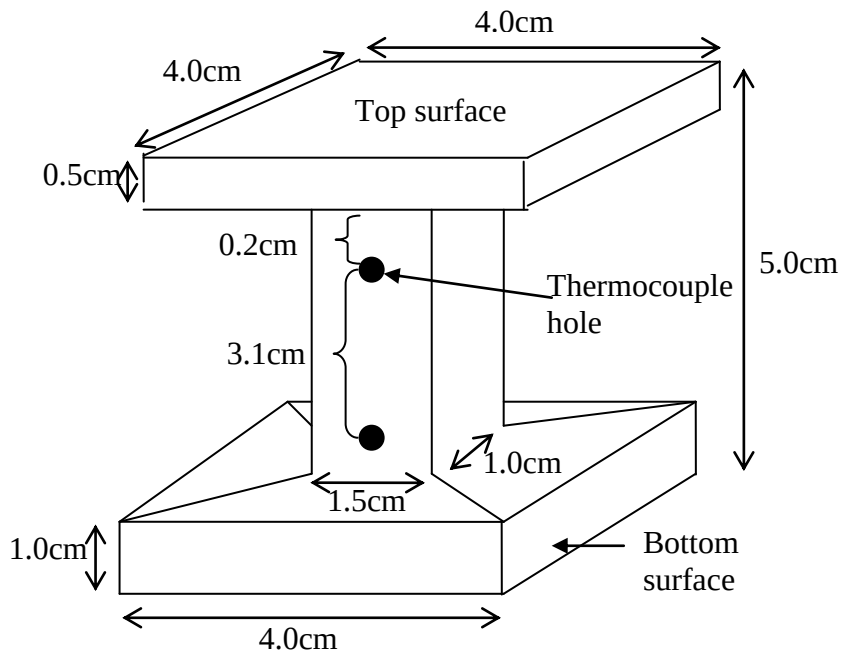

Figure 4.1: Schematic diagram of the heat flow meter.

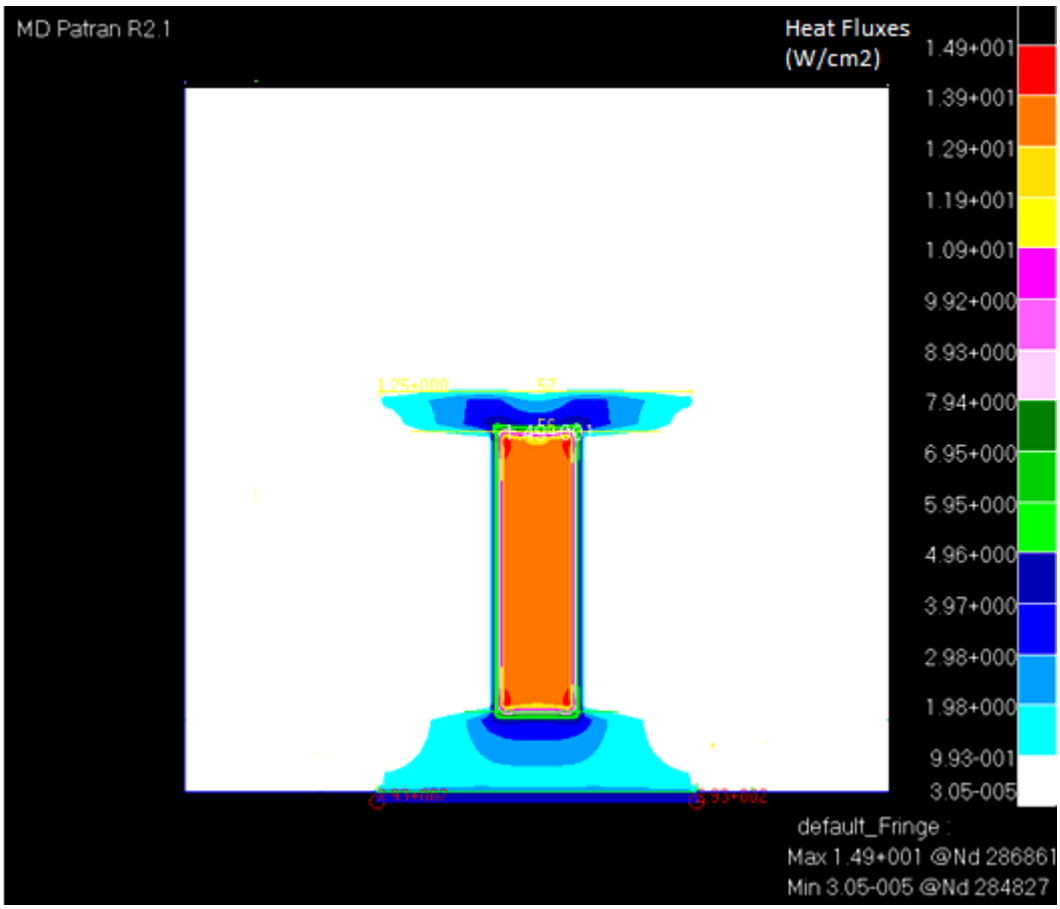

Figure 4.2: Simulation for optimization design of heat flow meter using MD Patran software.

Maintaining a constant heat flow requires minimizing heat loss at the copper block. Since the operating temperature of the thermoelectric module does not exceed 423 K, vacuum is not necessary, which will facilitate rapid measurement due to a non-complex assembly setup without compromising the result. However, to prevent heat loss from the heater and the copper block, they are wrapped with wool insulation ($\lambda \sim 4\times10^{-5}$ W/cmK) inside a box container.

The schematic design of the box container is shown in Figure 4.3. Polyoxymethylene was chosen as the material for the box container because of its low thermal conductivity ($\lambda \sim 0.3$ W/cmK) and machinability. More importantly, its strength, rigidity and toughness made it possible to hold the copper securely. The container is made of 2 pieces of 8.8×7 cm^2 and 2 pieces of 7×7 cm^2 with wall-thickness of 0.9 cm. Holes of diameter 1.5 cm were made on one side of the container to allow the connection wires to the heater and thermocouples to pass through to outside of the container. The top and bottom wall were made of 8.8×8.8 cm^2 with thicknesses of 1 cm and 0.9 cm respectively. A square opening of 4×4 cm^2 was made at the bottom wall of the container to allow the copper block to make contact with the examined module. The opening also acts as a holder for heat flow meter. In the previous design by Konstantinos, the container was much smaller and used wood as the bottom wall. A square of 4×4 cm^2 copper plate was held to the opening at the centre of the wood. The usage of wood was proven to be problematic as wood tends to bend when operated at high temperature, thus resulting in a loose opening to the copper

plate. A loose copper plate makes assembly more difficult and this effect is even more significant when this copper plate is used as a thermocouple mounting. Any movement will affect the position of thermocouple, thus giving an unreliable temperature reading.

Even though polyoxymethylene has low thermal conductivity, lateral heat loss by conduction at the holder cannot be neglected as temperature at the copper block increases. Because of direct contact with the copper block at the opening, the size of contact holder should be minimized to minimize heat loss yet be strong enough to hold the weight of copper. Four small holder legs of size 0.8×0.8 cm^2 were made at the centre of each side with half of the bottom thickness, as shown in Figure 4.4. The wall was assembled with screws made of the same material. The inner container had the dimensions of $7\times7\times7$ cm^3, enough to allow the heat flow meter to be covered with thick layer of wool. The heat sink component design was as before. It was made of a plastic box $8.8\times8.8\times4$ cm^3 with two holes at the side wall to allow water in and out. The top of the box was made out of copper plate. A groove was made on top for thermocouple insertion. The final assembly of the container on the heat sink is shown in Figure 4.5.

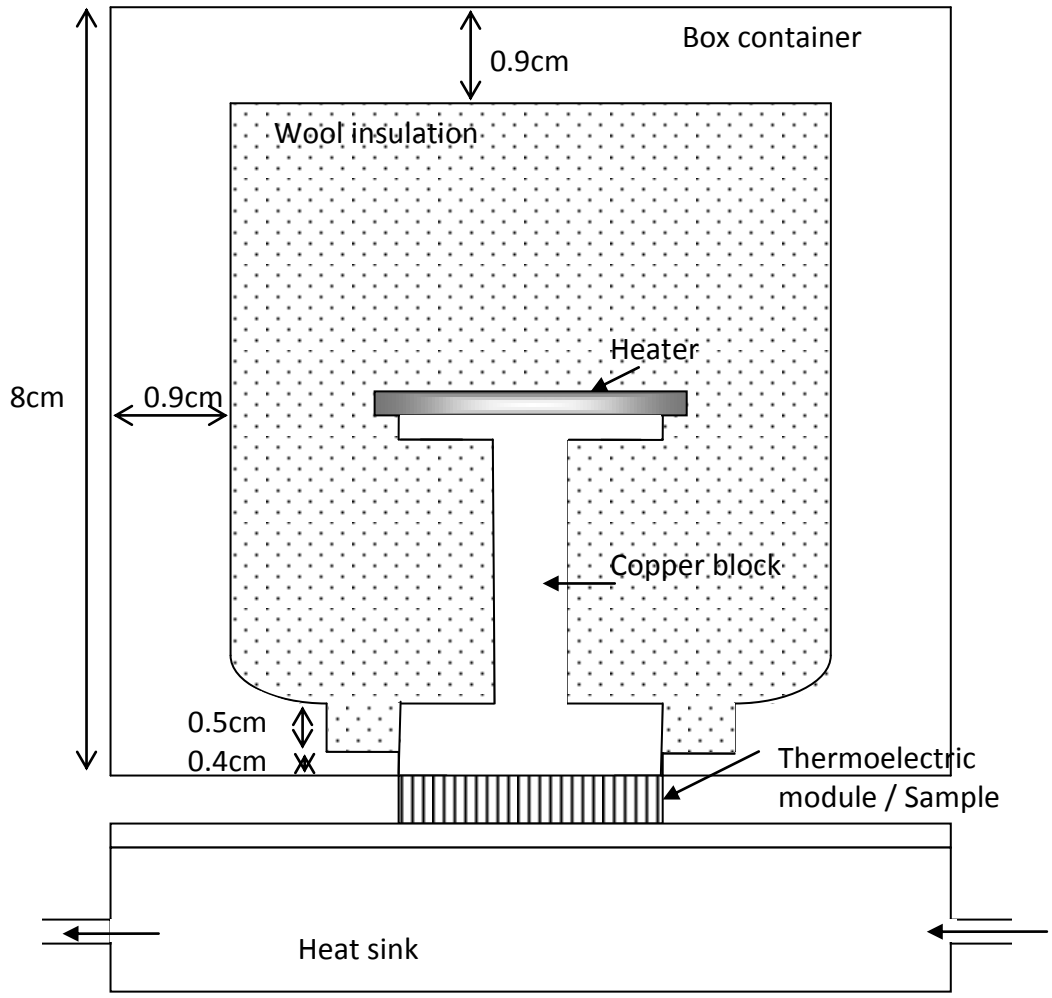

Figure 4.3: Schematic diagram of heat flow meter inside box container mounted on heat sink from side view.

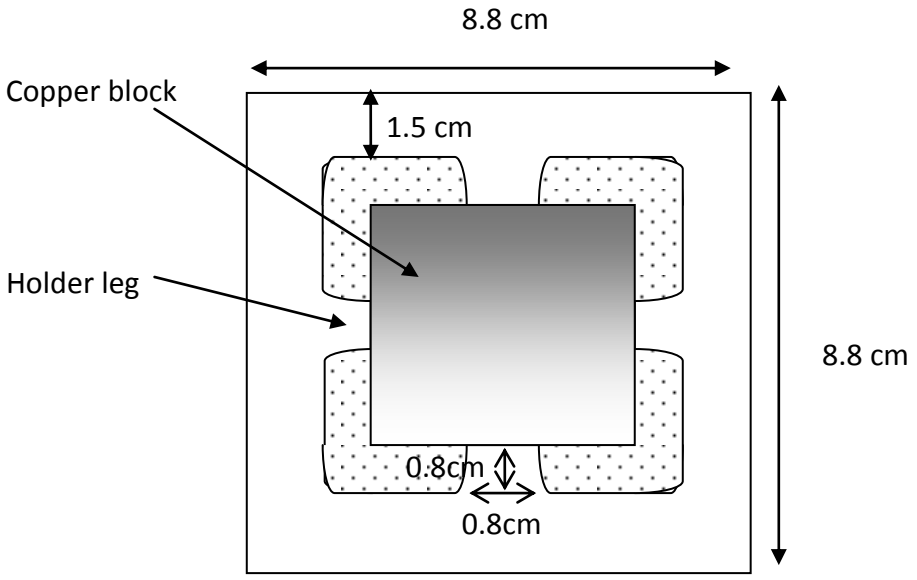

Figure 4.4: Bottom view of box container where copper block makes contact with the examined module.

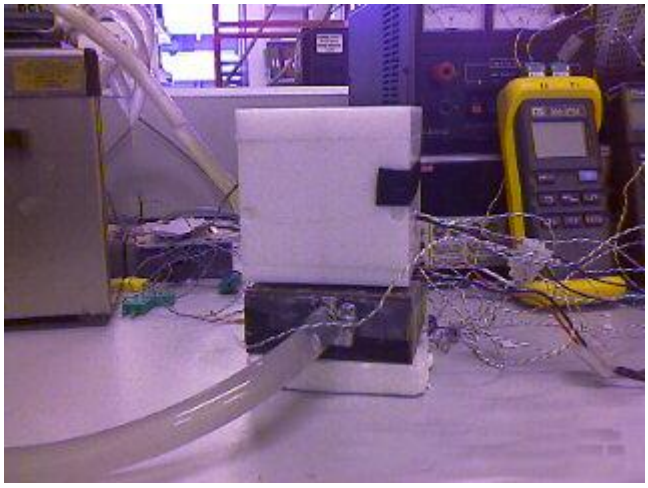

Figure 4.5: Heat flow meter inside box container mounted on top of heat sink. The thermoelectric module to be tested is sandwiched between the heat flow meter and heat sink.

Another issue that needs to be addressed is how to achieve the short circuit condition. This means that the electrical resistance of the external circuitry (i.e. wire, switch) should be negligible compared to the thermoelectric module resistance, R_i. Two types of bismuth telluride thermoelectric module were used. One was from the Nord thermoelectric supplier (Sample A) and another from Thermoelectric.com (Sample B). The size of both modules were 4×4 cm^2, consisting of 127 pairs of thermoelectric legs each with a cross sectional area of 0.14×0.14 cm^2. The resistance of each examined module, R_i, can be estimated from the knowledge of the thickness and cross sectional area of the legs. The thickness of the legs was measured using a travelling microscope, which excluded the thickness of the ceramic and electrodes at both sides. The cross sectional area of each leg can also be obtained from the manufacturer's specifications. The measured thickness of sample A and sample B were 0.171 cm and 0.115 cm respectively. By taking the electrical resistivity, ρ, of Bi_2Te_3 at room temperature as $1\times10^{-3}\,\Omega$cm, the resistances of the examined module were estimated as follows,

$$R_A = N\frac{\rho l}{A} = 2 \times 127 \times \frac{1 \times 10^{-3}\Omega cm \times 0.171cm}{0.14cm \times 0.14cm} = 2.22\Omega \ldots\ldots (4.4)$$

$$R_B = N\frac{\rho l}{A} = 2 \times 127 \times \frac{1 \times 10^{-3}\Omega cm \times 0.115cm}{0.14cm \times 0.14cm} = 1.49\Omega \ldots\ldots (4.5)$$

where R_A and R_B are module A and B resistance at room temperature, N is the number of thermocouple legs, ρ is Bi_2Te_3 electrical resistivity, l and A are

thickness and the cross sectional area of the legs respectively. To achieve low external resistance, a toggle switch with resistance R_{sw} ~ 10 mΩ was used while short and thick copper wire used as wire connections. Measurement showed that the total external resistance R_T was $\sim 15\,\mathrm{m}\Omega$ which was ~100 times smaller than the resistance of the modules.

Before proceeding with ZT measurement, it was important to have an estimate of the ZT value expected from the module measurement. The figure-of-merit of the sample can be estimated using the cooling method by measuring $\Delta T_{\max}$ and T_c of the module by use of the formula below,

$$\Delta T_{max} = \frac{1}{2} Z T_c^2 \quad \ldots\ldots (4.6)$$

where $\Delta T_{\max}$ is the maximum temperature difference across the module and T_c is the cold side temperature. To achieve this, sample A was mounted on the heat sink using heat compound with one thermocouple located between module and heat sink and another thermocouple mounted on another module surface. The exposed module was then covered by thick wool insulation to provide a condition of zero heat load. The module was then connected in series with a DC power supply as illustrated in Figure 4.6. Temperature differences produced for a given current were recorded. The process was repeated by increasing the current value until the maximum temperature difference was observed and the results were plotted as shown in Figure 4.7. Sample A shows a maximum temperature

difference of 64.3 K at I = 6.3 A (as shown in Table 1) when T_c = 230.4 K and T_{mean} = 262.5 K.

Table 1: Temperature difference changes with changes in current flow across Sample A.

Current, I (A)	ΔT (K)	T_H (K)	T_C(K)
2.0	39.7	289.5	260.6
3.0	50.2	290.3	240.1
3.5	54.1	290.6	236.5
4.0	57.2	291.1	233.9
4.5	59.9	291.7	231.9
5.0	61.8	292.3	230.5
5.5	63.2	293.0	229.8
5.6	63.4	293.3	229.9
5.7	63.6	293.4	229.9
5.8	63.8	293.6	229.8
5.9	63.9	293.8	229.9
6.0	64.0	294.0	230.0
6.1	64.1	294.2	230.1
6.2	64.2	294.4	230.2
6.3	64.3	294.6	230.4
6.4	64.1	294.7	230.6
6.5	64.1	294.9	230.8
6.6	64.1	295.1	231.0
6.7	64.1	295.3	231.3
6.8	64.0	295.6	231.7
6.9	63.7	295.9	232.2
7.0	63.6	295.8	232.2
8.0	60.5	298.4	237.9
9.0	45.0	302.7	257.5

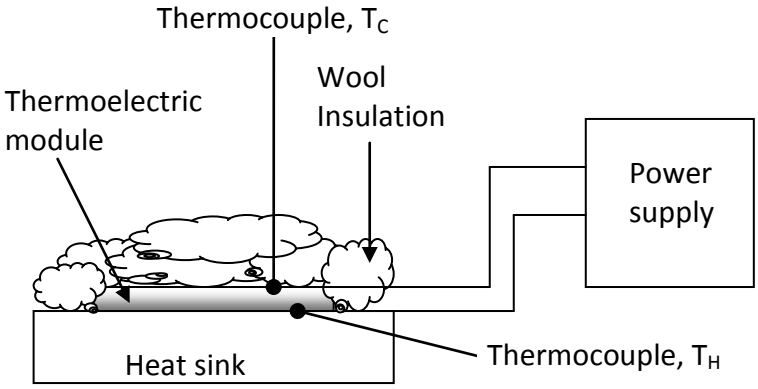

Figure 4.6: Schematic diagram of ΔT_{max} module measurement.

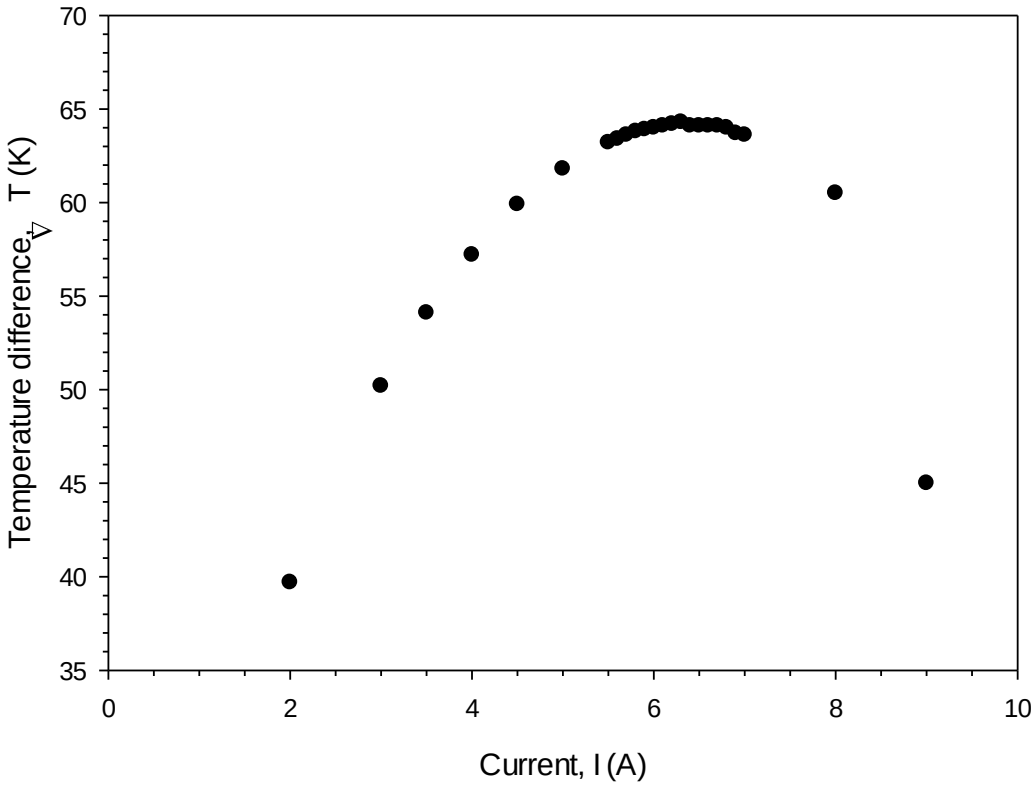

Figure 4.7: Changes in temperature difference ΔT with current I.

Z for Sample A can be estimated using equation 4.6,

$$Z = \frac{\Delta T_{max} \times 2}{T_c^2}$$

$$= \frac{64.3K \times 2}{(230.4K)^2} = 2.42 \times 10^{-3} K^{-1} \ldots\ldots (4.7)$$

The Z value observed was comparable with data obtained from the manufacturer where $\Delta T_{\max}$ = 71 K at T_h = 298 K, which gave calculated $Z = 2.76 \times 10^{-3} K^{-1}$ at T_{mean} = 262.5 K. The percentage of error between Z experimental value and the manufacturer's data value for Sample A was 12.3%. Considering factors that could cause this discrepancy include zero heat loads were not successfully achieved using wool insulation and the fact that the experiment was not done in an inert atmosphere increased the possibility of heat absorption from the surroundings. Besides that, additional thermal resistance was neglected during temperature difference measurement, where thermal resistance from ceramic and electrode connection at both sides were included. In addition, the degradation of the module performance due to operational factors might also contribute to the discrepancy since the module measured was not brand new. Despite this, it provides useful information as an initial reference for the expected figure-of-merit of module measurement.

4.3 Experimental Set-up & Procedure

The module under evaluation was sandwiched between a copper block and a heat sink. The heat flow was provided by an 80 watt, 5×5 cm^2 flat plat mica heater mounted on the top of the copper block. The other side of the copper block was attached to the hot side, T_h, of the thermoelectric module. The constant heat flow was monitored by two K-type thermocouples (T_1, T_2) inserted at the centre of the copper block with half the depth of the copper. The thermocouples were separated by a distance of 3.1 cm each. Heater and copper block were enclosed inside the 8.8×8.8×8 cm^3 box container filled with thick layer of insulating wools. The cold side, T_c, of the module was mounted on the copper heat sink where heat dissipated is removed by flowing water from a circulator. Once assembled, the entire gap between plastic container and heat sink was covered with wool insulation to prevent further heat loss from the side of the module. The assembled apparatus was connected in series with the switch and in parallel with the voltmeter.

The same type of thermocouple was used to monitor temperature differences between modules, attached underneath the copper block to measure T_h and on top of the copper plate to measure T_c. To get an accurate measurement, temperatures were measured at the centre instead at the corner or side of the module. Both thermocouples lay inside the copper groove to prevent uneven pressure due to the thickness of thermocouple at module

surfaces. The thermocouple was then connected to a PicoLog data logger that automatically recorded temperature measurement into a computer. Heat compound was applied on both sides of thermoelectric module surfaces, heater surface and inside the thermocouple holes to fill any remaining air gaps and ensure adequate thermal contact. Before measurement was made, the reliability of all four thermocouples were checked and calibrated. To make sure module and copper were in good contact, pressure was applied on top of the container after assembly. The examined module mounted on the heat sink was then connected in series to a low-resistance switch. The voltmeter was connected in parallel to the switch. Schematic diagram of experimental arrangement for module measurement is shown in Figures 4.8.

To start the measurement, water cooling from circulator to heat sink was switched on. For small ΔT measurement, cold end temperature, T_c, was set at ~286 K. The switch was set to open circuit and the voltmeter was switched on. Then the power supply was turned on, starting with modest power ~5-6 W to give a temperature difference across the module around 10 to 15 K. Temperature at the cold side, T_c, and the hot side, T_h, of the module was recorded to a computer using the data logger. Temperatures at the heat flow meter, T_1 and T_2 were simultaneously recorded where T_1 is temperature near the heater and T_2 is temperature near the module surface.

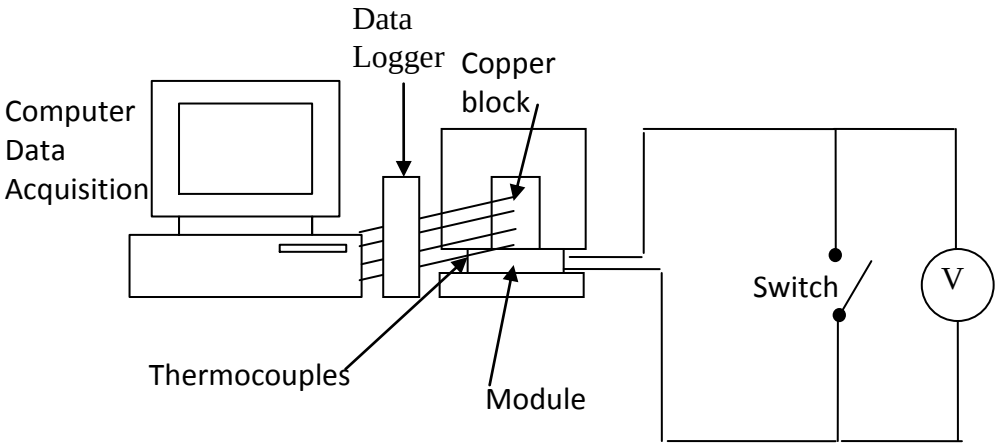

Figure 4.8: Schematic diagram of apparatus arrangement in ZT module measurement.

The temperature difference across the module, ΔT_m, and temperature difference between the heat flow meter, ΔT_c, were automatically calculated from the temperature observed and a graph was plotted. As the heater started supplying heat to the module, a temperature difference across the module and open circuit voltage began to increase due to the Seebeck effect. Measurement was then left to achieve stabilisation before the module's open circuit voltage, V_o, and heater's voltage and current supply (V_{ho}, I_{ho}) were recorded.

After the temperature was stabilized and while the power supply remain on, the switch was then closed. Instantaneously, voltage and temperature differences started to reduce drastically with time. The rate of temperature and

voltage reduction became slower after about a few minutes and started to stabilized ~30 minutes later. Once the short circuit temperature difference was stabilised, the short circuit voltage across module, V_s, as well as voltage and current supply from heater (V_{hs}, I_{hs}) were recorded. After that, the switch was set to "off" and the temperature of the water circulator was set to increase by 5-11 K for the next measurement. At the same time power supply to the heater was adjusted to give ΔT_s ~10-15 K. The same process was repeated until the temperature of the water circulator reached about ~100°C (this is the temperature of boiling water). As for large ΔT measurements, the same procedure are followed except that T_c is maintained at a fixed temperature around 15-27°C throughout the temperature range. Figure 4.9 shows one of the recorded results for small ΔT measurement.

4.4 Reliability

The reliability of the experimental setup and technique can be confirmed through the repeatability and accuracy assessment. As explained in Chapter 3, there are two ways to determined ZT from this novel technique, first using the temperature measurement method derived as $Z\overline{T} = \frac{\Delta T_o}{\Delta T_s} - 1$, and second using the electrical measurement method derived as $Z\overline{T} = \frac{V_o}{I_s R_i} - 1$.

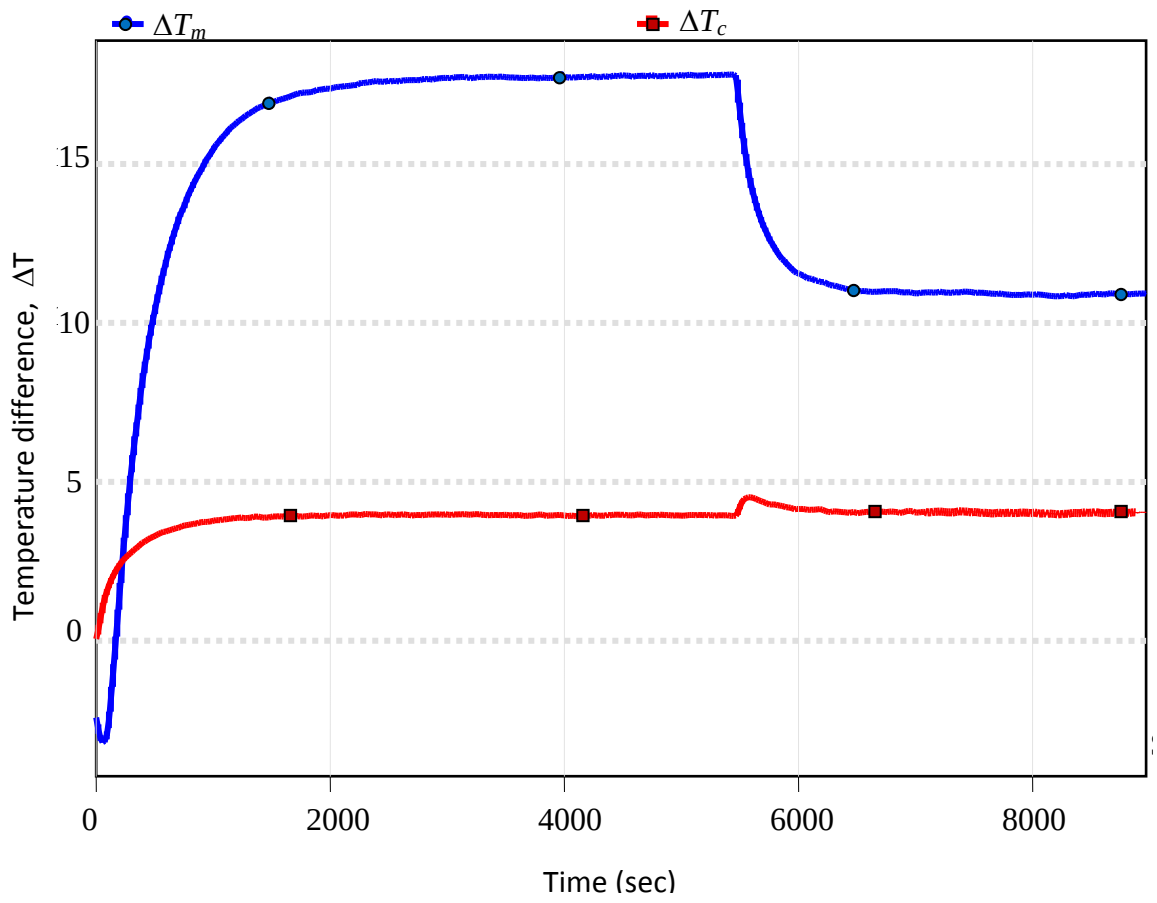

Figure 4.9: Temperature difference across the module ΔT_m and copper block ΔT_c over time recorded using a PicoLog data acquisition system.

In the electrical measurement method, open voltage, V_o , short circuit current, I_s , and resistance of sample, R_i, need to be obtained unlike in the temperature measurement method that only requires temperature difference. V_o and I_s can be directly measured during the experiment while R_i can be determined using equation 3.10. The results are plotted in Figure 4.10.

Measurement results obtained from the temperature measurement method show a clear trend throughout the temperature range compared with the electrical measurement method, where the distribution of ZT is more scattered. Theoretically, the electrical measurement method should give more accuracy due to the high accuracy of voltage and current measurement compared to the temperature measurement method. But in this case, the difficulty of obtaining and determining accurate instantaneous voltage drop, V_{s1} lead to significant error in internal resistance measurement. To prevent complexity, the rest of the thesis will focus on ZT measurement based on the temperature measurement method.

4.4.1 Repeatability

To investigate the maximum deviation and stabilization of the measurements under the same conditions, seven sets of small ΔT measurements (S1, S2, S3, S4, S5, S6 and S7) were conducted on sample A.

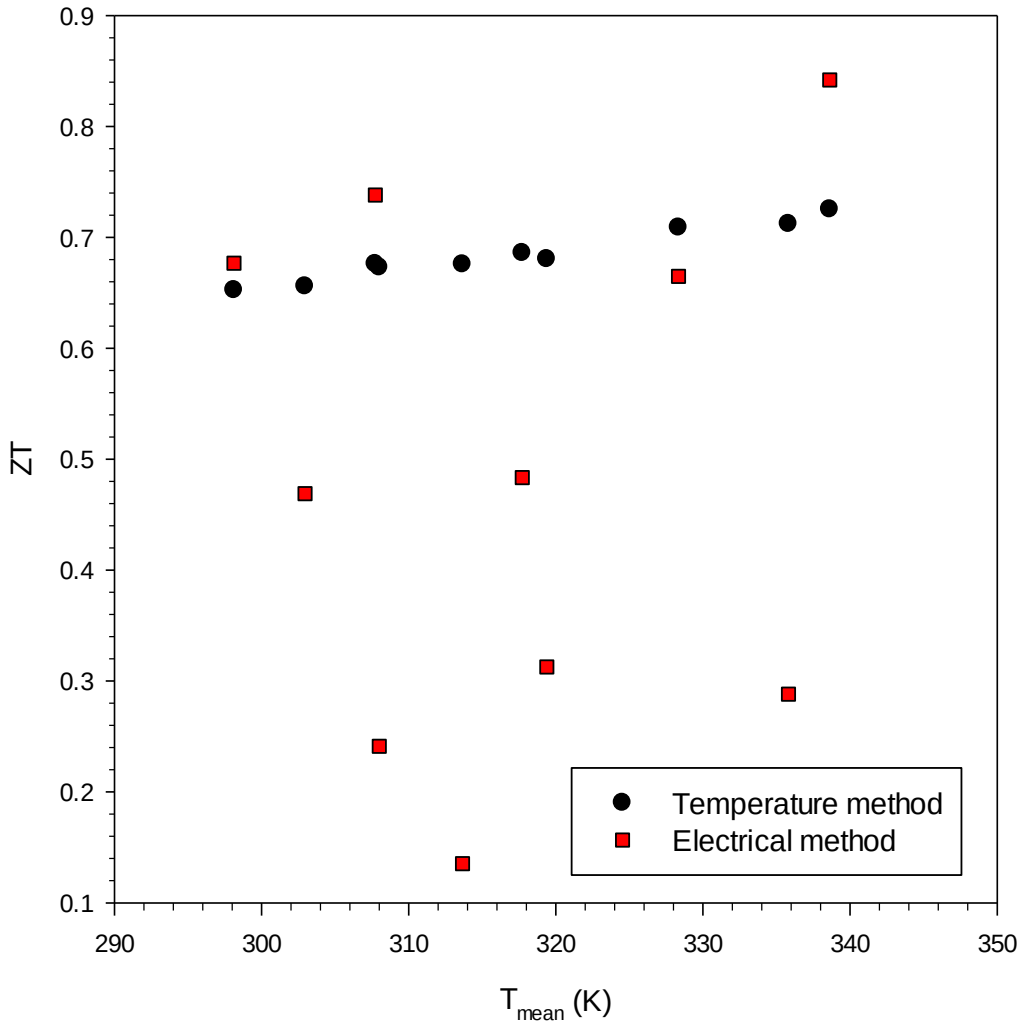

Figure 4.10: Comparison between ZT measurements obtained from temperature measurement method and electrical measurement method across different mean temperature.

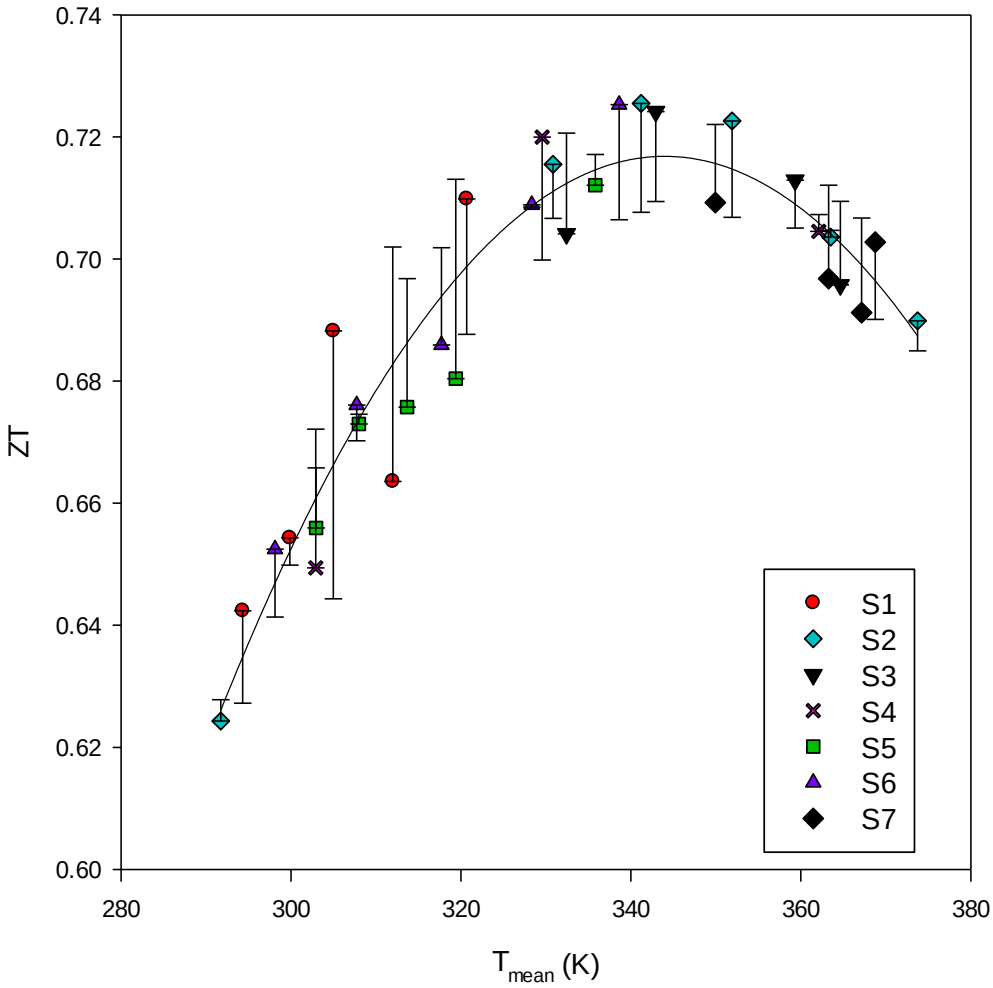

Figure 4.11: ZT of seven sets (S1, S2, S3, S4, S5, S6 and S7) small ΔT measurement on sample A with solid-line showing an average.

All the measurements were set within a temperature difference range of 8-16 K. The results are shown in Figure 4.11. The data presented in the figure has been adjusted to the constant heat flow. The details are discussed in Section 4.5.1. It can be seen that a high degree of repeatability has been achieved with the percentage of error less than 3.3%. For large ΔT, six different sets of (L1, L2, L3, L4, L5 and L6) measurements were taken, with repeatability less than 1.7% as shown in Figure 4.12. Large ΔT is expected to have higher repeatability than small ΔT as higher accuracy can be obtained at larger temperature. Both data for small and large ΔT measurement can be found in Appendix 2 and 3 respectively.

4.4.2 Accuracy

The accuracy of the system here is define as deviation of the measurement using open-short circuit technique as compared with the measurement measured using conventional method. To get an idea of how accurate is the data measured, the ZT result obtained from small ΔT measurement was compared with ZT calculated using data obtained from the manufacturer. The manufacturer material properties for given temperature range of 200 K to 350 K for both p and n-type can be found in Appendix 4. Theoretically the results were comparable because all properties were measured under small temperature differences.

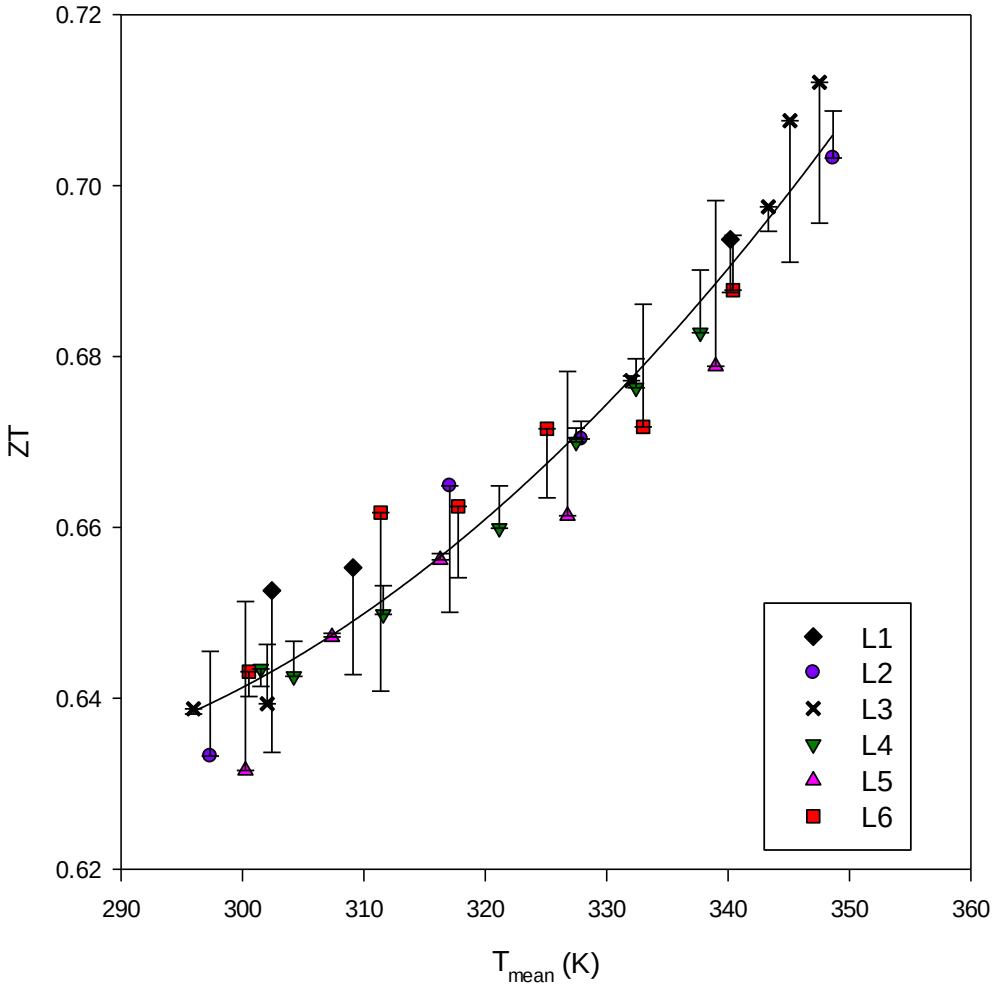

Figure 4.12: ZT of six sets (L1, L2, L3, L4, L5 and L6) large ΔT measurement on sample A with solid-line showing an average.

In general, the ZT of a thermoelectric module can be calculated from individual materials' properties using the formula,

$$ZT = \frac{\left(\alpha_p - \alpha_n\right)^2 T}{\left[\left(\rho_p \lambda_p\right)^{1/2} + \left(\rho_n \lambda_n\right)^{1/2}\right]^2} \ldots\ldots (4.8)$$

where α_n and α_p are the Seebeck coefficient, ρ_n and ρ_p are the electrical resistivity and λ_n and λ_p are the thermal conductivity of n and p-type respectively.

The experimental dimensionless figure-of-merit, ZT, obtained under small ΔT using temperature measurement method was compared with the conventional dimensionless figure-of-merit, ZT_c, calculated from equation (4.8) by plotting both together in Figure 4.13. The figure-of-merit, Z obtained by dividing the dimensionless figure-of-merit, ZT, with the mean temperature, $T = \frac{(T_h + T_c)}{2}$ are also shown in Figure 4.14 with conventional figure-of-merit, Z_c, as a comparison.

It can be seen from Figures 4.13 and 4.14 that the temperature dependence of the experimental results agrees with the calculated results as both ZT_c and ZT increased while Z_c and Z decreased with a mean temperature. However, the experimental results were lower between 22-30% than expected values.

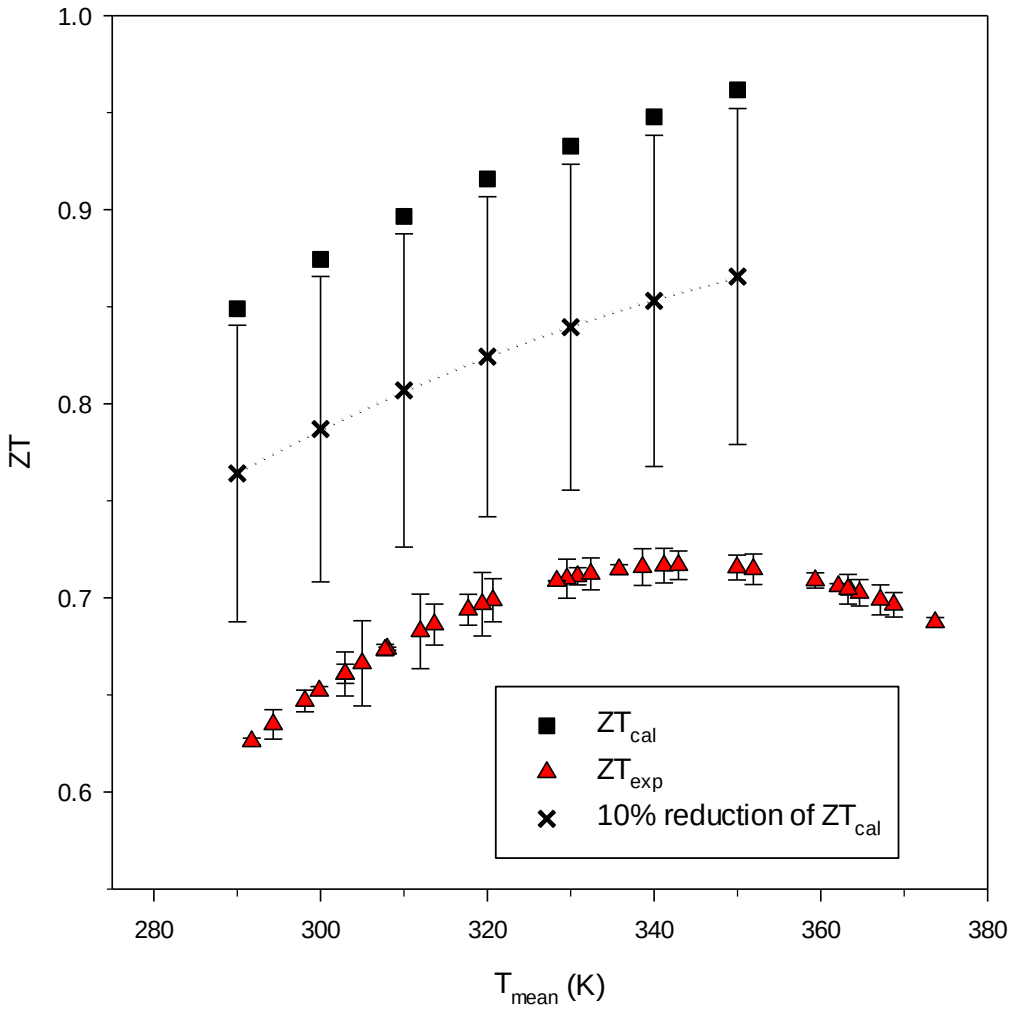

Figure 4.13: Temperature dependence of calculated ZT from manufacturer, (ZT_{cal}), and experimental ZT, (ZT_{exp}), values where ZT_{cal} data is from materials while ZT_{exp} is from module, which includes the influence of electrical and thermal contact. 10% ZT_{cal} shows an estimate of 10% reduction from material to device.

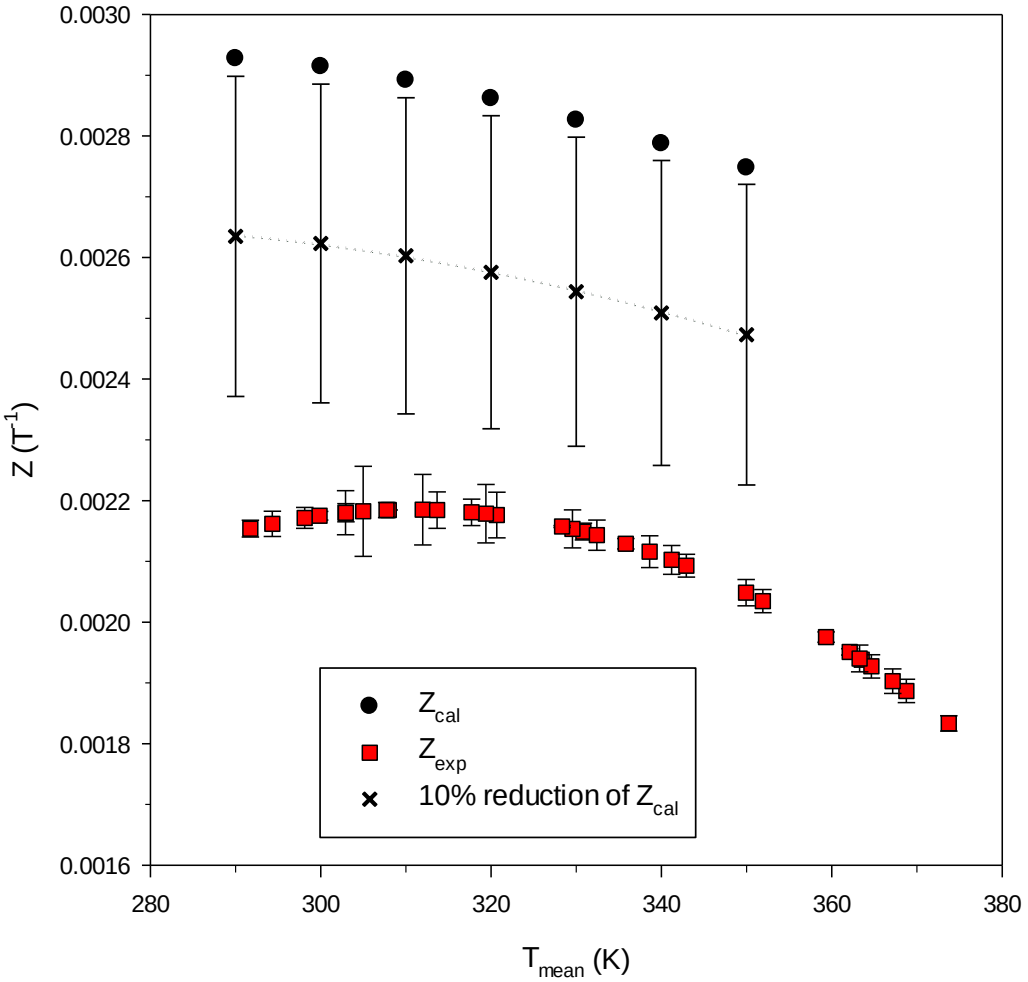

Figure 4.14: Temperature dependence of calculated Z from manufacturer, (Z_{cal}), and experimental Z, (Z_{exp}), values where Z_{cal} data is from materials while Z_{exp} data is from module, which include the influence of electrical and thermal contact. 10% Z_c shows an estimate of 10% reduction from material to device.

Although the percentage of relative error observed are big, the actual error could be much smaller than this due to the fact that ZT_c was calculated using equation (4.8) solely from materials and does not include thermal and electrical contact influences. It was expected that ZT_c would be ~10% lower due the transition from material to device as plotted as a dotted line in the graphs and within 10% error indicate by the error bars [102].

Another factor that contributed to this discrepancy was that the measured samples are not identical even though they are from the same Bi_2Te_3-based materials. If 10% reduction and error are taken into account, a deviation of 11% observed, which is agrees with ZT at room temperature measured using cooling method.

Based on the initial experimental results above, it is clear that the apparatus demonstrates good repeatability of the technique, which is promising evidence of reliability. However, because there is significant difference in the ZT values between the new and the established technique, further investigation was needed to identify the sources of error, as will be discussed below.

4.5 Error Analysis

4.5.1 Constant heat flow

One of the errors in ZT measurement came from non-constant heat flow during the open and short circuit. Previously, Konstantinos assumed a constant heat flow was achieved by maintaining a constant heating power. In this new

design, the heat flow meter was used to monitor the constant heat. Comparison was made between the two methods and no significant changes of heat from the power supply during open and short circuit states was observed, indicating that constant heat flows were achieved during both conditions. However, it was observed that temperature differences at the heat flow meter were slightly higher during the short circuit than that during the open circuit state. This indicates that heat flow through the thermoelectric module during short circuit was higher than that during the open circuit state (see Figure 4.15). An increased heat flow during the short circuit state may be due to less heat loss from the heater and the copper block or may be due to additional heat absorption from hot side of the sample because of the Peltier effect. The differences in heat flow between the two states ranging up to 4.5% over the measurement range. Although heat flow varies, the change cannot be detected by monitoring heater power supply. This might be due to the fluctuation in voltage and current measurement and heat loss at the heater's surfaces. Even though the variation appears to be small, it could lead to significant changes in ZT value.

Figure 4.16 shows heat flow through the copper block as well as heat supply from the heater calculated from the current and voltage measurement. Heat flow from the heater flowing through the copper block was greater than heat flow calculated from the copper block through the thermoelectric module. This indicates that heat loss takes place around the heater before reaching the copper block. The heat loss increased almost linearly as plotted in Figure 4.17.

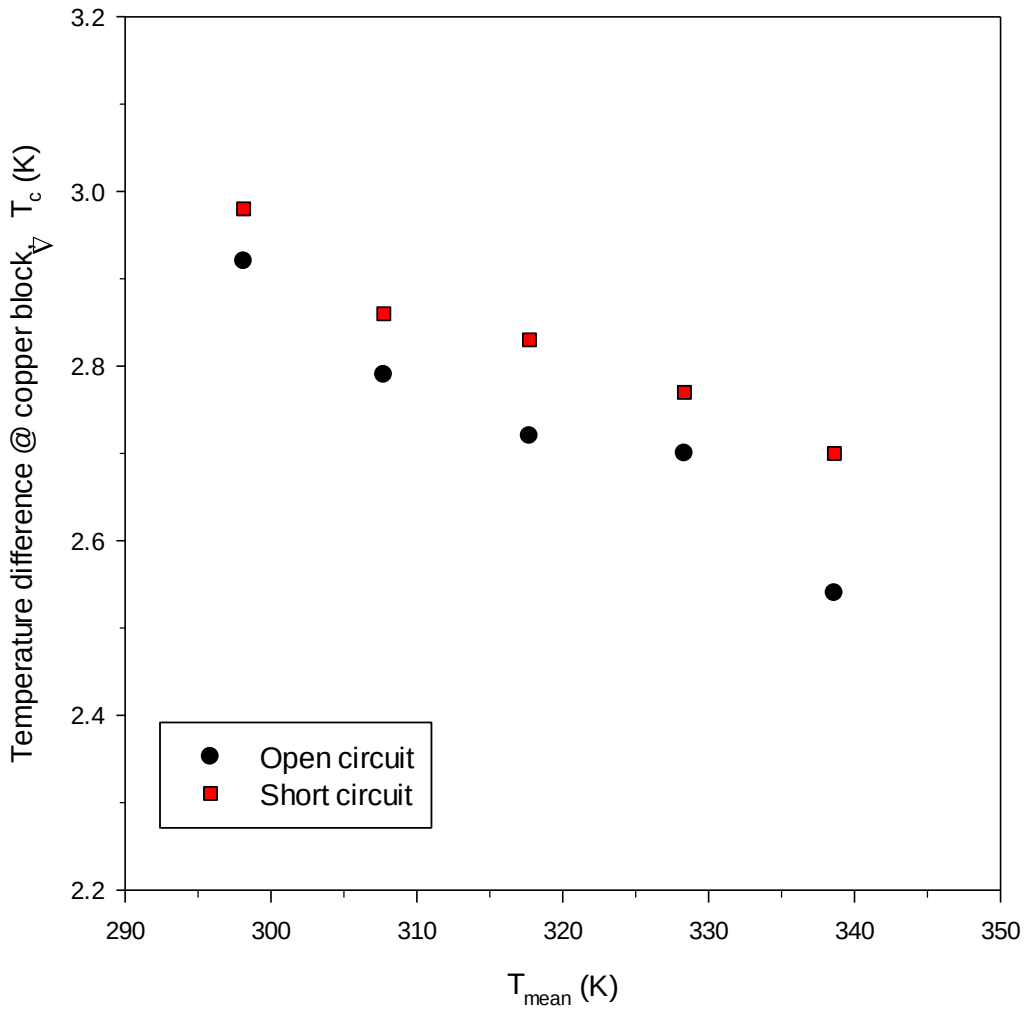

Figure 4.15: Temperature difference during open circuit and short circuit observed from heat flow meter.

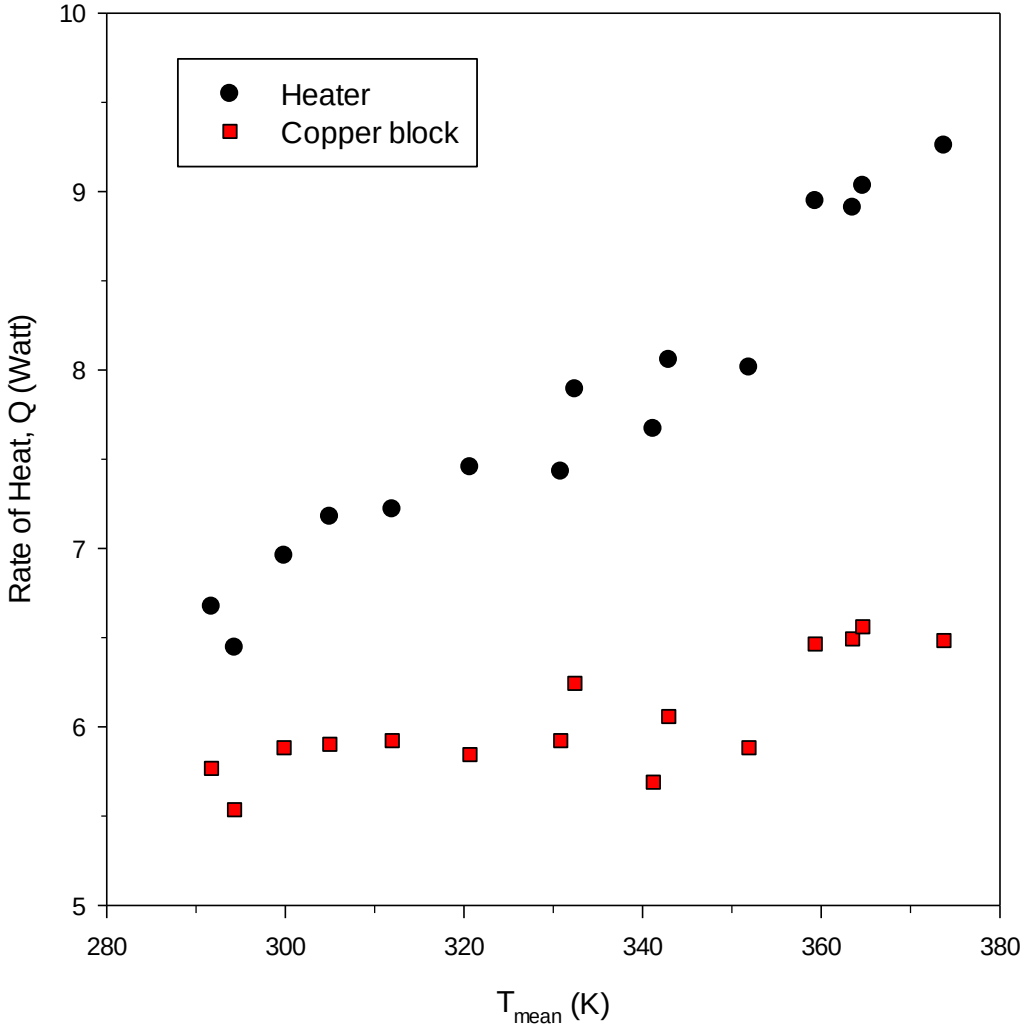

Figure 4.16: Rate of heat flow observed from heat flow meter and heater during open circuit.

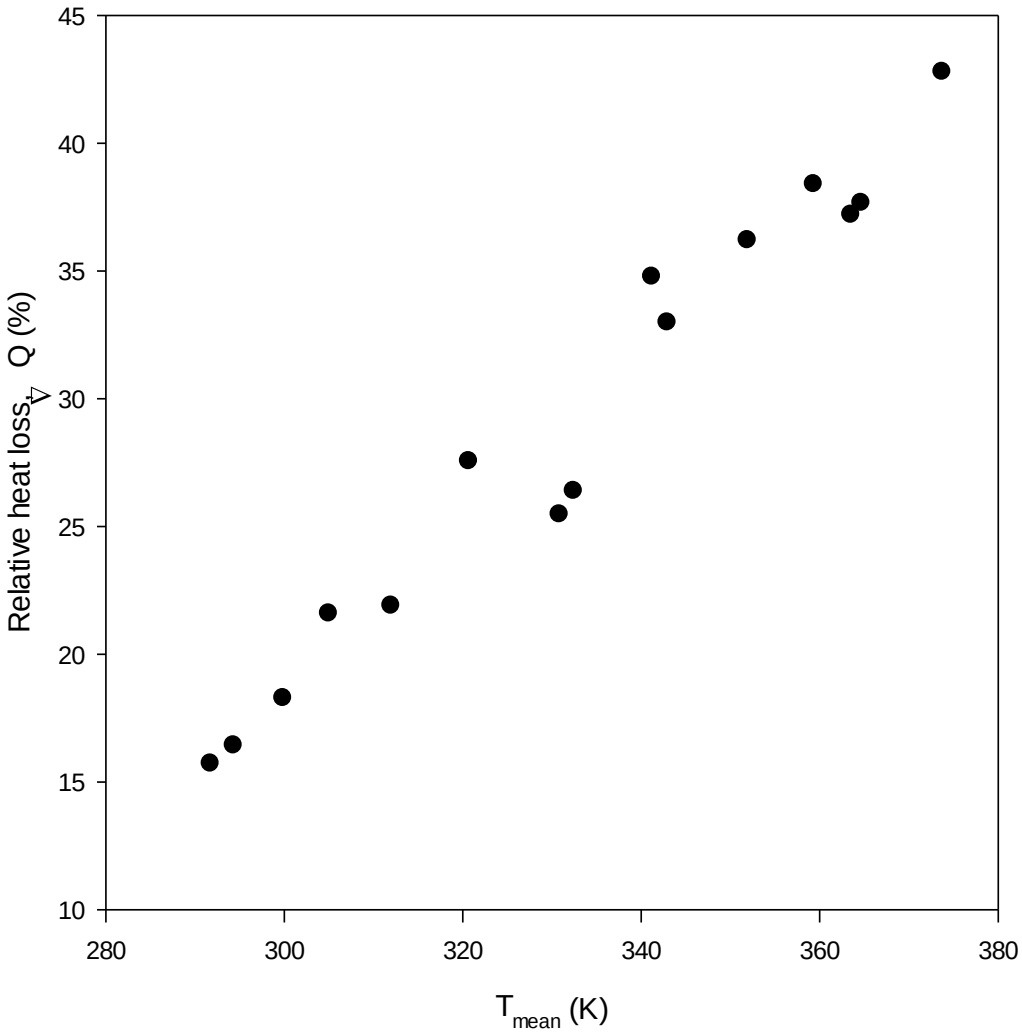

Figure 4.17: Percentage of difference between heat flow from heater power supply and heat flow meter during open circuit.

For lower mean temperatures, the difference is about 15% and it increases up to 54% with increasing mean temperature. Despite an increase in heat loss, in principle it is not a problem as long as the heat flow through the module remains constant during open and short circuit operation.

Heat loss is inevitable and to keep the heat flow constant between two states, a correction factor can be derived using equations (3.2), (3.3) and (3.4) to compensate for differences in heat flow during open and short circuit as shown below,

$$\frac{Q_s}{Q_o} = \frac{\bar{\alpha}T_h I_s - \frac{1}{2}{I_s}^2 R_i + K\Delta T_s}{K\Delta T_o}$$

$$= \frac{\bar{\alpha}T_h}{K\Delta T_o}\left(\frac{\bar{\alpha}\Delta T_s}{R_i}\right) - \frac{\frac{1}{2}R_i}{K\Delta T_o}\left(\frac{\bar{\alpha}^2\Delta T_s^2}{{R_i}^2}\right) + \frac{\Delta T_s}{\Delta T_o}$$

$$= \left(\frac{\bar{\alpha}^2}{KR_i}\right)\frac{T_h\Delta T_s}{\Delta T_o} - \left(\frac{\bar{\alpha}^2}{KR_i}\right)\frac{\frac{1}{2}\Delta T_s^2}{\Delta T_o} + \frac{\Delta T_s}{\Delta T_o}$$

$$= Z\left(\frac{T_h\Delta T_s}{\Delta T_o}\right) - Z\left(\frac{\frac{1}{2}\Delta T_s^2}{\Delta T_o}\right) + \frac{\Delta T_s}{\Delta T_o}$$

$$\left(\frac{Q_s}{Q_o}\right)\left(\frac{\Delta T_o}{\Delta T_s}\right) = ZT_h - \frac{1}{2}Z\Delta T_s + 1$$

$$\left(\frac{Q_s}{Q_o}\right)\left(\frac{\Delta T_o}{\Delta T_s}\right) - 1 = Z\left(\frac{T_h + T_c}{2}\right)$$

$$Z\bar{T} = \left(\frac{Q_s}{Q_o}\right)\left(\frac{\Delta T_o}{\Delta T_s}\right) - 1$$

$$\therefore Z\bar{T} = \left(\frac{\Delta T_{cs}}{\Delta T_{co}}\right)\left(\frac{\Delta T_{mo}}{\Delta T_{ms}}\right) - 1 \qquad \ldots\ldots (4.9)$$

where Q_o and Q_s are heat flow during open and short circuit, ΔT_{co} and ΔT_{cs} are the temperature difference across heat flow meter while ΔT_{mo} and ΔT_{ms} are temperature difference across module during open and short circuit respectively.

The dimensionless figure-of-merit measurement on sample A without the correction factor, ZT_{wo}, and with correction factor, ZT_w, are shown in Figure 4.18. ZT_w clearly shows a trend of slowly increasing until T_{mean} ~350 K before decreasing significantly. The results for ZT_{wo} appear to be more scattered, even though the similar trend was observable. Note that ZT_{wo} values are lower than ZT_w values. The larger the heat flow differences between open and short circuit, the greater the deviation. Hence, it is important to keep a constant heat flow during open and short circuit measurement and accurate detection of heat flux change. Thus only corrected dimensionless figure-of-merit, ZT_w will be plotted throughout the rest of the thesis and will be represented as ZT.

4.5.2 Seebeck Coefficient

The Seebeck coefficient, α, can be calculated from the open circuit voltage, V_o, and the temperature difference, ΔT_{mo}, using

$$\alpha = \frac{V_o}{\Delta T_{mo}} \quad \ldots\ldots\ldots (4.10)$$

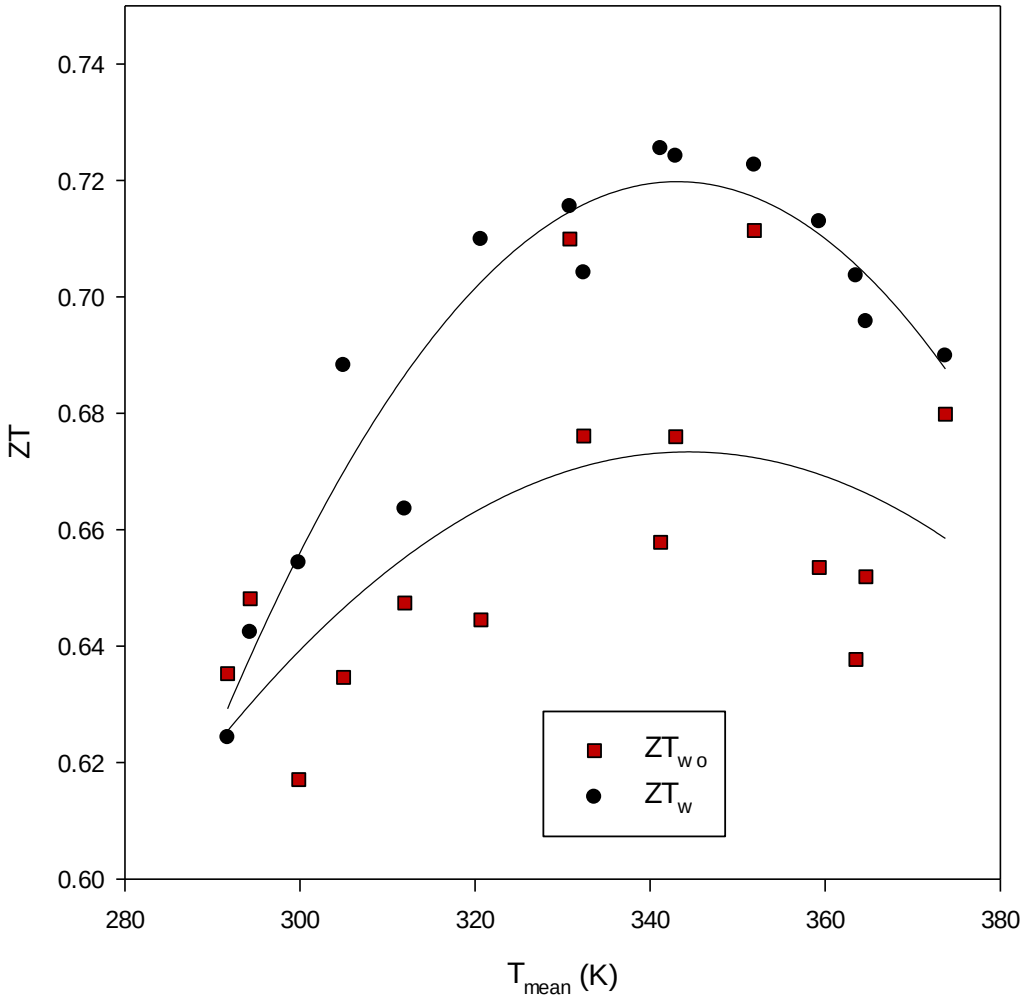

Figure 4.18: Dimensionless figure-of-merit without correction factor ZT_{wo} and with correction factor ZT_w as a function of T_{mean} for sample A.

High repeatability was observed for the Seebeck coefficient measurement with an error of <1%. The Seebeck coefficient obtained from experiment showed high accuracy as well as having a relative error of 4-7% compared with the expected result from the manufacturer's data as plotted in Figure 4.19.

4.5.3 Electrical resistivity

Before the electrical resistivity can be determined, the resistance of the thermoelectric module needs first to be obtained. Resistance could be found using equation 3.3, $R_i = \frac{\overline{\alpha}\Delta T_s}{I_s}$. Figure 4.20 shows the resistance of sample A as a function of mean temperatures for seven sets of measurements. The resistance measurement shows good repeatability with achieved standard deviation of 0.07. Measured resistance at T_{mean} = 304 K was 2.29 Ω which was comparable with the estimated resistance of 2.22 Ω at room temperature as calculated in section 4.2.

Once the resistance of the thermoelectric module is determined, the electrical resistivity of the material can be calculated by,

$$\rho = \frac{1}{N}\left(\frac{R_m A}{l}\right) \ldots\ldots (4.11)$$

where N is the number of thermoelectric pellets and A and l are the cross sectional area and thickness of each pellet respectively. The electrical resistivity, ρ, observed from experiments is shown in Figure 4.21, which agrees well with reference data from the manufacturer with an error <6.3%.

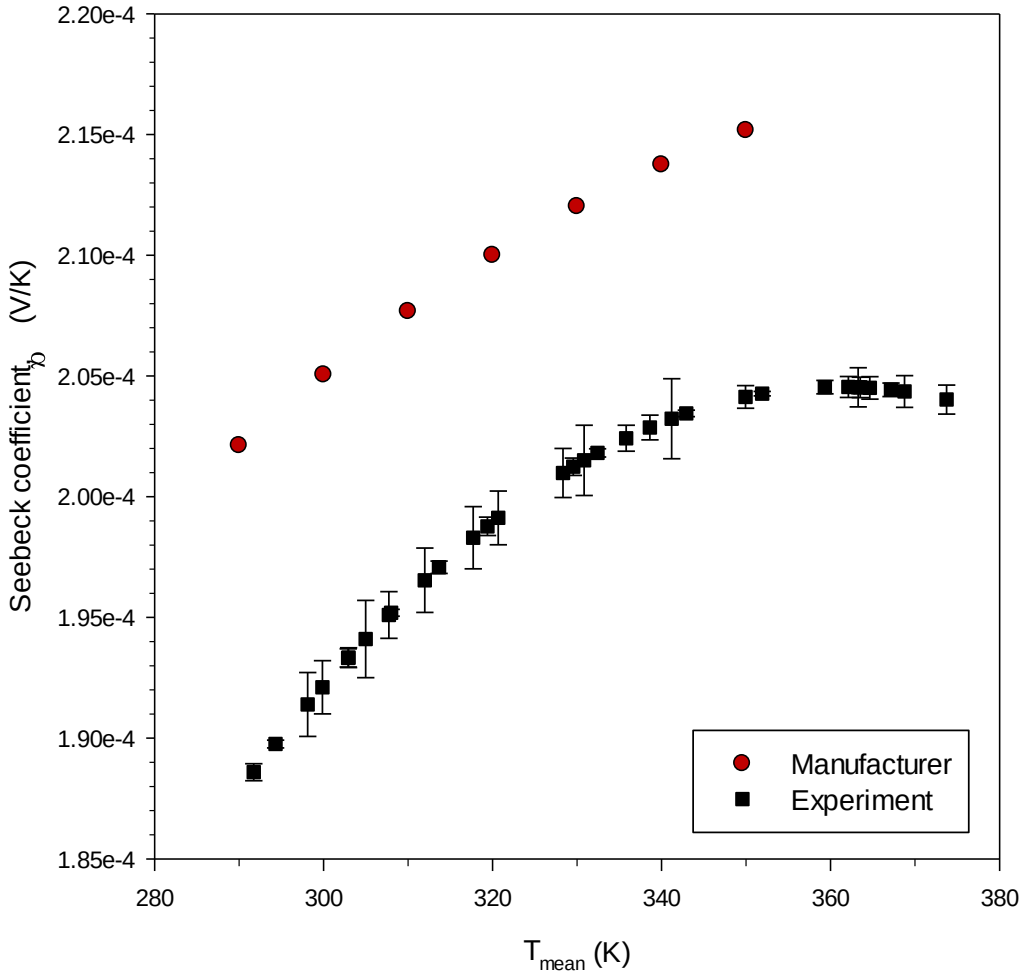

Figure 4.19: An average of Seebeck coefficient (from seven different experiments) from module measurement as a function of T_{mean} as compared with manufacturer data [Appendix 4] as reference material.

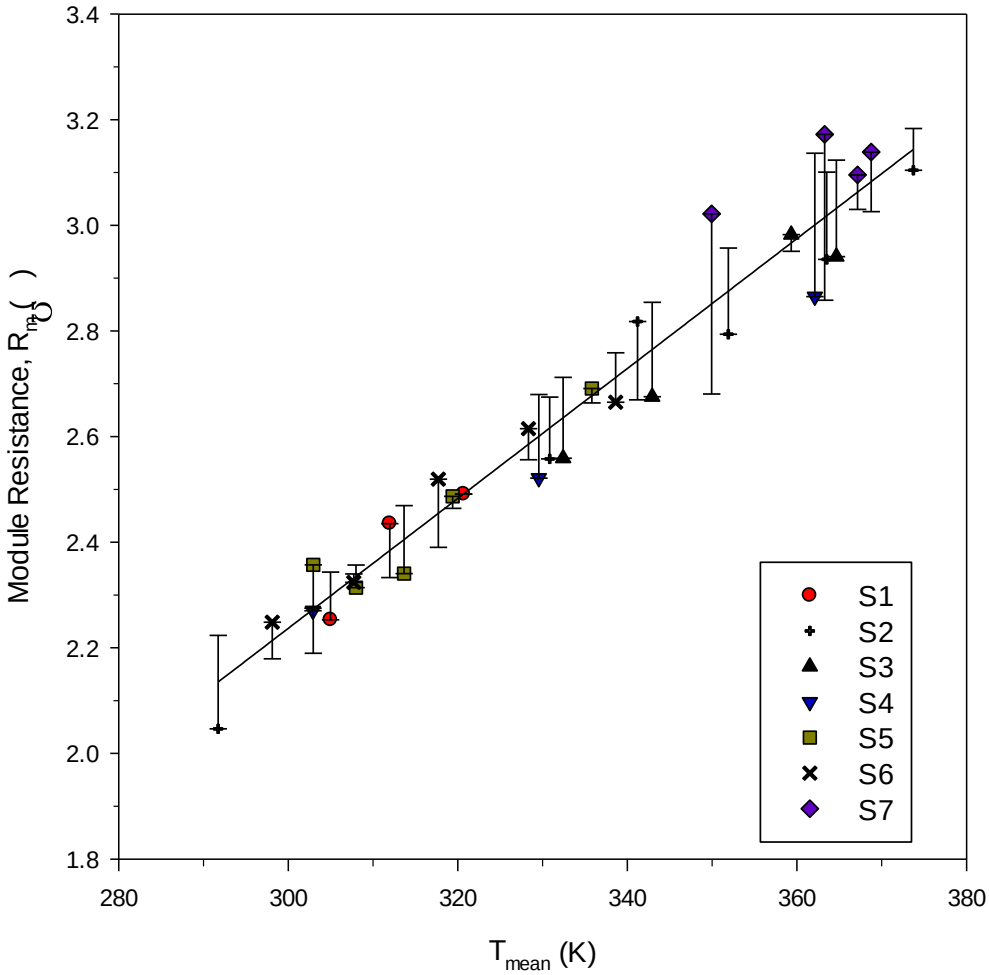

Figure 4.20: Module resistance of seven sets of measurement as a function of T_{mean}.

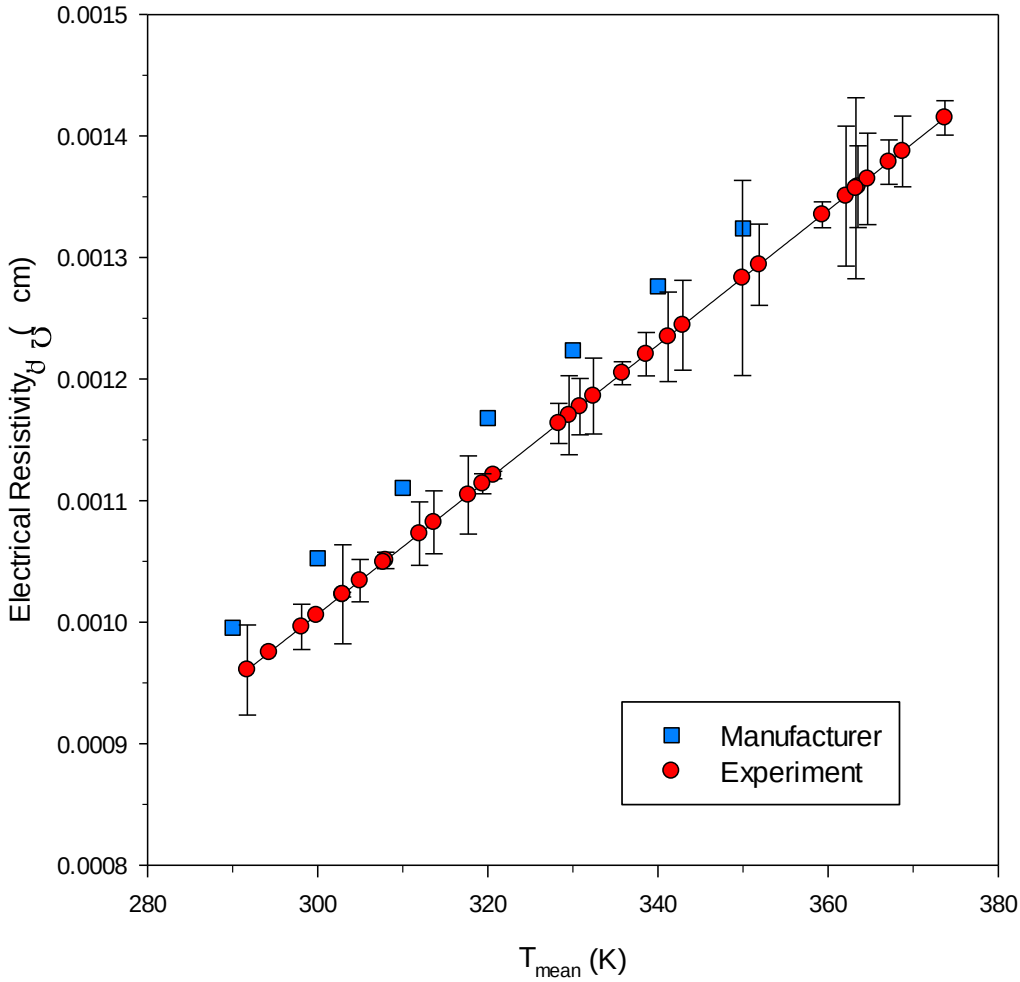

Figure 4.21: An average of electrical resistivity (from seven different experiments) from module measurement as a function of T_{mean} as compared with manufacturer data [Appendix 4] as reference material.

4.5.4 Thermal conductivity

Two possible ways to determine the thermal conductivity of the sample from this experimental set up are by calculation from measured Z, α and ρ or from calculation of heat flow through copper and module. Thermal conductivity can easily be calculated by using obtained values of α, ρ and ZT employing,

$$\lambda_1 = \frac{\alpha^2}{\rho Z} \dots \dots (4.12)$$

Another way to obtain thermal conductivity was by measuring the module's thermal conductance. This can be achieved by knowing the total heat flowing to the sample by observing the temperature difference produced at the heat flow meter during open circuit. Assuming that heat loss from the copper to the examined module was negligible, the module's conductance and hence thermal conductivity of the material can be calculated using equation,

$$K_m = \frac{Q_o}{\Delta T_o} = \frac{K_c \Delta T_{co}}{\Delta T_o} \dots \dots (4.13)$$

$$\frac{\lambda_2 A}{l} = \frac{K_c \Delta T_{co}}{\Delta T_o}$$

$$\lambda_2 = \frac{K_c \Delta T_{co}}{\Delta T_o} \cdot \frac{l}{A} \dots \dots (4.14)$$

where K_m and $K_c = 1.935\ W/K$ are the thermal conductance for the module and the copper respectively, ΔT_{co} and ΔT_o are the temperature difference between the copper block and module during open circuit, Q_o is total heat flow

during open circuit and $l = 0.171\ cm$ and $A = 0.0196\ cm^2$ are length and cross sectional area of the legs of module A.

Thermal conductivity derived from Z, α and ρ measurement is plotted in Figure 4.22 together with the reference data from manufacturer. Experimental results show thermal conductivity produced is higher than expected with deviation of 23-27% from the reference value. Despite the differences, thermal conductivity behaves in similar ways with reference data. The only possible reason for this deviation is due to an overestimation of heat flowing through the sample. This can be confirmed from the measurement of heat flow through the copper flow meter throughout the temperature range. Negligible heat loss obtained at low temperature but worsened as the temperature increased. This meant that more heat was lost during the transition from copper block to examined module and getting worst with an increase in temperature. As a result, an increase in temperature differences was observed at the copper block. Due to significant heat loss at the heat flow meter, the derivation of thermal conductivity from heat flow at open circuit will introduce significant error. Besides that, the assumption of copper thermal conductivity is the same throughout the temperature range might introduce more discrepancy. Because of that, thermal conductivity derived from ZT, α and ρ measurement was used as comparison in Figure 4.22.

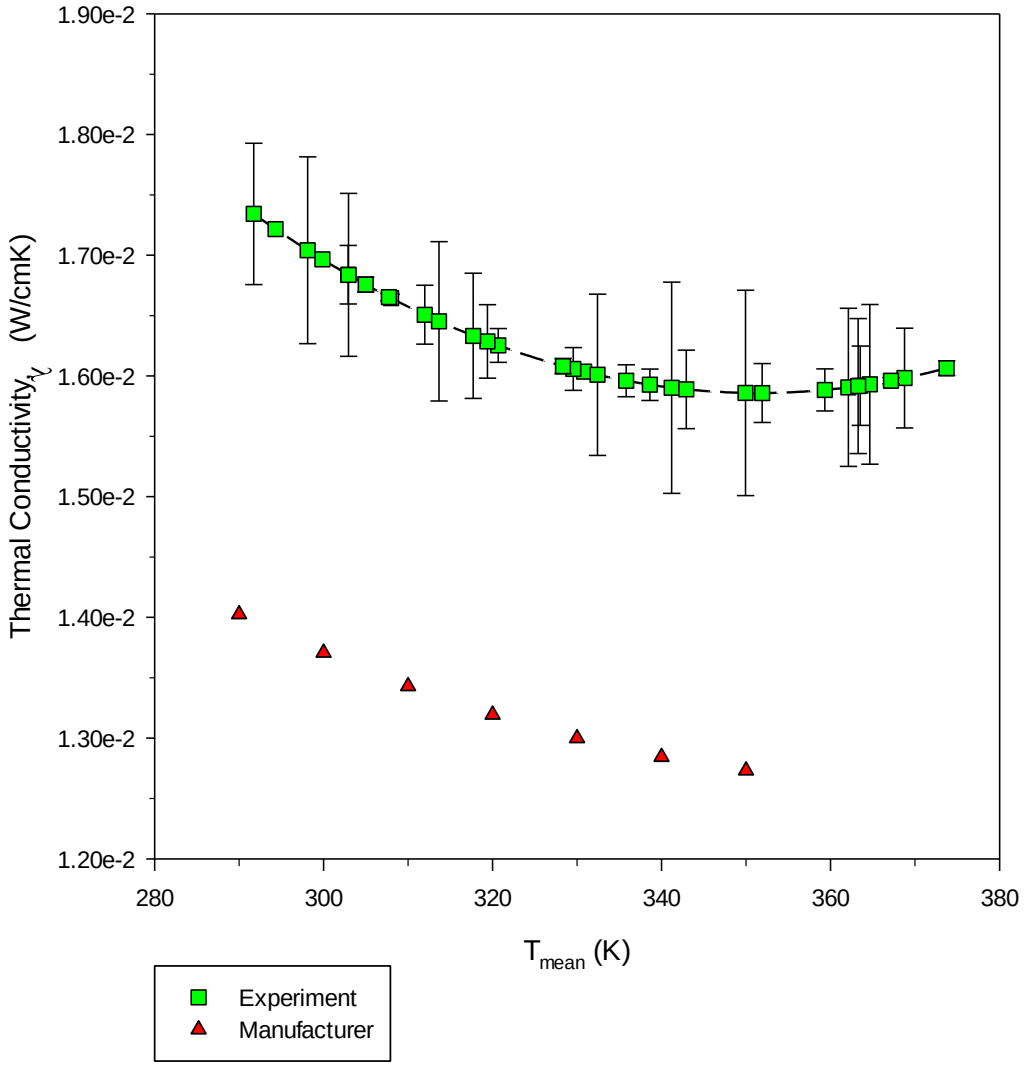

Figure 4.22: An average thermal conductivity λ_1 calculated using measured ZT, α and ρ; and thermal conductivity λ_2 using heat flow meter, together with manufacturer data [Appendix 4] as material reference as a function of T_{mean}.

From all the thermoelectric properties results, it was obvious that the reduction in ZT obtained from experiment as compared to the manufacturer's reference data was most likely due to an overestimate of thermal conductivity. As discussed above, significant error appears to occur in the thermal conductivity. The errors in electrical resistivity and Seebeck coefficient are relatively smaller. This indicates that the accuracy of the ZT measurement can be improved by minimizing the heat loss from the copper block. With careful insulation and proper design of the experimental setup, this technique is capable providing more accurate ZT measurement.

4.6 Conclusion

In conclusion, this study has proved that the temperature method technique is feasible and reliable when measuring thermoelectric ZT. Using a heat flow meter, a constant heat with a deviation of 4.5% is achieved during open and short circuit. Good repeatability is achieved for ZT, α and ρ measurement with an error of <3.3%, <1% and <6.3% respectively under small ΔT and repeatability error are less for large ΔT measurement. The accuracy of ZT measurement shows less than 13% error compared with ZT from the cooling method at room temperature and from materials properties considering 10% reduction and error. Even though the ZT results show a large deviation from the original materials properties of manufacturer's data, a good temperature dependency was observed, which indicates that the main error is due to heat

loss at the copper flow meter. However, since the main objective of this investigation is to prove the feasibility of the novel measurement method, further efforts will not focus on improving the accuracy of measurements of module system but rather to the development of a measurement system which is suitable for the evaluation of single materials. The results from this chapter demonstrate the feasibility and reliability of the proposed technique. In the following chapters, efforts will be made to focus on a more challenging task – the ZT measurement of single materials where the short circuit condition is difficult to achieve. Further improvements are required.

CHAPTER 5

Design and Construction of Large Temperature Difference (L∆T) Facility for Single Thermoelement Measurement

5.1 Introduction

Measurements of the dimensionless figure-of-merit, ZT, using the proposed novel technique have been successfully demonstrated using a thermoelectric module structure as discussed in chapter 4. However, it would be more useful if the technique could also be used to evaluate a single piece of material. The evaluation of thermoelectric material's performance at this level will determine the behaviour of final device development as in module structures. This will not only reduce cost, time and energy of production, but more importantly it is necessary in the process to determine the optimization of an existing thermoelectric composition which requires a lot of tests. Nevertheless, researches on possible new thermoelectric materials have proved to be of great help. Because of this, an approach was taken involving the design and construction of new measuring equipment catering for thermoelements, and investigating the applicability of the novel technique over a large temperature differences. It is worth mentioning that application of this technique at the thermoelement can be fully optimised by neglecting the contribution from the thermal resistance of the ceramic layer which exists in module measurement.

5.2 Design of equipment

A lot of effort has been made to achieve accurate and reliable measuring equipment which is able to measure thermoelement under a large temperature difference. Although the principle technique has been demonstrated using a module, it cannot be directly applied to material measurement. Due to the difficulty of achieving a “short-circuit” condition, the implementation to thermoelement and thermocouples is not as easy and straightforward as in module measurement. As a result, significant modification is needed. The main challenges in this design involve: 1) to overcome non-short circuit condition; 2) to provide constant heat flows into the sample at higher temperature and 3) to design a high temperature apparatus which involves careful selection of the materials used.

The schematic diagram of the developed apparatus is shown in Figure 5.1. The design consists of four important components: heat flow meter, heat sink, sample holder and vacuum chamber, which will be explained in detail below.

5.2.1 Heat flow meter

The heat flow meter is a crucial part of the equipment that is responsible for heat supply to the sample and allows monitoring of constant heat fluxes during the open and closed circuit state. A schematic diagram of heat flow construction is shown in Figure 5.2.

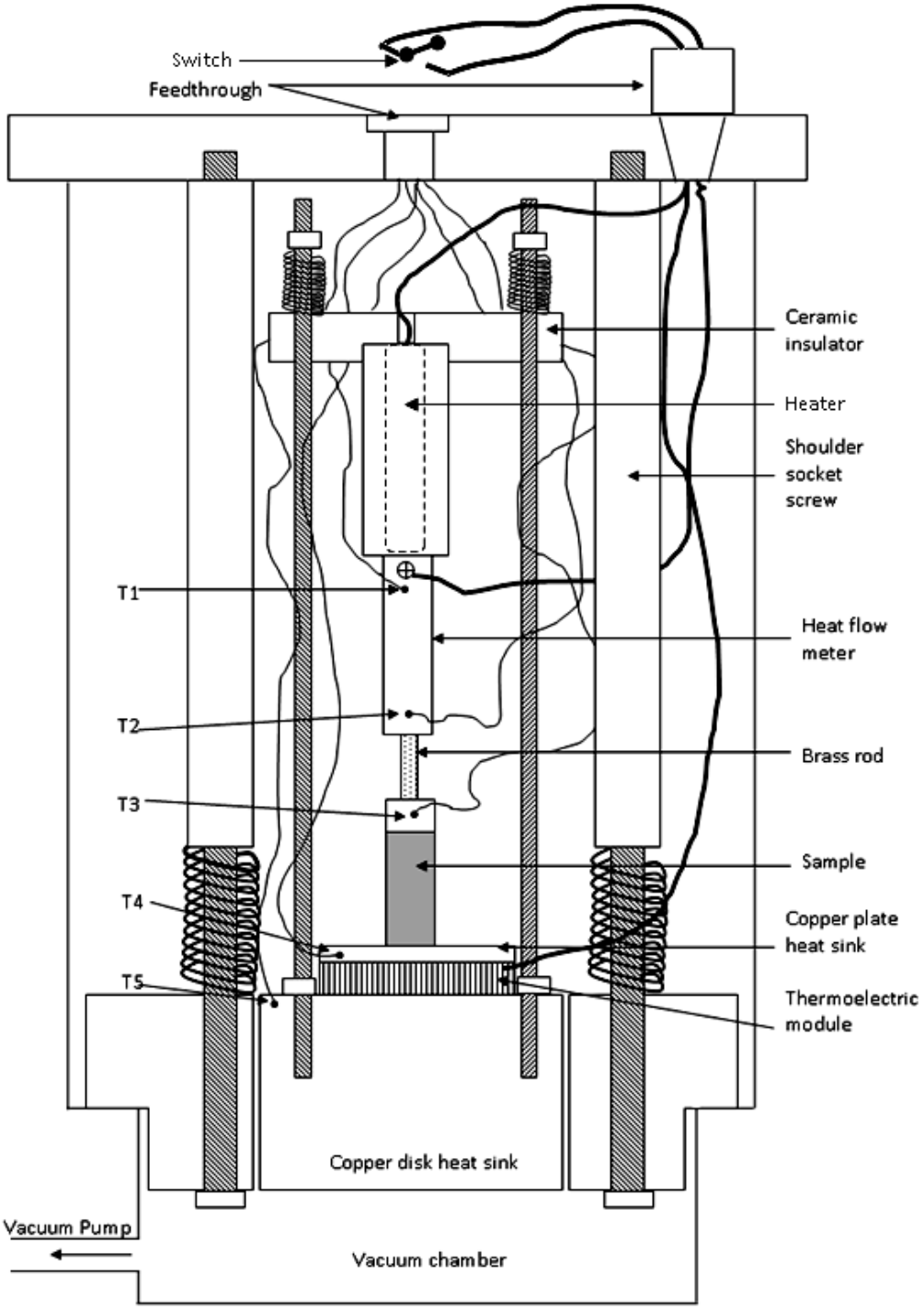

Figure 5.1: Schematic diagram of apparatus for large temperature difference ZT measurement setup inside vacuum chamber.

The flow meter consists of two parts, heater and brass heat regulator. The heater holder is made of copper with dimensions of 8mm×8mm×48mm. Holes with diameter 3.2 mm and 28 mm depth were bored from the top side of the copper heater holder for heater insertion. High powered density cartridge heater (Omega CSS series) with a maximum output of 15 Watt was used. The heater had been tested and was able to withstand operational temperatures up to 500°C in a vacuum environment without deterioration.

The lower part of the copper block was cut to a dimension of 4mm×4mm×18mm (referred to as the heater arm). Screw type wire connection and temperature sensors were located here. Two thermocouple holes separated by a distance of 11 mm were responsible for measuring heater temperature, T1, and the hot side temperature of brass, T2. They are located at 15 mm and 4 mm from the bottom respectively. All the thermocouples holes were 1 mm in diameter and 2 mm in depth. At the end of the heater arm, a hole with a 3 mm depth was bored to allow brass rod insertion.

The brass heat regulator consists of a brass rod and a copper contact. The length and diameter of the rod were 12 mm and 1 mm, respectively. It was tightly inserted into the hole at the end of heater arm to form a good pressure contact. Similarly, the other end of the rod was tightly inserted. The total distance from the end of heater arm to the copper contact was 8 mm as shown in Figure 5.2.

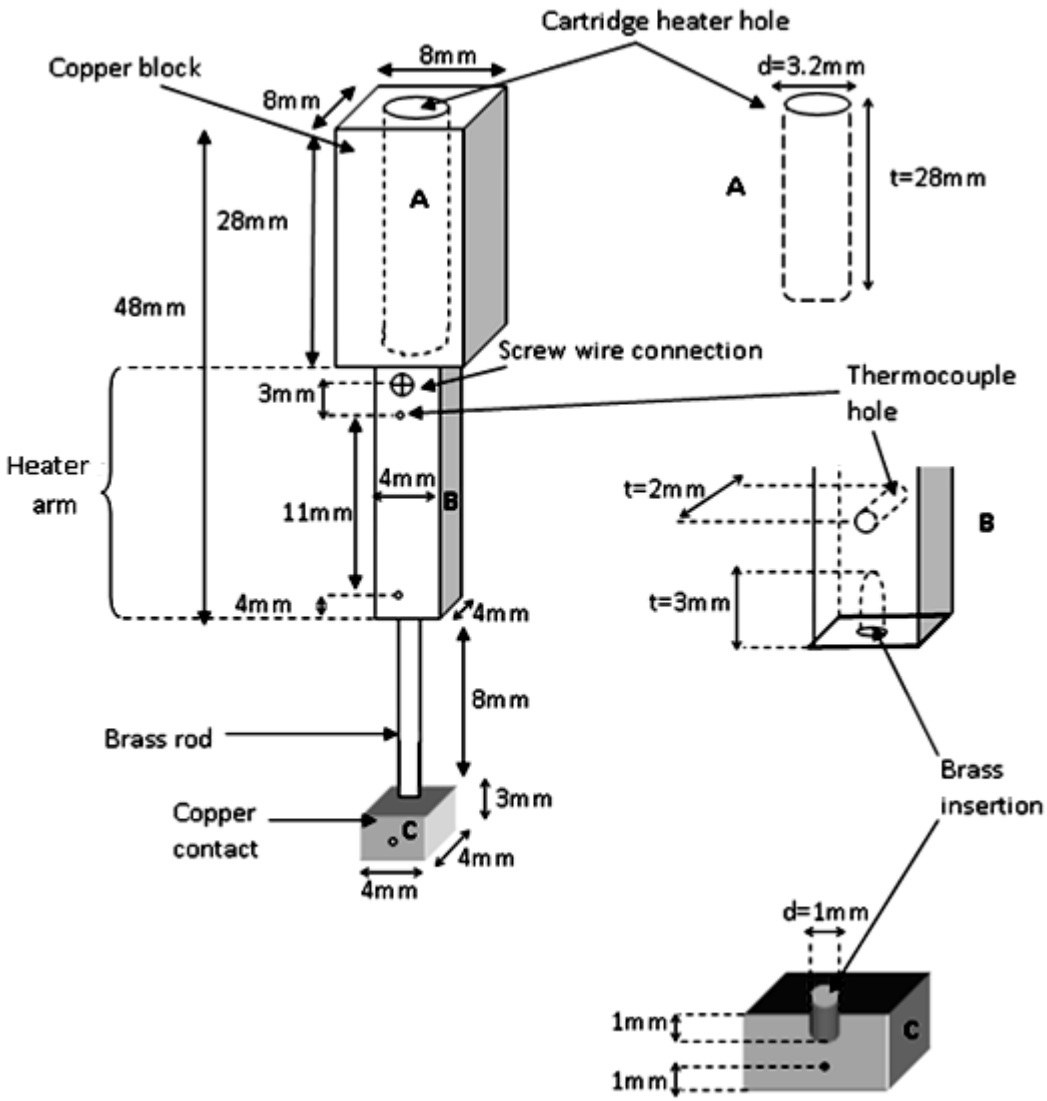

Figure 5.2: Heat flow meter design to provide heat and measure heat flux to the sample.

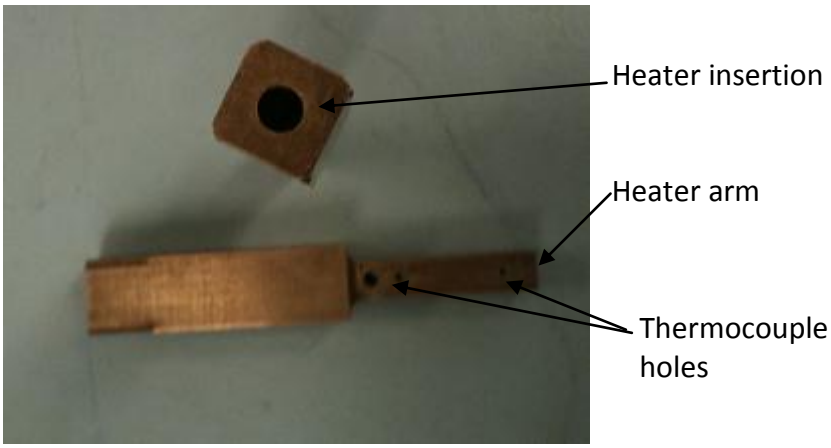

(a)

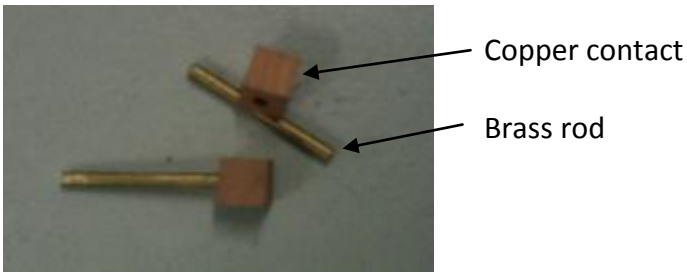

(b)

Figure 5.3: Heat flow meter assembly consists of two components (a) heater and (b) the brass heat regulator.

The brass rod acted as a flow meter responsible for measuring the changes in heat flux into the sample during open and closed circuit by monitoring the temperature difference across it. The copper contact was responsible for distributing the heat evenly to the sample by making the cross sectional area equal to that of the sample. Due to limited space on the brass rod itself, the temperature difference was measured at the heater arm, T2, at the hot side and at the copper contact, T3, at the cold side.

There are three main reasons why the contact between the brass rod with heater arm and copper contact was made using tight insertion instead of permanent contact such as by soldering or brazing because 1) this makes it easier to change the copper contact to other dimensions depending on the contact area of the samples to be measured, 2) this facilitates measurements of a different range of heat flow through the samples by only changing the brass rod with different materials and length and 3) if good contact is still needed between copper and sample, copper contact can easily reproduced without removing the whole structure.

Brass was selected due to its properties of high thermal conductivity and low electrical resistivity (λ= 1.09 W/cmK and $\rho = 0.09 \times 10^{-6}\ \Omega m$) besides having relatively high strength at high temperature. By using a hot probe apparatus, measurement on Seebeck coefficient of the brass rod relative to copper is small (α= 1.0μV/K), thus will not give significant change to the produced Seebeck voltage when measured against thermoelectric samples. According to Fourier's

law, the 8 mm length of the brass rod is capable of detecting heat flux as small as 10.7 mW if the temperature difference can be measured to an accuracy of 1 K.

In the initial design, the heater arm was used as the heat flow meter for heat flux measurements but no significant temperature drop between samples was observed from open to close circuit after several attempts. Significant efforts were made to identify the problem. It was found that due to large heat capacity of the copper heater arm, the temperature drop at the moment of a closed circuit cannot be observed as a result of heat compensation. Consequently, brass rod of a smaller dimension with lower thermal conductivity was used instead.

The copper contact should have the same cross sectional area as that of the samples in order to allow equal heat flux distribution from the brass rod. In addition, to prevent high heat capacity at the contact, it should be as thin as possible. Taking into consideration the minimum hole depth of 1 mm that is required for stable brass rod insertion and at least 1 mm distance from the 1 mm diameter hole required for the insertion of thermocouples, the minimum thickness of the copper contact had to be 3 mm. Copper contacts with two different cross sectional areas (4mm$\times$4mm and 3mm$\times$3mm) were prepared. The sizes of the cross sectional areas were selected to match the cross sectional area of the samples measured. In order to avoid heat loss from the copper contact, the electrical contact was attached to the heater arm and not directly to the copper contact.

5.2.2 Heat sink

The amount of heat required in the measurement depended on the size and thermal conductivity of the samples. The heat sink in this measurement system consisted of two parts: copper disk and copper plate. The huge copper disk (diameter = 148 mm, thickness = 16 mm) could dissipate heat quickly and was mounted directly onto the vacuum chamber. This copper disk was important in the design not only to stabilize the cold side temperature but also serves as a foundation for the whole structure (see Figure 5.1).

To allow the apparatus to measure a sample under small ΔT throughout the temperature range, a heater was needed to increase the temperature at the cold side/heat sink. A thermoelectric module (30mm$\times$30mm) was chosen over a resistive heater because of its ability to operate as both heater and cooler which is needed for large ΔT measurement. Moreover, resistive heater that is mounted on the huge copper disk would require a large power to heat up the sample. The module chosen (HZ-2, Hi-Z Technology) was placed on top of the copper disk heat sink. The module is able to operate at temperatures as high as 250^{o}C in continuous operation and intermittently as high as 400^{o}C without degrading the module. This is an important consideration because the cold side of the samples needs to be at high temperature in order to achieve higher mean temperature during small ΔT measurement. A small copper plate with dimensions 30mm$\times$30mm$\times$3mm (the same cross sectional area as the module) was mounted on a thermoelectric module. During large ΔT measurements, this plate will

dissipate the heat and ensure the cold side of the sample remains cool. Meanwhile, during small ΔT measurement the copper plate will distribute heat from the module equally to the sample. Theoretically, 0.84 Watt of heat flux is required to heat up Bi_2Te_3 sample of dimensions 3mm×3mm×8mm to temperature difference of 500 K, assuming the thermal conductivity is 1.5 W/cmK and T_c is 300 K. Due to the very small amount of heat flux, the temperature of cooper plate of this size did not change significantly, which was enough to be used as a heat sink to cool the sample. 1 mm diameter holes with 3 mm depth was bored on one side of the copper plate for temperature measurement, T4, while one side of the cooper plate was grooved for the easy soldering of a wire connection as shown in Figure 5.4. A temperature solder with melting point of ~200°C (AgSnPb, CuP Alloys Ltd.) was used to prevent melting at high temperature during small ΔT measurement.

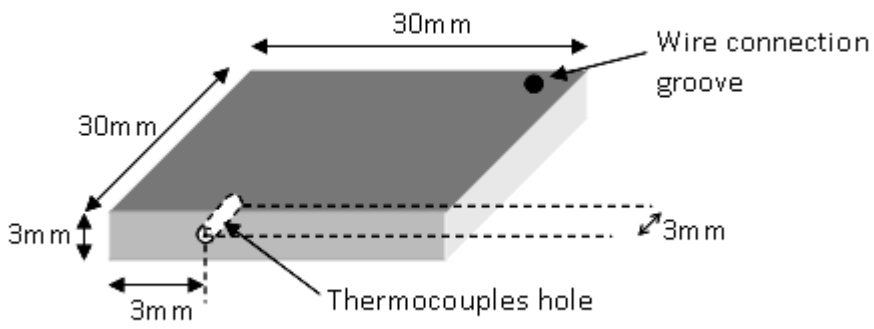

Figure 5.4: Schematic diagram of copper plate heat sink design.

5.2.3 Holders

Two types of holders were developed for this experimental assembly; 1) sample holder, and 2) chamber holder. The sample holder was responsible for holding the sample together and at the same time providing sufficient pressure to the sample to achieve good contact. The chamber holder was responsible for holding the heater/sample assembly to the top flange of the vacuum chamber for easy insertion and removal during assembly.

The sample holder held the sample between the heat flow meter and heat sink as shown in Figure 5.1. Sufficient pressure was given by tightening all nuts at all four points of stainless steel rods. To allow for the expansion of heated materials, compression springs were placed on top of the ceramic insulator. A low thermal conductivity ceramic plate was employed to hold the heater assembly in place and at the same time minimize the heat loss from the heater assembly. The ceramic plate was supported by four 5 mm diameter stainless steel rods. Each rod goes through the ceramic plate at one end and the other end was fixed into the copper disc heat sink.

The sample holder was placed inside the chamber holder. The chamber holder was attached to the top of the vacuum chamber flange so that the whole setup could be lifted out or inserted together with the top flange during open and closed circuit conditions. This is a convenient design because;

1) it prevent from having long thermocouples and wire connections inside the vacuum chamber and thus possibilities of short circuit and extra resistance due to long thin wires;
2) it prevent the thermocouples from being damaged due to the movement of the top flange during assembly.

Four steel socket shoulder screws (M6, 10 mm diameter, Buck & Hickman) were fixed on the top flange while the opposite ends were fixed to the copper disk heat sink. The screws were strong enough to hold the top flange and copper disk weight when lifted out the chamber and at the same time could provide compression during the sealing of the chamber. To allow easy access to the samples, the steel screws at the copper disc heat sink were put in line with the stainless steel rods of the sample holder, as shown in Appendix 5.

5.2.4 Vacuum

By designing the assembly setup inside a vacuum chamber could minimize heat loss through convection. The vacuum was achieved by a two-stage system that comprised of a RV8 rotary vane pump and an EXT250 turbomolecular pump (Edwards). This pump took about 10-15 minutes to achieve up to 2×10^{-5} Torr and the pressure slightly increased as the temperature increased. However, less time is required to achieve a similar pressure if the vacuum chamber remains un-open in the next measurements. The dimensions of the vacuum chamber used can be found in Appendix 6.

Two types of feed-through were employed and were located at the top flange of the vacuum chamber; one was for thermocouples access, which was a solder-type sealing and another one for wire connection access (WFP series, Spectite) sealed by tightening the nuts to a pre-set torque to compress an internal sealant. Both feed-through were electrically and thermally insulated.

5.2.5 Wire Connection

One of the challenges in thermoelement measurement is to accomplish a short circuit condition. Due to very low sample resistance (~0.01 Ω), it is important to obtain a closed circuit ($R_L \neq 0$) with an external resistance (i.e. wire connection, switch and contact) as low as possible. In order to achieve this, copper wires should be thick and short. The copper wires of 1.626 mm (16swg) in diameter and length of about 15 cm long were employed to form the total closed circuit. Ideally, smaller external resistance can be achieved if a closed circuit were to be made inside the vacuum chamber where only a short wire is required, but switching the circuit would require the use of a relay switch. The typical resistance of a relay switch found in the market is around 0.15 Ω and this contributes to the total wire connection resistance. In the case where only long and thick copper wire was used, the total wire connection resistance measured was 0.025 Ω, while the switching resistance contribute around 0.01 Ω, making the total external resistance is ~0.035 Ω, much smaller than achievable if using a relay switch inside the vacuum. In addition, the penalty of using of a relay switch

will get worse as the temperature inside the chamber increases. Due to the complexity and significant difference in resistance between the use of a switch inside and outside the vacuum chamber, the switch placed outside vacuum chamber was employed. In order to avoid more additional resistance to the circuit, measurement of the current was made using a clamp meter.

Another consideration was to avoid the copper wire being connected close to the location of temperature measurement to prevent conduction heat loss through thick copper wire becoming significant. Consequently, the connection at the hot side was located at the heater arm just below the heater.

5.2.6 Thermocouple

A bare fine thermocouple type-J, 0.25 mm in diameter (IRCO, Omega) was used for temperature measurement in this setup. Type-J thermocouples consist of iron as the positive leg and constantan as the negative leg was chosen over a typical type-K thermocouples due to its ability to operate in a vacuum environment over a wide temperature range 0-750°C. For most thermocouples, the operating temperature is limited by the temperature of the insulating sleeve (typically up to 300°C), consequently, bare thermocouples wires are employed for high temperature operation. In addition, the bare thermocouple is needed for feed-through soldering termination. Fine thermocouples help to minimize heat loss through wire conduction. The total length of each thermocouple was 1 m with about 0.4 m was assembled inside the vacuum chamber while the rest

was outside and connected to a data logger. To prevent a short circuit, all the thermocouples wires inside the chamber were insulated using stack of single hole ceramic beads (maximum temperature 1600°C) while the thermocouples wires outside the chamber were insulated by PVC insulating sleeves.

5.3 Experimental Setup

Figure 5.5 shows a schematic diagram of experimental setup for ZT measurement of a small resistance sample. The heat flux at the hot side of the sample was provided by a cartridge heater powered by an AC power supply (MKII, Regavolt). The current and voltage of the power supply were monitored by Keithley 199 and Fluke 8842A digital multimeters respectively. The cold end of the sample was placed on a thermoelectric module which was powered by a programmable DC power supply (TSX3510P, Thurlby Thandar Instruments). The whole measurement assembly was placed inside a vacuum chamber which was connected to a turbomolecular pump. Five pairs of thermocouples were positioned at T1, T2, T3, T4 and T5 where the temperature of heater, brass hot junction, brass cold junction/ sample hot junction, sample cold junction and copper disk heat sink were measured respectively. The thermocouple was inserted inside small holes filled with heat sink compound (RS) to provide good thermal contact. All the data were recorded by a data logger (TC-08, PicoLog) which recorded the measurements every second and displayed them on the computer.

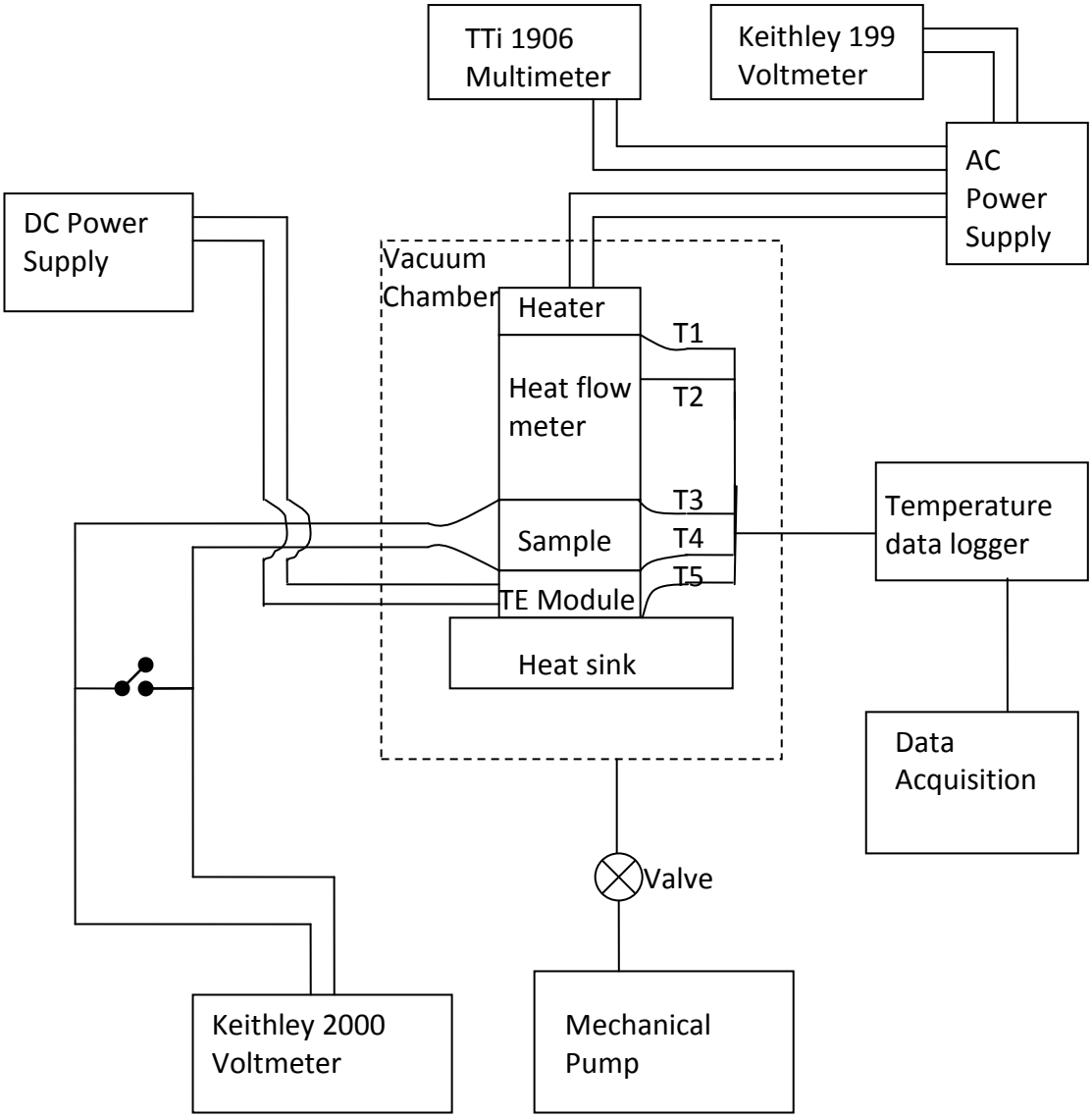

Figure 5.5: Schematic diagram of experimental setup for single leg thermoelement measurements.

Meanwhile, a Keithley 2000 multimeter was used to measure the voltage produced in the samples by connecting it across the switch. The electric current during closed circuit is measured using a clamp meter (ST-337, Farnell). The completed experimental setup is shown in Figure 5.6.

5.4 Experimental Procedure

5.4.1 Preparation of sample

Samples of disk shape were cut into squares with dimensions of 2mm×2mm and 3mm×3mm using a MKII microslice precision slicing machine (Malvern Instruments). A few attempts were made to cut segmented samples but these were not successful because the samples were too fragile and proved to be easily broken at the join during cutting. However, successful attempts were achieved by using a wire-cutter from Wire Cut Technology Ltd. The samples were then cleaned using acetone and deionised water a few times to remove dirt and residue. Prior to that, all surfaces of the samples were polished using fine sand paper (P2500, Hermes) to obtain flat surfaces. The average cross sectional area and thickness of each sample were then measured using a precision micrometer.

5.4.2 Contact material

Contact material is an important layer that will connect the samples to an electrode to ensure low electrical and thermal contact resistances.

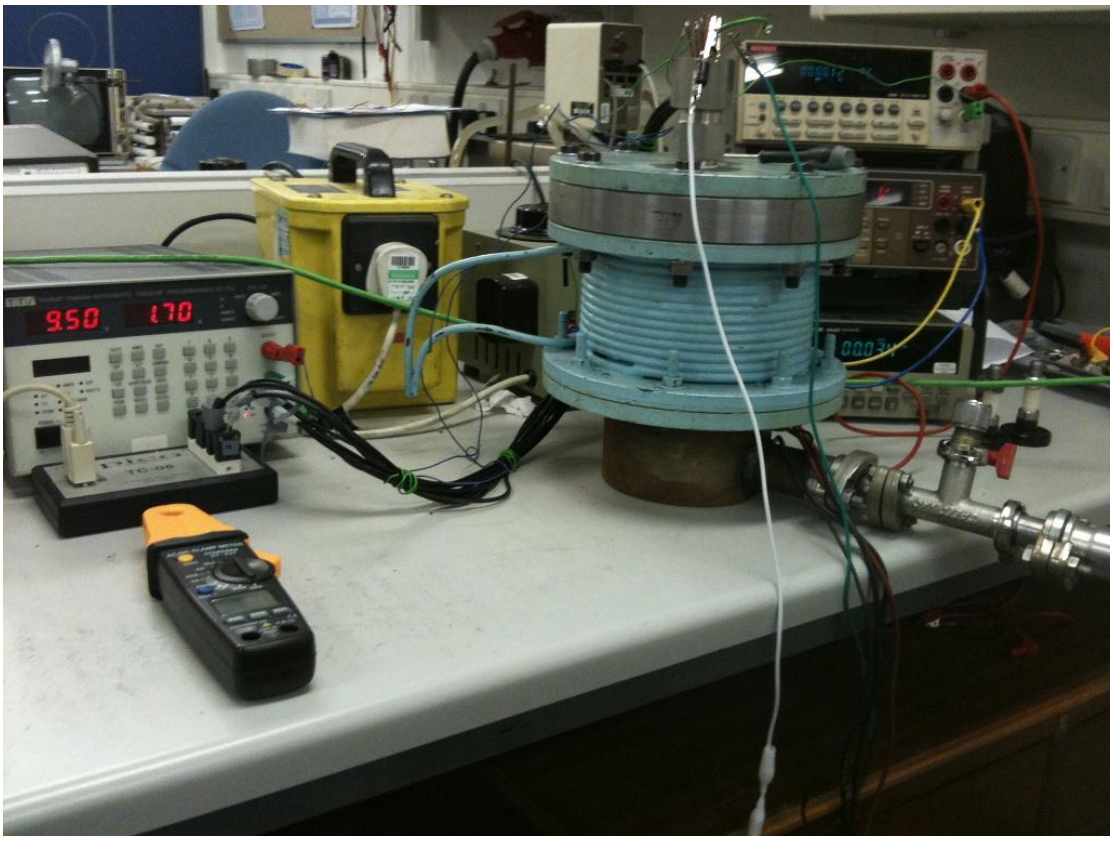

Figure 5.6: The completed (except computer data acquisition system is not in the picture) measurement system for single leg thermoelement.

In this apparatus, the electrodes were the copper contact at the hot junction and the copper plate at the cold junction. There are a few considerations in making contact to the samples which include;

1) material will not react with samples,

2) high melting temperature, and

3) high thermal and electrical conductivity.

PbSn solder and indium could have been used as a good contact material. However, it's low melting temperature (<200°C) limit the usage to low temperature operation only and thus was not suitable for this type of measurement. Hence, pure platinum foil (99.998%, Alfa Aesa) with 0.1mm thickness was chosen as a contact material due to its high melting temperature (1768°C) and high thermal conductivity (71.6 W/mK) which is close to indium (81.8 W/mK) [105]. Platinum's high resistance to oxidation also provides a low and relatively stable contact resistance. Because platinum is not as soft as indium, folding the platinum foils into a few layers helps to decrease the contact resistance.

Prior to forming the contact, the sample at each junction was plated with nickel using a nickel plating pen (Hunter Product). Nickel layers act as a barrier to prevent the diffusion of copper atoms into the sample that would change the carrier concentration and even may change the conducting type of the sample [106,107].

5.4.3 Assembly

The prepared sample was placed vertically between the sample holders with layers of platinum foil placed at each junction. Prior to that, the thermoelectric module was sandwiched between the copper plate and the copper disk heat sink. Once assembled, the nuts on top of the spring of each rod were tightened to ensure sufficient pressure across the sample. Two opposite nuts were tightened simultaneously to prevent tilt and unbalanced pressure on the sample. Then all thermocouples were inserted into the respective holes. Figure 5.7 shows the assembled setup of thermoelement measurement. A close-up of sample mounting inside the sample holder is shown in Figure 5.8.

5.4.4 Measurement

Once the sample was assembled, the total resistance at room temperature was measured. Measurement was made using 4-wires and the average of a few measurements was recorded. Then the apparatus was sealed inside the vacuum chamber to be evacuated to a vacuum pressure of 2×10^{-5} Torr and after 10 minutes or as soon as the pressure was reached, a low power was applied to the heater (under open circuit) to produce small temperature difference (~15 K). Temperature produced (T1-T5) were recorded to the computer. When the temperature reading was stabilized, the open voltage reading was recorded. This was followed by the closed circuit measurement in a similar manner, except that the switch was on.

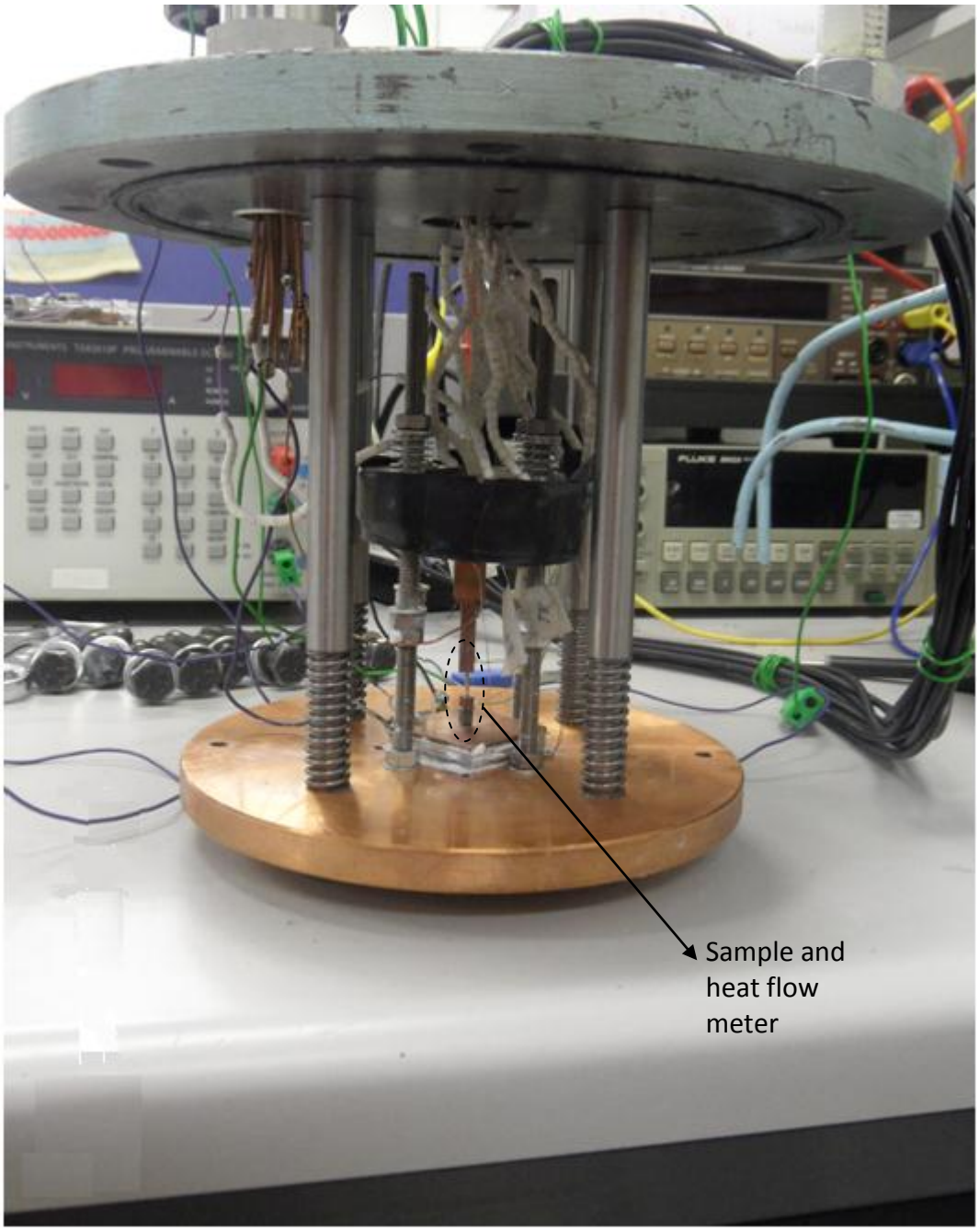

Figure 5.7: Measurement setup (before put inside vacuum chamber).

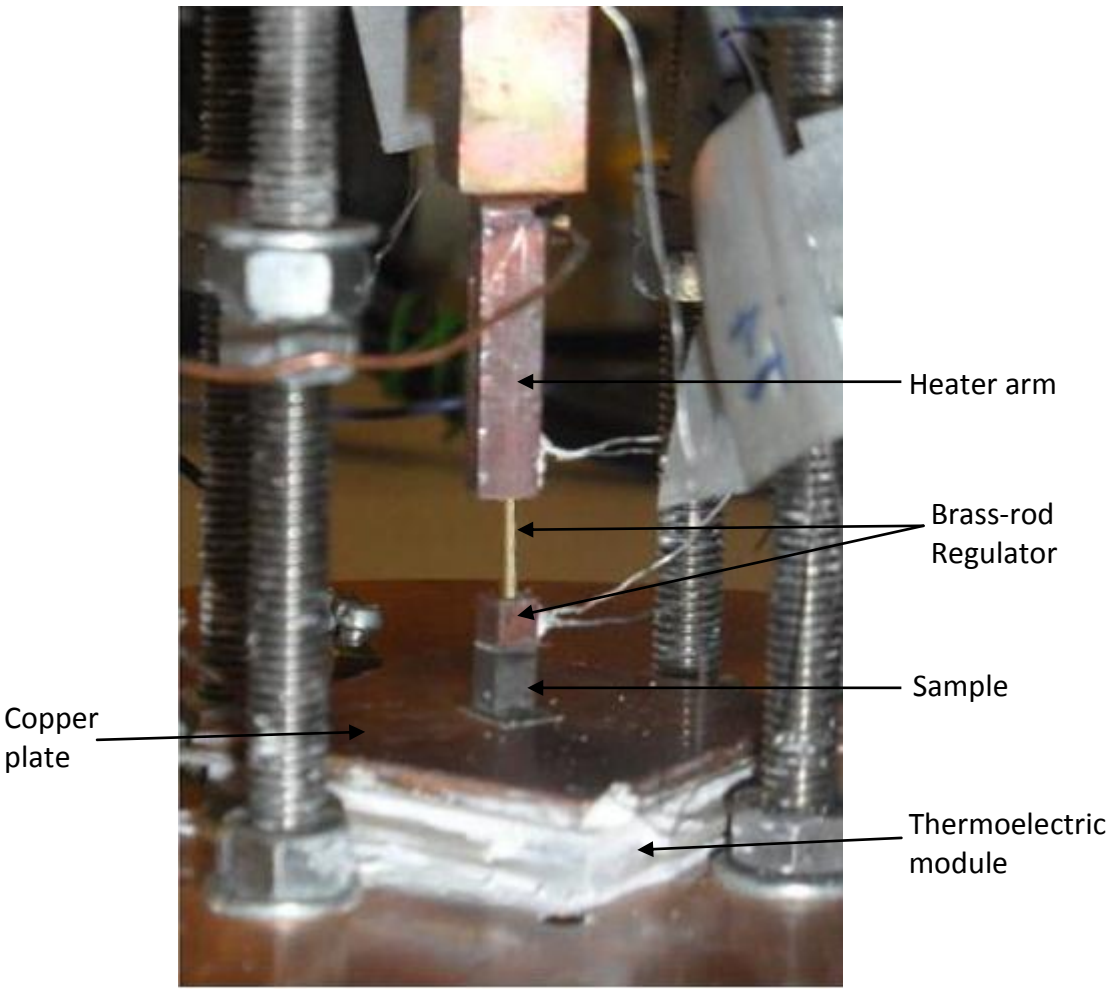

Figure 5.8: Close-up of mounting sample between heat flow meter and heat sink.

For large ΔT measurements, this measurement cycle was repeated for different T_h by increasing the heating power, while keeping the cold side at a constant T_c (295 K-300 K). The highest T_h that can be reached with this equipment is ~570 K, when the brass rod start becomes soft and bended.

For small ΔT measurement, a similar procedure was repeated except that the current to the thermoelectric module was reversed so that the temperature at the cold junction, T_c, could be adjusted to keep the same temperature difference (~15-30 K) with the change on the hot side during open circuit. The process was repeated until T_h not exceeded ~570 K. Usually, large ΔT method was measured first (i.e., increasing ΔT across the sample with increasing temperature), so that practical temperature difference for small ΔT measurement (i.e., ΔT keeps almost constant with increasing temperature) could be determined. The minimum observable temperature difference for the different samples was determined by its ZT and dimensions.

5.5 ZT Calculation

Due to the relatively small thermoelement resistance in comparison to the external wiring resistance in the measurement setup (i.e., R_L is not << R_i), the short circuit condition cannot be obtained. In this case, equation 3.15, ($ZT_m = \frac{\Delta T_o}{\Delta T_c} - 1$, as explained in chapter 3) will be used for ZT calculation where

$T_m = \frac{(2a-1)T_h + T_c}{2a^2}$ is an effective mean temperature and $a = \frac{R_i + R_L}{R_i}$ is the ratio of total to internal resistance.

5.5.1 Closed circuit

Equation 3.15 indicates that the resistance of sample, R_i, is needed for the determination of ZT values. Determination of internal resistance became more complex at higher temperature due to the fact that sample's resistance changed with temperature.

To determine R_i, method using extrapolation of ΔT_c with changes in R_L [101] as successfully proved in module measurement described in chapter 3 has been tried but not successful due to the very small changes of ΔT_c. To solve this problem, larger temperature difference (ΔT>200°C) is required. Since the research involved comparison measurement of ZT at small ΔT, so this method is not suitable for determination of the sample resistance. Alternative approach for determination of R_i can be determined using equation 3.14, $\overline{\alpha}\Delta T_c = I_c(R_i + R_L)$. Since value of I_c, ΔT_c and $\bar{\alpha}$ are already obtainable in the measurements, we only need to know the external resistance, R_L, to determine the value of R_i.

External resistance consists of a contribution from leads and contacts as illustrate schematically in Figure 5.9. R_1 and R_2 represent wire resistances at the hot side and cold side respectively meanwhile R_3 is the resistance of the switch. R_{c1} and R_{c2} are the contact resistances at the hot and cold side respectively.

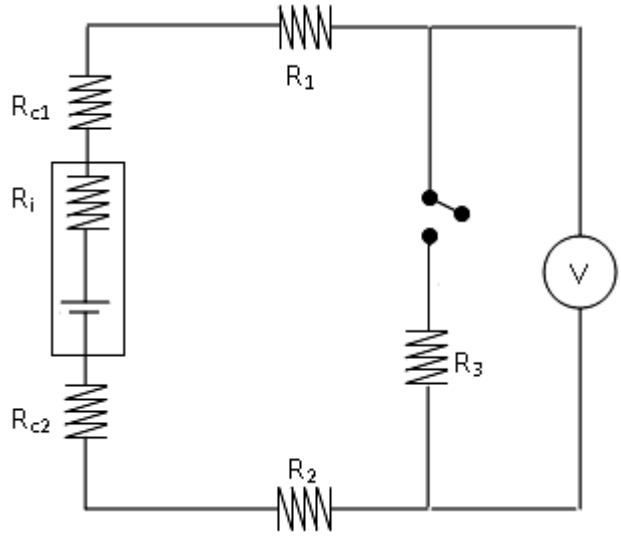

Figure 5.9: Schematic diagram of total circuit resistance.

Although R_1, R_2 and R_3 are very small, they can be measured quite accurately using 4-wires. On the other hand contact resistance cannot be determined readily. Contact resistance should not be ignored because it can make a significant contribution to the total external resistance. The total external resistance which includes contact resistances can be determined from the measured overall resistance, $R_i + R_L$, and the sample resistance, R_i, at room temperature by using,

$$[R_L]_{T=T_{room}} = [(R_i + R_L) - R_i]_{T=T_{room}} \dots\dots (5.1)$$

In contrast with total resistance measurement which can be measured during assembly of the sample measurement, the sample resistance need to be measured separately. R_i at room temperature can be measured using an

apparatus developed by Srivatsan [108] which will be explained further in section 5.5.3. The total resistance, $R_T = (R_i + R_L)$ at room temperature was measured using the 4-wires method available on a digital multimeter. With the assumption that wire and contact resistance does not change significantly over the temperature range, the sample resistance at different temperatures, $R_i(T)$ can be determined using equation 3.14,

$$R_i(T) = \frac{\alpha \Delta T_c}{I_c} - [R_L]_{T=T_{room}} \dots \dots (5.2)$$

where $[R_L]_{T=room} = R_1 + R_2 + R_3 + R_{c1} + R_{c2}$ is the total external resistance at room temperature. Note that R_i calculated from this equation represents resistance under actual operating conditions with a temperature difference established across the sample. It is to be noted also that R_T needs to be determined whenever a new contact is formed because the formation of the contacts has a negligible influence on R_T.

5.5.2 Sample Resistance at room temperature

The sample resistance at room temperature was determined from resistivity measurement measured using an apparatus developed by Srivatsan, originally to evaluate the electrical contact resistance at the thermoelectric junction. The concept of the measurement used a three-probe technique where a small ac current was applied at the end of the sample while the voltage produced between one movable probe and one fixed probe were measured.

Plotting R_i as a function of distance, , the resistivity of the sample can be calculated from the slope of the graph,

$$R(x) = \left(\frac{\rho}{A}\right) \cdot x + R_c \ldots\ldots (5.3)$$

where $R(x)$ is the resistance measured at a particular distance x, R_c is the contact resistance, ρ, x and A are resistivity, length and cross sectional area of the sample respectively.

The apparatus for resistivity measurement and the schematic diagram of the measurement principles used are shown in Figures 5.10 and 5.11 respectively. The current flowing into the samples can be determined accurately by measuring the voltage, V_1, across known resistance, R_L. $R(x)$ can then be calculated using the Ohm's Law, $R(x) = \frac{V_2}{I}$, where V_2 is the voltage drop across the sample.

It is to be noted that only one or two sets of measurements are required for determination of the resistance of each sample. However, the total resistance measurement is always required at the start of each run of measurement. Once R_i at room temperature and R_T are successfully measured, a and T_m values can be calculated and thus ZT at that particular temperature can also be determined.

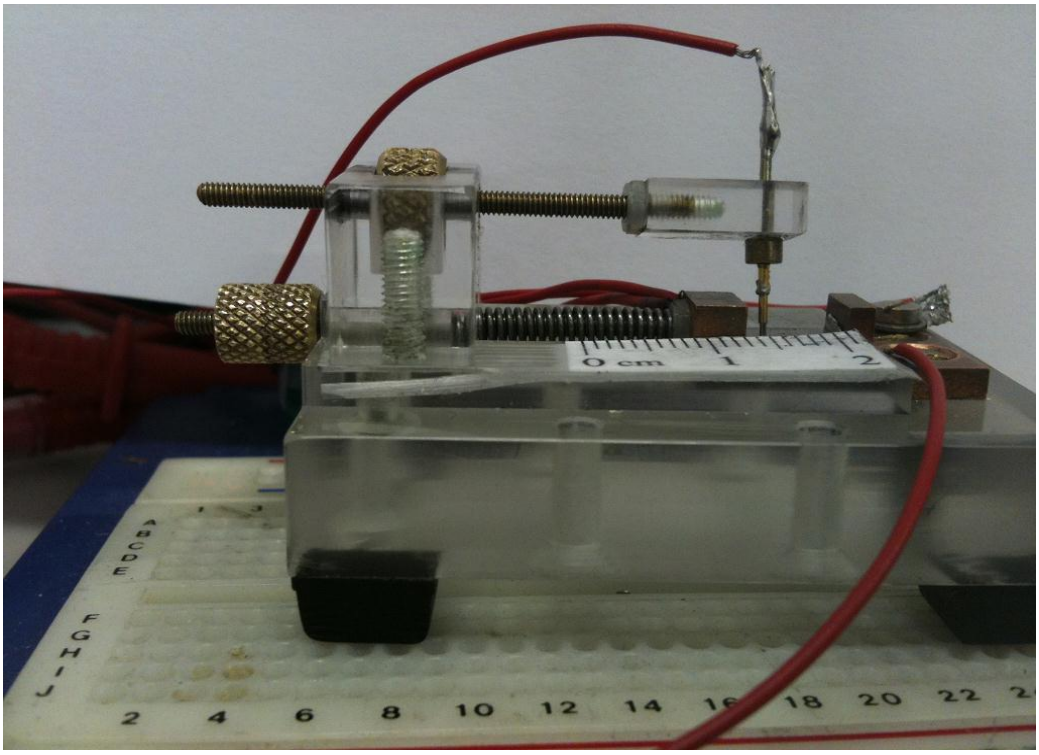

Figure 5.10: Apparatus used for sample resistivity measurement at room temperature (Photograph from recent equipment, Srivatsan, 2008).

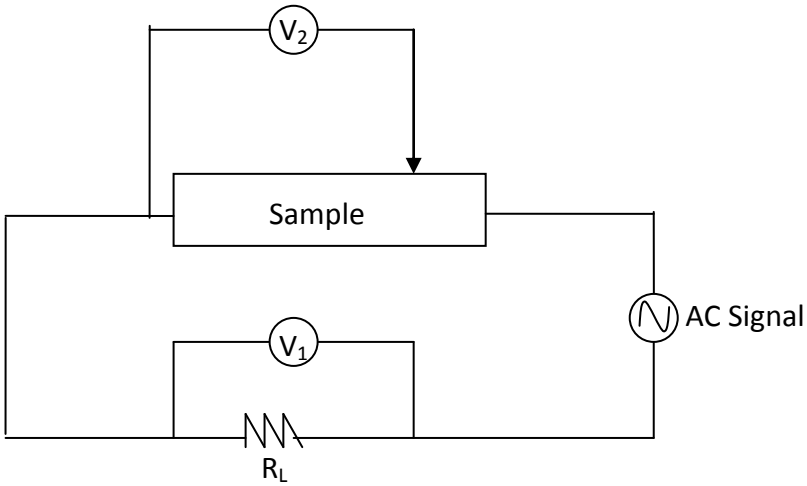

Figure 5.11: Schematic diagram of resistivity measurement [1].

5.5.3 Expected results

After all the data are available, modified dimensionless figure-of-merit, ZT_m , with correction could be calculated using,

$$ZT_m = \left(\frac{\Delta T_o}{\Delta T_c} \times \frac{\Delta T_{bc}}{\Delta T_{bo}}\right) - 1 \ldots\ldots (5.4)$$

where ΔT_o and ΔT_c are the temperature difference across the sample during open and closed circuit respectively while ΔT_{bo} and ΔT_{bc} are the temperature difference across the brass regulator during open and closed circuit respectively. Figures 5.12 and 5.13 show the results of the temperature difference measurement across the sample and the temperature difference across the brass heat regulator as a function of time. Compared to the ZT module measurement described in chapter 4, the temperature drop between open and closed circuit in a single thermoelement measurement is much smaller. On the other hand, thermoelement measurement requires less time to stabilize compared to module measurement. Because of the relatively small drop during open and closed circuit, a small change in heat flux can result in significant change to ZT. Therefore, the observation of the ratio of the temperature difference across the sample to the temperature difference across the brass regulator serves as an accurate indicator for the steady state condition (see Figure 5.15).

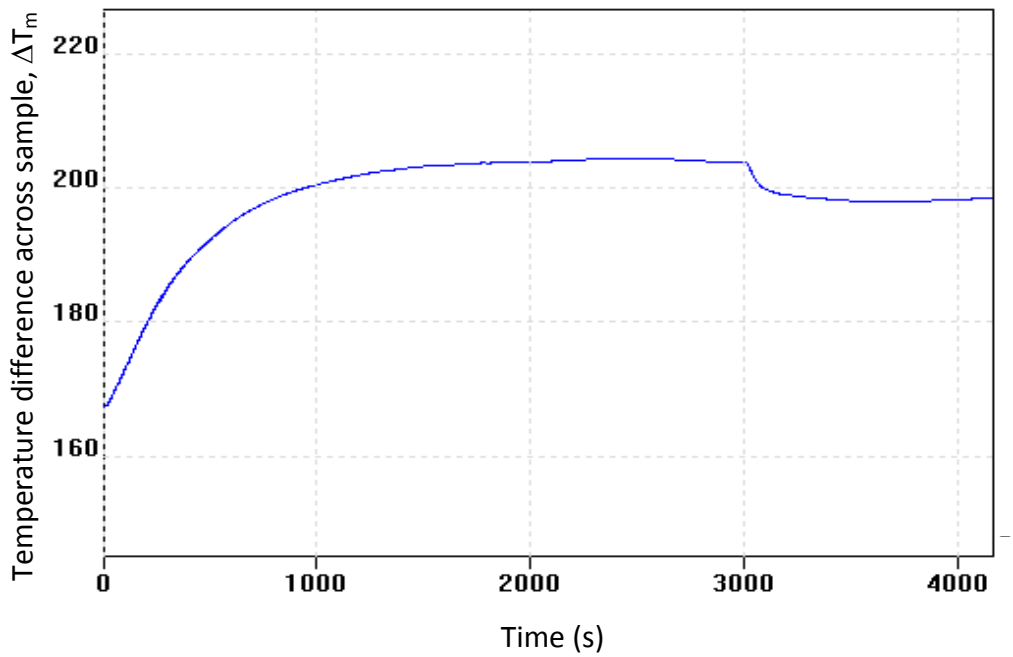

Figure 5.12: Temperature difference across the sample as function of time at $\Delta T_o = 205°C$.

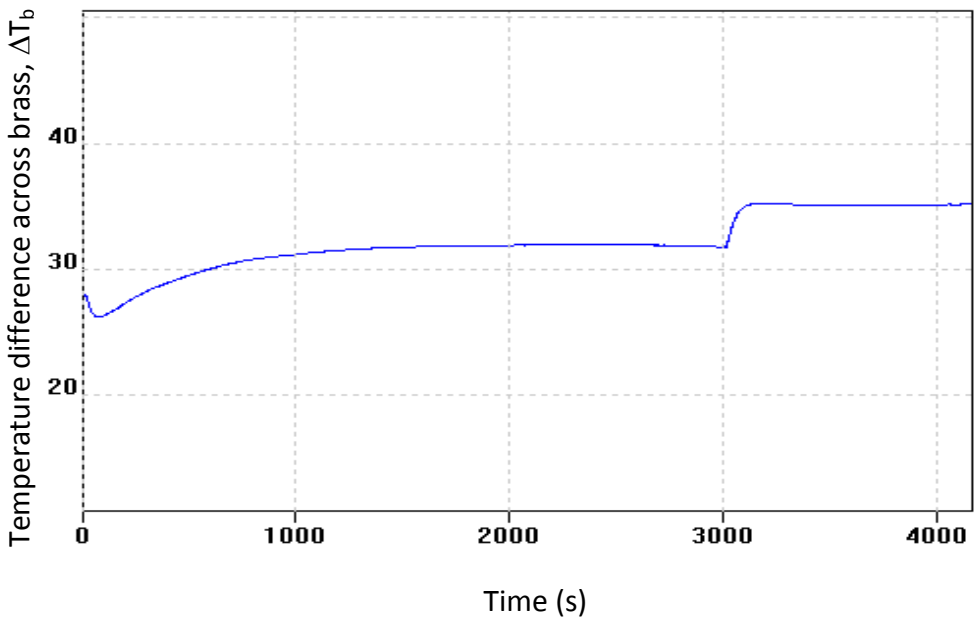

Figure 5.13: Temperature difference across the brass heat regulator as a function of time at $\Delta T_{bo} = 32°C$.

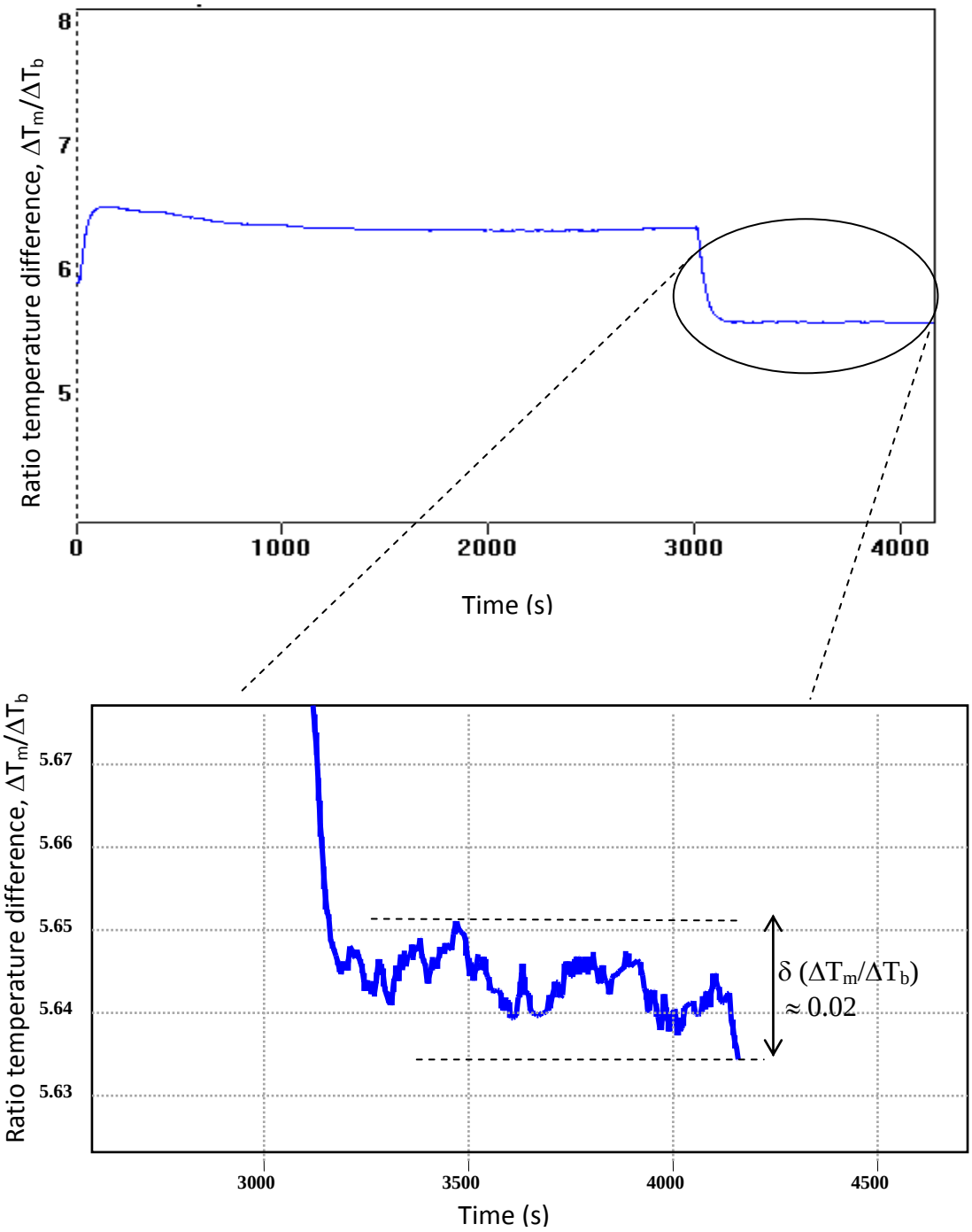

Figure 5.14: The ratio of the temperature difference across the sample and temperature difference across the brass, $\frac{\Delta T}{\Delta T_b}$, as a function of time.

5.6 Performance evaluation of the equipment

5.6.1 Calibration

Since temperature difference and current are involved directly in the measurement of ZT_m , all thermocouples and the current meter were calibrated. The temperature of a copper block placed inside the vacuum chamber was measured using all thermocouples involved from the same position during a period in which the heater power kept increasing.

The results were compared with one of the calibrated thermocouples (T4 as reference). Figure 5.15 shows the measurement results of all thermocouples from 0-50°C and Figure 5.16 shows the measurement results from 50-250°C. The relative error for all thermocouples with T4 showed an error of less than 3.6%, 1.1%, 2.7% and 4.4% in the high temperature range and less than 0.7%, 0.3%, 0.4% and 0.7% observed for the low temperature range for T1, T2, T3, and T5 respectively.

The clamp meter used for current measurement in determination of T_m and R_T was calibrated against a precision 1021 DC Current Source (Time Electronics) in a range of 1 to 99 mA. It showed an error of less than 2%. At the higher current range, the clamp meter was calibrated against the current measured by a TTi 1906 multimeter from Thurlby DC Power source in 0.1 to 1 A ranges. The error observed was less than 1.2%.

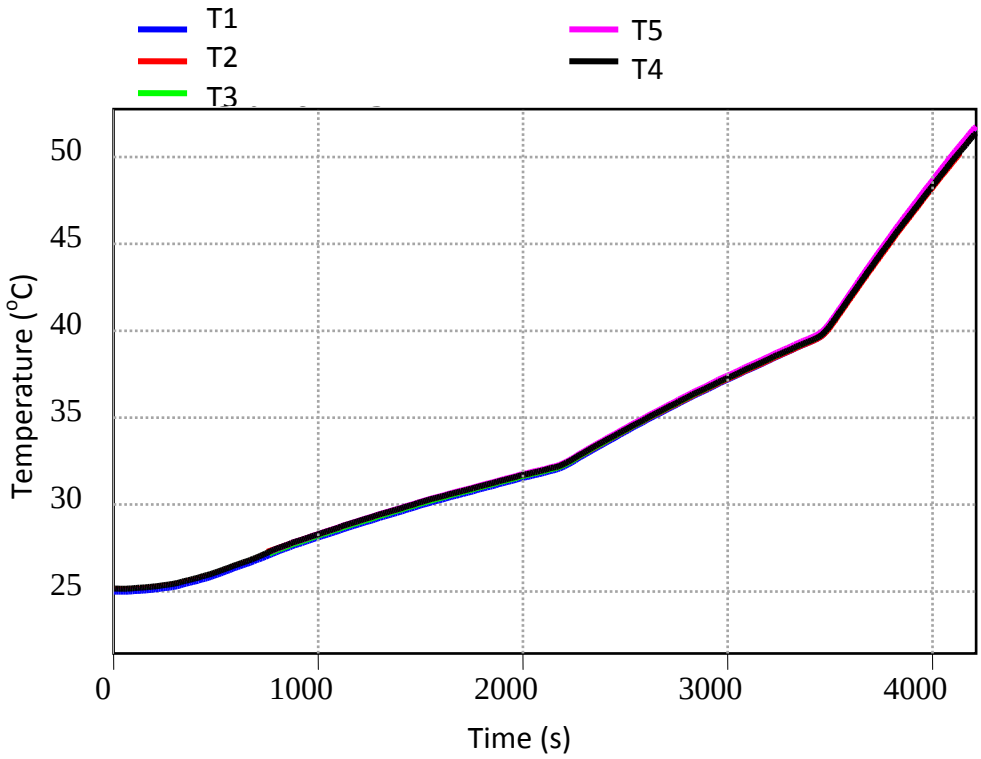

Figure 5.15: Calibration of all thermocouples at lower temperature (0-50 °C).

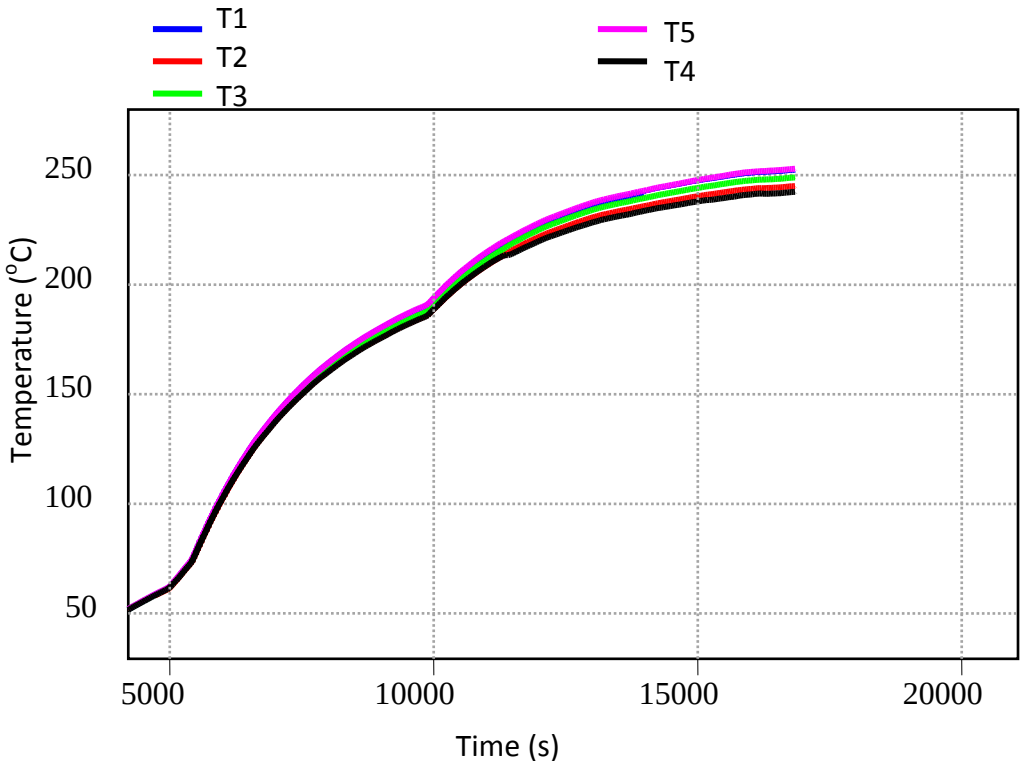

Figure 5.16: Calibration of all thermocouples at higher temperature (50-250 °C).

5.6.2 Repeatability

The developed equipment shows good repeatability under the same measurement conditions. The repeatability tests were done on a n-type Bi_2Te_3 sample with dimensions of 3mm×3mm×8mm (sample C). The measurements were made with and without moving the sample out throughout the test. It was observed that the repeatability is slightly affected when a new contact was required. Figure 5.17 is shows four sets of small ΔT measurements that were carried out under temperature differences of 17-35 K throughout the temperature range of 300-428 K. On the other hand, four sets of large ΔT measurements were made with an increasing temperature difference from 12 K to 243 K is shown in Figure 5.18. Measurement data for small and large ΔT can be found in Appendixes 9 and 10 respectively. Both results show a maximum error of less than 10% and 7% respectively. It was also found that repeatability for thermoelement measurement was slightly lower than for module measurement.

The uncertainty in temperature measurement can be estimated using the theory of propagation error. The fluctuation of temperature measurement observed from the experiment gives an estimated error of ratio temperature difference, $\delta\left(\frac{\Delta T_m}{\Delta T_b}\right)$ of 0.02-0.06 K (as shown in Figure 5.14). The estimated error of figure-of-merit, $\delta(ZT)$, determine by equation 5.4, can be calculated by,

$$\delta(ZT) = ZT \times \left[\left(\frac{\delta(\Delta T_{mo}/\Delta T_{bo})}{(\Delta T_{mo}/\Delta T_{bo})}\right)^2 + \left(\frac{\delta(\Delta T_{mc}/\Delta T_{bc})}{(\Delta T_{mc}/\Delta T_{bc})}\right)^2\right]^{1/2} \quad \dots\dots (5.5)$$

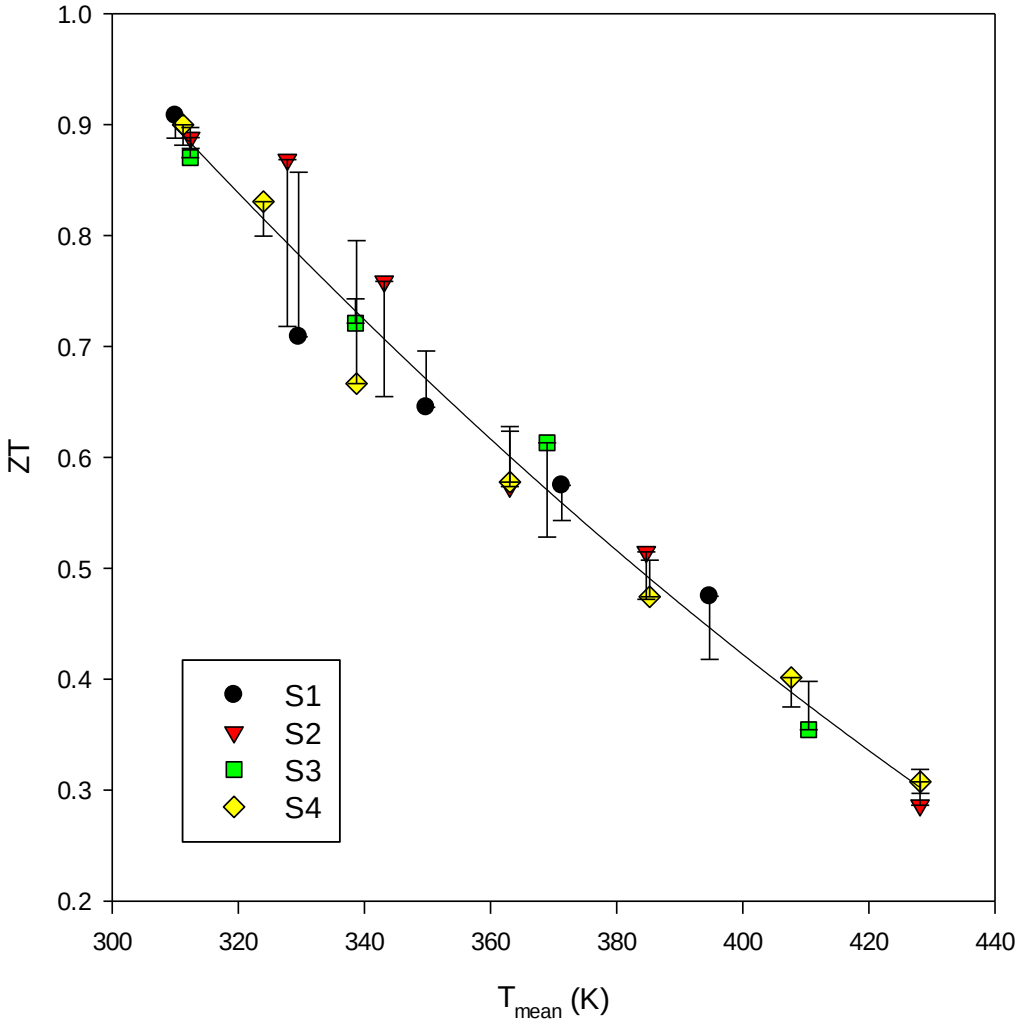

Figure 5.17: Repeatability test of ZT measurement under small ΔT for sample C. The results of four set of measurements shows maximum repeatability error of less than 10%.

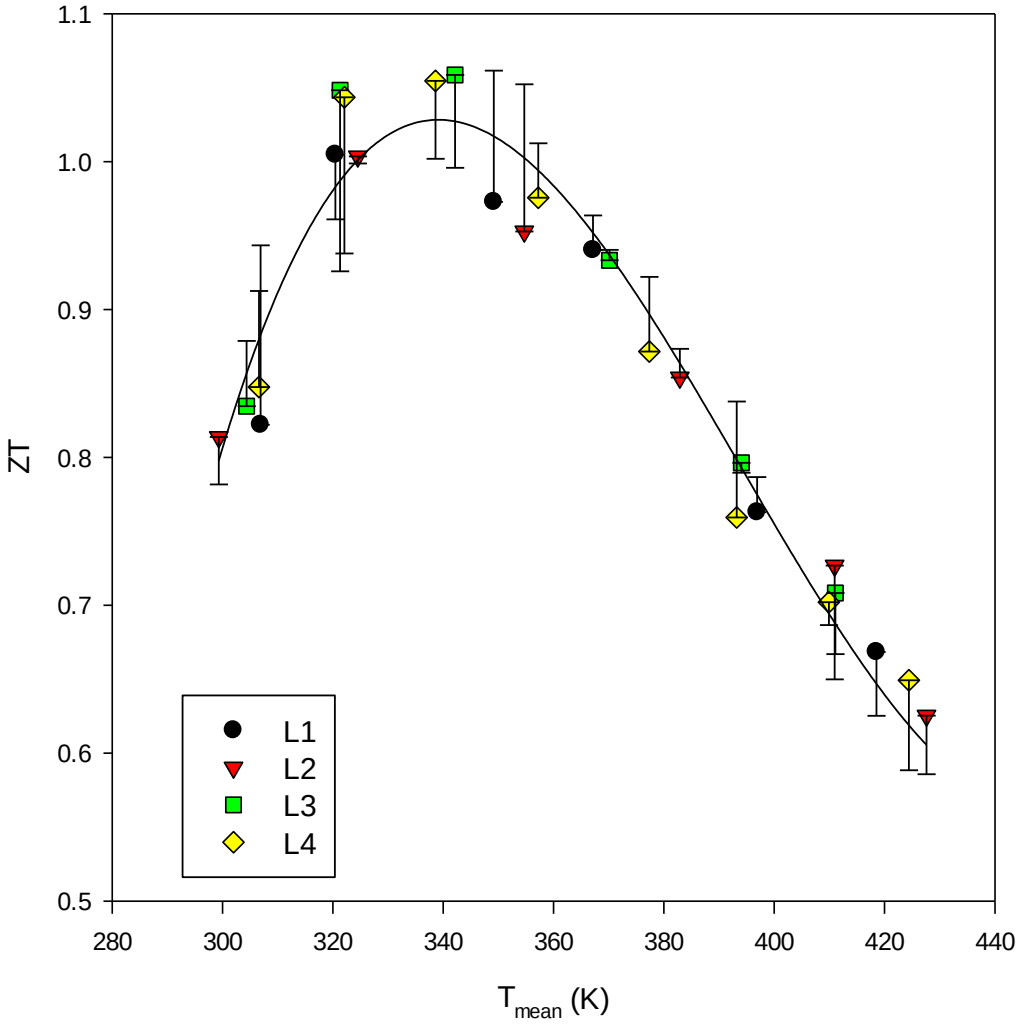

Figure 5.18: Repeatability test of ZT measurement under large ΔT for sample C. The results of four set of measurements shows maximum repeatability error of less than 7%.

where ΔT_{mo} and ΔT_{mc} are temperature difference across sample during open circuit and ΔT_{bo} and ΔT_{bc} are temperature difference across brass heat regulator during open and close circuit respectively. It was calculated that the maximum error of less than 1% are observed if maximum $\delta\left(\frac{\Delta T_m}{\Delta T_b}\right) = 0.06$ are used in the calculation. Due to the small uncertainty in temperature measurement, this did not significantly contribute to repeatability errors. It suggested that the error in repeatability came from the difficulty of achieving a good contact using platinum foil especially when a new contact is required. Unlike in the module measurement, all thermoelements are already in good contact. Repeatability could be improved if high temperature solder was used at the junction.

5.6.3 Accuracy

The accuracy of the measurement has been compared with a similar material using other commercial PPMS equipment (Quantum Design Inc) as a reference. However, the reference data was only available up to a temperature of 360 K. Comparison between these two results is shown in Figure 5.19. The results show that a relative error of 13% up to 32% was obtained within the temperature range of 300-362 K. ZT measurement from the new setup equipment decrease more rapidly compared with measurement using PPMS (data can be found in Appendix 11). Investigation on the deviation is carried out as discussed below.

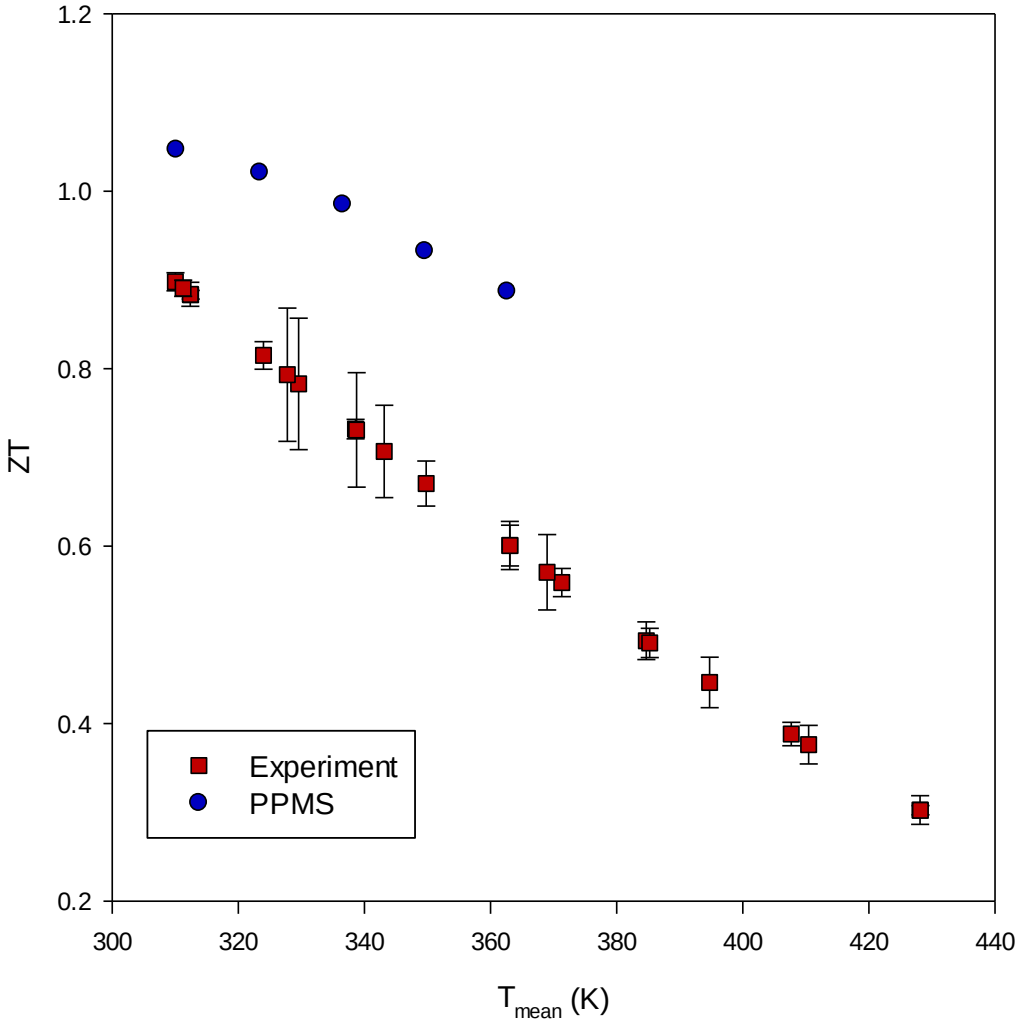

Figure 5.19: Temperature dependence of sample C based on an average experimental ZT using novel technique as compared with PPMS measurement technique [Appendix 11].

5.7 Error Analysis

5.7.1 Constant heat

As observed in module measurement, temperature differences across the heat flow meter were higher at closed circuit compared with that during open circuit, which indicates that heat flux through the sample during short circuit is higher than during open circuit. The differences observed in thermoelement measurement were 3% to 15% for all temperatures. These differences can be compensated using for equation (4.9). Figure 5.20 shows the results of small ΔT measurement (ΔT~15-35 K) on Bi_2Te_3 with (ZT_w) and without (ZT_{wo}) correction. Deviation in heat flow temperature difference during open and close circuit is larger compared to module measurement corresponding to higher mean temperature measured.

5.7.2 Seebeck Coefficient

The Seebeck coefficient is calculated using equation 4.10. The results were then compared with reference data as shown in Figure 5.21. The experimental Seebeck coefficient result shows 9-12% lower than the reference material. Despite this, the curves show similar behaviour as expected which means that the ZT curve is only shifted to lower ZT without changing its behaviour.

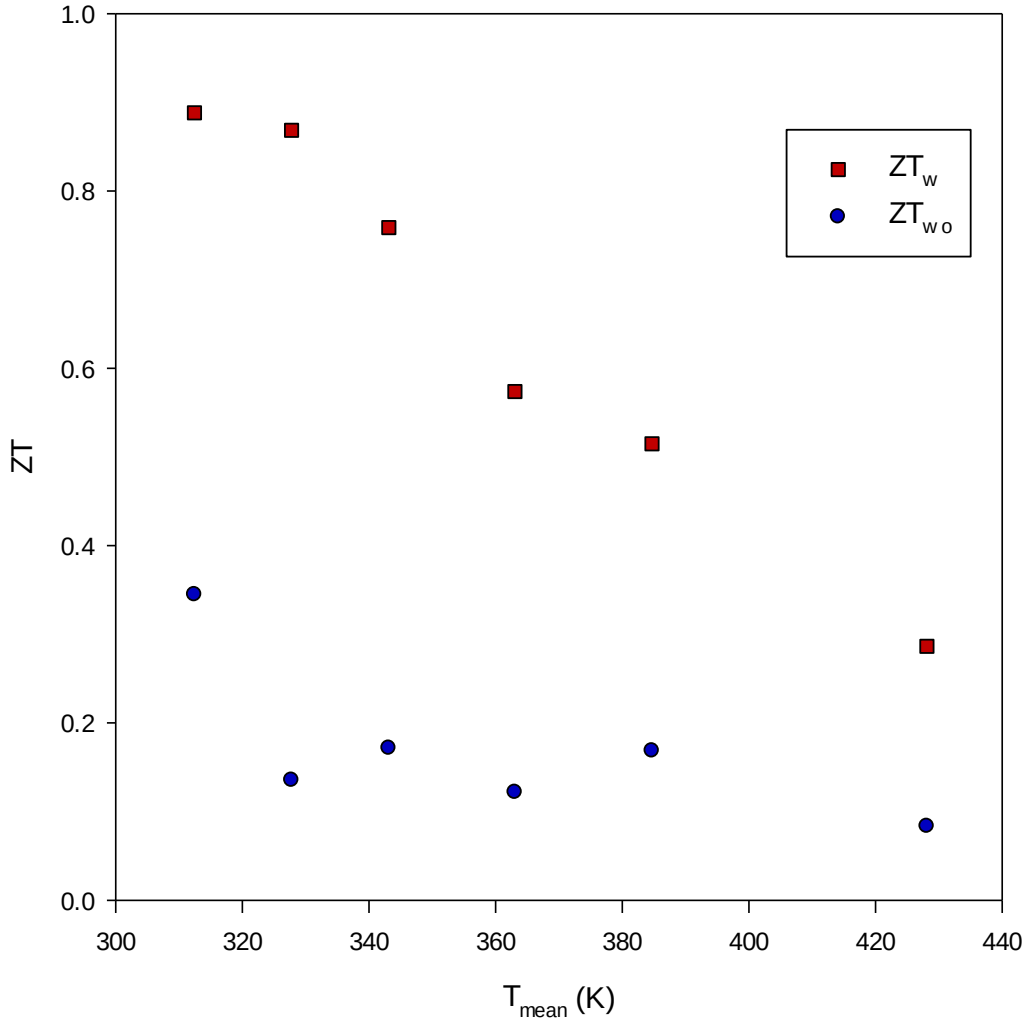

Figure 5.20: Dimensionless figure-of-merit of sample C (from S2 data) obtained from small ΔT measurements with (ZT_w) and without (ZT_{wo}) correction.

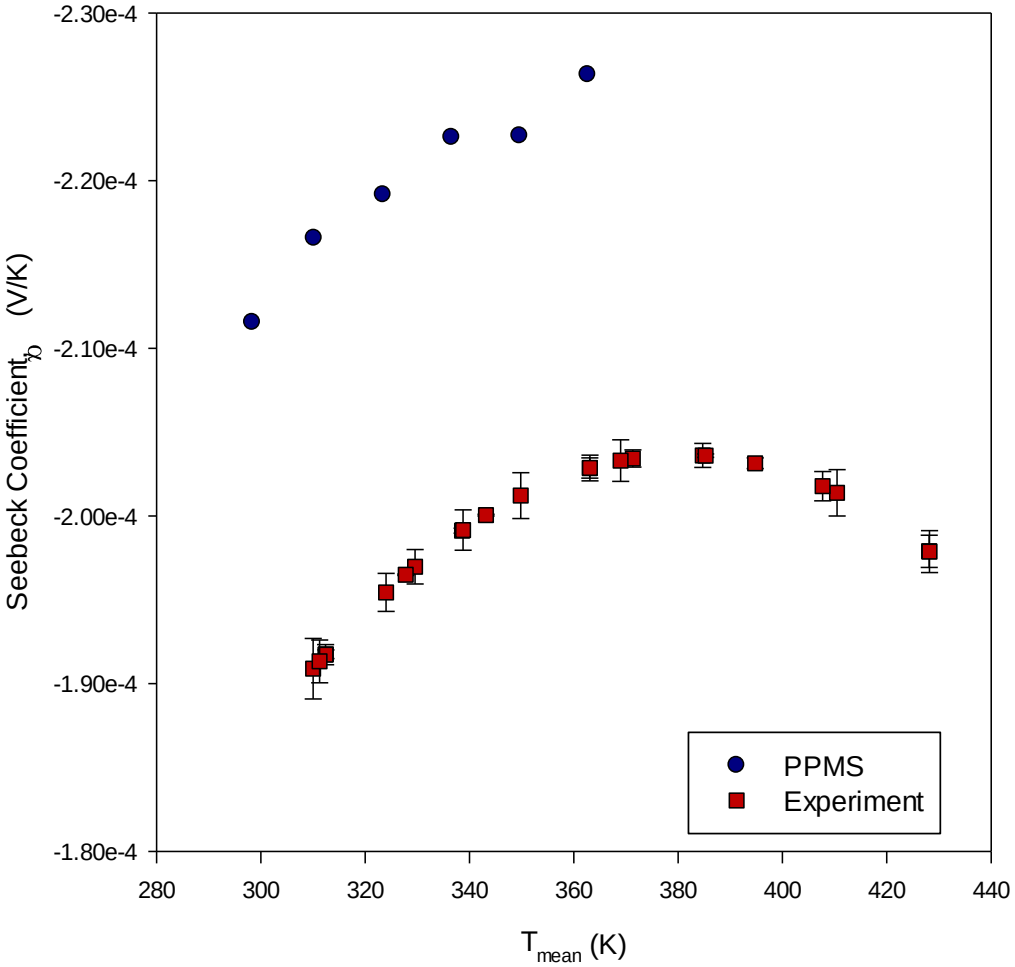

Figure 5.21: An average Seebeck coefficient of sample C obtained from four different sets of measurements (S1, S2, S3 and S4) as comparison with PPMS measurement data [Appendix 11] as material reference as a function of T_{mean}.

5.7.3 Electrical resistivity

Electrical resistance of non-short circuited condition can be determined from equation 5.2 with the assumption that R_L was constant throughout the temperature range. The result of electrical resistivity measurement is shown in Figure 5.22. The deviation of ~25% compared with the reference material is observed. As can be seen, the large overestimate of sample resistance mainly contributes to the reduction of ZT. Because determination of sample resistance requires the measurement of current as well as of the external resistance at room temperature, the low resolution of current clamp meter and resistance meter contribute to the reduction in the accuracy of ZT measurement.

5.7.4 Thermal conductivity

Thermal conductivity was calculated using equation 4.12. The plotted result is shown in Figure 5.23. The graph indicates reduced heat loss was achieved as smaller deviation of thermal conductivity was observed from the reference data as the temperature increased. However, λ at low temperature show much larger deviation. As shown in Figure 5.24, the error decreased linearly from 29% to 4% as a function of temperature. ZT of measured sample is being overestimate at lower mean temperature due to underestimate of thermal conductivity. This is because of smaller heat flux through the sample which reduced the capability of constant heat flow detection at lower temperature.

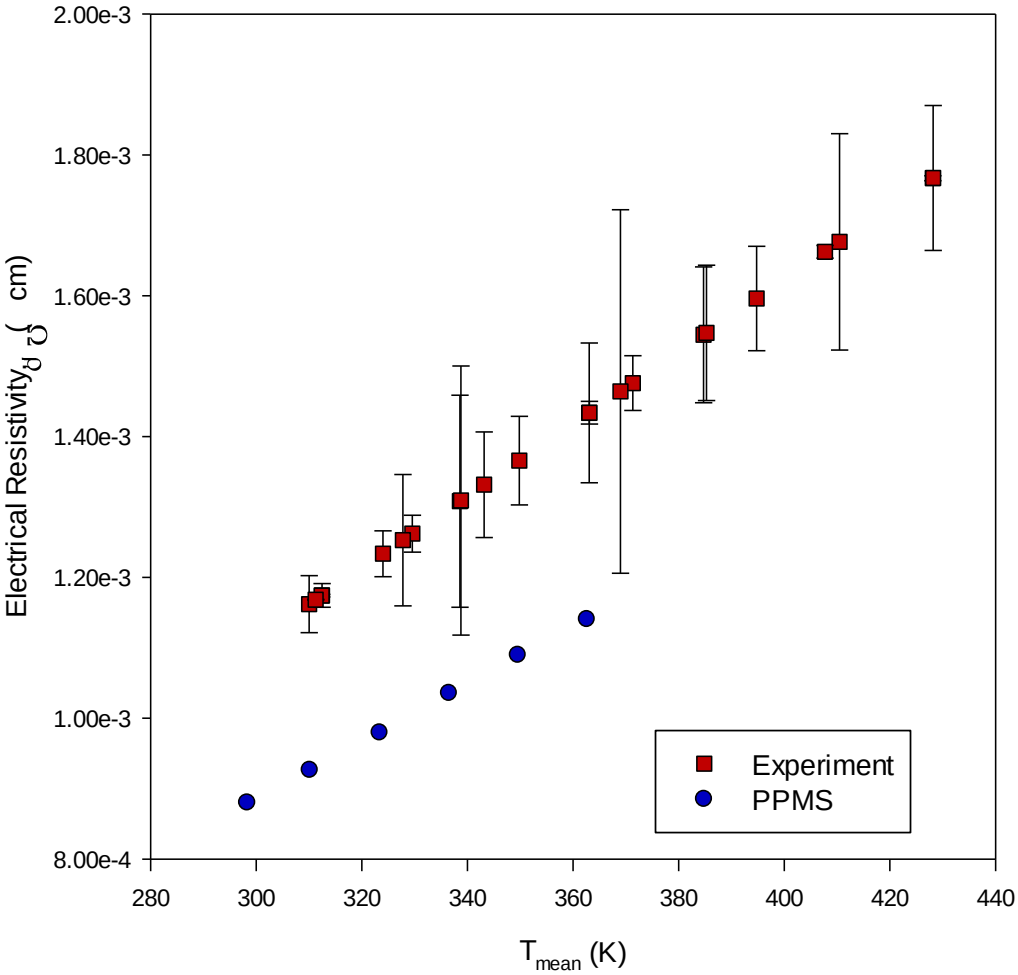

Figure 5.22: An average electrical resistivity of Sample C obtained from four different set of measurements (S1, S2, S3 and S4) as comparison with PPMS measurement data [Appendix 11] as material reference as a function of T_{mean}.

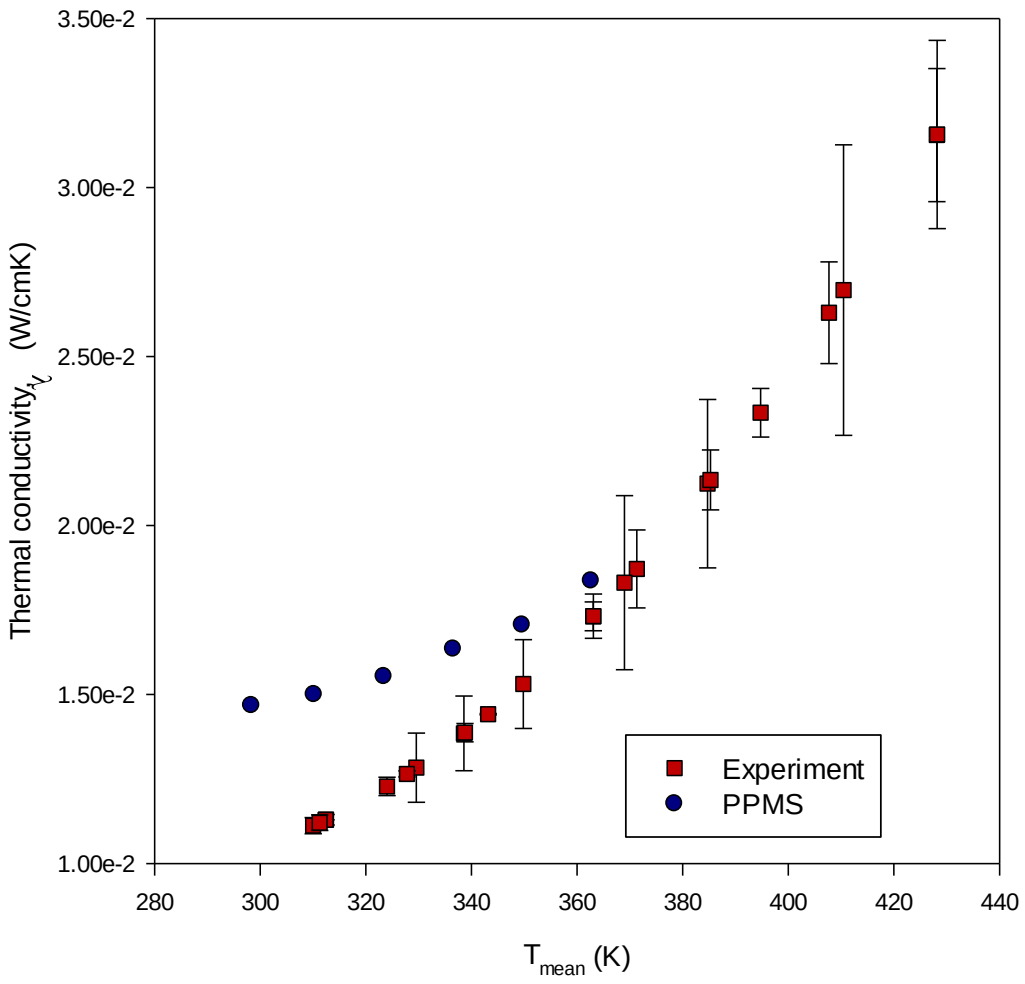

Figure 5.23: An average thermal conductivity of Sample C obtained from four different sets of measurements (S1, S2, S3 and S4) as comparison with PPMS measurement data [Appendix 11] as material reference as a function of T_{mean}.

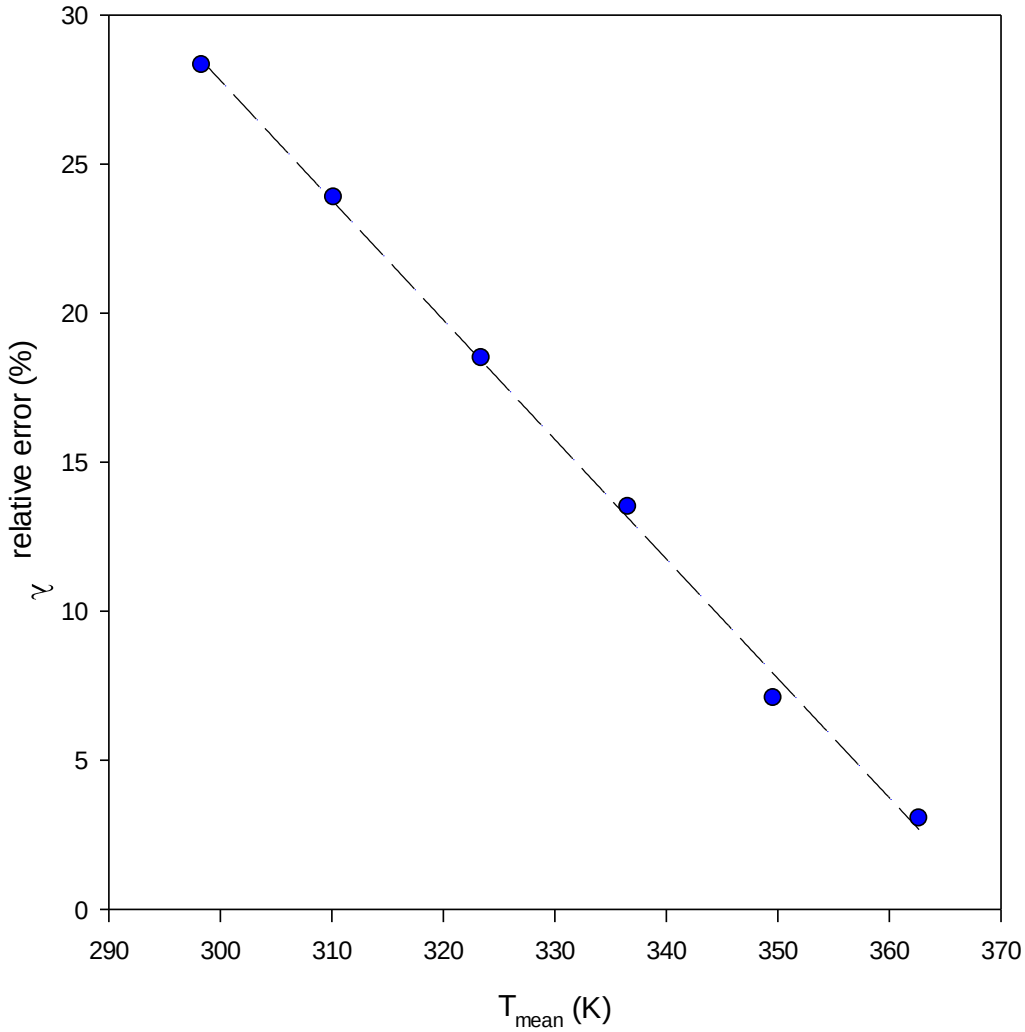

Figure 5.24: Percentage of thermal conductivity relative error as compared with material reference as a function of T_{mean}.

Compromise has been made between longer heat flux meter and heat loss along the meter. That is also the reason why reduction in ZT looks more rapidly from the reference materials. Thermal conductivity could also be calculated from equation 4.13 using total heat flow to the sample using brass rod conductance, $K_b = 10.7 \times 10^{-3}\ W/K$ (taken $\lambda_b = \frac{1.09W}{cmK}, l = 0.8\ cm$ and $A = \pi j^2$; with $j = 0.05$ cm). It is found out that the results are similar with thermal conductivity obtained using Z, α and ρ measurements. This gives an indication that the heat loss across heat flow meter is almost negligible as a result of vacuum usage as compared in module measurement where heat loss is significant.

5.8 Conclusion

The large temperature difference facility for measuring ZT of a thermoelement using the proposed novel technique has been successfully developed. The design allows for both types of measurement (small ΔT and large ΔT) by appropriate control of heater and cooling stage. Measurement can be done on different cross sectional area of samples without major changes to the facility. However, the facility operating temperature is limited due to brass rod properties.

The facility successfully demonstrates ZT measurement using the proposed technique for thermoelements. ZT of n-type Bi_2Te_3 under small ΔT measurement showed acceptable agreement with a similar sample measure using commercial PPMS equipment. Good repeatability was achieved with an

error of less than 10% and 7% under small and large ΔT respectively. On the other hand, the accuracy of ZT measurement suggested a 13% to 32% deviation from the reference sample. In addition, the Seebeck coefficient and electrical resistivity can also be measured, although noticeable deviations are observed.

CHAPTER 6

Results and Discussions

6.1 Introduction

Following the successful development of the proposed measurement technique on thermoelement, a number of carefully selected samples were investigated using the new apparatus. In this chapter, measurement results are presented and discussed. The key focuses of this investigation are 1) to confirm if there exists, in general, a noticeable difference in ZT evaluation between measurements under a large ΔT and those under a small ΔT; 2) to identify possible factors that are responsible for the observed differences.

6.2 Samples

A number of samples were used in the study of ZT measurement under a large ΔT. These include homogeneous thermoelements of an n-type (sample C) and a p-type (sample D) Bi_2Te_3 and three segmented samples of an n-type BiTe+PbTe (sample E), p-type BiTe+TAGS-85 (sample F) and p-type BiTe+TAGS-80 (sample G). The Bi_2Te_3 samples were made previously by the Cardiff thermoelectric group. Samples E and F (segmented) were supplied by Zhejiang University, China. Sample G was formed by joining sample D to a TAGS-80 (from Zhejiang University) using an indium contact. The exact compositions for the n-

type segmented sample were made up from $Bi_2Se_{0.9}Te_{2.1}$ and $Pb_{9.6}Sb_{0.2}Te_2Se_8$. The composition for the p-type segmented sample were $Bi_{0.5}Sb_{1.5}Te_3$ and $(AgSbTe_2)_{15}(GeTe)_{85}$. Both were prepared using the SPS method. A summary of the samples employed in this study is given in Table 6.1 below.

Table 6.1: Type and dimensions of the samples used in the experiments.

Sample	Structure	Material	Type/No. of legs	Cross sectional area (mm^2)	Thickness (mm)
A	Module	Bi_2Te_3	127	1.4×1.4	1.71
B	Module	Bi_2Te_3	127	1.4×1.4	1.15
C	Single	Bi_2Te_3	n-type	3.0×3.0	8.00
D	Single	Bi_2Te_3	p-type	3.0×3.0	8.00
E	Segmented	Bi_2Te_3+PbTe	n-type	2.0×2.0	10.00
F	Segmented	Bi_2Te_3+TAGS-85	p-type	2.0×2.0	5.00
G	Segmented	Bi_2Te_3	p-type	3.0×3.0	8.00
		TAGS-80	p-type	1.5×3.0	7.00

6.3 Sample Resistivity at Room Temperature

As discussed in chapter 5, it is necessary to obtain the resistance of the tested samples at room temperature for ZT calculation. The resistance of each sample was measured using an apparatus developed by Srivatsan [108]. The measurement was carried out using a small ac signal of <10 mA for the single element and <100 mA for segmented element samples, with frequency ranging between 100-500 Hz. The results are shown in Table 6.2.

Table 6.2: Electrical resistivity of all samples measured at room temperature.

Sample	Structure	Material	Frequency (Hz)	Current (mA)	Electrical Resistivity (Ωcm)	Resistance (Ω)
C	Single leg	n-BiTe	100	9.43	1.368×10^{-3}	12.16×10^{-3}
D	Single leg	p-BiTe	100	6.59	1.008×10^{-3}	8.24×10^{-3}
E	Segmented	n-BiTe	400	22	1.318×10^{-3}	6.59×10^{-3}
		n-PbTe	400	22	8.358×10^{-4}	5.11×10^{-3}
F	Segmented	p-BiTe	300	91.2	1.552×10^{-3}	9.7×10^{-3}
		p-TAGS 85	300	91.2	7.84×10^{-4}	4.9×10^{-3}
G	Segmented	p-BiTe	100	6.59	1.008×10^{-3}	8.24×10^{-3}
		p-TAGS 80	500	91.2	0.801×10^{-3}	12.46×10^{-3}

6.4 Module Measurement Results

ZT results for sample A (thermoelectric module) under small ΔT and large ΔT obtained in chapter 3 are shown in Figure 6.1 for comparison. The plotted ZT are calculated based on equation 4.9 with measurement data for small and large ΔT can be obtained in Appendix 2 and 3. It can be seen that the ZT of the module starts at 0.65 at room temperature and then shows an increasing trend as the mean temperature increases. Large ΔT measurements show a much slower increase in ZT than small ΔT measurements for the same mean temperature. Large ΔT measurements then continue to increase up to ΔT= 110 K while the ZT of small ΔT starts to decrease at a temperature of 341 K.

A similar test was performed on another module of the same cross sectional area, sample B. The result is shown in Figure 6.2, with both curves showing an increasing ZT with increasing mean temperature. It can be seen that ZT behaviour is similar with to that observed in sample A but the ZT of large ΔT became bigger than that of small ΔT for temperature above 336 K. The ZT of sample B is much lower than sample A, with 0.52 at room temperature. It is noted that the ZT for this module degrades after it has operated at a high temperature for a period of time. The initial measurement of large ΔT shows ZT as high as 0.57 can be achieved at a temperature of 304 K as represented by solid triangle in Figure 6.2. Measurement data for sample B can be obtained at Appendix 7 and 8.

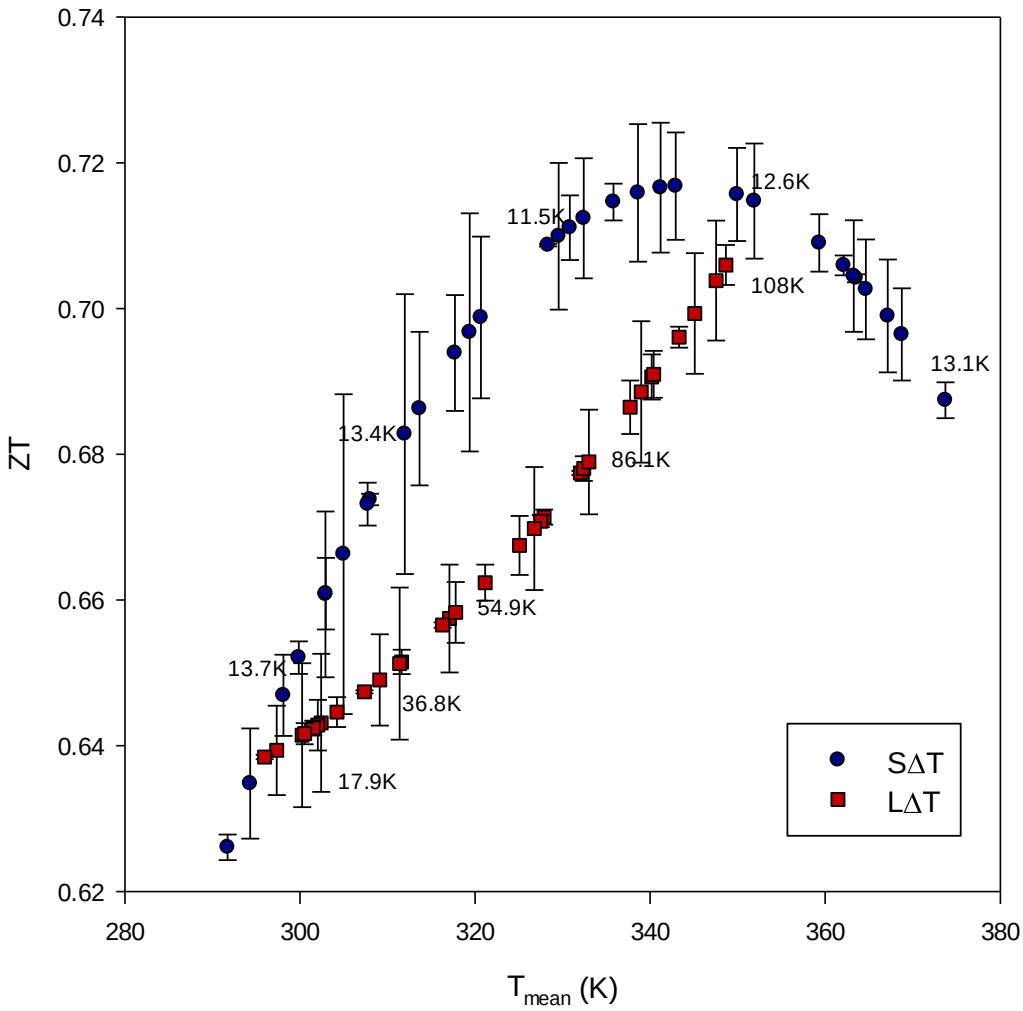

Figure 6.1: An average ZT (from 4 set of measurements for SΔT and LΔT) as a function of mean temperature for Sample A. The dots represent the ZT value obtained under constant ΔT (small ΔT); the solid square represent the ZT values measured under increased ΔT (large ΔT).

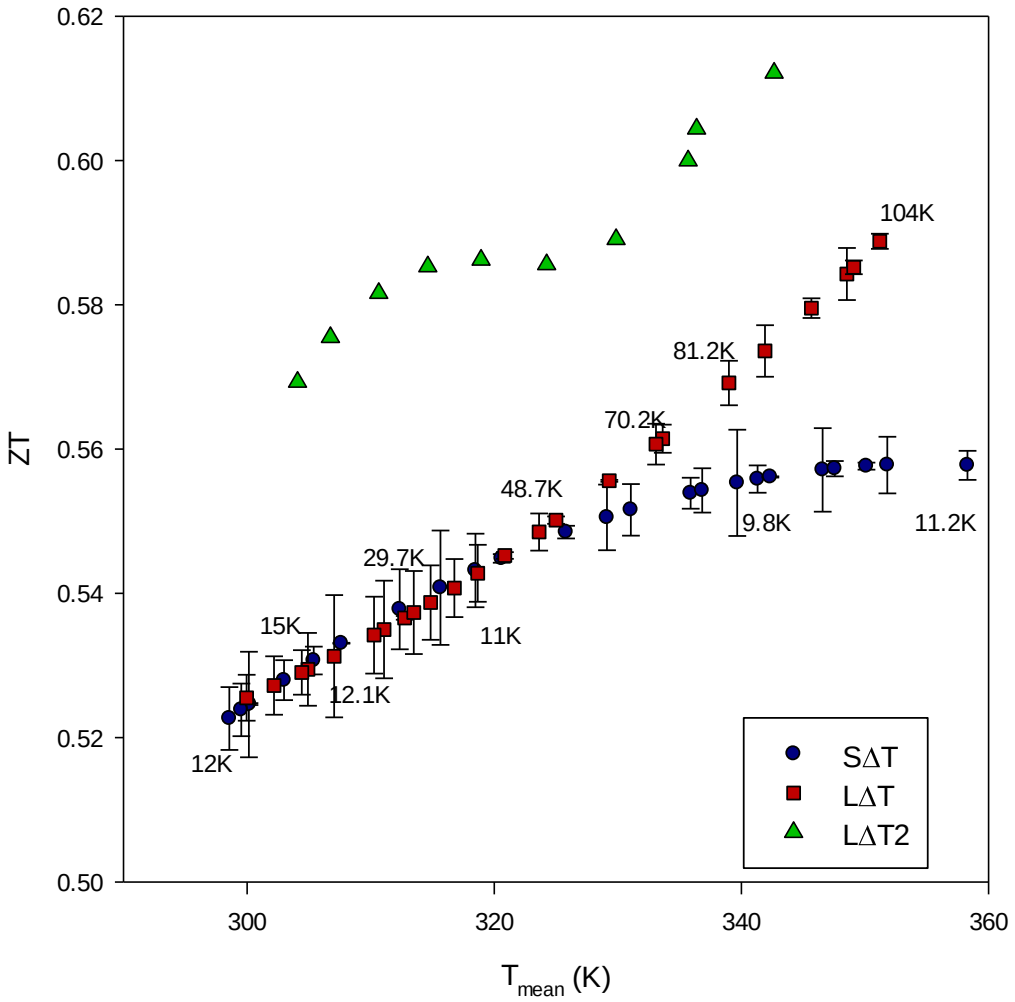

Figure 6.2: An average ZT (from 4 sets of measurements of SΔT and LΔT) as a function of mean temperature for Sample B. The dots represent the ZT value obtained under constant ΔT (small ΔT); the solid square represent the ZT values measured under increased ΔT (large ΔT) and the triangle represents initial large ΔT measurement.

6.5 Single and segmented ZT measurements

ZT measurement for single leg thermoelement and segmented materials is obtained based on equation 5.4. For single leg measurements of samples C and D, the temperature difference was set between 11-38 K for a small ΔT while those under large ΔT were measured at up to 243 K for sample C and to 210 K for sample D. (Measurements data for sample C and D can be found in Appendix 9, 10 and 12, 13 respectively.)

The ZTs of n-type and p-type Bi_2Te_3 samples are shown in Figure 6.3 and 6.4 respectively. Small ΔT measurements for both samples show a decrease in ZT with increasing mean temperature. When the large ΔT measurement of sample C was compared to the small ΔT measurements, ZT initially shows an increasing trend up to a temperature of 344 K before decreasing, following the same trend as small ΔT. On the other hand, the ZT for sample D did not show any significant difference with measurements under small ΔT except toward the end of the temperature range.

Measurements on the segmented thermoelectric structure were investigated for n-type and p-type of sample E, F and G. Sample E consisted of Bi_2Te_3 and PbTe materials, sample F consist of Bi_2Te_3 and TAGS-85 materials and sample G consist of Bi_2Te_3 and TAGS-80 materials. Since samples E and F were made from nanostructure materials using the SPS method, sample G which was joined together using an indium layer will be used as a reference material to study the segmentation influences toward the final result.

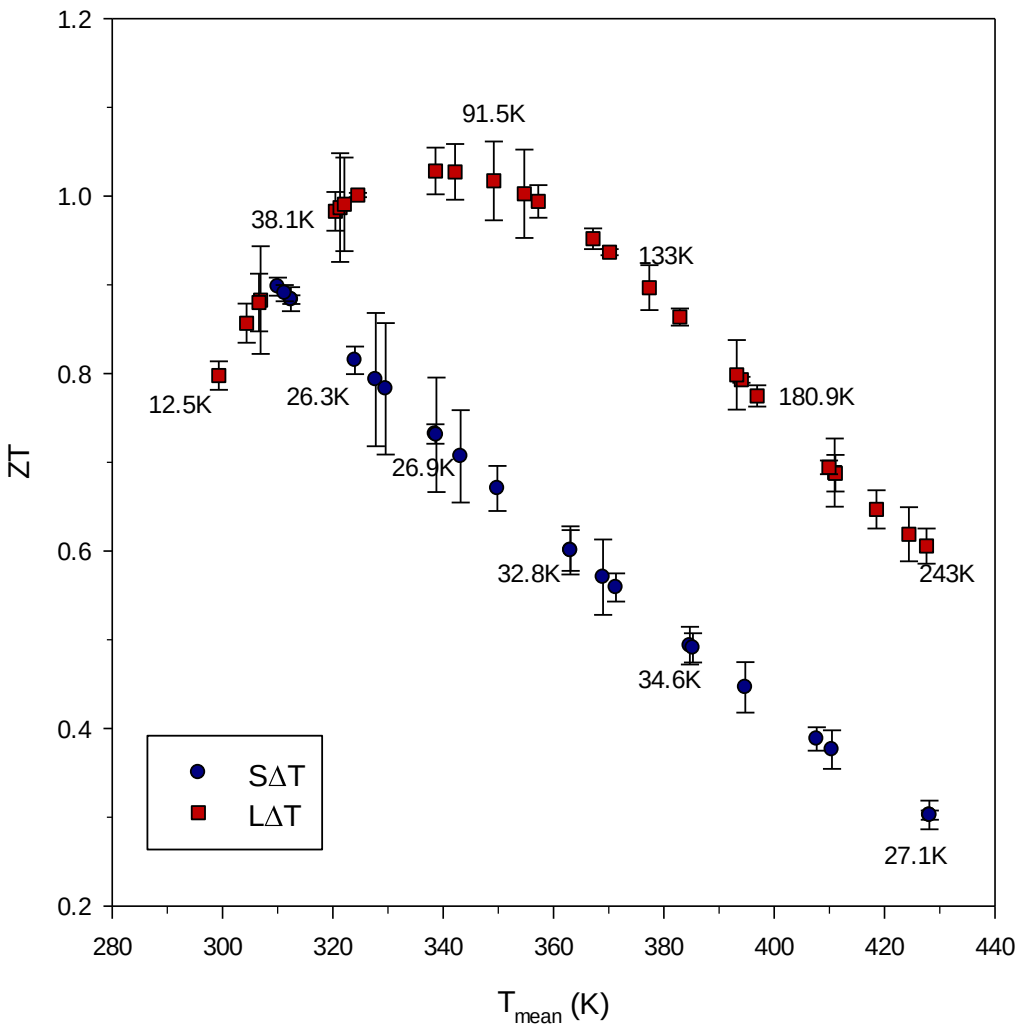

Figure 6.3: An average (from 5 sets of measurements for SΔT and 4 sets for LΔT) ZT as a function of mean temperature for Sample C. The dots represent the ZT value obtained under small ΔT; the solid square represents the ZT values measured under increased ΔT (large ΔT).

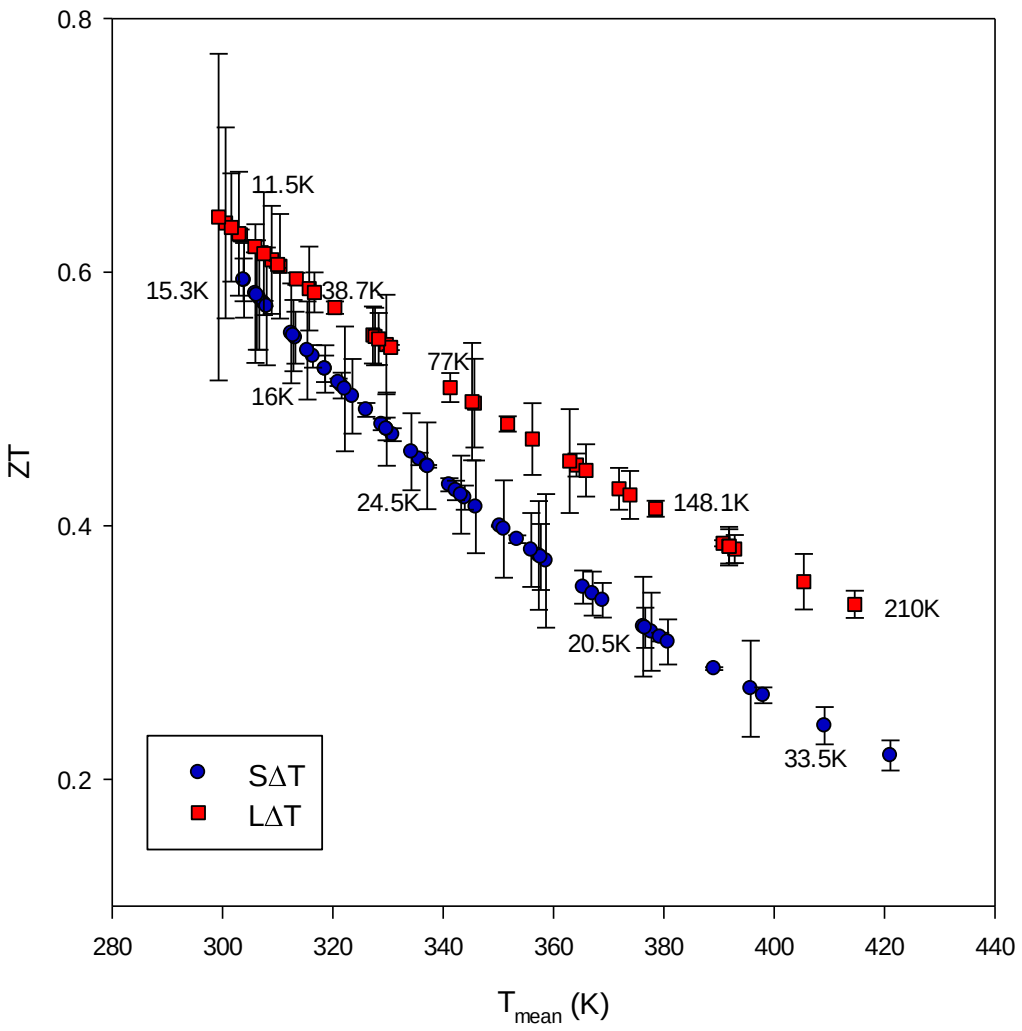

Figure 6.4: An average (from 8 sets of measurements for SΔT and 5 sets for LΔT) ZT as a function of mean temperature for Sample D. The dots represent the ZT value obtained under small ΔT; the solid square represents the ZT values measured under increased ΔT (large ΔT).

The segmented samples were arranged in such way that the low temperature material (Bi_2Te_3) was located at the cold side while the high temperature materials (PbTe or TAGS-85 or TAGS-80) were located at the hot side. ZT results for sample E and F are plotted in Figures 6.5 and 6.6. For sample E, no significant difference was observed between large and small ΔT measurements for the same mean temperature. Under large ΔT, that ZT showed an increase from a measurement at ΔT= 26 K to ΔT= 94 K before starting to decrease with further increase in mean temperature. Temperature difference for small ΔT measurement was set at a much higher than homogenous sample to the range 64-77 K to reduce the error. Sample F observed a significant difference between large ΔT and small ΔT measurements. ZT obtained from large ΔT measurements increases up to ~0.6 at ΔT= 101 K, and then decreases to 0.27 at ΔT= 237 K. ZT obtained from small ΔT decreases monotonically from 0.4 to 0.13 when measured under ΔT~56-79 K. (Measurement data for sample E and F can be obtained in Appendixes 14-17).

The segmented sample G was made in-house by putting together Bi_2Te_3 sample of dimension 3mm×3mm×8mm (from sample D) and a TAGS-80 sample of dimensions 1.5mm×3mm×7mm with an indium layer in between. The result (Appendix 18) is plotted in Figure 6.7. Temperature differences for measurement under small ΔT were set at ΔT ~30 K; while T_c of measurements under large ΔT were set at ~300 K. In this sample, a significant difference can be seen between ZT under large ΔT measurements and that under small ΔT measurements.

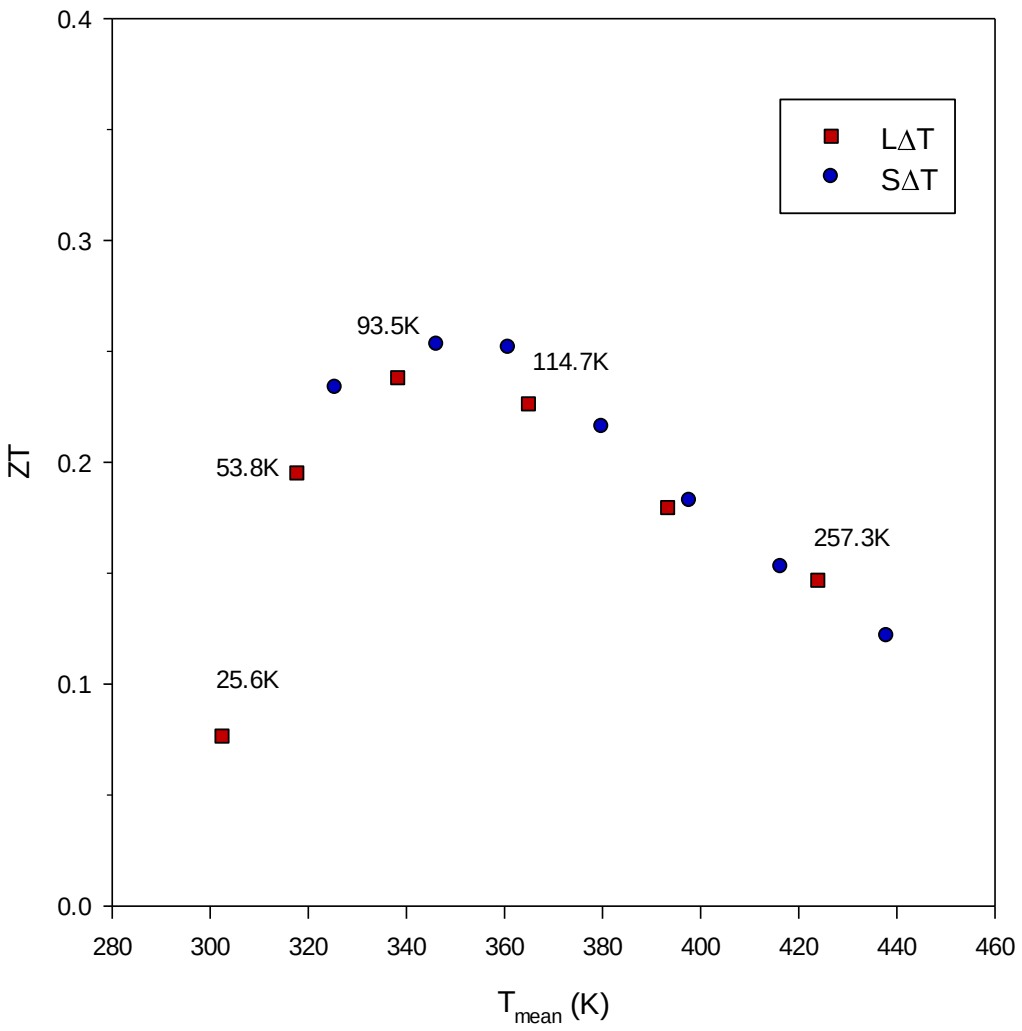

Figure 6.5: ZT as a function of mean temperature for Sample E with Bi_2Te_3 at the cold side. The dots represent the ZT value obtained under a small ΔT; the solid squares represent ZT values measured under an increased ΔT (large ΔT).

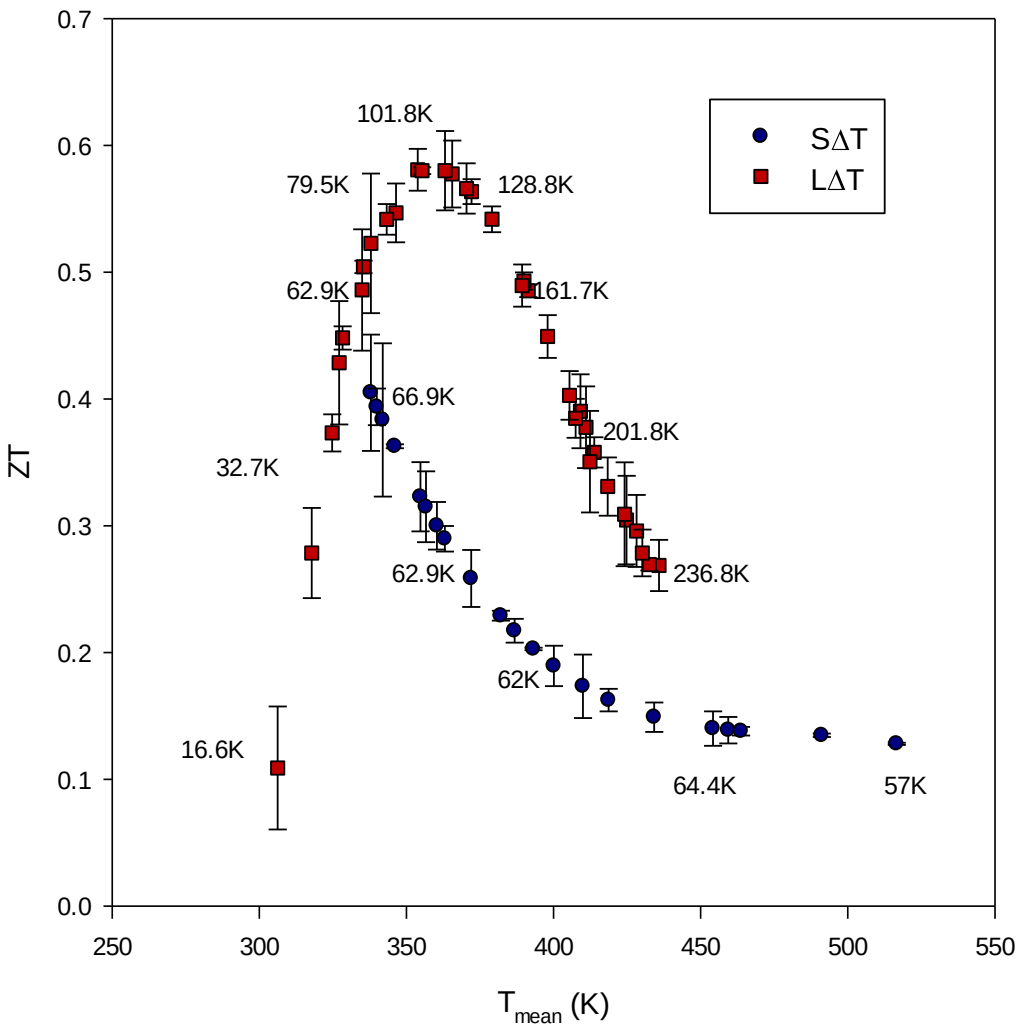

Figure 6.6: An average (from 5 sets of measurements for SΔT and 7 sets for LΔT) of ZT as a function of mean temperature for sample F with Bi_2Te_3 at the cold side. The dots represent the ZT value obtained under small ΔT; the solid squares represent ZT values measured under an increased ΔT (large ΔT).

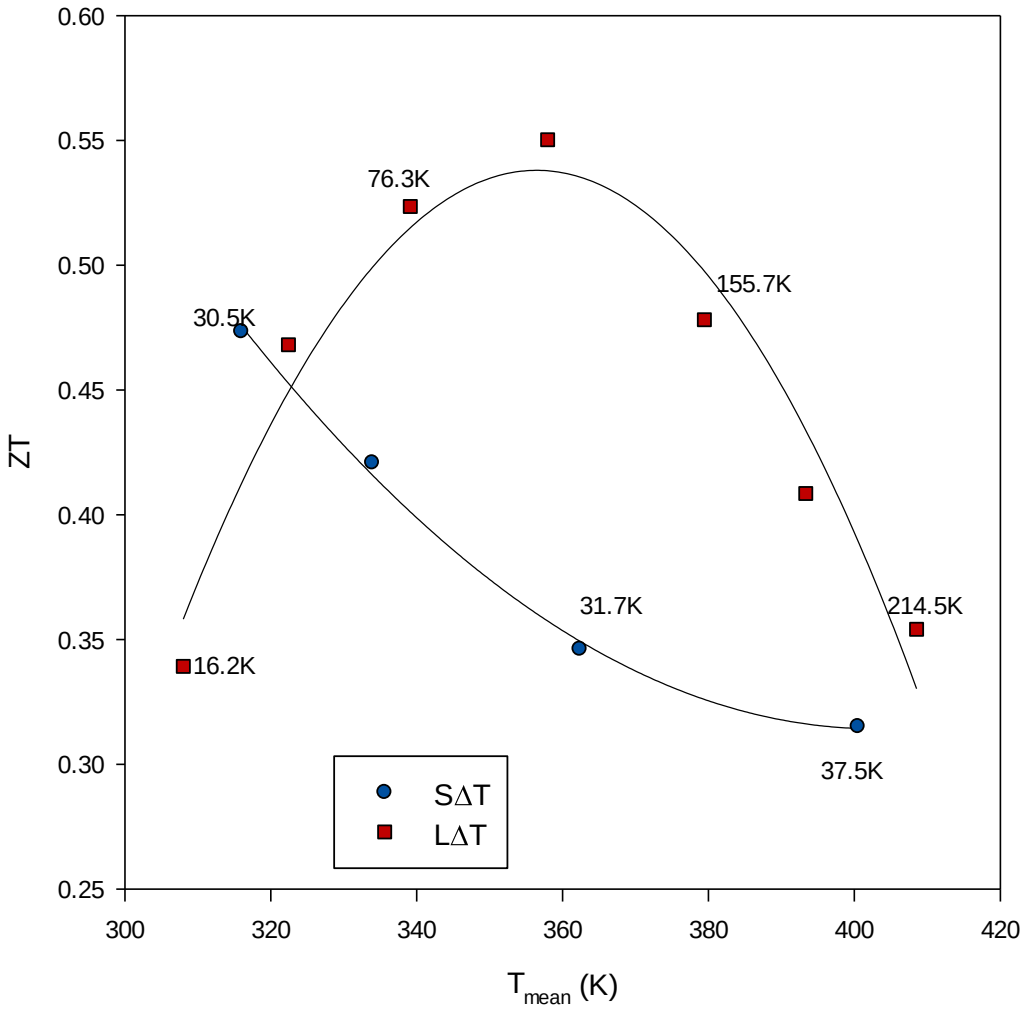

Figure 6.7: ZT as a function of mean temperature for Sample G with Bi_2Te_3 at the cold side. The dots represent the ZT value obtained under a small ΔT; the solid squares represent ZT values measured under an increased ΔT (large ΔT).

6.6 Influence of material "polarity"

The portion of segmented materials in contact with the hot or cold sides was investigated by flipping the sample position by 180°, so that the higher temperature portion (PbTe or TAGS-85) was placed at the cold side while the lower temperature portion (Bi_2Te_3) was place at the hot side. This is referred to as changing the "polarity". The results of measurement for both samples E and F are shown in Figures 6.8 and 6.9, respectively.

The ZT of samples E and F under small ΔT measurements behave almost the same when the sample is change in polarity. Temperature differences for small ΔT measurements were set at 34-38 K and 41-52 K respectively. However, large ΔT measurements show an increase of up to ΔT= 240 K when Bi_2Te_3 was at the hot side. By contrast, sample F did not show a significant difference under large ΔT except towards the end of the temperature range. It is anticipated that ZT obtained under large ΔT should be significantly higher than that obtained under small ΔT for both samples E and F. However, this was not observed in all of the measurement results. In order to understand the reasons behind this, a detail knowledge of samples E and F are needed. Unfortunately, this is not readily available and is outside the scope of this project.

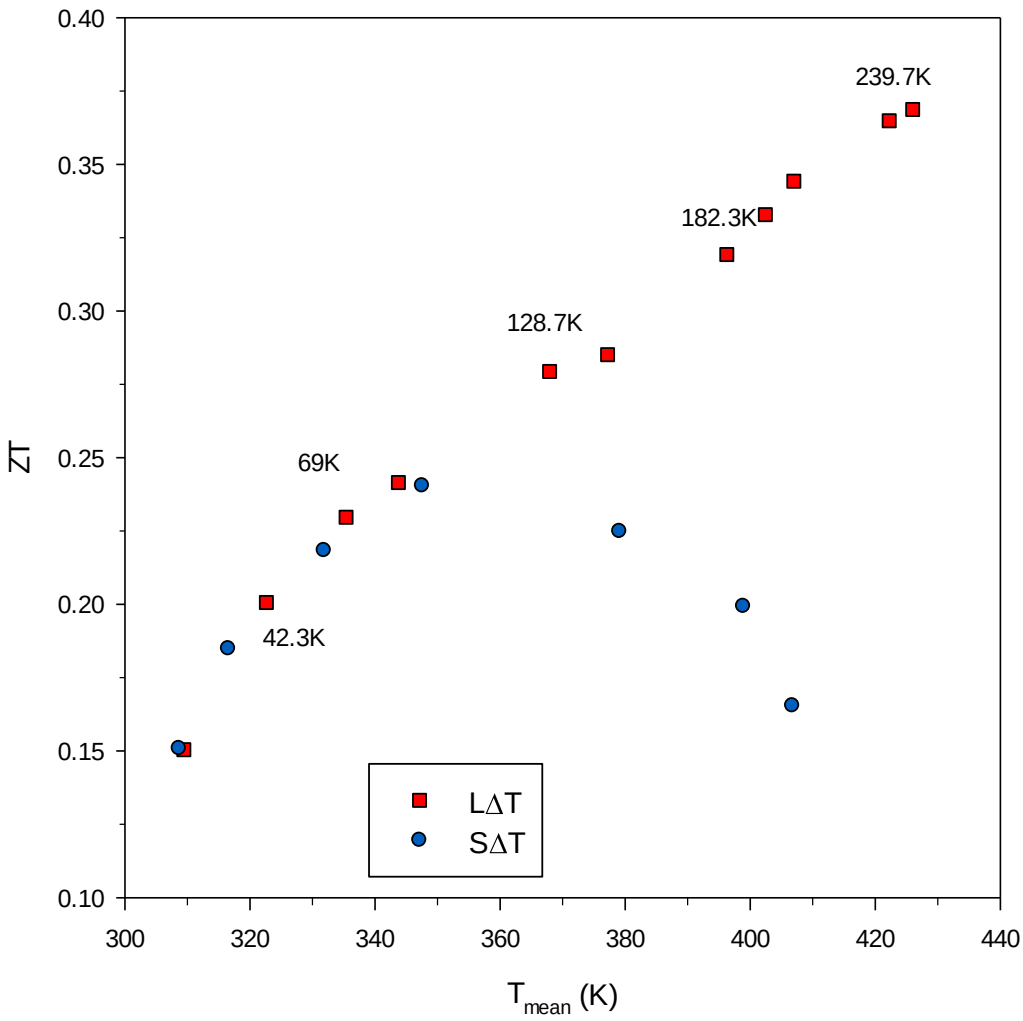

Figure 6.8: ZT as a function of mean temperature for Sample E with Bi_2Te_3 at the hot side. The dots represent the ZT value obtained under small ΔT; the solid squares represent ZT values measured under an increased ΔT (large ΔT).

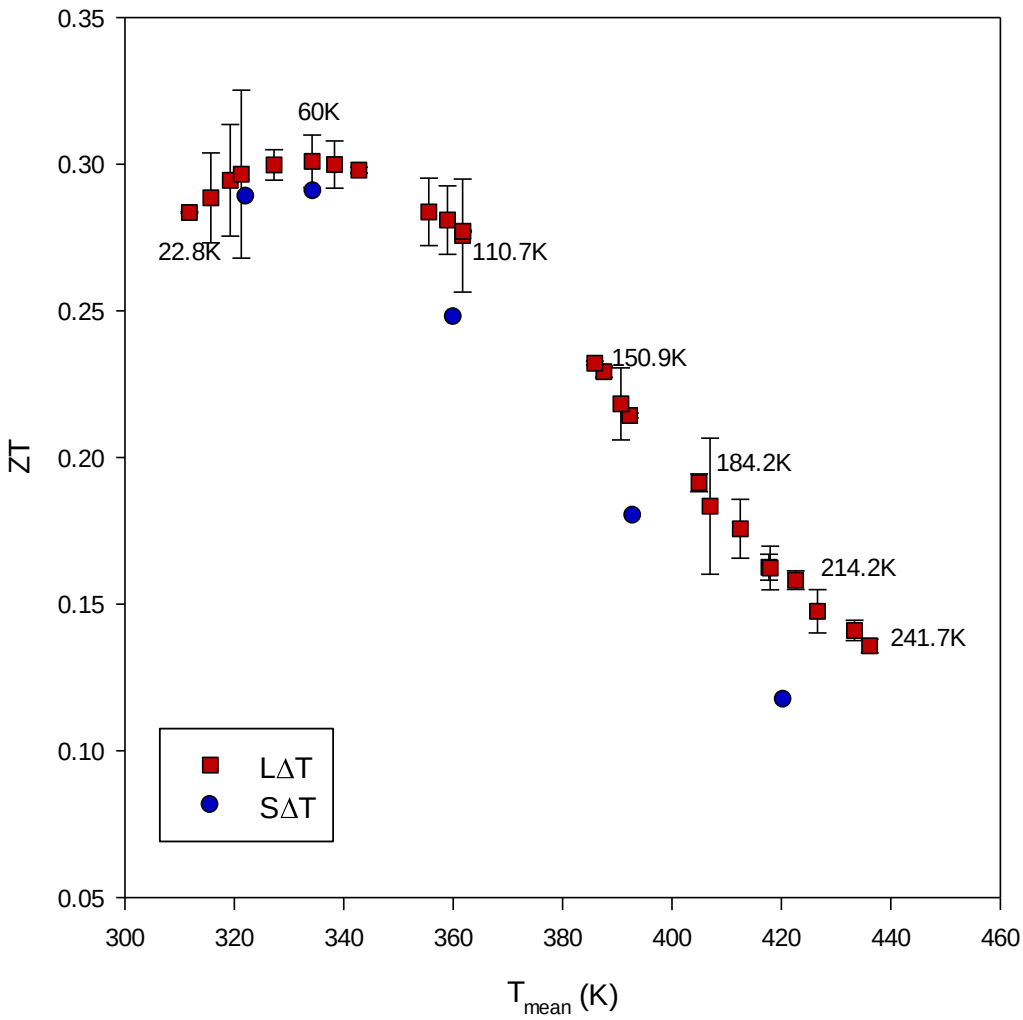

Figure 6.9: An average (from 7 sets of measurements for LΔT) ZT as a function of mean temperature for sample F with Bi_2Te_3 at the hot side. The dots represent the ZT value obtained under small ΔT; the solid squares represent the ZT values measured under an increased ΔT (large ΔT).

It can be seen from Figure 6.6 that sample F (Bi_2Te_3+TAGS-85) displayed a similar trend to sample G (as shown in Figure 6.7). This was expected due to the use of almost similar samples for both measurements. Consequently it was proved that the significant difference observed under both methods was not due to the change in properties of the segmented material made using the SPS technique. On the other hand, the polarity effect on this material cannot be further proved because no measurement was made on sample G when it was in the opposite position due to smaller size of TAGS-80 makes it difficult to hold the segment tightly without breaking the Bi_2Te_3/TAGS-80 junction.

6.7 Influence of contact material

As mentioned in chapter 5, platinum was chosen to replace indium as the contact material between sample and copper due to its high melting temperature and low electrical resistivity. However, platinum is not as soft as indium, which introduces gaps at the junction and thus increases the total contact resistance. To minimize this effect, a few layers of platinum were used. It was observed that the total electrical resistance at room temperature was increased by ~31-36% compared with that produced by the indium. The changes were observed using the 4-wire method. The total resistance using indium produced an average resistance of 0.040 Ω while total resistance using platinum produced an average resistance of 0.062 Ω.

The influence of indium and platinum contact materials on measured ZT values at higher temperature was also investigated. Measurements were made on the same n-type and p-type Bi_2Te_3 samples under large ΔT. Figures 6.10 and 6.11 show the results of indium and of platinum contacts on samples C and D respectively. It was shown that both contacts gave similar ZT despite the higher total resistance of the platinum contact. The maximum temperature difference measured using indium was <100 K because the melting point of the indium is 429.7 K.

6.8 Thermoelectric Transport Properties

Key thermoelectric transport properties include the Seebeck coefficient, α, electrical resistivity, ρ and thermal conductivity, λ. The Seebeck coefficient can be readily measured using this technique under large ΔT and small ΔT. The Seebeck coefficients of samples A and B are shown in Figures 6.12 and 6.13, respectively. The temperature difference for small ΔT measurement was kept in range 8-16 K for both modules, while T_c were maintained between 288-295 K and 293-300 K for samples A and B respectively, with a maximum achievable ΔT of ~110 K. It can be seen from the figures that for both modules, the Seebeck coefficients obtained under large ΔT measurements are lower than those obtained under small ΔT measurements as the mean temperature increases.

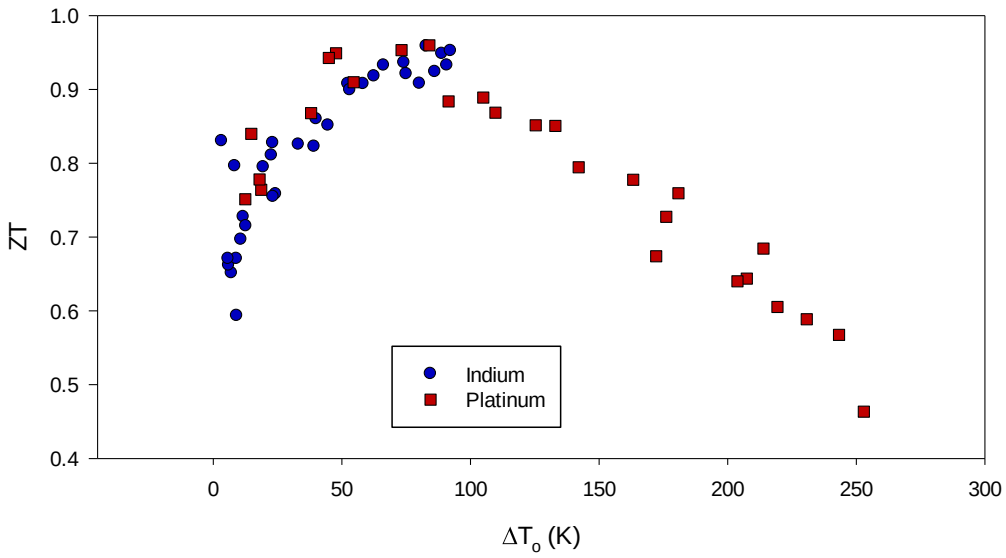

Figure 6.10: ZT measurements made under large ΔT on n-type Bi_2Te_3 (sample C) using indium and platinum as contact material.

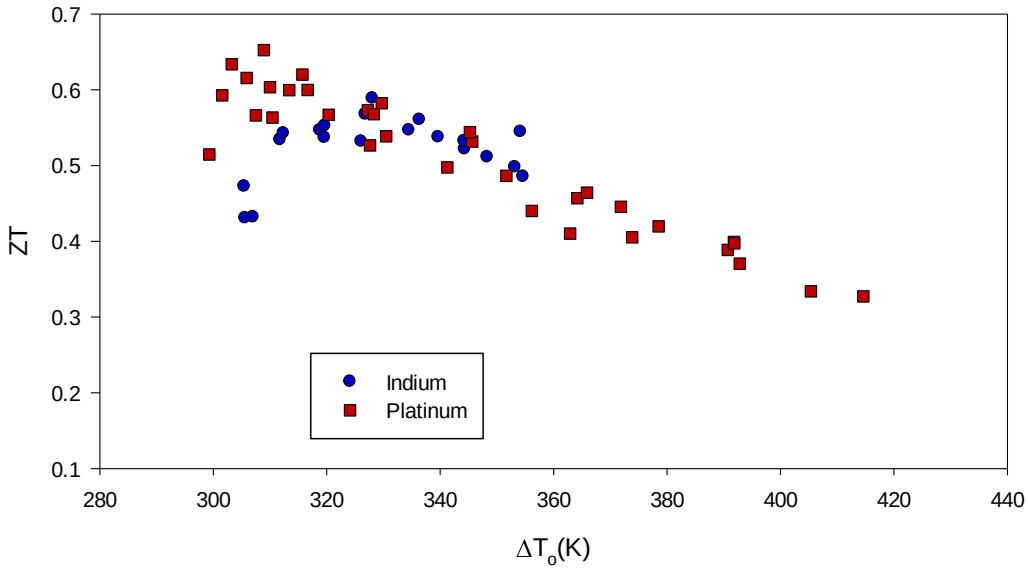

Figure 6.11: ZT measurements made under large ΔT on p-type Bi_2Te_3 (sample D) using indium and platinum as contact material.

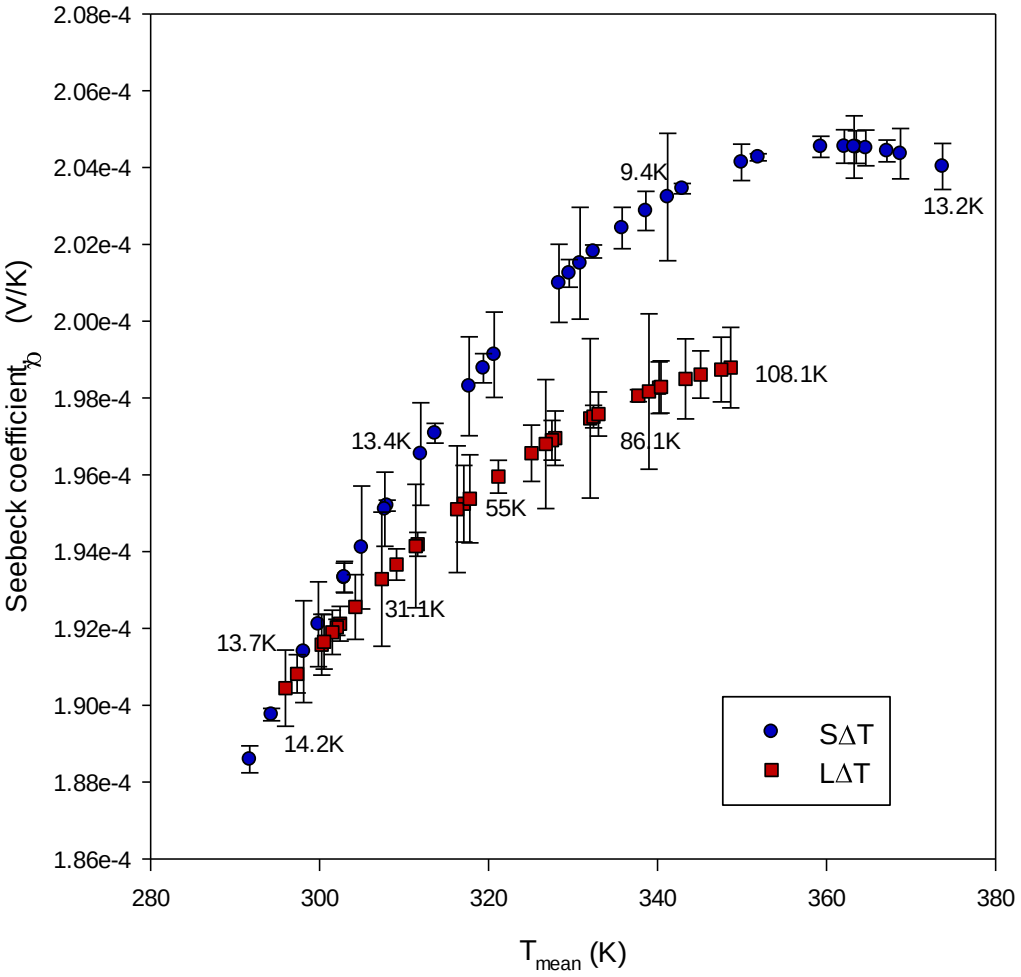

Figure 6.12: An average (from 7 sets of measurements for SΔT and 6 sets of LΔT) of the Seebeck coefficient of sample A under small ΔT and large ΔT.

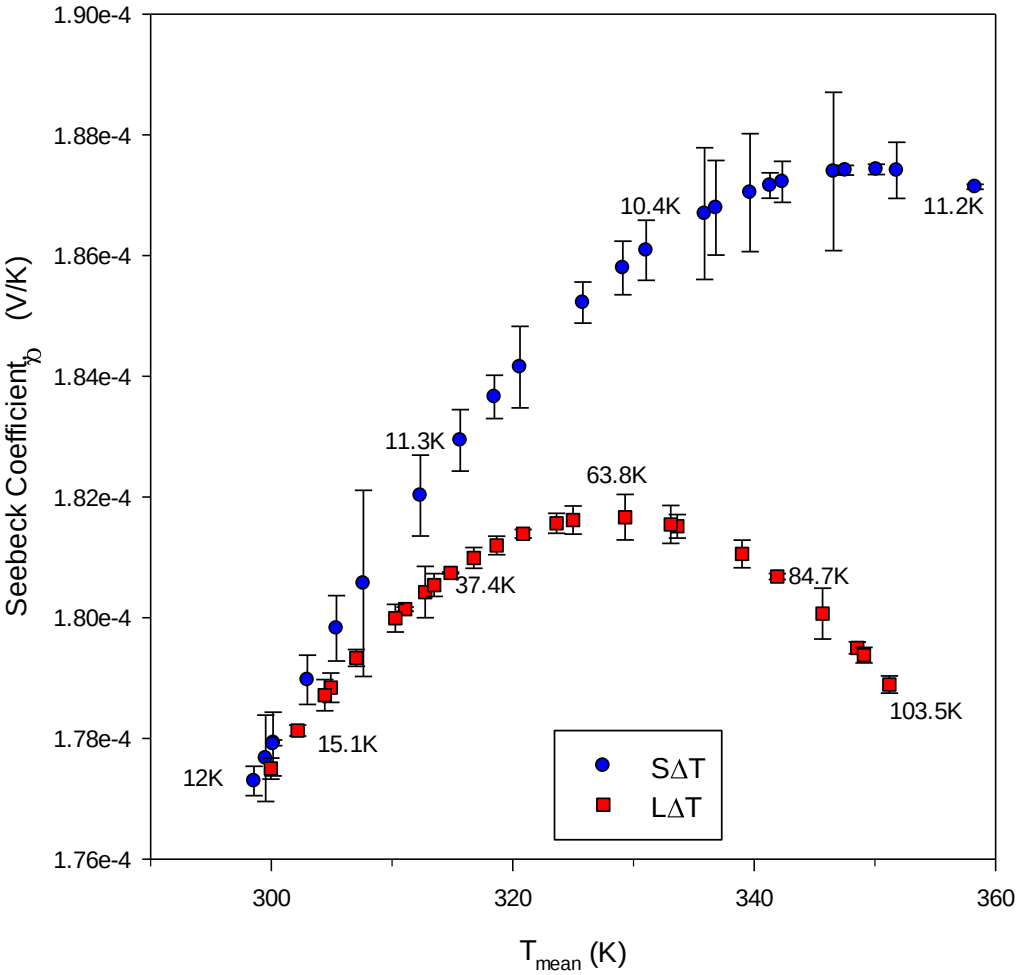

Figure 6.13: An average (from 4 sets of measurements for SΔT and LΔT) of the Seebeck coefficient of sample B under small ΔT and large ΔT.

Figures 6.14 and 6.15 show the Seebeck coefficient of n-type and p-type thermoelements for samples C and D. Similar to the behaviour observed in the modules, the Seebeck coefficient under large ΔT is lower than that under small ΔT for the same mean temperatures. For segmented samples, the Seebeck coefficients change with the material "polarity" as shown in Figures 6.16-6.20. When placing low temperature materials, Bi_2Te_3 parts of sample E and F at the cold side, the Seebeck coefficient under large ΔT measurements is bigger than small ΔT measurements under the same mean temperatures. It behaved in the opposite fashion when the polarity changed. Such behaviours are anticipated due to the inhomogeneity of the segmented samples. Unfortunately, an in-depth analysis of these results is not straight forward and is complicated by other factors. For example, it has been observed that the temperature profiles along the samples are non-linear for segmented samples as shown in Figure 6.21 (a) and (b). This may also contribute to the observed difference in α when changing the "polarity". Further investigations are needed.

$\rho\lambda$ can be calculated using Z and the Seebeck coefficient values, $\rho\lambda = \frac{\alpha^2}{Z}$. Figures 6.22 and 6.23 show $\rho\lambda$ values for samples A and B (thermoelectric modules), Figures 6.24-6.27 show the results for samples C, D, E and F (thermoelements), respectively. Except for sample E, all $\rho\lambda$ obtained under large ΔT were lower than those under small ΔT.

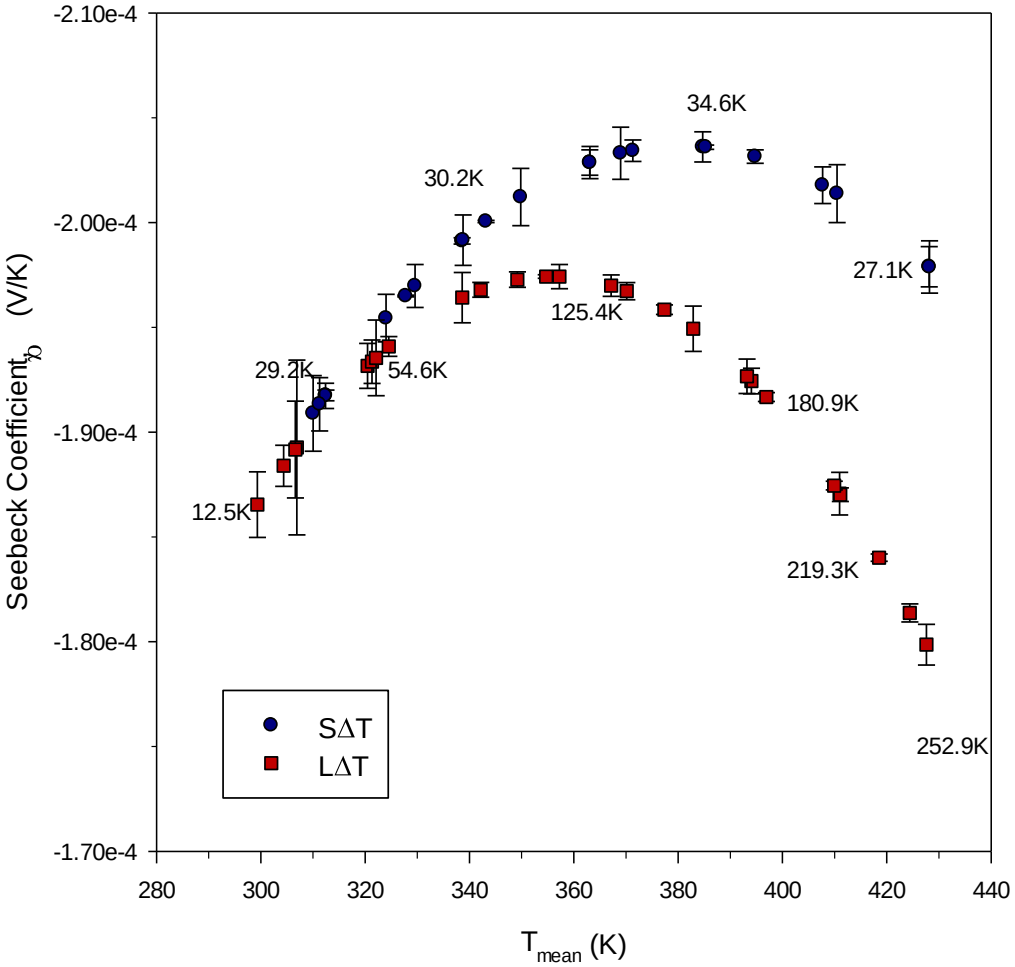

Figure 6.14: An average (from 4 sets of measurements for SΔT and LΔT) of the Seebeck coefficient for sample C under small ΔT and large ΔT.

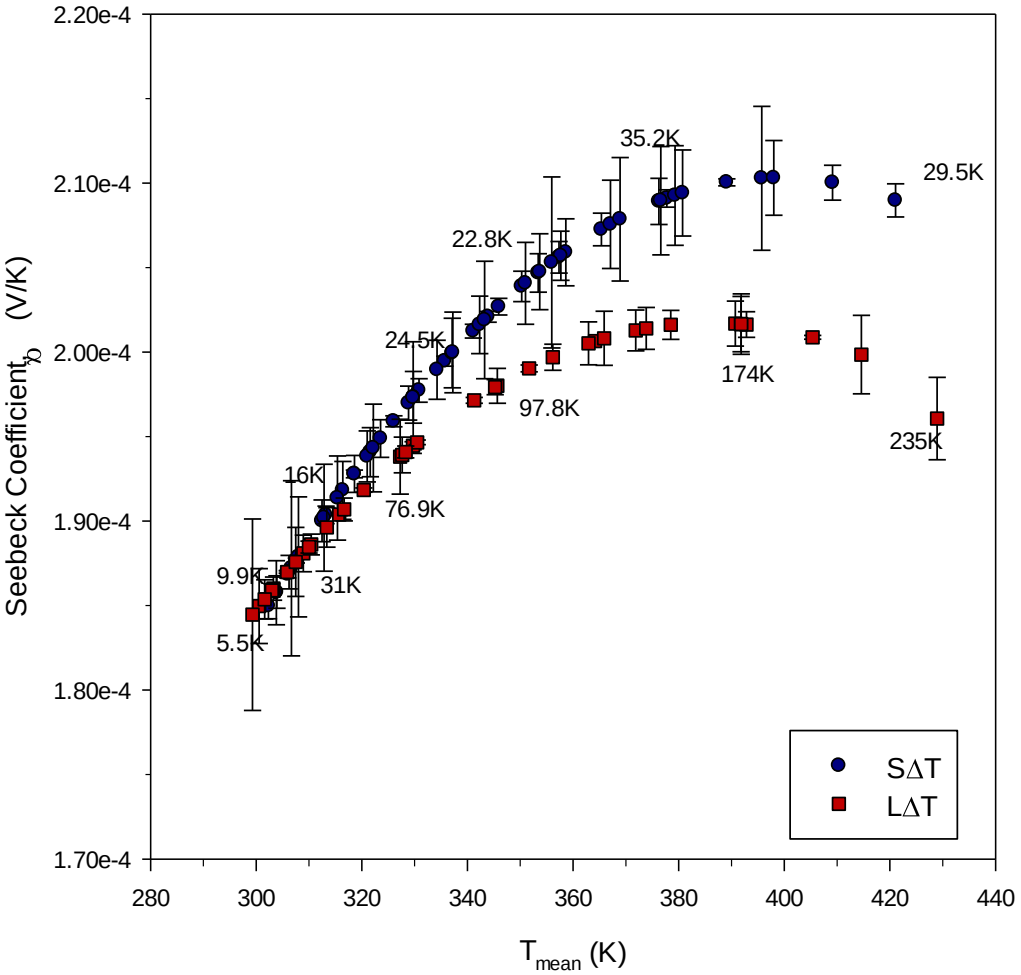

Figure 6.15: An average (from 8 sets of measurements for SΔT and 5 sets for LΔT) of the Seebeck coefficient for sample D under small ΔT and large ΔT.

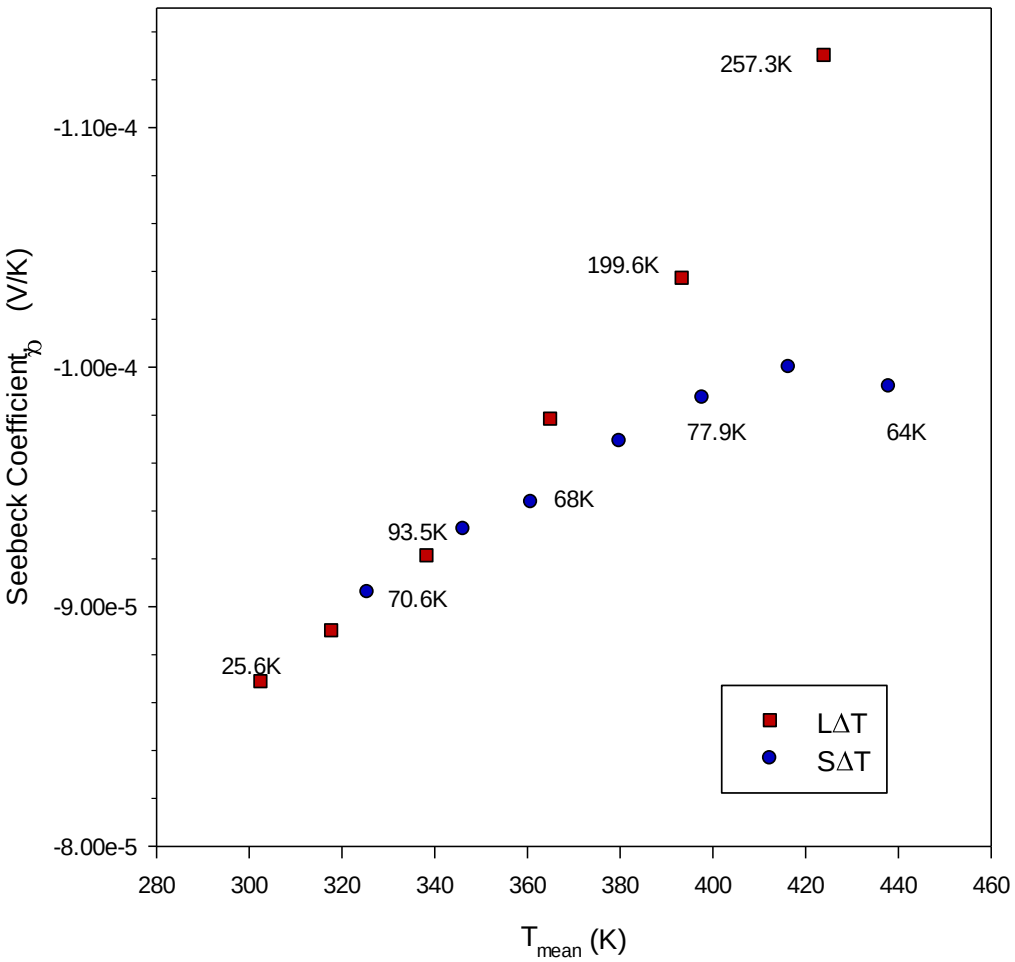

Figure 6.16: The Seebeck coefficient for sample E under small ΔT and large ΔT with the Bi_2Te_3 segment at the cold side.

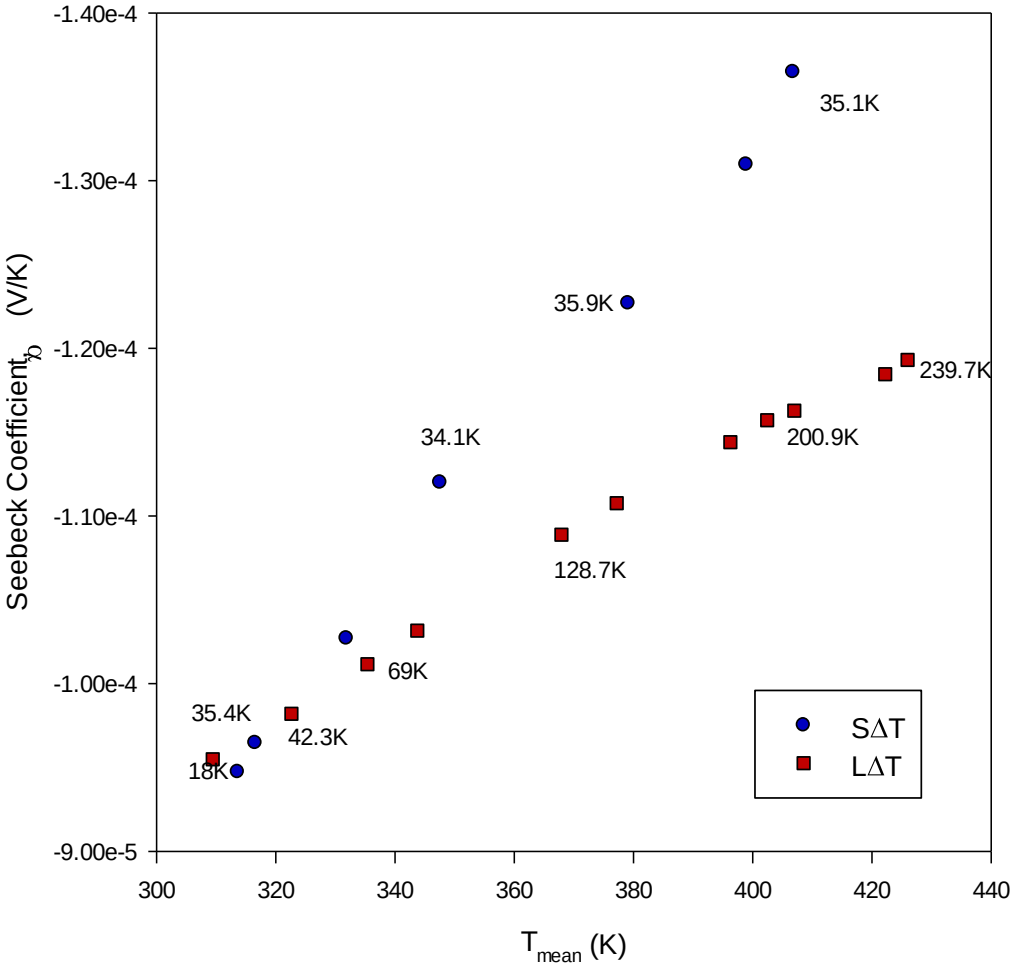

Figure 6.17: The Seebeck coefficient for sample E under small and large ΔT with the Bi_2Te_3 parts at the hot side.

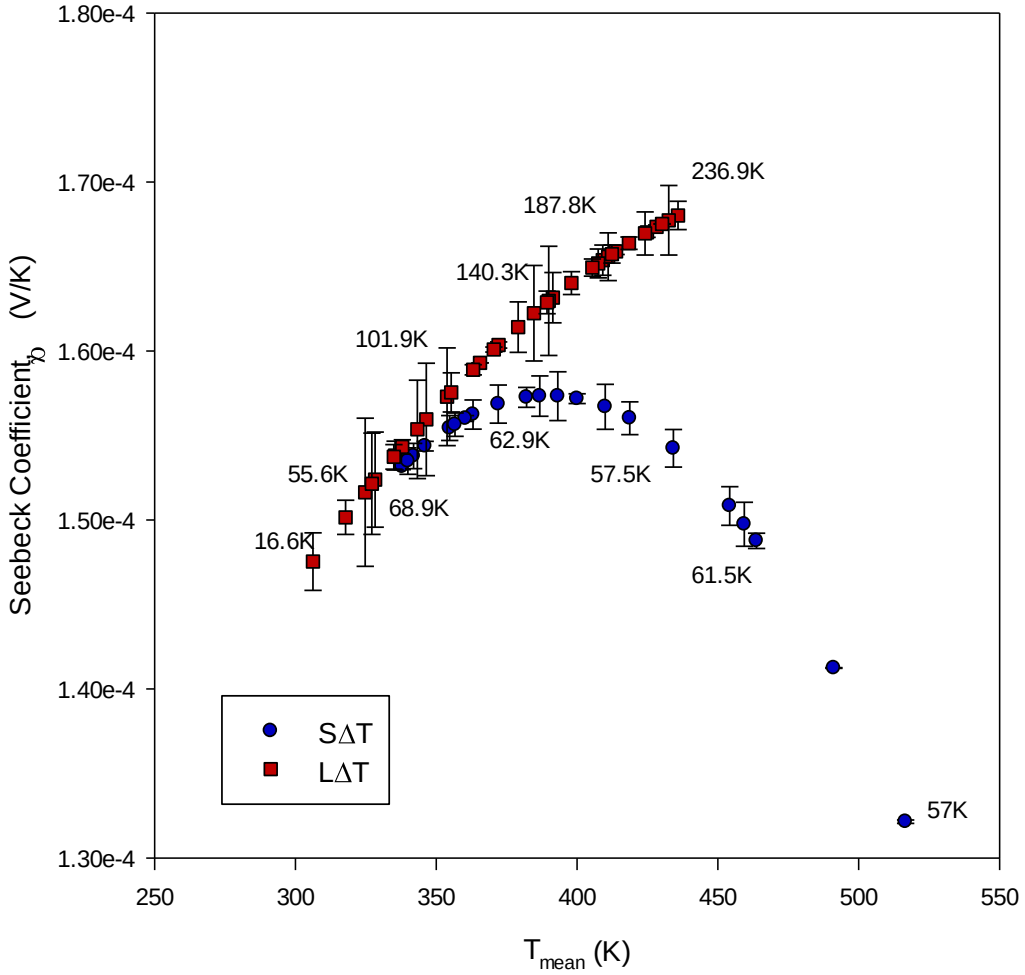

Figure 6.18: An average (from 5 sets of measurements for SΔT and 7 sets for LΔT) of the Seebeck coefficient for sample F under small and large ΔT with the Bi_2Te_3 part at the cold side.

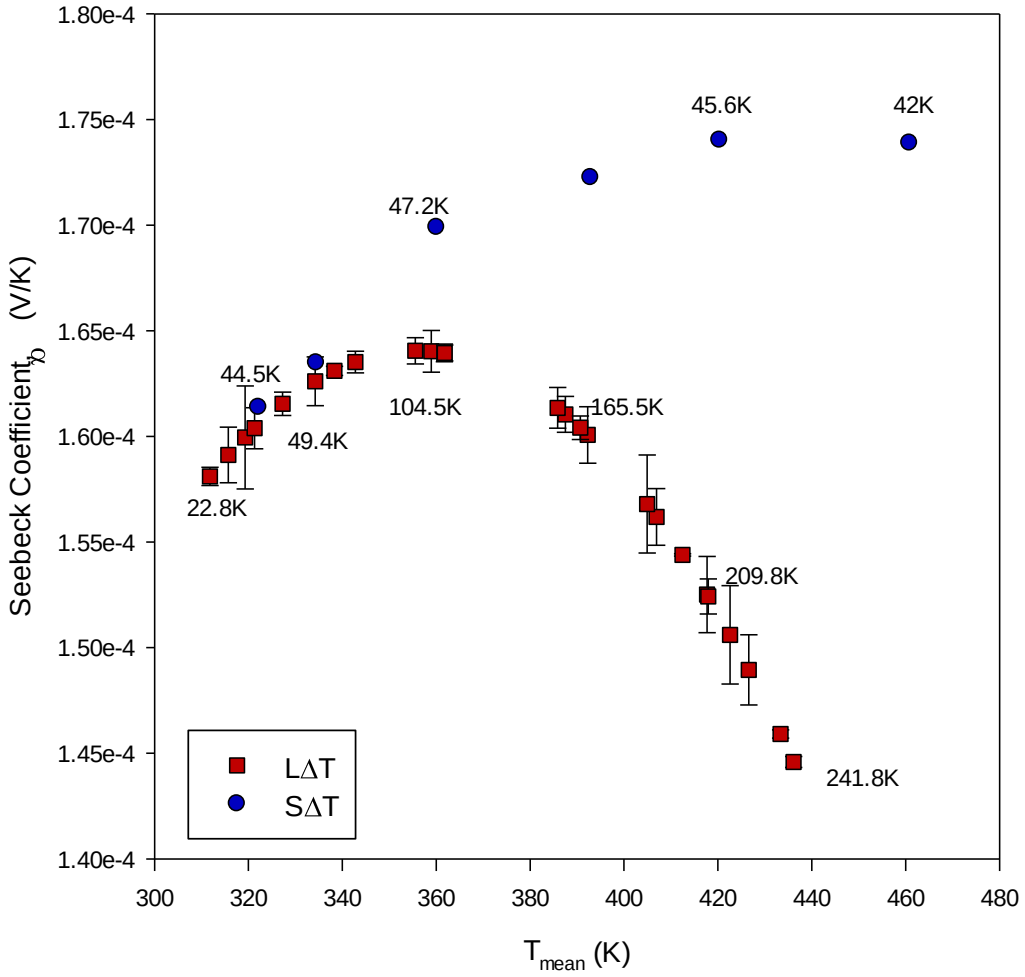

Figure 6.19: An average (from 4 sets of measurements for LΔT) of the Seebeck coefficient for sample F under small and large ΔT with the Bi_2Te_3 part at the hot side.

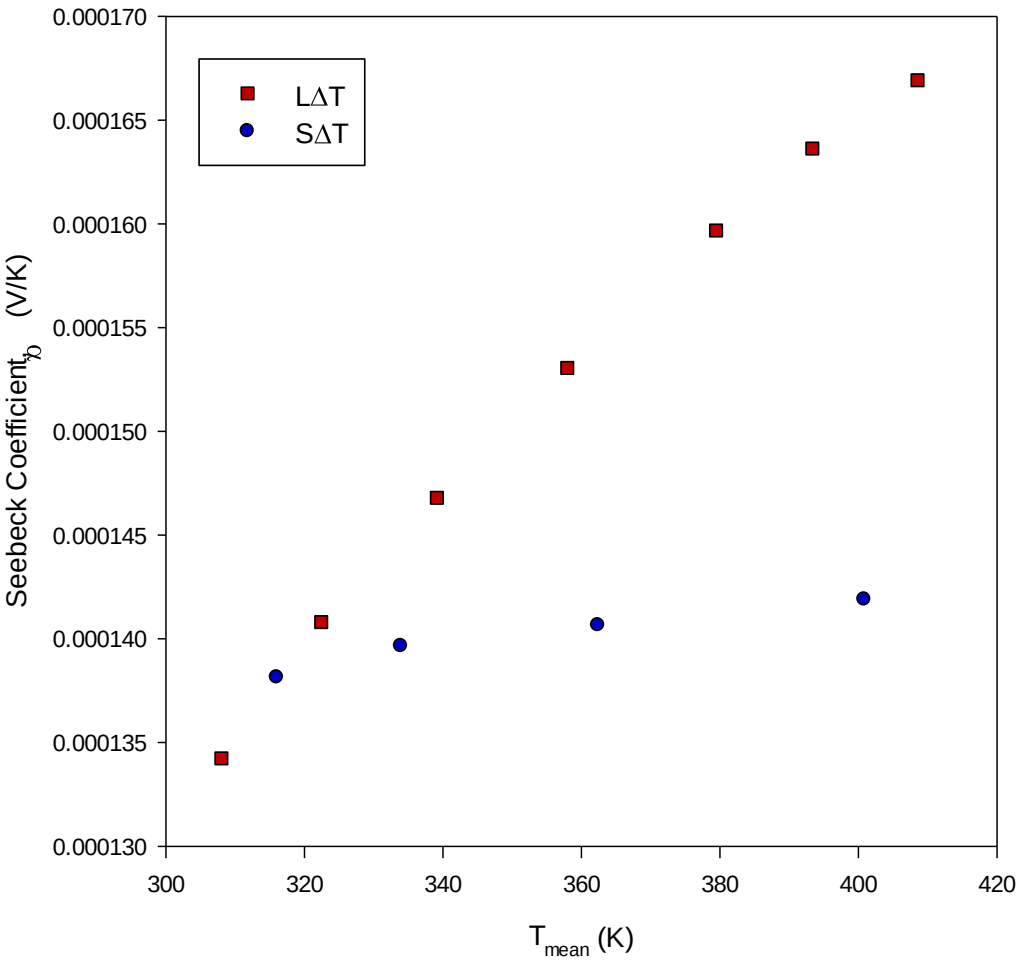

Figure 6.20: The Seebeck coefficient for sample G under small and large ΔT with the Bi_2Te_3 part at the cold side.

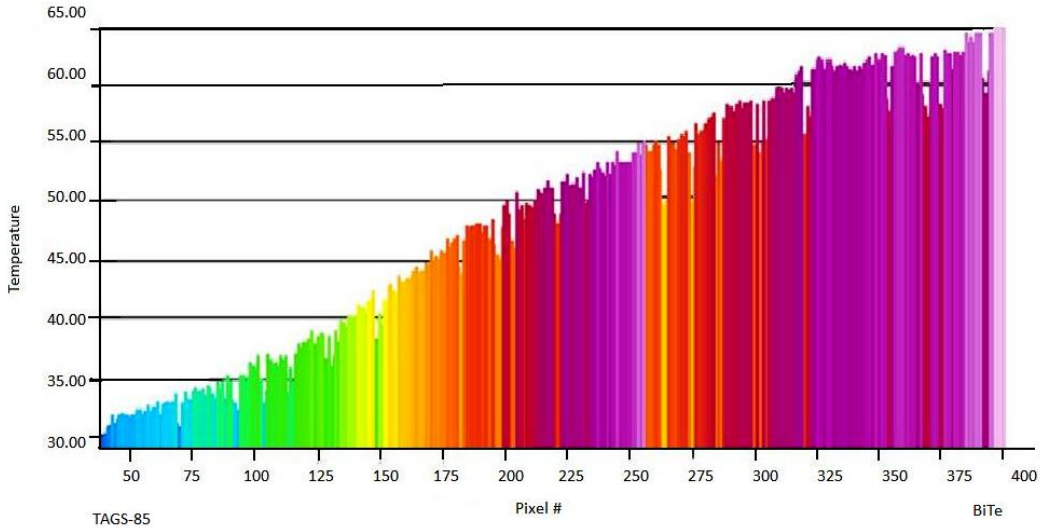

(a)

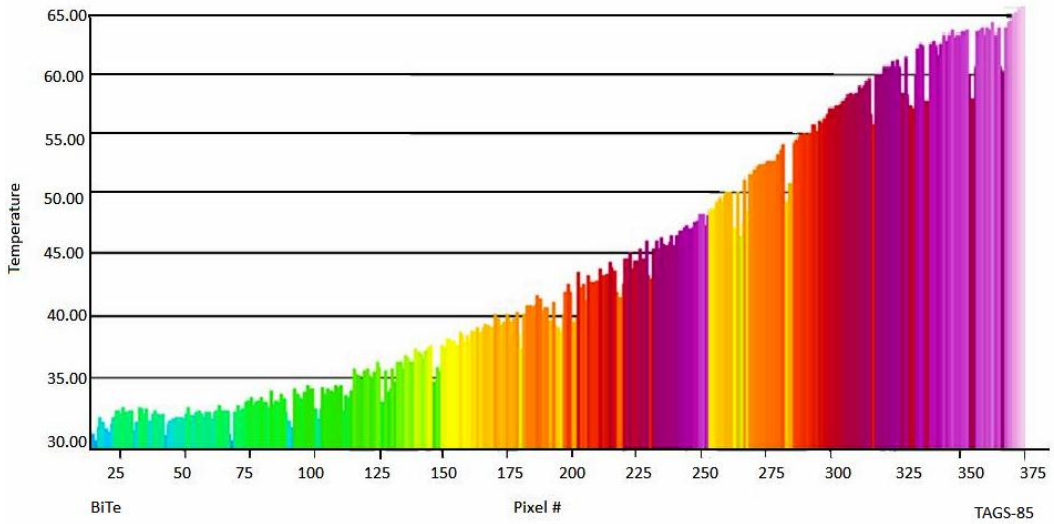

(b)

Figure 6.21: Temperature distribution along sample F when (a) Bi_2Te_3 is located at the hot side and (b) TAGS-85 is located at the hot side.

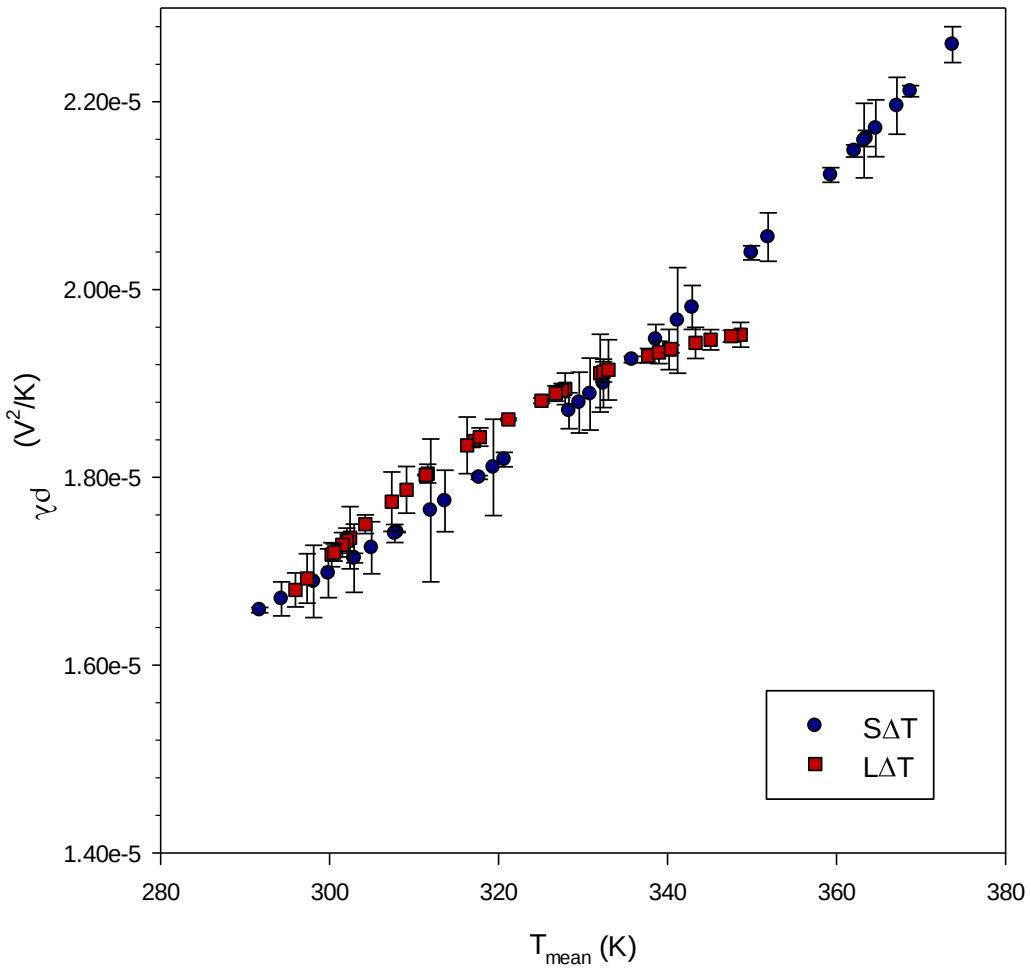

Figure 6.22: An average (from 7 sets of measurements for SΔT and 6 sets of LΔT) of the product of electrical resistivity and thermal conductivity, ρλ of sample A under small ΔT and large ΔT.

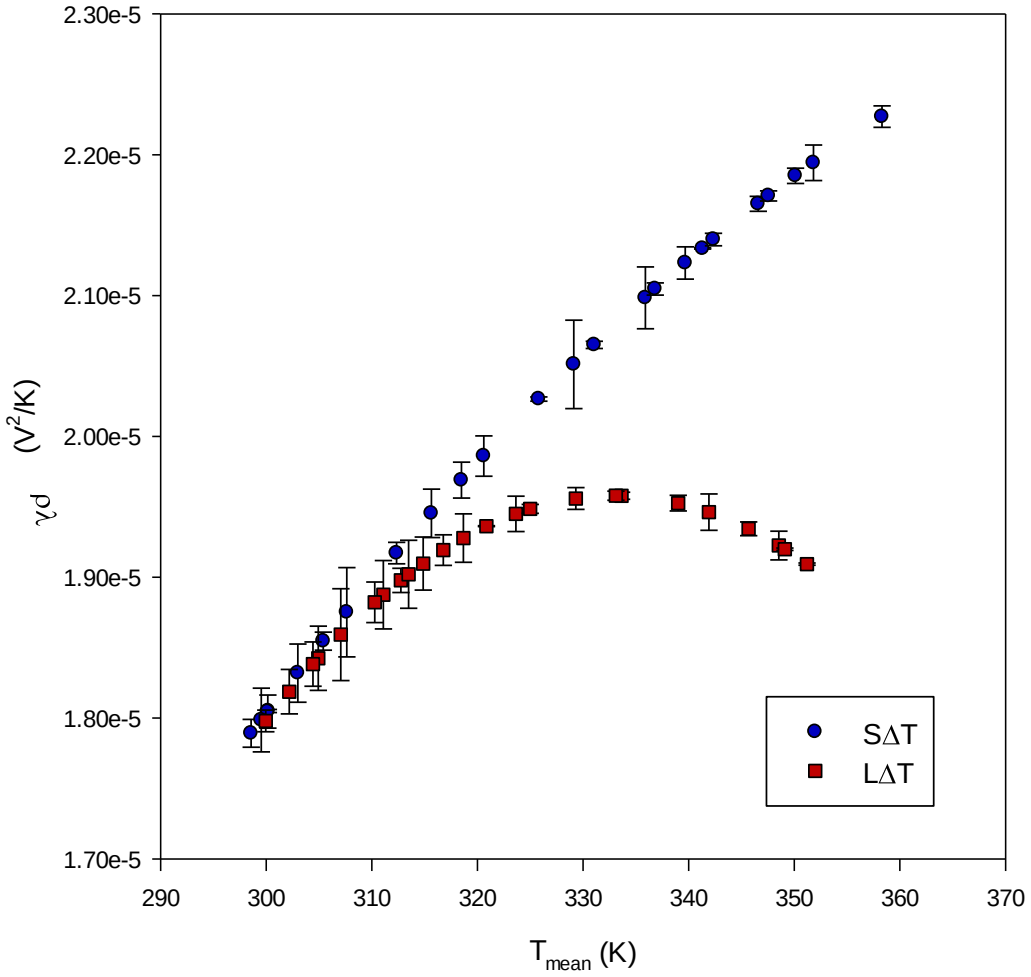

Figure 6.23: An average (from 4 sets of measurements for SΔT and LΔT) of the product of electrical resistivity and thermal conductivity, ρλ of sample B under small ΔT and large ΔT.

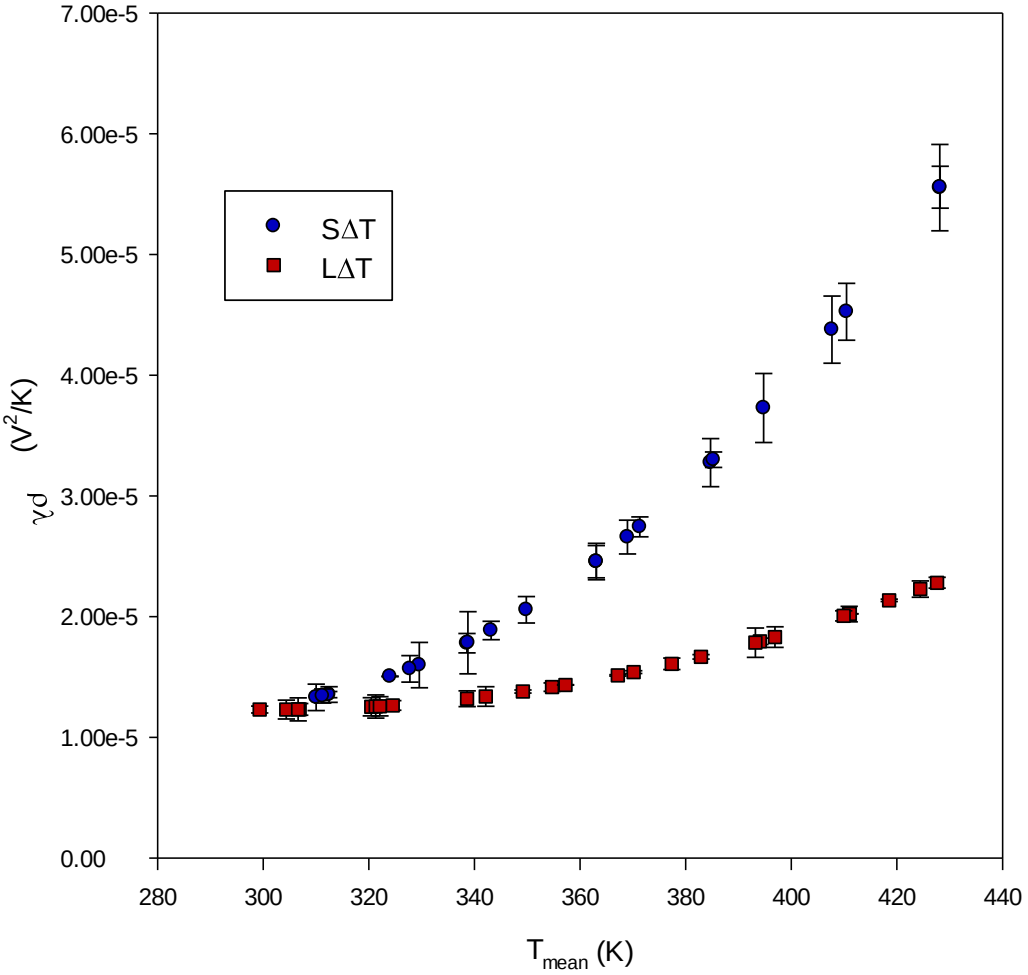

Figure 6.24: An average (from 4 sets of measurements for SΔT and LΔT) of the product of electrical resistivity and thermal conductivity, ρλ of sample C under small and large ΔT.

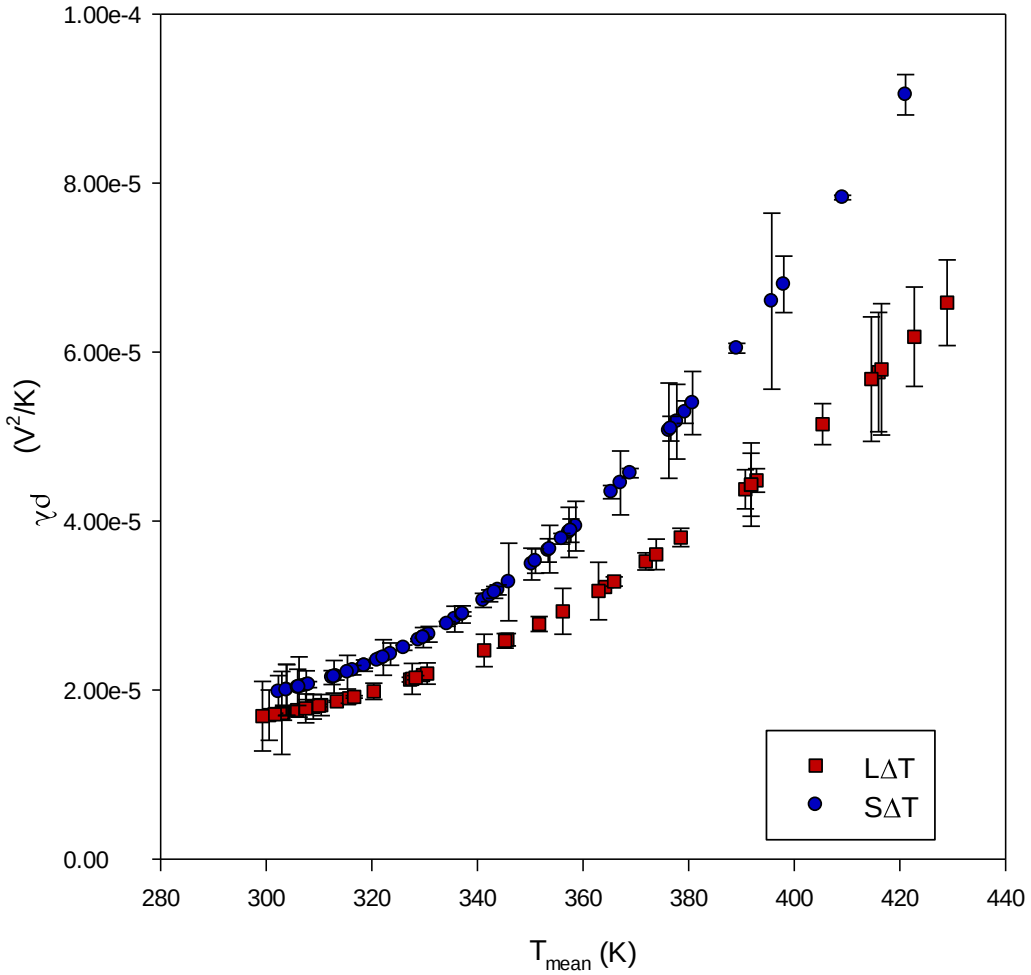

Figure 6.25: An average (from 8 sets of measurements for SΔT and 5 sets for LΔT) of the product of electrical resistivity and thermal conductivity, ρλ of sample D under small and large ΔT.

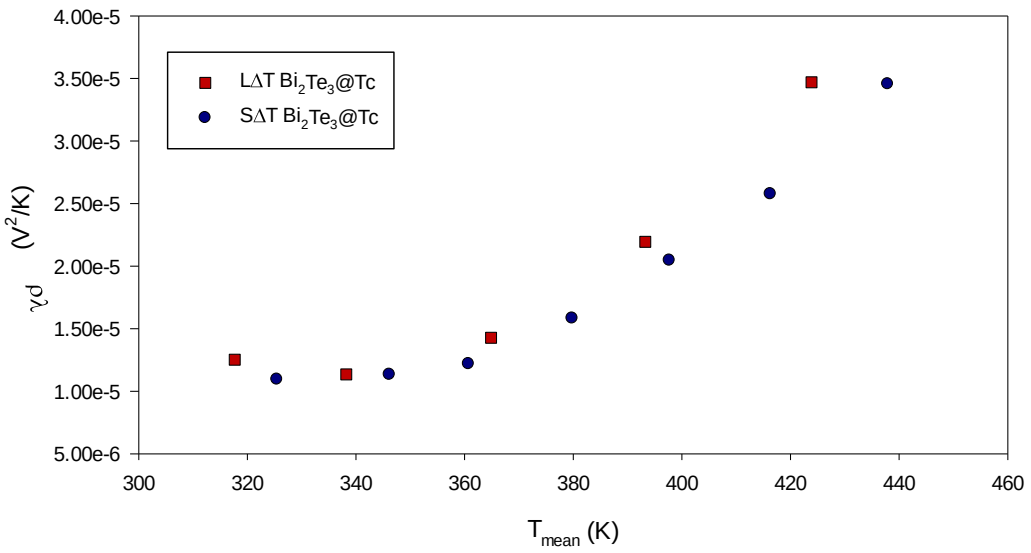

(a)

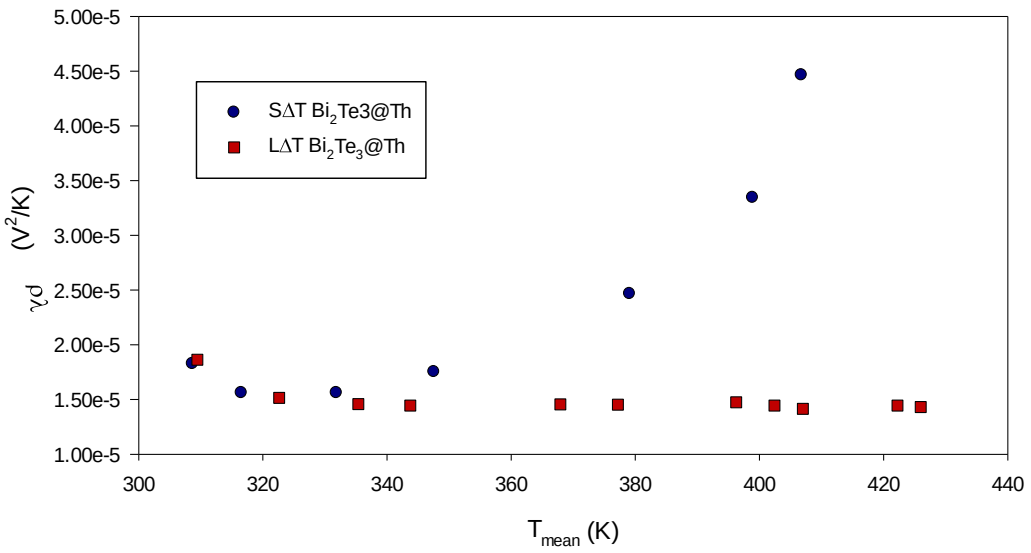

(b)

Figure 6.26: A product of electrical resistivity and thermal conductivity, $\rho\lambda$ of sample E under small and large ΔT when (a) Bi_2Te_3 at the cold side and (b) Bi_2Te_3 at the hot side.

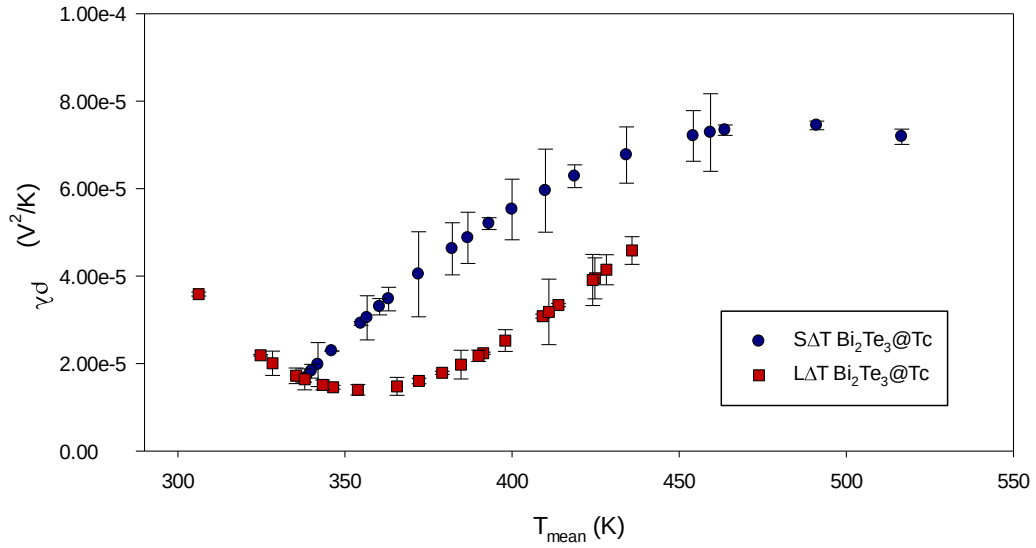

(a)

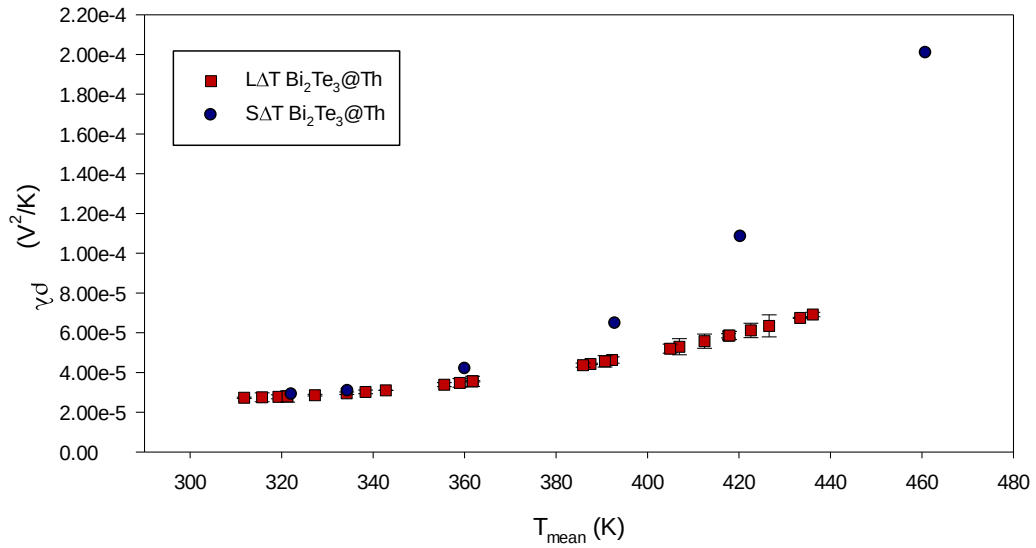

(b)

Figure 6.27: A product of electrical resistivity and thermal conductivity, $\rho\lambda$ for sample F under small and large ΔT when (a) Bi_2Te_3 at the cold side and (b) Bi_2Te_3 at the hot side.

6.9 Influence of the Thomson Effect

Most of the ZT measurements presented above show a significant difference between small ΔT and large ΔT which is not due to experimental error. This is evident by examining the errors bars in the figures. In fact, one of the reasons for the observed differences is the Thomson effect, which becomes significant under larger temperature differences. The Thomson effect will introduce additional heat absorption or dissipation to the sample and consequently affects the ZT values.

The Thomson coefficient can be determined from the measured Seebeck coefficients using,

$$\beta = T\frac{d\alpha}{dT} \text{ .....(6.1)}$$

where T is mean temperature and $d\alpha/_{dT}$ is the derivative of the Seebeck coefficient for small ΔT. The Thomson heat being absorbed or released can be calculated using,

$$Q_{\beta} = \beta I \Delta T \text{ .....(6.2)}$$

where β is the Thomson coefficient, I is the electrical current flowing through the samples and ΔT is the temperature difference across the sample. Since Thomson heat occurred throughout the whole sample, it is assumed that half of the Thomson heat flowed to the hot end.

Using the experimental data, the total heat flows into the sample which include the Thomson effect can then be obtained using equation (3.19).Thus, the

effective figure-of-merit for different temperature differences can be calculated using;

$$ZT_{eff} = \frac{\left(\alpha_{eff}\right)^2}{\rho\lambda} \cdot T$$

$$= \frac{\left(\alpha_h - \frac{\beta \Delta T}{2T_h}\right)^2}{\rho\lambda} \cdot T \ldots\ldots (6.3)$$

As shown previously, almost all ρλ values obtained under large ΔT differ significantly from ρλ obtained under small ΔT. In order to investigate the influence of the Thomson effect only, ZT values were calculated using ρλ values derived under small ΔT measurements. However, it was also necessary to identify the influences of ρλ on ZT. This was achieved by using ρλ values obtained from large ΔT measurements. Those calculated results were plotted together with experimental results under small ΔT as well large ΔT measurements for comparison. Effective ZT which includes the influence of Thomson heat only, is referred to as ZT_{eff1}, while ZT_{eff2} represents the calculated ZT which included the influence of both the Thomson effect and the product ρλ.

Figures 6.28 and 6.29 show the calculated effective figure-of-merit, compared with ZT obtained from small ΔT and large ΔT measurements for samples A and B. Average ZT_{eff1} curves for both modules exhibited similar trends to those of large ΔT measurements. It was expected that ZT values from large ΔT measurements would be in agreement with ZT_{eff2} because it included the influence of both the Thomson effect and ρλ values under large ΔT.

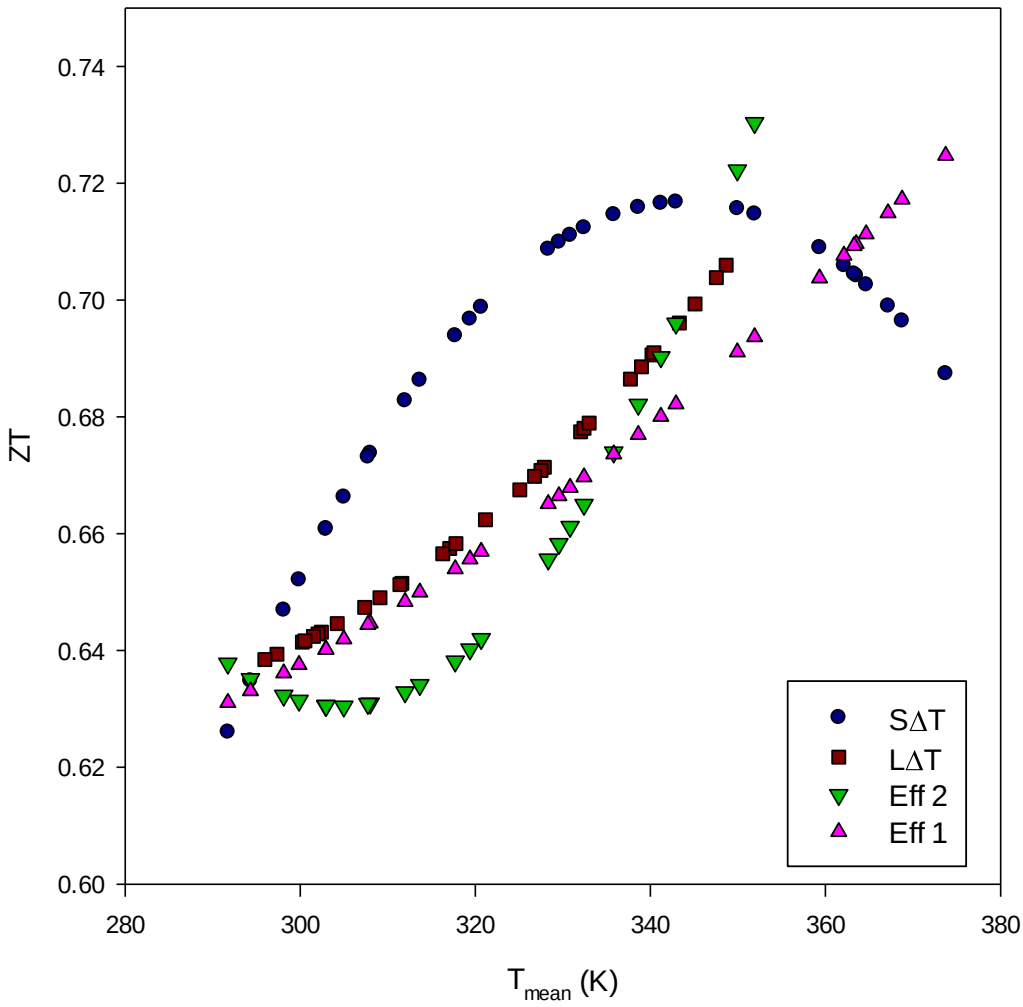

Figure 6.28: Calculated ZT_{eff1} and ZT_{eff2} for sample A, an average experimental ZT under small and large ΔT.

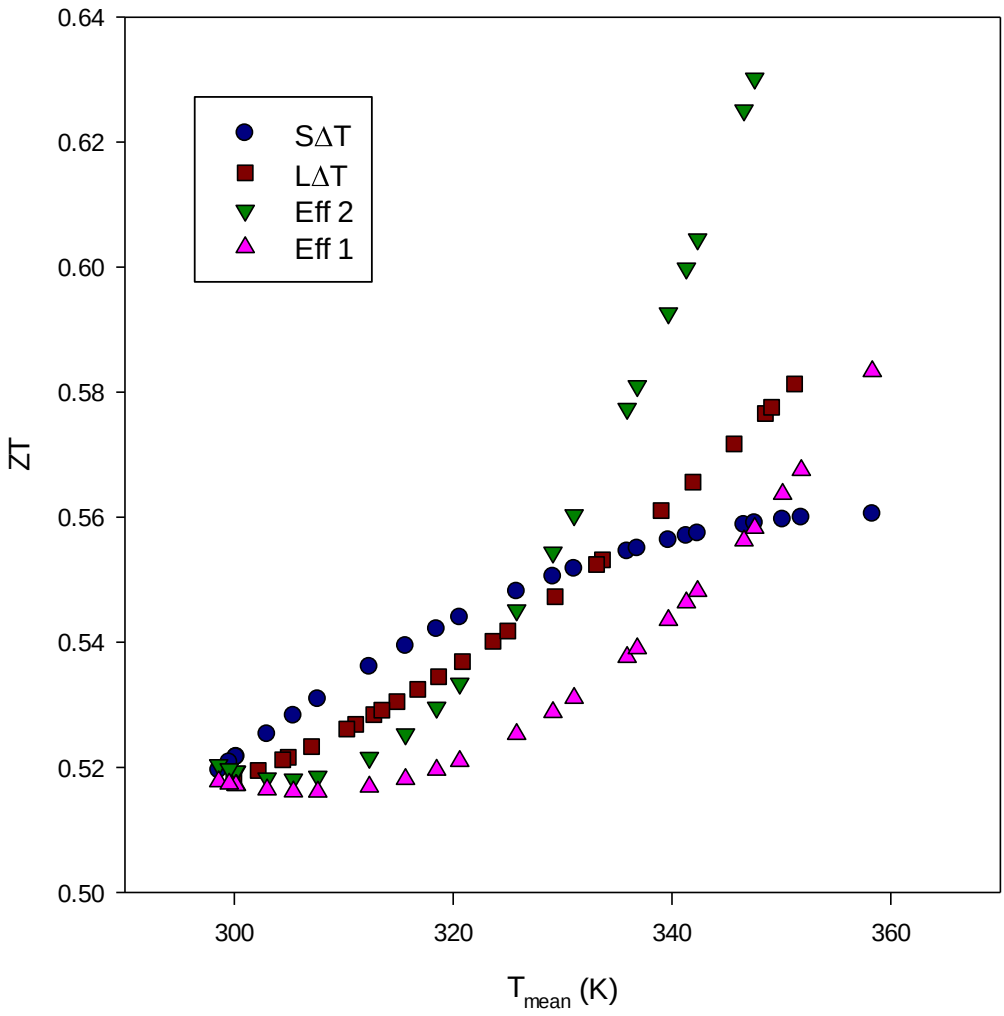

Figure 6.29: Calculated ZT_{eff1} and ZT_{eff2} for sample B, an average experimental ZT under small and large ΔT.

Figures 6.30 and 6.31 show the results of samples C and D. In these two single element samples, the calculated ZT_{eff2} is in better agreement with ZT values obtained from large ΔT measurements than ZT_{eff1}. This result may indicate that changes in $\rho\lambda$ due to operating under large ΔT and current also contribute to the observed change in ZT.

The calculated ZT_{eff1} and ZT_{eff2} for segmented samples E and F are shown in Figures 6.32-6.35. The results from the segmented samples are more complex and difficult to explain due to the fact that the temperature profile along the samples exhibited significant non-linearity. Nevertheless, the results also indicate that both the Thomson heat and $\rho\lambda$ product under large ΔT are different from those when operated under small ΔT.

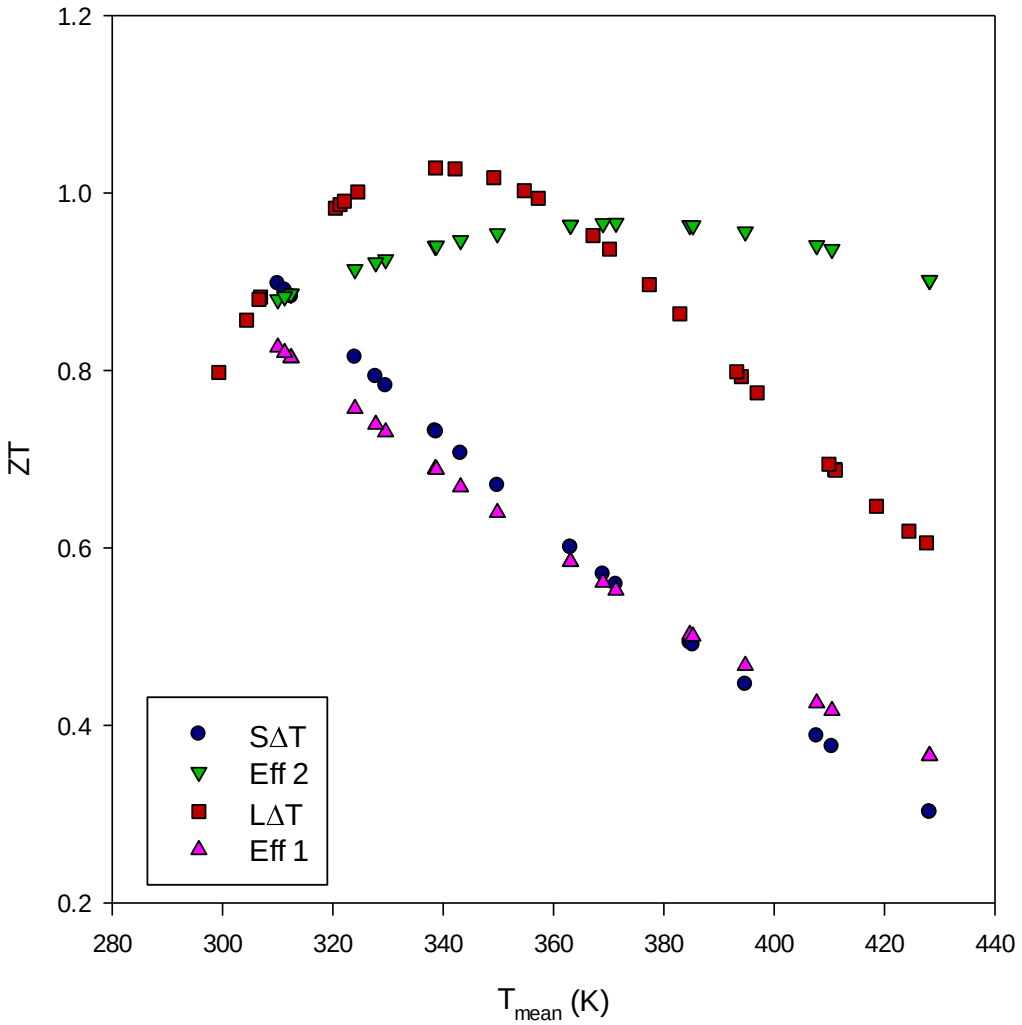

Figure 6.30: Calculated ZT_{eff1} and ZT_{eff2} for sample C, an average experimental ZT under small and large ΔT.

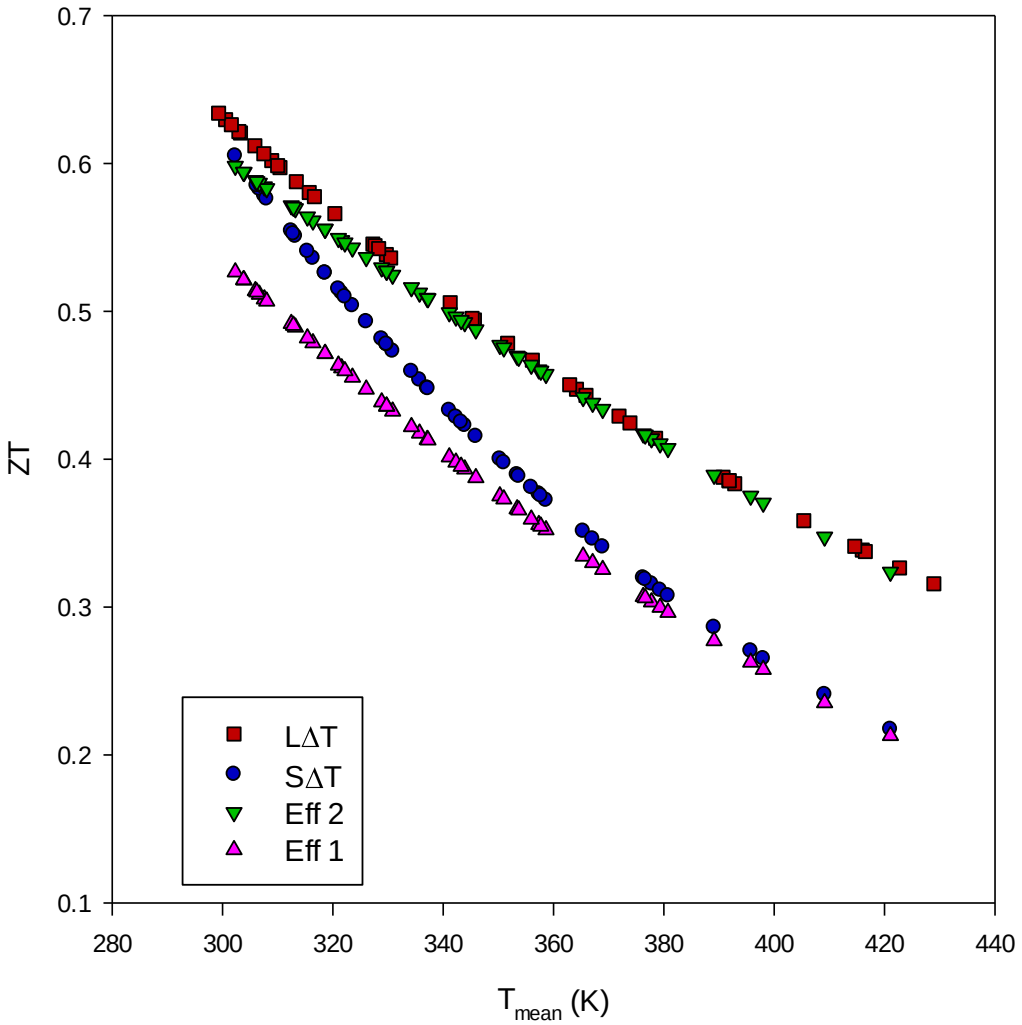

Figure 6.31: Calculated ZT_{eff1} and ZT_{eff2} for sample D, an average experimental ZT under small and large ΔT.

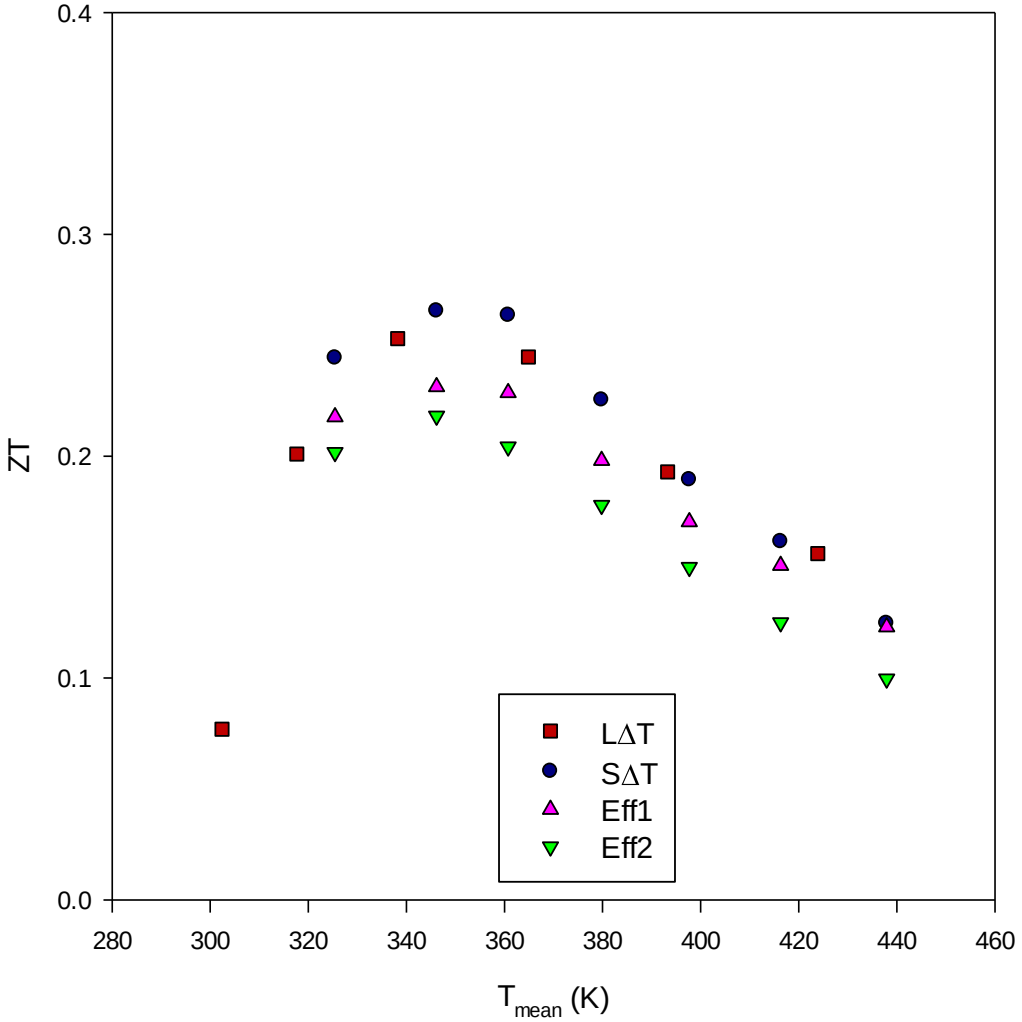

Figure 6.32: Calculated ZT_{eff1} and ZT_{eff2} for sample E with the Bi_2Te_3 part at the cold side, experimental ZT under small and large ΔT.

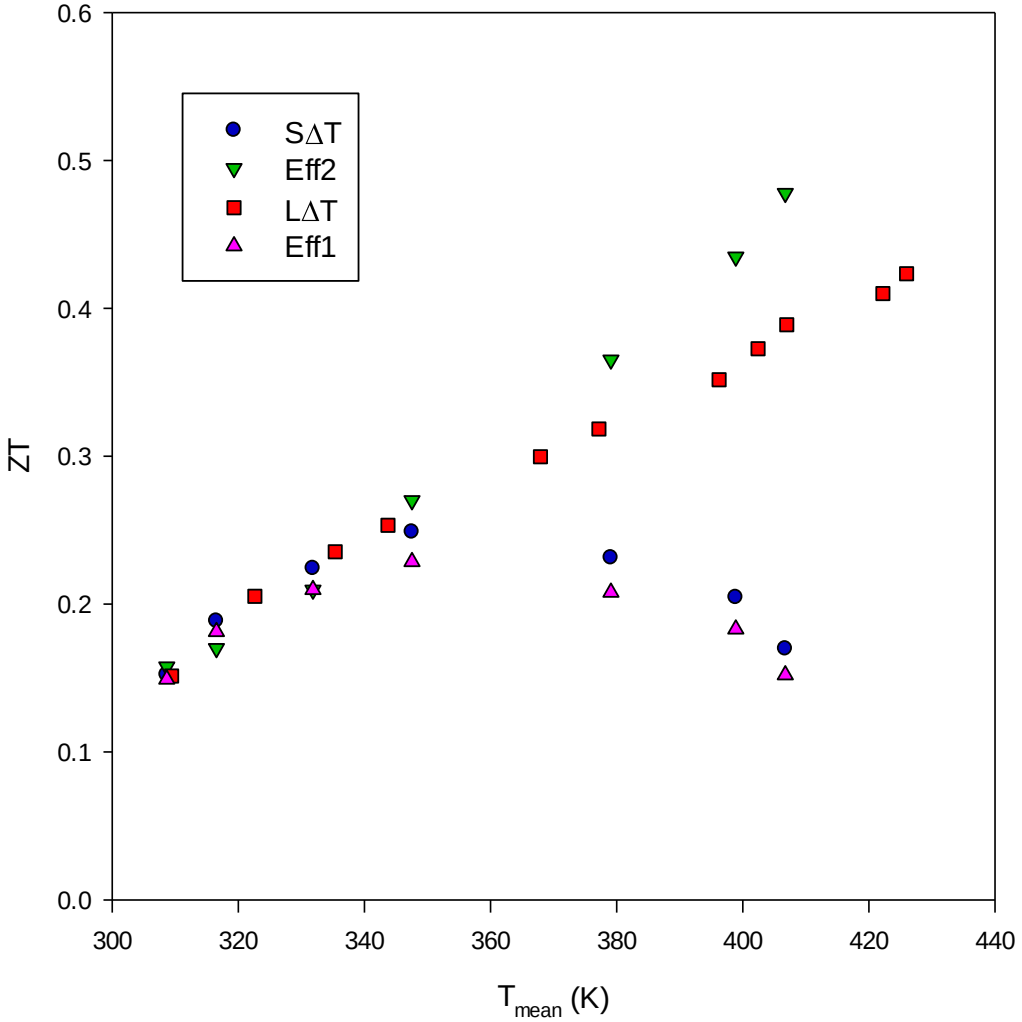

Figure 6.33: Calculated ZT_{eff1} and ZT_{eff2} for sample E with the Bi_2Te_3 part at the hot side, experimental ZT under small and large ΔT.

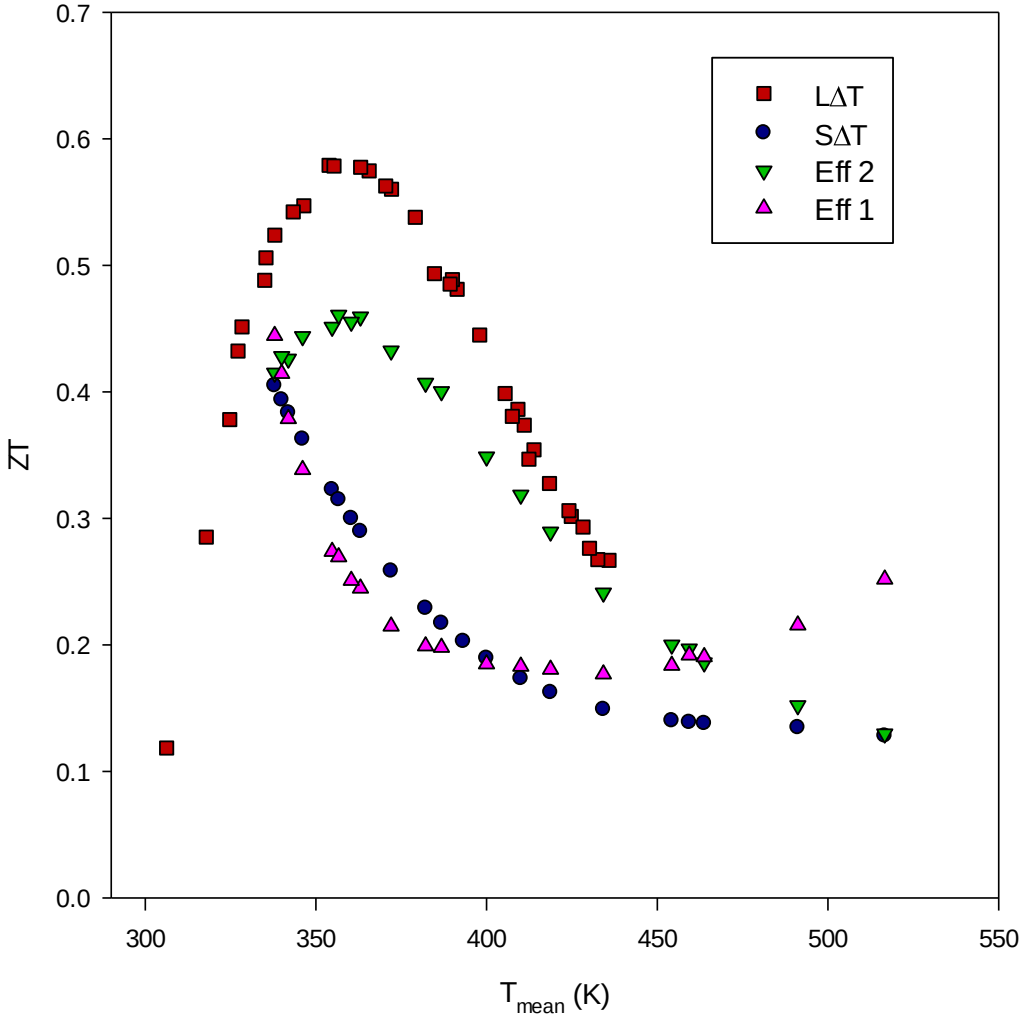

Figure 6.34: Calculated ZT_{eff1} and ZT_{eff2} for sample F with the Bi_2Te_3 part at the cold side, experimental ZT under small and large ΔT.

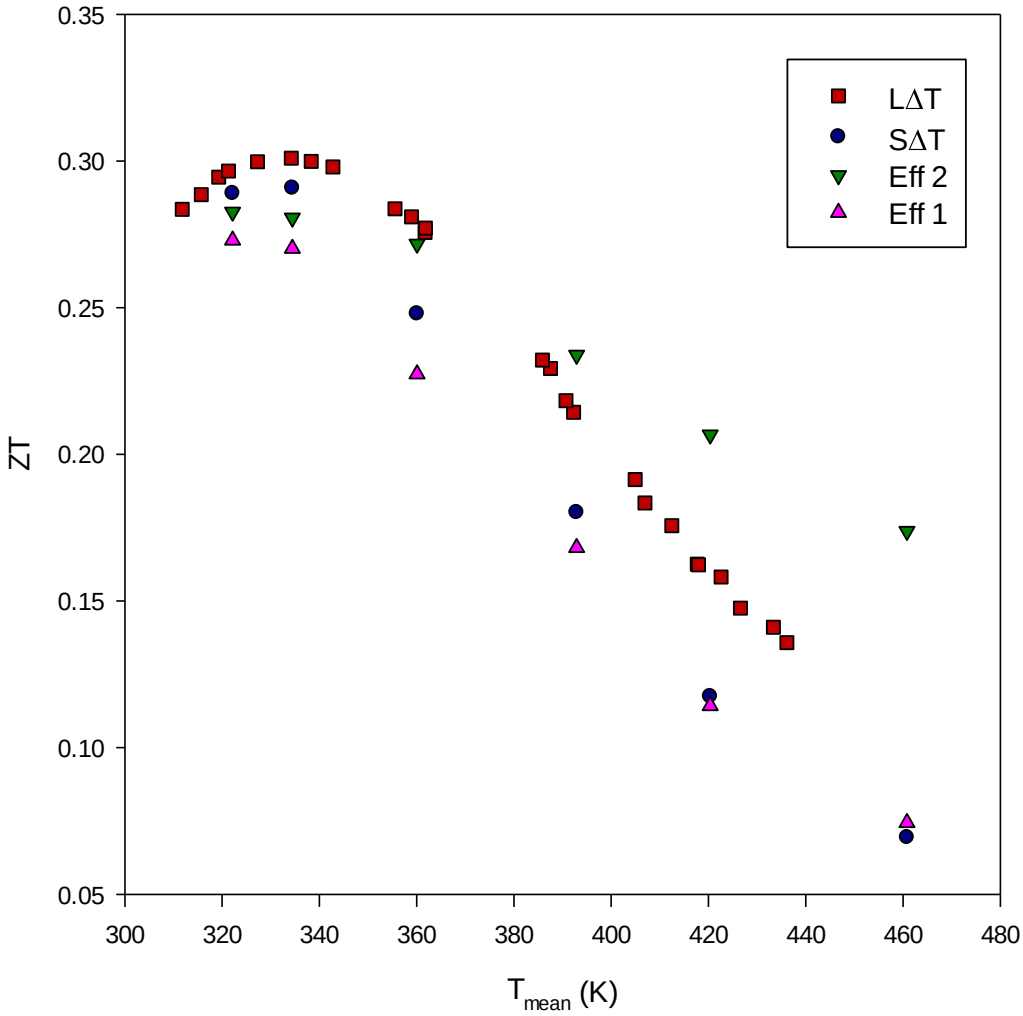

Figure 6.35: Calculated ZT_{eff1} and ZT_{eff2} for sample F with the Bi_2Te_3 part at the hot side, experimental ZT under small and large ΔT.

6.10 Conclusion

Measurements results presented in this chapter showed that ZT values obtained under large ΔT were different from those obtained under small ΔT. This finding was observed in a variety of samples including thermoelectric modules, homogeneous single thermoelements (both n and p-types) and segmented structures.

Measurements of the Seebeck coefficient under large ΔT and small ΔT enabled the deduction of $\rho\lambda$ values under respective Ts. Experimental data analysis indicated that in addition to the Thomson effect, the change in $\rho\lambda$ also contributed to the observed difference in ZT values under large ΔT.

The ZT of segmented materials over large ΔT were measured for the first time. This demonstrates the unique capability of this new technique. However it should be noted that the experimental results on the segmented samples were not conclusive due to the fact that the temperature profile along the sample exhibit non-linearity. In order to achieve accurate measurement, linear temperature profile along the samples is required.

CHAPTER 7

Conclusions and Further Work

7.1 Conclusions

The main aim of the research in this thesis was to develop a novel ZT measurement technique. The studies embodied in this thesis describe experimental attempts toward fulfilling this aim. Since specific conclusions have been discussed at the end of each chapter, this final chapter will focus on the major conclusions that contribute to the successful establishment of this novel ZT measurement technique and facility. The key achievements are as follows:

1)

An initial measurement system was constructed to investigate the feasibility of this novel technique. The system was designed for studying the feasibility using thermoelectric modules because the “short circuit” condition required by this technique can be readily achieved with thermoelectric modules, which have a relatively large internal resistance (a few ohms). An important feature of this system is the capability to monitor heat flow using an in-house designed heat flow meter, so that a constant heat flow across the sample is ensured. This facility can also be used for measuring the power output of the thermoelectric modules. Extensive experimental studies of ZT measurement using this system

confirmed the feasibility of the proposal measurement principle. The "temperature method" has proved to be more feasible and reliable, with ZT measurements showing a repeatability of <3.3% and an accuracy of <13%. The results from small ΔT measurements agree well with other measurement methods and the data supplied by the module manufacturers. Furthermore, the experimental results obtained from this initial study demonstrated that ZT obtained under a large ΔT measurement is different from that obtained under small ΔT measurement.

2)

Following on from the success of the feasibility study using thermoelectric modules, research efforts were focused on the implementation of this technique for the evaluation of single thermoelectric materials, which have dimensions of approximately 3mm×3mm×8mm. A major problem associated with small-dimension samples is the difficulty in achieving the short circuit condition. The investigation of ΔT dependence on the ratio of the load resistance to the internal resistance led to a viable solution – determination of ZT by measuring the temperature differences at open and closed circuits, rather than at the unattainable short circuit condition. The theoretical outline for the modified technique was established (equations 3.15 and 3.16). Extensive experimental investigation on the influence of contact resistance and constant heat flux were carried out, which helped to identify suitable materials and structures for a

successful design of the proposed measurement system. Those include vacuum assembly, a multi-function heat flux meter as well as indium and platinum contacts for the cold and hot sides.

3)

A novel ZT measurement system was successfully designed, constructed and calibrated. The system is capable of measuring ZT values of *small dimension samples* under *real operating conditions* (i.e., under a large temperature difference and with electrical current flowing through the sample). This provides a radically new characterisation method for the investigation of the thermoelectric parameters and processes that was not possible previously. The system has been successfully tested at high temperatures up to 570 K, with a large temperature difference of ~260 K. The calibration against a standard n-type Bi_2Te_3 based sample shows that both the repeatability and accuracy of the system is better than 10% and 32% errors respectively. The system can be used to measure a homogeneous single piece or inhomogeneous segmented or functionally graded samples with different cross-sectional areas and lengths with a typical dimension of 3mm×3mm×8mm. The heat flux meter has ability to detect changes with 3% error between open and close circuit. A better accuracy and reliability of measurement is achieved with an established correction procedure.

4)

The measurement system developed in this project was employed to investigate a variety of different types of thermoelectric materials. Those include: homogenous single piece p- and n-type Bi_2Te_3 based alloys, inhomogeneous n-type Bi_2Te_3+PbTe, p-type Bi_2Te_3+TAGS-85 and p-Bi_2Te_3+TAGS-80 segmented samples. Taking advantage of being capable of measuring ZT under both small and large temperature difference of the developed system, a comparative study was carried out to investigate if the ZT obtained under a large temperature difference (which represents real operating conditions) differs from that under a small temperature difference (which represent the values obtained from conventional ZT measurement techniques). Experimental results show clearly a noticeable difference in ZT values between large and small ΔT measurements. Analysis of experimental data indicates that the observed difference can be attributed to the Thomson effect and the changes in the product of the electrical resistivity and thermal conductivity under a large temperature difference. ZT for segmented materials was measured for the first time and a change with the sample “polarity” was observed. However, the result is not fully understood but an initial study suggests that it may be partly due to the non-linear temperature profile that occurred along the sample during measurement. Further investigation is needed.

7.2 Further Work

Several improvements in the design of the apparatus and of the measurement technique have been identified. This study has also highlighted several potential areas which suggest further investigation that could be carried out in the future.

1. The ZT measurement system developed in this project has a temperature limitation of 570 K. This is mainly due to the fact that the thin brass rod of the heat flow meter becomes soft when the operating temperature is higher than 570 K and it is likely to get bent under pressure. To increase the measurement temperature and hence to achieve a larger temperature difference, the brass rod used in the current system should be replaced with a high strength and high temperature material which also needs to satisfy the requirements of high electrical conductivity and relatively low thermal conductivity.
2. The current system demonstrated the capability of ZT measurement but only with materials which have relatively large ZT values (ZT > 0.2). In order to improve its ability to measure small ZT materials, the electrical resistance in the measurement loop needs to be further reduced. This may be achieved by employing high temperature soldering material as an interconnector between sample and copper contact/copper plate to reduce the total contact resistance and increase repeatability. Since the temperature change between open and closed circuit is small when

measuring small dimension samples, a more accurate temperature measurement system such as a higher resolution data logger and more accurate current measurement system should be incorporated to improve measurement accuracy.

3. The results from this investigation show that the Thomson effect has a noticeable influence on ZT values under large temperature difference (i.e., real operating conditions). An in-depth investigation of the influence of the Thomson effect on ZT values will provide useful insight into further improvement of thermoelectric efficiency. Since the Thomson coefficient can be positive or negative depending on the temperature dependence of the Seebeck coefficient, it can either increase or decrease ZT values when under a real operating temperature. It is anticipated that the optimal operating temperature region is where the Thomson effect contributes to improving ZT values, which can be identified by ZT measurement using the system developed in this project.
4. The experimental results also indicate that the product of electrical resistivity and thermal conductivity under large temperature differences is significantly smaller from that under small temperature differences. This finding has not been investigated in this project. The determination of why and how they are responsible for the observed reduction will provide useful insights into the understanding of the electrical and the thermal transport mechanisms under a large temperature difference.

5. As demonstrated in the experiments, segmented materials exhibit directional dependence. Unfortunately, non-linearity in the temperature profile of those materials was also observed, which complicated the interpretation of the results. Further investigation is required to study the influences of non-linear temperature distribution along the sample and its correlation to the changes in thermoelectric properties. Moreover, careful preparation of samples and measurement conditions may help to minimize the non-linear temperature distribution and consequently allow a direct comparison of ZT values measured in different "polarities" under large temperature differences.
6. It has been predicted theoretically that the efficiency of thermoelectric devices over a large operating temperature difference can be significantly improved by employing appropriately segmented thermoelements. Very little experimental work has been done in this area due to lack of simple procedures. The measurement system developed in this project provides an effective method. It is now possible to design segmented samples based on theoretical calculation and then to evaluate their ZT values experimentally using the developed technique. This investigation will be able to provide a direct verification of improved thermoelectric performance by using segmented structures. In addition, it will provide experimental guidelines for the appropriate design of segmented structures.

APPENDIXES

Appendix 1

Heat absorbed at cold side thermoelectric cooler given as:

$$Q_c = \alpha I T_c - \frac{1}{2} I^2 R - K\Delta T$$

By setting $\frac{dQ_c}{dI} = 0$, maximum current obtained:

$$I_{max} = \frac{(\alpha_p - \alpha_n)T_c}{R}$$

Therefore, maximum heat absorbed at cold side can be calculated by replace I_{max} into equation:

$$(Q_c)_{max} = \frac{(\alpha_p - \alpha_n)^2 T_c^2}{2R} - K(T_h - T_c)$$

By setting $(Q_c)_{max} = 0$, maximum ΔT obtained is:

$$(T_h - T_c)_{max} = \frac{(\alpha_p - \alpha_n)^2 {T_c}^2}{2KR}$$

From definition of maximum efficiency of heat engine, $\frac{T_h - T_c}{T_c}$, thermoelectric figure-of-merit can be defined as:

$$Z = \frac{\alpha^2}{\rho\lambda}$$

Appendix 2

Measurements data for sample A under small temperature differences condition.

Exp	T_{mean} (K)	ΔT_{mo}	ΔT_{ms}	ΔT_{co}	ΔT_{cs}	ZT_{wo}	ZT
S1	294.315	13.35	8.1	2.86	2.85	0.648148	0.642385
	299.855	13.81	8.54	3.04	3.11	0.617096	0.654332
	304.99	13.78	8.43	3.05	3.15	0.634638	0.688233
	311.975	13.41	8.14	3.06	3.09	0.64742	0.663571
	320.675	13.37	8.13	3.02	3.14	0.644526	0.709872
S2	330.835	12.91	7.55	3.06	3.07	0.709934	0.715522
	341.2	12.5	7.54	2.94	3.06	0.657825	0.725491
	351.905	12.63	7.38	3.04	3.06	0.711382	0.722641
	363.505	13.724	8.38	3.355	3.49	0.637709	0.703608
	373.725	13.17	7.84	3.35	3.37	0.679847	0.689876
	291.73	13.72	8.39	2.98	2.96	0.63528	0.624305
S3	332.41	13.878	8.28	3.226	3.28	0.676087	0.704143
	342.925	13.458	8.03	3.13	3.22	0.675965	0.724156
	364.655	13.81	8.36	3.39	3.48	0.651914	0.69577
	359.33	13.84	8.37	3.34	3.46	0.653524	0.712933
S4	302.92	8.12	5.03	1.84	1.88	0.614314	0.649408
	329.555	8.29	5.04	1.97	2.06	0.644841	0.719986
	362.1	8.892	5.25	2.345	2.36	0.693714	0.704548
S5	302.955	8.03	4.93	1.8	1.83	0.628803	0.65595
	308	7.448	4.53	1.71	1.74	0.64415	0.672995
	313.66	8.08	4.95	1.88	1.93	0.632323	0.675736
	319.39	8.54	5.26	2	2.07	0.623574	0.680399
	335.81	9.38	5.72	2.27	2.37	0.63986	0.712101
S6	298.125	13.65	8.43	2.92	2.98	0.619217	0.652489
	307.735	12.59	7.7	2.79	2.86	0.635065	0.676088
	317.715	11.91	7.35	2.72	2.83	0.620408	0.685939
	328.34	11.46	6.88	2.7	2.77	0.665698	0.708882
	338.615	10.55	6.5	2.54	2.7	0.623077	0.725318
S7	368.745	10.85	6.51	2.77	2.83	0.666667	0.702768
	363.27	11.12	6.69	2.88	2.94	0.662182	0.696811
	349.945	16.47	9.93	3.93	4.05	0.65861	0.709255
	367.15	8.26	5.06	2.22	2.3	0.632411	0.691237

Appendix 3

Measurements data for sample A under large temperature differences condition.

Exp	T_{mean} (K)	ΔT_{mo}	ΔT_{ms}	ΔT_{co}	ΔT_{cs}	ZT_{wo}	ZT
L1	302.425	17.87	10.98	3.89	3.95	0.627505	0.652607
	309.105	30.15	18.65	6.69	6.85	0.616622	0.655286
	340.185	87.05	53.31	19.07	19.78	0.632902	0.693697
L2	348.66	108.12	66.96	23.71	25.01	0.614695	0.703228
	297.34	8.54	5.51	1.86	1.96	0.549909	0.633238
	317.07	45.54	28.49	10.11	10.53	0.598456	0.66486
	327.895	65.45	41.12	14.57	15.29	0.591683	0.670338
L3	343.315	110.49	68.39	24.65	25.9	0.615587	0.697513
	295.965	14.19	8.77	3.12	3.16	0.618016	0.63876
	302.045	25.19	15.72	5.64	5.77	0.602417	0.639352
	332.035	79.63	47.93	17.88	18.05	0.661381	0.677177
	345.105	103.55	63.29	22.89	23.89	0.636119	0.707597
	347.535	108.75	66.51	24	25.13	0.635092	0.712078
L4	301.52	17.444	10.95	3.77	3.89	0.593059	0.643447
	304.23	22.54	14.36	4.93	5.16	0.569638	0.642575
	311.6	36.1032	22.82	7.88	8.22	0.582086	0.649828
	321.155	53.8706	33.44	11.65	12.01	0.610963	0.659905
	327.495	65.42284	39.91	14.184	14.46	0.639259	0.669999
	332.425	74.5094	45.62	16.17	16.61	0.633262	0.676346
	337.72	84.4172	51.65	18.33	18.89	0.634409	0.68278
L5	300.245	17.85	11.08	3.92	3.97	0.611011	0.631559
	307.37	31.12	19.25	6.88	7.01	0.616623	0.64717
	316.29	47.54	29.55	10.52	10.83	0.608799	0.656206
	326.775	66.847	41.09	14.894	15.21	0.626844	0.66136
	338.98	89.32	55.44	19.74	20.57	0.611111	0.678853
L6	300.535	14.8895	9.34	3.42	3.52	0.594165	0.643117
	311.38	34.726	21.59	7.77	8.02	0.60843	0.66172
	317.78	46.6376	28.73	10.35	10.59	0.623307	0.662456
	325.09	60.1982	37.2	13.33	13.76	0.618231	0.671548
	333.015	74.5833	45.35	16.42	16.68	0.644615	0.671764
	340.405	88.1245	54.2	19.32	20.05	0.625913	0.687767

Appendix 4

Temperature dependence of thermoelectric properties data showing (a) Seebeck coefficient, (b) thermal conductivity and (c) electrical resistivity [109] from manufacturer for given sample A.

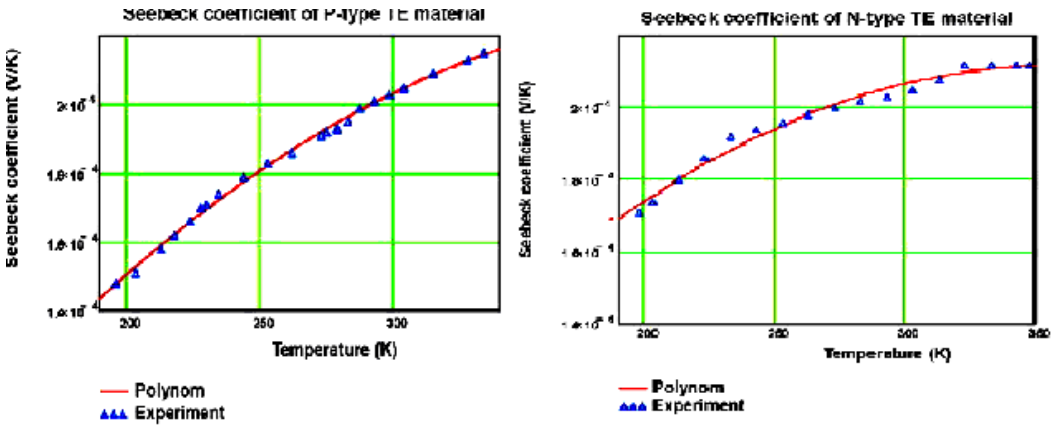

(a)

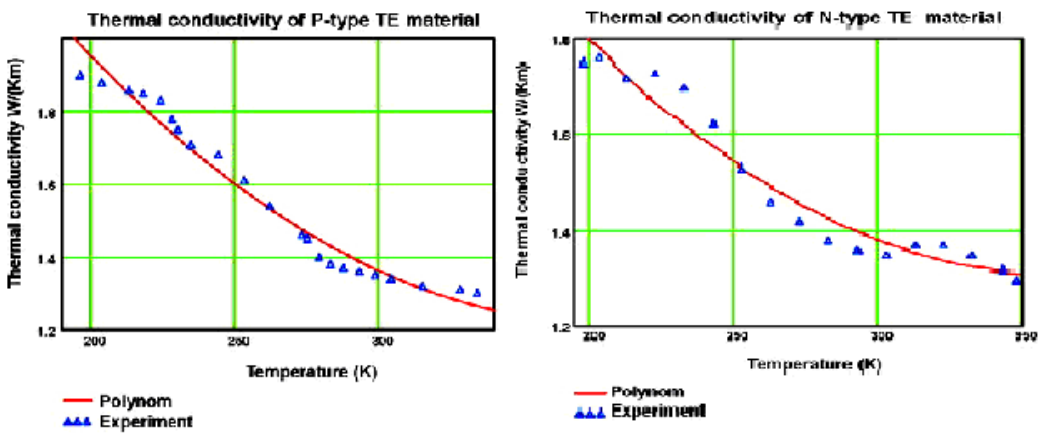

(b)

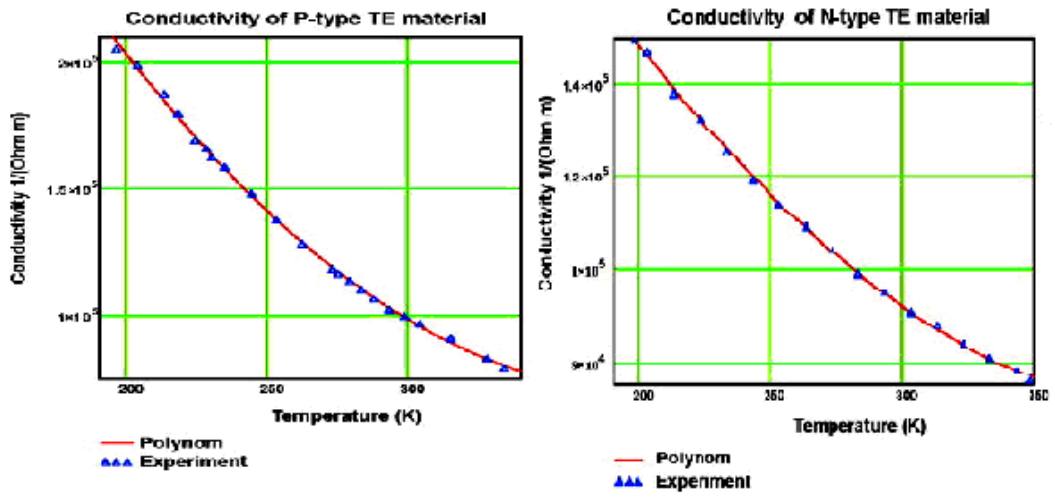
Conductivity of P-type TE material
Conductivity 1/(Ohm m)
Temperature (K)
Polynom
Experiment
Conductivity of N-type TE material
Conductivity 1/(Ohm m)
Temperature (K)
Polynom
Experiment

(c)

Appendix 5

Diagram showing design of the bottom heat sink where position of screw and rod made in line for easy access and assembly of the sample at the centre.

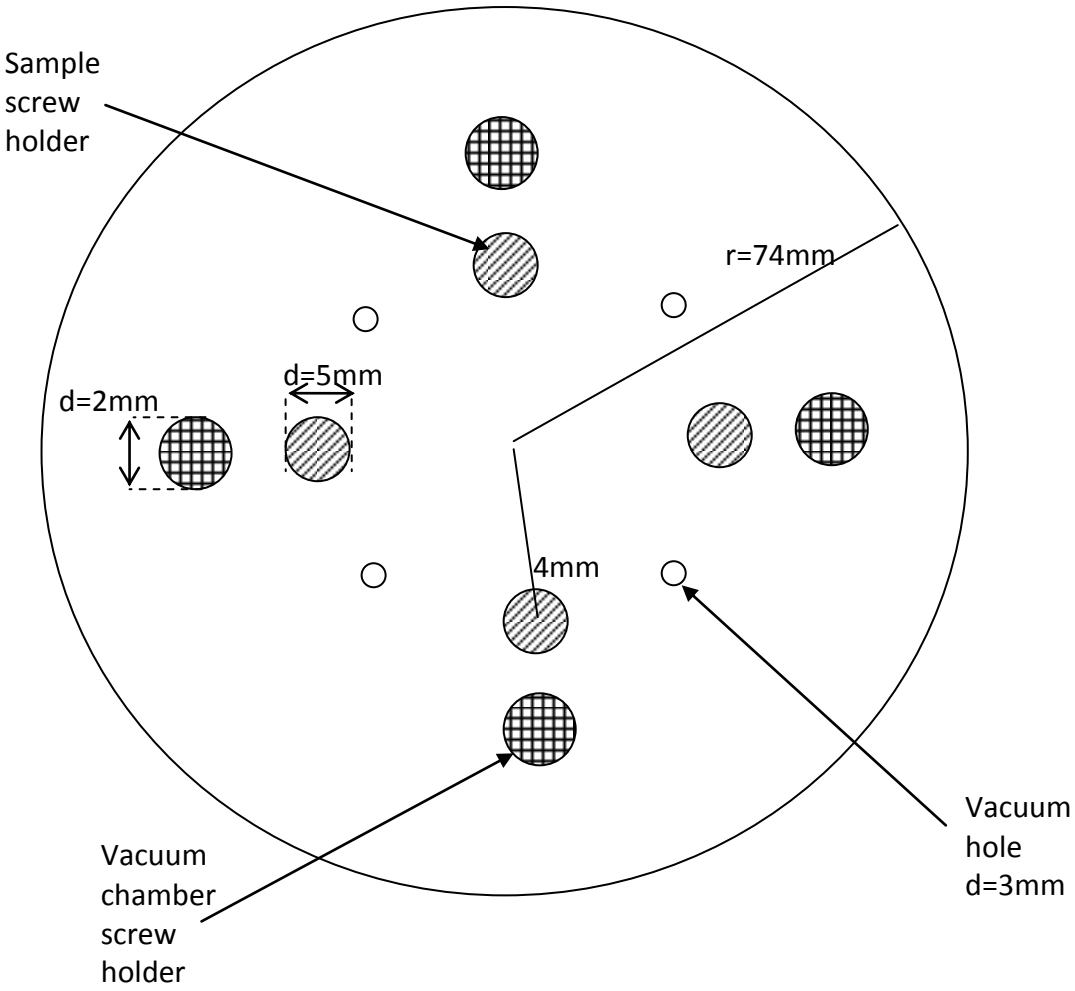

Appendix 6

Size and dimension of vacuum chamber used in high temperature thermoelement measurement.

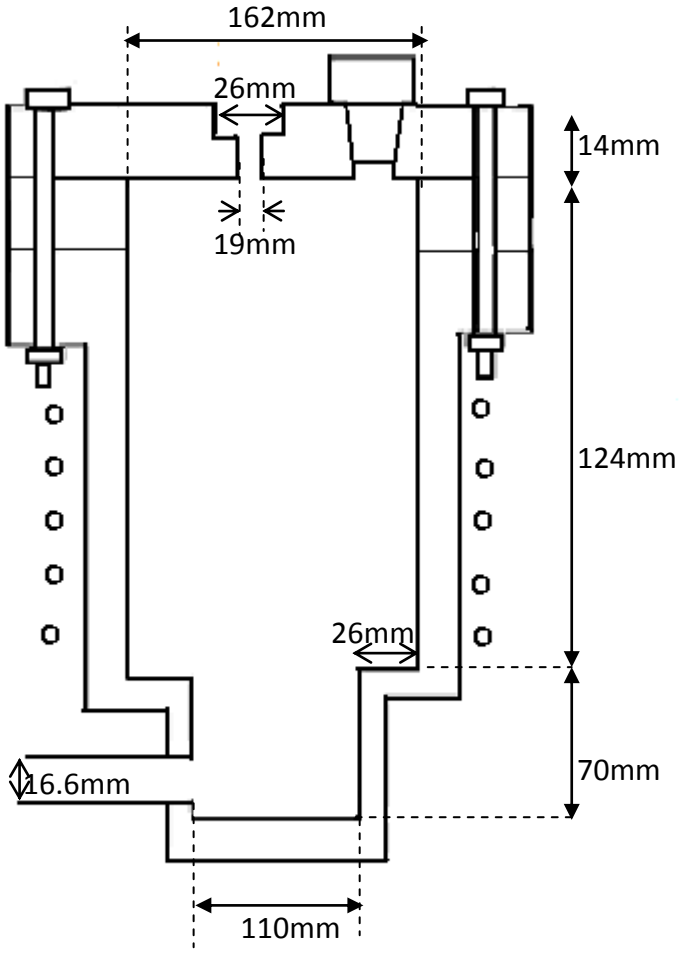

Appendix 7

Measurements data for sample B under small temperature differences condition.

Exp	T_{mean} (K)	α (V/K)	ΔT_{so}	ΔT_{bo}	ΔT_{sc}	ΔT_{bc}	ZT	β (V/K)
S1	298.575	1.77E-04	11.97	3.85	8.15	3.98	0.518305	1.185E-04
	300.195	1.78E-04	11.93	3.83	8.11	3.97	0.524795	1.154E-04
	305.405	1.80E-04	11.75	3.78	7.91	3.9	0.532619	1.050E-04
	312.35	1.83E-04	11.04	3.7	7.54	3.9	0.543336	9.054E-05
	315.65	1.83E-04	11.338	3.79	7.63	3.95	0.548709	8.340E-05
S2	320.605	1.83E-04	10.95	3.73	7.3	3.84	0.544236	7.236E-05
	325.805	1.86E-04	10.53	3.67	7	3.78	0.549373	6.036E-05
	331.055	1.87E-04	10.43	3.64	7.02	3.81	0.555145	4.783E-05
	335.895	1.86E-04	9.87	3.54	6.72	3.74	0.55173	3.589E-05
	341.31	1.87E-04	9.82	3.53	6.57	3.67	0.553952	2.211E-05
	346.58	1.89E-04	9.52	3.47	6.351	3.618	0.56291	8.252E-06
	351.82	1.88E-04	9.08	3.39	6.02	3.51	0.561697	-5.951E-06
S3	302.99	1.79E-04	11.56	3.8	7.85	3.95	0.530741	1.099E-04
	336.835	1.86E-04	11.51	4.07	7.73	4.24	0.551198	3.353E-05
	342.335	1.87E-04	11.53	4.1	7.68	4.25	0.556228	1.945E-05
	347.565	1.87E-04	11.25	4.08	7.52	4.25	0.558344	5.615E-06
	358.3	1.87E-04	11.18	4.16	7.48	4.33	0.555732	-2.411E-05
	300.145	1.77E-04	11.97	3.93	8.13	4.05	0.517281	1.155E-04
S4	299.535	1.77E-04	10.33	3.17	7.04	3.3	0.527504	1.167E-04

	307.63	1.82E-04	12.113	4.02	8.115	4.129	0.533141	1.005E-04
	318.49	1.83E-04	12.84	4.32	8.58	4.44	0.538073	7.712E-05
	329.13	1.86E-04	12.5	4.3	8.33	4.43	0.545967	5.248E-05
	339.67	1.86E-04	12.3	4.31	8.37	4.54	0.547955	2.633E-05
	350.115	1.88E-04	11.89	4.29	7.88	4.43	0.558124	-1.283E-06

Appendix 8

Measurements data for sample B under large temperature differences condition.

Exp	T_{mean} (K)	α (V/K)	ΔT_{mo}	ΔT_{co}	ΔT_{ms}	ΔT_{cs}	ZT
L1	314.86	1.81E-04	37.36	24.64	12.06	12.28	0.543893
	323.64	1.81E-04	52.74	34.65	16.8	17.12	0.55107
	333.64	1.82E-04	70.2	46.08	22.12	22.7	0.563383
	341.92	1.81E-04	84.74	55.39	26.67	27.37	0.570033
	304.935	1.79E-04	19.95	13.3	6.52	6.67	0.534509
	311.095	1.80E-04	30.81	20.84	10.09	10.43	0.528224
	318.665	1.81E-04	44.07	29.36	14.29	14.65	0.538836
L2	299.965	1.77E-04	11.19	7.37	3.76	3.77	0.522356
	302.185	1.78E-04	15.11	9.92	5.18	5.18	0.523185
	304.43	1.79E-04	19.16	12.67	6.61	6.67	0.52596
	307.055	1.79E-04	23.97	15.87	8.23	8.39	0.539761
	310.275	1.80E-04	29.71	19.43	10.24	10.31	0.539531
L3	312.75	1.80E-04	34.34	23.16	11.89	12.32	0.536352
	316.775	1.81E-04	41.53	27.09	14.4	14.51	0.544749
	320.855	1.81E-04	48.73	31.75	16.89	17.01	0.545708
	325	1.81E-04	56	36.51	19.4	19.6	0.549639
	329.31	1.82E-04	63.8	42.27	22.12	22.8	0.555744
	333.1	1.81E-04	70.82	46.31	24.6	25.06	0.557855
	339	1.81E-04	81.16	52.64	27.95	28.39	0.566065

	345.67	1.80E-04	93.14	61.3	31.81	33.04	0.578164
L4	313.49	1.81E-04	35.9	24.31	11.9658	12.41	0.531005
	348.535	1.80E-04	98.67	68.25	33.2416	36.51	0.58947
	351.205	1.79E-04	103.51	68.23	34.8292	36.5	0.591537
	349.095	1.80E-04	99.85	63.41	33.5356	33.78	0.587691

Appendix 9

Measurements data for sample C under small temperature differences condition.

Exp	T_{mean} (K)	α (V/K)	ΔT_{so}	ΔT_{bo}	ΔT_{sc}	ΔT_{bc}	I_c (A)	ZT_m+1	a	T_m	*ZT*	β (V/K)
S1	310.04	-1.89E-04	25.94	3.65	24.88	4.03	0.076	1.15115	6.208807	51.60354	0.908124	-1.12E-04
	329.57	-1.96E-04	23.22	4.16	22.64	4.59	0.07	1.131632	5.534725	61.21076	0.70873	-8.61E-05
	349.81	-2.00E-04	26.52	5.56	25.93	6.09	0.081	1.120246	5.524327	65.20127	0.645131	-5.52E-05
	371.31	-2.03E-04	27.77	7.01	26.42	7.48	0.082	1.121571	4.855233	78.54396	0.574723	-1.77E-05
	394.75	-2.03E-04	30.01	9.04	29.28	9.71	0.091	1.100895	4.839418	83.89538	0.474742	2.85E-05
S2	312.45	-1.91E-04	29.15	4.06	27.42	4.44	0.09	1.162594	5.669598	57.19662	0.888222	-1.09E-04
	327.77	-1.96E-04	32.46	5.01	31.67	5.67	0.107	1.159967	5.641212	60.38117	0.868359	-8.87E-05
	343.14	-2.00E-04	30.19	5.49	29.21	6.1	0.099	1.148389	5.282862	67.11427	0.758691	-6.58E-05
	363.07	-2.02E-04	32.8	6.95	31.91	7.65	0.105	1.13142	4.510783	83.17025	0.573697	-3.27E-05
	384.71	-2.03E-04	34.58	8.6	33.23	9.29	0.108	1.124118	4.279674	92.7612	0.514757	7.99E-06
	428.11	-1.99E-04	27.07	11.58	26.51	12.16	0.083	1.072268	4.052237	108.0216	0.286417	1.04E-04
S3	312.39	-1.92E-04	25.94	3.74	25.27	4.2	0.079	1.152769	5.885371	54.8416	0.870208	-1.09E-04
	338.58	-1.99E-04	26.93	4.91	25.75	5.4	0.08	1.150195	4.93885	70.53122	0.72101	-7.29E-05
	368.98	-2.05E-04	17.75	5.63	16.99	5.97	0.056	1.107824	5.790023	64.89142	0.61311	-2.20E-05
	410.46	-2.03E-04	19.99	9.09	19.51	9.54	0.061	1.075326	4.790978	87.22517	0.354468	6.26E-05
S4	311.25	-1.93E-04	26.71	3.76	26.32	4.3	0.084	1.160563	5.80883	55.54035	0.899813	-1.11E-04
	324.00	-1.97E-04	26.25	4.2	25.31	4.66	0.082	1.150731	5.683247	58.80499	0.830501	-9.39E-05
	338.76	-2.00E-04	19.88	4.17	18.64	4.472	0.059	1.143273	4.748692	72.82311	0.666479	-7.26E-05
	363.09	-2.04E-04	27.66	6.37	26.82	6.93	0.087	1.121985	4.870625	76.66916	0.577699	-3.26E-05

	385.25	-2.03E-04	30.71	8.28	29.79	8.92	0.094	1.110565	4.414605	89.79194	0.474381	9.08E-06
	407.70	-2.01E-04	31.15	10.29	30.22	10.92	0.094	1.093883	4.394987	95.34317	0.401461	5.64E-05
	428.17	-1.97E-04	28.96	11.95	28.06	12.49	0.083	1.078712	3.998954	109.5815	0.307552	1.04E-04

Appendix 10

Measurements data for sample C under large temperature differences condition.

Exp	T_{mean} (K)	α (V/K)	ΔT_{so}	ΔT_{bo}	ΔT_{sc}	ΔT_{bc}	I_c (A)	ZT_m+1	a	T_m	*ZT*
L1	306.9	-1.85E-04	14.76	2.17	14.4	2.41	0.042	1.138364	6.056468	51.65241	0.822109
	320.455	-1.92E-04	38.05	5.39	37.16	6.08	0.116	1.155031	6.794248	49.44996	1.004663
	349.185	-1.97E-04	91.51	13.1	88.47	14.79	0.28	1.167803	6.39938	60.23515	0.972756
	367.14	-1.96E-04	125.34	18.86	121.04	21.16	0.385	1.161809	6.600227	63.18277	0.940234
	396.895	-1.92E-04	180.87	29.48	175.56	32.71	0.54	1.143126	6.2996	74.4612	0.762893
	418.535	-1.84E-04	219.33	38.16	214.41	41.84	0.638	1.121596	6.676692	76.13701	0.668427
L2	299.325	-1.85E-04	12.45	1.82	11.71	1.97	0.033	1.15082	5.492249	55.47708	0.813743
	324.53	-1.95E-04	54.56	7.44	52.61	8.35	0.164	1.163911	6.518882	53.00676	1.00353
	354.7	-1.97E-04	109.7	15.29	105.37	17.19	0.33	1.170464	6.262191	63.46449	0.952715
	382.875	-1.94E-04	163.27	24.23	158.53	27.22	0.489	1.15699	6.368552	70.38079	0.854034
	410.935	-1.86E-04	213.937	35.766	210.41	39.76	0.63	1.130305	6.788836	73.6729	0.726818
	427.58	-1.81E-04	243.3	42.24	237.64	46.06	0.688	1.116407	6.620838	79.58111	0.625442
L3	304.36	-1.89E-04	18.64	2.61	17.93	2.89	0.056	1.151126	5.645403	55.10713	0.834679
	321.295	-1.94E-04	47.75	6.46	44.95	7.15	0.147	1.175756	6.301182	53.87135	1.048229
	342.15	-1.97E-04	84	11.25	80.07	12.71	0.265	1.18523	6.259855	59.86792	1.058602
	370.14	-1.96E-04	133.04	18.26	128.79	20.81	0.421	1.177257	6.011334	70.2985	0.933306
	394.055	-1.92E-04	176.11	25.8	169.37	28.73	0.539	1.15788	5.91186	78.1286	0.796293
	411.065	-1.87E-04	207.45	32.87	201.49	36.3	0.63	1.137017	6.207712	79.52383	0.70825

L4	306.62	-1.91E-04	18	2.5	17.56	2.81	0.053	1.152164	5.700076	55.05184	0.847502
	322.075	-1.95E-04	44.95	6.06	43.71	6.87	0.139	1.165824	6.650956	51.18121	1.043503
	338.615	-1.98E-04	73.21	9.8	70.59	11.08	0.227	1.172576	6.641909	55.41269	1.054573
	357.245	-1.98E-04	104.99	14.06	100.84	15.87	0.321	1.175186	6.207525	64.15079	0.975583
	377.36	-1.96E-04	142.08	19.6	137.405	22.018	0.433	1.161588	6.205482	69.96088	0.871586
	393.185	-1.92E-04	172.21	25.09	167.47	28.08	0.51	1.150848	5.903775	78.10878	0.759338
	409.91	-1.87E-04	203.803	31.801	198.17	35.09	0.597	1.134789	6.241449	78.70203	0.702034
	424.415	-1.82E-04	230.73	38.02	225.31	41.6	0.666	1.120482	6.58254	78.75012	0.649323

Appendix 11

Measurements data for n-type Bi2Te3 sample using commercial PPMS method.

T_{mean} (K)	α (V/K)	ρ (Ωcm)	λ (W/cmK)	ZT
362.67	-2.26E-04	1.14E-03	1.84E-02	0.886960076
349.61	-2.23E-04	1.09E-03	1.71E-02	0.932481153
336.57	-2.23E-04	1.04E-03	1.64E-02	0.98508119
323.42	-2.19E-04	9.79E-04	1.55E-02	1.021016673
310.18	-2.17E-04	9.26E-04	1.50E-02	1.046851661
298.34	-2.12E-04	8.80E-04	1.47E-02	1.033873254
287.97	-2.08E-04	8.42E-04	1.44E-02	1.022277126

Appendix 12

Measurements data for sample D under small temperature differences condition.

Exp	α (V/K)	T_{mean}	ΔT_{so}	ΔT_{bo}	ΔT_{sc}	ΔT_{bc}	I_c	ZT_m+1	a	T_m	ZT	β (V/K)
S1	1.92E-04	318.595	31.81	5.3	31.04	6	0.111	1.160159	3.256864	101.0465	0.504973	1.389E-04
	1.96E-04	328.845	33.77	6.02	32.89	6.82	0.117	1.163202	3.065476	110.7806	0.484454	1.251E-04
	2.02E-04	345.925	32.89	6.86	32.27	7.69	0.111	1.142529	2.730796	130.3142	0.378349	9.952E-05
	2.05E-04	357.32	38.72	8.31	37.6	9.26	0.137	1.147513	2.937713	125.6761	0.419405	8.070E-05
S2	1.88E-04	307.585	20.03	3.24	19.36	3.6	0.068	1.149564	3.920129	80.28581	0.572998	1.525E-04
	1.93E-04	318.58	25.2	4.46	24.37	4.95	0.087	1.147666	3.714667	88.07243	0.534143	1.390E-04
	1.97E-04	330.85	31.34	5.93	30.69	6.65	0.107	1.145168	3.316641	102.9305	0.466613	1.223E-04
	2.01E-04	341.115	31.43	6.51	30.75	7.26	0.108	1.139869	3.221815	109.0714	0.437432	1.070E-04
	2.04E-04	353.4	34.4	7.59	32.91	8.31	0.108	1.144432	2.748715	132.1394	0.386275	8.733E-05
	2.06E-04	365.375	34.37	8.4	33.03	9.12	0.113	1.129761	2.889437	130.0407	0.364589	6.654E-05
	2.09E-04	377.76	35.2	9.39	34.21	10.26	0.118	1.124272	2.873482	135.2252	0.347161	4.339E-05
	2.10E-04	389.09	32.74	9.97	31.84	10.76	0.106	1.109744	2.670976	149.23	0.286137	2.076E-05
	2.09E-04	409.115	33.47	11.85	32.84	12.7	0.105	1.09229	2.521862	165.992	0.227464	-2.265E-05
	2.08E-04	421.065	29.51	12.29	28.78	12.96	0.093	1.081263	2.594915	165.4214	0.206849	-5.063E-05
S3	1.90E-04	316.385	31.73	5.03	30.48	5.66	0.113	1.171396	3.158573	103.3426	0.52473	1.418E-04
	1.93E-04	321.59	32.68	5.37	31.71	6.08	0.118	1.16685	3.096698	107.2497	0.500303	1.350E-04
	1.96E-04	329.755	34.95	5.98	33.11	6.63	0.124	1.170308	3.060062	111.1971	0.50505	1.238E-04
	2.00E-04	335.71	24.46	4.93	23.42	5.44	0.089	1.152449	3.001546	114.3106	0.447714	1.152E-04
	2.02E-04	343.89	27.18	5.69	26.1	6.3	0.098	1.153021	2.887725	121.9094	0.431652	1.027E-04

	2.08E-04	358.635	37.55	7.76	35.27	8.46	0.132	1.160682	2.720899	135.5834	0.425023	7.843E-05
	2.08E-04	376.27	34.98	8.52	33.41	9.3	0.121	1.142843	2.58333	149.4054	0.359744	4.626E-05
S4	1.87E-04	303.9	15.26	2.54	14.89	2.82	0.055	1.137824	4.168651	74.25521	0.564066	1.568E-04
	1.88E-04	303.825	10.53	1.85	10.11	2.03	0.037	1.142882	4.088187	75.23715	0.576992	1.569E-04
	1.91E-04	312.46	16	2.92	15.39	3.2	0.056	1.139327	3.741004	84.97	0.512348	1.467E-04
	1.95E-04	321	18.88	3.71	18.21	4.08	0.068	1.140193	3.754446	87.22323	0.515939	1.358E-04
	2.01E-04	334.245	18.63	4.34	17.77	4.69	0.068	1.132944	3.743388	90.93541	0.488654	1.174E-04
	2.05E-04	350.28	22.78	5.8	21.94	6.31	0.08	1.129584	3.143746	113.6894	0.399251	9.249E-05
S5	1.90E-04	306.67	15.5	2.68	15.07	2.97	0.047	1.13983	3.923503	79.58438	0.53882	1.536E-04
	2.01E-04	342.32	17.82	4.78	17.24	5.16	0.056	1.115815	3.828073	91.03751	0.435489	1.052E-04
	2.05E-04	357.7	22.1	6.23	21.48	6.74	0.07	1.113089	3.622974	100.8055	0.401287	8.004E-05
	2.08E-04	367.09	20.06	6.59	19.58	7.09	0.062	1.102247	3.27793	114.0394	0.329132	6.343E-05
	2.10E-04	379.315	20.55	7.48	19.72	7.94	0.06	1.106175	2.95631	130.4514	0.308726	4.037E-05
	2.12E-04	395.735	17.27	8.29	16.84	8.74	0.051	1.081203	2.915259	137.5836	0.233566	6.837E-06
S6	1.85E-04	305.97	13.02	2.28	12.59	2.51	0.041	1.138477	3.873279	80.18136	0.528423	1.544E-04
	1.89E-04	313.21	16.12	2.99	15.72	3.32	0.052	1.138622	3.877508	82.26942	0.52775	1.457E-04
	1.94E-04	323.545	15.93	3.42	15.55	3.76	0.055	1.126282	4.285835	76.88021	0.531449	1.324E-04
	2.00E-04	337.12	15.68	4.09	15.23	4.44	0.052	1.11765	3.565656	96.03966	0.412977	1.131E-04
	2.10E-04	376.615	18.75	6.98	18.16	7.46	0.06	1.103491	2.978297	128.3926	0.303571	4.560E-05
	2.10E-04	398.01	20.78	8.93	19.7	9.34	0.062	1.103252	2.676536	150.8442	0.272436	1.960E-06
S7	1.90E-04	308.025	15.41	2.66	14.85	2.93	0.054	1.143042	3.745855	83.67591	0.526561	1.520E-04
	1.92E-04	315.38	13.66	2.68	13.28	2.95	0.052	1.132244	4.431771	72.2988	0.576869	1.430E-04
	1.94E-04	326.07	13.26	3.13	12.79	3.39	0.049	1.122867	4.011198	82.45559	0.485877	1.290E-04
	2.04E-04	350.995	12.93	4.48	12.51	4.79	0.047	1.105093	3.457312	102.7737	0.358915	9.132E-05
	2.10E-04	380.755	21.41	7.56	20.65	8.05	0.073	1.104004	2.842033	136.2747	0.29059	3.754E-05

S8	1.85E-04	306.215	14.63	2.48	13.93	2.7	0.046	1.143419	4.437737	70.2589	0.625073	1.541E-04
	1.90E-04	312.845	15.51	2.83	14.92	3.11	0.05	1.142397	4.132433	77.06713	0.578043	1.462E-04
	1.94E-04	322.18	19.14	3.75	18.44	4.09	0.064	1.132069	4.309004	76.37735	0.557104	1.342E-04
	1.98E-04	329.72	18.04	3.98	17.5	4.34	0.059	1.124101	3.837243	87.55498	0.467345	1.239E-04
	1.99E-04	337.235	19.43	4.58	18.93	4.97	0.066	1.113815	3.996376	86.11843	0.445694	1.129E-04
	2.02E-04	343.26	17.3	4.61	16.37	4.91	0.056	1.125584	3.683572	94.69828	0.455215	1.037E-04
	2.07E-04	355.975	16.21	5.17	15.24	5.44	0.052	1.119197	3.488044	103.498	0.40997	8.299E-05
	2.08E-04	368.9	20.5	6.59	19.7	7.04	0.066	1.111667	3.233943	116.0918	0.354841	6.012E-05

Appendix 13

Measurements data for sample D under large temperature differences condition.

Exp	α (V/K)	T_{mean}	ΔT_{so}	ΔT_{bo}	ΔT_{sc}	ΔT_{bc}	I_c	ZT_m+1	a	T_m	*ZT*
L1	1.83E-04	300.575	10.03	1.98	9.79	2.18	0.039	1.128001	5.652897	53.87398	0.714147
	1.88E-04	313.39	31.02	5.72	29.95	6.36	0.113	1.151612	4.097624	79.2619	0.59945
	1.92E-04	327.25	55.32	10.04	53.01	11.18	0.197	1.16207	3.737141	92.57817	0.572895
	1.97E-04	345.66	88.54	16.37	84.43	18.23	0.312	1.167833	3.429437	109.1288	0.531602
	2.01E-04	364.175	122.29	23.58	116.4	26.1	0.419	1.162879	3.094516	129.8046	0.456968
	2.02E-04	378.505	148.17	29.67	142.61	33.03	0.51	1.156648	3.002524	141.2517	0.419762
	2.02E-04	392.83	174.04	36.62	167.37	40.44	0.58	1.148324	2.829143	157.2456	0.370541
	2.01E-04	405.37	196.26	43.46	189.61	47.81	0.643	1.138674	2.755735	168.3424	0.333929
L2	1.85E-04	303.255	11.51	2.18	11.09	2.4	0.046	1.142611	4.504902	68.24991	0.633665
	1.87E-04	308.925	20.01	3.67	19.39	4.11	0.08	1.1557	4.289891	73.73848	0.652299
	1.93E-04	327.635	53.79	9.54	52.18	10.79	0.203	1.165925	3.346451	103.2538	0.526497
	1.99E-04	351.665	97.79	17.84	93.39	20.03	0.357	1.175656	3.002455	127.032	0.486271
	2.02E-04	371.855	134.59	25.95	130.06	29.41	0.493	1.172807	2.862876	144.2239	0.445552
	2.03E-04	390.715	167.59	34.34	161.47	38.4	0.597	1.160612	2.725026	161.5114	0.38854
L3	1.86E-04	302.98	9.92	1.91	9.66	2.12	0.039	1.139822	4.917857	62.37226	0.679201
	1.88E-04	310.43	22.5	4.07	21.78	4.54	0.082	1.152354	3.79021	83.95756	0.563325
	1.94E-04	329.7	57.28	9.92	55.63	11.29	0.212	1.171861	3.58786	97.3275	0.582186
	1.98E-04	345.24	85.3	14.88	79.73	16.37	0.3	1.176991	3.303221	112.3029	0.544102

	2.02E-04	365.885	123.09	22.69	119.19	25.79	0.434	1.173815	2.952316	137.0091	0.464177
	2.03E-04	391.79	169.9	34.15	164.29	38.21	0.593	1.157094	2.879062	154.2162	0.399101
L4	1.84E-04	301.59	11.46	2.02	10.86	2.17	0.039	1.133609	4.501153	67.99672	0.592603
	1.87E-04	305.875	16.27	2.78	15.64	3.06	0.055	1.145058	4.327867	72.08242	0.615539
	1.89E-04	309.995	21.73	3.64	20.95	4.03	0.074	1.148363	4.17058	76.22881	0.603341
	1.90E-04	315.715	31.11	5.14	29.92	5.68	0.107	1.14901	4.310128	75.86065	0.620144
	1.92E-04	320.355	38.71	6.34	37.64	7.11	0.129	1.153331	3.856621	86.6173	0.567096
	1.95E-04	330.48	57	9.2	54.32	10.22	0.184	1.165677	3.429813	101.6764	0.538501
	1.97E-04	341.27	76.9	12.38	74.51	13.97	0.25	1.164629	3.243912	112.9363	0.497474
	1.99E-04	356.175	104.35	16.85	99.67	18.69	0.323	1.161281	2.968765	130.5538	0.440005
	2.03E-04	373.86	136.82	22.55	132.69	25.38	0.425	1.16053	2.80549	148.0568	0.405357
L5	1.90E-04	299.295	5.47	0.96	5.38	1.05	0.018	1.112047	4.624092	65.17133	0.514568
	1.90E-04	307.5	15.8	2.71	15.28	2.98	0.05	1.137053	4.208902	74.44098	0.566137
	1.91E-04	316.645	31.73	5.27	30.49	5.82	0.102	1.149278	4.161146	78.81396	0.599742
	1.94E-04	328.285	52.85	8.65	50.56	9.57	0.167	1.156468	3.825675	90.47608	0.567733
	1.99E-04	362.91	117.02	18.92	111.3	20.69	0.343	1.149752	3.002225	132.5296	0.410071
	2.00E-04	391.845	170.11	29.09	164.56	32.3	0.514	1.147795	3.05702	145.7677	0.397295
	1.98E-04	414.59	210.1	38.38	204.71	42.27	0.614	1.130353	2.909289	165.1668	0.327204

Appendix 14

Small and large ΔT measurement for sample E (BiTe@Tc).

Exp	α (V/K)	T_{mean}	ΔT_{so}	ΔT_{bo}	ΔT_{sc}	ΔT_{bc}	I_c	ZT_m+1	a	T_m	*ZT*	β (V/K)
L1	-8.69E-05	302.4	25.56	4.62	25.47	4.68	0.026	1.016566	4.798615	65.1013	0.076952	
	-8.90E-05	317.67	53.83	9.967	53.39	10.08	0.064	1.019672	10.98572	31.09127	0.201	
	-9.22E-05	338.22	93.519	17.49	92.95	17.76	0.117	1.021653	13.16999	28.94696	0.253002	
	-9.79E-05	364.88	144.68	27.7	145.52	28.55	0.192	1.024881	11.68583	37.10127	0.244694	
	-1.04E-04	393.25	199.57	39.89	199.23	40.88	0.27	1.026521	8.906502	54.06201	0.192916	
	-1.13E-04	423.87	257.3	49.56	255.46	50.6	0.363	1.028339	6.917847	76.95547	0.156088	
S1	-9.92E-05	437.92	64.06	20.14	63.92	20.49	0.085	1.019607	6.757984	68.83129	0.124742	-2.788E-06
	-1.00E-04	416.3	77.62	19.08	78.74	19.65	0.113	1.015225	11.52653	39.22901	0.161571	-1.511E-05
	-9.87E-05	397.7	77.88	17.22	78.53	17.8	0.107	1.025126	8.197077	52.74439	0.189453	-2.467E-05
	-9.69E-05	379.8	77.14	15.73	76.22	15.94	0.104	1.025582	9.579435	43.11545	0.225347	-3.296E-05
	-9.44E-05	360.73	67.99	13.36	67.92	13.68	0.092	1.025007	11.44023	34.2311	0.263534	-4.083E-05
	-9.33E-05	346.15	74.76	13.36	74.91	13.74	0.1	1.026077	11.17846	33.9912	0.265551	-4.616E-05
	-9.06E-05	325.44	70.55	11.59	70.91	11.93	0.092	1.02411	11.147	32.11709	0.244307	-5.273E-05

Appendix 15

Small and large ΔT measurement for sample E (BiTe@Th).

Exp	α (V/K)	T_{mean}	ΔT_{so}	ΔT_{bo}	ΔT_{sc}	ΔT_{bc}	I_c	ZT_m+1	a	T_m	*ZT*	β (V/K)
L1	-9.55E-05	309.435	17.95	4.15	17.93	4.24	0.022	1.022826	6.795417	46.66832	0.151351	
	-9.82E-05	322.625	42.29	9.41	42.32	9.63	0.056	1.022654	9.595037	35.61265	0.205228	
	-1.03E-04	343.74	82.44	18.13	82.11	18.54	0.115	1.026724	10.50109	36.26867	0.253283	
	-1.09E-04	367.925	128.69	28.49	129.65	29.66	0.191	1.033358	10.42832	40.96479	0.299608	
	-1.14E-04	396.245	182.33	40.58	180.4	41.65	0.281	1.037348	11.34855	42.07866	0.351699	
	-1.16E-04	406.98	202.76	45.49	201.29	46.78	0.323	1.035868	13.30605	37.53452	0.388909	
	-1.19E-04	425.99	239.68	55.4	239.49	57.44	0.396	1.037646	14.18847	37.87233	0.42344	
	-1.11E-04	377.2	149.34	30.99	147.52	31.65	0.229	1.033897	11.03977	40.15833	0.318391	
	-1.01E-04	335.37	68.98	14.22	68.53	14.51	0.096	1.027094	9.478982	38.60068	0.235399	
	-1.16E-04	402.42	200.9	42.69	198.95	44.02	0.322	1.041262	11.04259	44.54949	0.372721	
	-1.18E-04	422.245	244.91	54.159	242.41	55.76	0.407	1.040179	12.87686	41.38101	0.409981	
S1	-9.49E-05	308.66	18.96	4.15	18.93	4.23	0.026	1.020892	7.482383	42.35616	0.152248	-4.05E-05
	-9.65E-05	316.555	35.35	7.44	35.2	7.58	0.05	1.023159	8.54183	38.87452	0.188582	-4.05E-05
	-1.03E-04	331.84	35.84	8.79	35.66	8.95	0.055	1.023342	10.06602	34.5607	0.224122	-4.02E-05
	-1.12E-04	347.565	34.07	9.83	34.44	10.15	0.059	1.02146	12.1301	29.98495	0.248754	-3.98E-05
	-1.23E-04	379.095	35.878	13.29	35.54	13.5	0.065	1.025462	9.476567	41.71182	0.23141	-3.82E-05
	-1.31E-04	398.9	38.66	15.56	38.32	15.84	0.073	1.027027	7.886917	52.69875	0.204581	-3.68E-05
	-1.36E-04	406.76	35.14	15.82	35.13	16.16	0.07	1.021783	8.083032	52.19662	0.169748	-3.61E-05

Appendix 16

Small and large ΔT measurement for sample F (BiTe@Tc).

Exp	α (V/K)	T_{mean}	ΔT_{so}	ΔT_{bo}	ΔT_{sc}	ΔT_{bc}	I_c	ZT_m+1	a	T_m	*ZT*	β (V/K)
L1	1.53E-04	335.355	67.03	13.31	66.63	14	0.135	1.058155	9.533477	38.31084	0.509064	
	1.66E-04	413.86	201.84	42.86	200.85	45.42	0.414	1.064953	6.420518	77.71004	0.345919	
	1.67E-04	424.79	220.54	47.45	217.829	49.817	0.452	1.06295	6.550398	78.79666	0.339364	
	1.60E-04	379.08	140.26	25.86	138.47	27.29	0.29	1.06894	8.947735	49.16577	0.531541	
L2	1.55E-04	337.95	71.78	13.79	70.88	14.42	0.145	1.058963	10.72333	34.4935	0.577689	
	1.65E-04	391.375	161.75	31.93	155.52	32.36	0.336	1.054066	10.42696	44.04952	0.480367	
	1.66E-04	409.155	191.63	39.27	188.31	40.97	0.389	1.061684	6.996656	69.89666	0.361079	
	1.67E-04	428.225	223.99	47.37	221.68	49.91	0.43	1.0646	4.995225	103.4089	0.267512	
	1.67E-04	435.87	236.86	50.24	233.03	52.56	0.445	1.063373	4.739011	111.1548	0.248504	
L3	1.60E-04	372.14	128.82	23.5	126.535	24.66	0.268	1.068311	9.652729	44.34455	0.57327	
	1.63E-04	397.96	173.4	31.41	170.55	33.06	0.358	1.07012	7.874815	59.86695	0.466113	
	1.66E-04	424.13	218.78	43.36	215.66	45.57	0.443	1.066173	6.408286	80.19981	0.349952	
	1.53E-04	346.475	79.456	13.983	79.45	14.83	0.162	1.060654	10.34849	36.87219	0.569941	
L4	1.56E-04	324.755	44.15	7.7	43.82	7.99	0.054	1.045477	8.347531	41.19964	0.358469	
	1.58E-04	343.325	77.63	13.47	77.5	14.09	0.101	1.047783	12.23276	30.97765	0.529577	
	1.59E-04	365.555	117.33	20.6	117.06	21.57	0.154	1.049502	12.77368	32.84003	0.551031	
	1.60E-04	389.965	159.13	28.81	157.37	29.88	0.206	1.048739	11.80395	39.09234	0.486196	
	1.64E-04	411.005	195.55	36.62	193.22	37.86	0.245	1.046328	7.306765	67.55082	0.28188	
L5	1.46E-04	306.24	16.58	2.79	16.56	2.9	0.016	1.040682	4.498085	69.54275	0.179148	

	1.55E-04	328.32	55.652	8.88	55.53	9.24	0.067	1.042827	11.52377	30.74608	0.457321	
	1.60E-04	353.84	101.85	15.84	100.86	16.49	0.127	1.051254	13.17935	30.369	0.597175	
	1.60E-04	370.45	127.16	22.09	125.35	22.72	0.163	1.043371	15.62205	27.42586	0.585827	
	1.66E-04	407.52	193.36	35.13	191.71	36.37	0.251	1.044208	10.9736	45.03489	0.400038	
L6	1.49E-04	327.145	52.35	9.29	52.07	9.56	0.059	1.034597	11.78064	29.7921	0.379909	
	1.56E-04	355.295	100.45	17.31	99.58	17.87	0.121	1.041371	15.78373	25.46138	0.577296	
	1.64E-04	389.305	160.35	27.73	155.77	28.09	0.196	1.042766	13.97023	32.89889	0.506071	
	1.70E-04	432.56	236.48	44.07	235.77	45.93	0.287	1.045344	7.473961	71.60156	0.273933	
	1.66E-04	412.39	204.26	34.45	202.52	35.81	0.243	1.048408	7.775595	64.31369	0.310403	
L8	1.49E-04	317.85	32.68	6.95	32.53	7.17	0.036	1.036412	6.964777	47.63895	0.242942	
	1.53E-04	334.965	62.93	13.11	62.71	13.52	0.077	1.034892	13.64658	26.67938	0.438073	
	1.59E-04	363.095	113.428	24.148	113.7	25.03	0.149	1.034045	20.66599	20.22207	0.611293	
	1.65E-04	405.41	187.76	41.07	187.34	41.89	0.255	1.022253	21.04531	23.51969	0.383569	
	1.67E-04	418.435	210.85	46	208.82	47.57	0.27	1.044184	9.790634	52.24643	0.35386	
	1.68E-04	430.17	231.72	50.71	229.77	52.57	0.291	1.045477	8.045774	65.88814	0.296911	
S1	1.58E-04	410.005	56.47	17.78	56.41	18.34	0.078	1.032593	4.80126	90.08999	0.148334	-2.61E-05
	1.51E-04	459.38	60.06	23.32	60.07	23.96	0.08	1.027273	4.94612	97.66799	0.128279	-1.00E-04
S2	1.53E-04	337.91	68.9	13.33	67.85	13.91	0.139	1.05966	8.215286	44.72887	0.450706	5.47E-05
	1.55E-04	346.06	65.72	13.11	64.83	13.72	0.129	1.060896	6.393175	58.36376	0.361077	4.72E-05
	1.57E-04	363.045	61.91	13.24	61.1	13.85	0.117	1.05994	4.974148	77.85217	0.279517	3.02E-05
	1.59E-04	386.77	60.42	14.24	59.97	14.93	0.111	1.056322	4.259276	96.13373	0.226599	3.51E-06
	1.57E-04	418.745	57.48	16.016	57.04	16.66	0.1	1.048234	3.726679	117.867	0.17136	-3.81E-05
	1.48E-04	463.735	61.49	21.95	60.47	22.4	0.102	1.037715	3.924438	123.7338	0.141349	-1.07E-04
	1.41E-04	491.145	59.95	25.6	58.99	26.16	0.092	1.038505	3.612654	141.7755	0.133391	-1.56E-04
	1.32E-04	516.62	56.96	28.35	56.48	28.94	0.089	1.029487	4.555124	118.2098	0.128868	-2.05E-04
S3	1.53E-04	341.935	75.63	13.86	74.48	14.48	0.153	1.060864	5.77853	64.43083	0.323006	5.10E-05

	1.55E-04	354.775	70.25	13.36	69.36	14.04	0.139	1.064383	4.944026	77.29843	0.295497	3.87E-05
	1.56E-04	360.375	79.15	14.84	77.96	15.57	0.155	1.065206	4.673743	83.58606	0.281133	3.30E-05
	1.57E-04	382.105	60.79	13.18	60	13.78	0.116	1.05929	4.157663	97.28166	0.232879	9.04E-06
	1.57E-04	399.995	61.83	14.29	60.96	14.91	0.114	1.058278	3.715975	113.5631	0.205268	-1.29E-05
	1.50E-04	454.225	64.35	18.62	63.4	19.23	0.108	1.048236	3.336475	142.6383	0.153604	-9.17E-05
S4	1.54E-04	339.975	66.89	13.89	66.56	14.01	0.035	1.01364	32.74979	11.36141	0.408161	5.28E-05
	1.56E-04	356.65	57.64	13.37	57.5	13.51	0.0305	1.012931	28.56906	13.45244	0.342838	3.68E-05
S5	1.56E-04	372.045	62.93	13.72	63.07	14.07	0.051	1.023234	8.321584	48.01976	0.18001	2.05E-05
	1.56E-04	393.145	63.51	16.05	62.78	16.24	0.051	1.023604	8.549255	49.18655	0.188662	-4.27E-06
	1.53E-04	434.22	71.82	21.63	71.4	21.97	0.055	1.021694	6.774092	68.55825	0.137399	-6.05E-05

Appendix 17

Small and large ΔT measurement for sample F (BiTe@Th).

Exp	α (V/K)	T_{mean}	ΔT_{so}	ΔT_{bo}	ΔT_{sc}	ΔT_{bc}	I_c	ZT_m+1	a	T_m	*ZT*	β (V/K)
L1	1.58E-04	319.28	36.72	6.43	36.15	6.79	0.074	1.072638	3.952082	84.1927	0.275462	
	1.63E-04	355.54	101.04	17.53	99.35	18.73	0.2	1.086629	3.454049	113.145	0.272218	
	1.61E-04	392.27	165.48	30.05	162.26	31.71	0.311	1.076182	3.195279	139.9719	0.2135	
	1.58E-04	406.95	190.98	35.29	187.66	37.34	0.346	1.076809	3.103982	151.2931	0.206603	
	1.54E-04	417.7	209.84	39.17	204.96	40.74	0.363	1.064846	2.984869	162.1702	0.167022	
	1.51E-04	426.585	225.77	42.05	222.45	44.07	0.351	1.06368	2.543404	193.7637	0.140196	
L2	1.60E-04	315.72	28.28	5.22	27.86	5.5	0.049	1.069524	4.058537	80.35106	0.273177	
	1.64E-04	334.215	59.97	10.78	59.02	11.37	0.11	1.071708	4.61842	77.32738	0.309928	
	1.63E-04	358.96	104.54	18.682	102.33	19.66	0.186	1.075077	4.325768	92.09511	0.292629	
	1.62E-04	387.53	153.3	27.95	149.68	29.12	0.26	1.067058	3.863462	114.322	0.227313	
	1.54E-04	412.47	197.7	37.39	196.03	39.32	0.3	1.060577	3.180865	150.8382	0.165649	
	1.46E-04	433.355	233.98	45.59	232.31	47.81	0.32	1.056234	2.874893	177.1081	0.137595	
L3	1.59E-04	321.29	40.7	6.85	40.39	7.28	0.076	1.070931	4.812948	70.06808	0.325245	
	1.63E-04	338.325	69.67	11.45	68.79	12.14	0.13	1.073825	4.497758	81.12549	0.307881	
	1.64E-04	361.73	110.68	18.24	108.82	19.29	0.195	1.075642	3.757139	106.7084	0.256419	
	1.60E-04	390.68	162.26	27.9	160.04	29.42	0.268	1.069108	3.406233	131.0679	0.205992	
	1.52E-04	417.93	210.08	38.01	208.79	40.13	0.322	1.062298	3.193934	153.3547	0.169777	
	1.44E-04	436.12	241.76	45.92	239.27	47.91	0.335	1.054194	2.900373	177.1434	0.133423	
L4	1.59E-04	311.78	22.84	5.03	22.72	5.19	0.031	1.037259	7.859807	40.92527	0.283848	

	1.62E-04	327.27	49.36	10.51	48.83	10.83	0.068	1.041632	7.796495	44.68784	0.304888	
	1.64E-04	342.76	76.2	15.92	75.69	16.54	0.105	1.045945	7.074653	53.03308	0.29695	
	1.64E-04	361.8	109.014	23.284	108.02	24.05	0.151	1.042403	7.369036	55.4049	0.276895	
	1.60E-04	385.875	150.91	32.95	149.22	33.98	0.198	1.042939	6.296587	71.14977	0.232877	
	1.54E-04	404.93	184.24	41.37	182.53	42.66	0.228	1.040842	5.635324	85.07848	0.194389	
	1.48E-04	422.605	214.21	49.2	212.82	50.63	0.253	1.035786	5.431866	93.72471	0.16136	
S1	1.61E-04	322.145	44.49	9.65	44.85	10.13	0.07	1.041315	7.423246	46.06329	0.288937	7.596E-05
	1.63E-04	334.43	48.2	10.82	47.51	11.15	0.074	1.045465	6.778879	52.29268	0.290766	7.017E-05
	1.70E-04	360.07	47.18	12.03	46.74	12.47	0.073	1.046333	5.634339	67.29489	0.247912	5.603E-05
	1.72E-04	392.89	52.62	15.77	52.04	16.25	0.078	1.041922	4.517558	91.42113	0.180164	3.387E-05
	1.74E-04	420.345	45.63	17.06	45.5	17.54	0.066	1.031074	3.932357	111.1991	0.117461	1.183E-05
	1.74E-04	460.82	41.98	20.61	42.02	21.04	0.059	1.019892	3.601	132.1176	0.069382	-2.648E-05

Appendix 18

Small and large ΔT measurement for sample G (BiTe@Tc).

Exp	α (V/K)	T_{mean}	ΔT_{so}	ΔT_{bo}	ΔT_{sc}	ΔT_{bc}	I_c	ZT_m+1	a	T_m
L1	1.67E-04	408.535	214.51	27.66	213.23	29.34	1.067105	6.434085	77.42199	0.354095
	1.64E-04	393.33	183.44	22.15	181.98	23.41	1.065364	7.492787	62.94004	0.408479
	1.60E-04	379.425	155.67	17.98	154.37	19.04	1.067872	8.294666	53.85926	0.478143
	1.53E-04	357.955	113.29	12.58	113	13.37	1.065526	9.582519	42.62385	0.550284
	1.47E-04	339.12	76.26	8.33	75.54	8.73	1.058008	9.917956	37.57848	0.523485
	1.41E-04	322.415	43.67	4.73	43.16	4.94	1.056739	8.732987	39.07929	0.468109
	1.34E-04	308.005	16.15	2	15.8	2.03	1.037484	9.253369	34.03477	0.339221
S1	1.38E-04	315.98	30.46	3.59	30.35	3.72	1.039967	12.36619	26.6778	0.473385
	1.40E-04	333.9	32.5	4.81	32.04	4.95	1.043881	9.99821	34.82101	0.420776
	1.41E-04	362.355	31.67	6.66	31.369	6.83	1.035333	10.17362	36.9906	0.346117
	1.42E-04	400.82	37.49	10.29	36.91	10.53	1.029237	11.23242	37.15845	0.31511

REFERENCES

[1] L. I. Anatychuk, “On the Discovery of Thermoelectricity by Volta”, Journal of Thermoelectricity No. 2, (2004), pp. 5-11.

[2] A. F. Ioffe, “Semiconductor Thermoelements and Thermoelectric Cooling”, Infosearch Limited, London, (1957).

[3] A. F. Jofle, “The Revival of Thermoelectricity”, Scientific American Vol. 199 No. 5, (1958), pp. 31-37.

[4] D. M. Rowe, “Introduction”, CRC Handbook of Thermoelectrics, CRC Press LLC, Boca Raton, (1995), pp. 1-6.

[5] G. Chen, M. S. Dresselhaus, G. Dresselhaus, J. P. Fleurial, and T. Caillat, "Recent developments in thermoelectric materials," International Materials Reviews, Vol. 48, (2003), pp. 45-66.

[6] I. A. Nishida, “Thermoelectric Energy Conversion Material”, J. FGM Forum, (1994), pp. 32-37.

[7] G. J. Snyder and E. S. Toberer, “Review Article: Complex Thermoelectric Materials”, Nature Materials Vol. 7, (2008), pp. 105-114.

[8] R. F. Service, “Temperature Rises for Devices that turn Heat into Electricity”, Science, Vol. 306, 2004, pp. 806-807.

[9] M. Arun, “Thermoelectricity in Semiconductor Nanostructures”, Science Vol. 33, (2004), pp. 777-778.

[10] T. Harman, P. J. Taylor, D. L. Spears, M. P. Walsh, “Thermoelectric quantum-dot superlattices with high ZT”, J. Electron. Mater. 29, (2000), pp. 1-2.

[11] R. Venkatasubramanian, E. Siivola, T. Colpitts and B. O’Quinn, “Growth of one-dimensional Si/SiGe heterostructures by thermal CVD”, Nature 413, (2001), pp. 597-602.

[12] G. A. Slack, “New Materials and Performance Limits for Thermoelectric cooling”, CRC Handbook of Thermoelectrics edited by D. M. Rowe, CRC Press LLC, Boca Raton, (1995), pp. 407-440.

[13] B. C. Sales, D. Mandrus, R. K. Williams, "Filled Skutterudite Antimonides: A New Class of Thermoelectric Materials", Science Vol. 272, (1996), pp. 1325-1328.

[14] G. S. Nolas, J. L. Cohn, G. A. Slack, and S. B. Schujman, "Semiconducting Ge clathrates: Promising candidates for thermoelectric Applications", Appl. Phys. Lett. Vol. 73 No. 2, (1998), pp. 178-180.

[15] H. Kleinke, "New bulk Materials for Thermoelectric Power Generation: Clathrates and Complex Antimonides", Chem. Mater. Vol. 22 No. 3, (2010), pp. 604–611.

[16] C. Uher, "Transport properties of pure and doped *M*NiSn (*M*=Zr, Hf)", Physical Review B Vol. 59, No. 13, (1999), pp. 8615-8621.

[17] K. Kurosaki, H. Muta, S. Yamanaka, "Thermoelectric properties of titanium-based half-Heusler compounds", Journal of Alloys and Compounds 384, (2004), pp. 51–56.

[18] H. Ohta, "Thermoelectrics Based on Strontium Titanate", Materials Today Vol. 10 No. 10, (2007), pp. 44–49.

[19] T. Tani, S. Isobe, Y. Masuda, K. Koumoto, "Thermoelectric properties of highly textured $(ZnO)_5In_2O_3$ ceramics", J. Mater. Chem. 11 , (2001), pp. 2324-2328.

[20] M. Ohtaki, H. Koga, T. Tokunaga, K. Eguchi, H. Arai, "Electrical transport properties and high temperature Thermoelectric performance of $(Ca_{0.9}M_{0.1})MnO_3$ (M=Y, La, Ce, Sm, In, Sn, Sb, Pb, Bi)", J. Solid State Chem. 120, (1995), pp. 105-111.

[21] S. Ohta, T. Nomura, H. Ohta, K. Koumoto, "High-temperature carrier transport and thermoelectric properties of heavily La- or Nb-doped $SrTiO_3$ single crystals", J. Appl. Phys. 97, (2005), pp. 034106 (1-4).

[22] J. Androulakis, P. Migiakis, J. Giapintzakis, "$La_{0.95}Sr_{0.05}CoO_3$: An efficient room-temperature thermoelectric oxide", Appl. Phys. Lett. 84, (2004), pp. 1099-1101.

[23] T. Okuda, K. Nakanishi, S. Miyasaka, Y. Tokura, "Large thermoelectric response of metallic perovskites: $Sr_{1-x}La_xTiO_3$ ($0 \leq x \leq 0.1$)", Phys. Rev. B Vol. 63, (2001), pp. 113104 (1-4).

[24] S. B. Riffat and Xiaoli Ma, "Thermoelectrics: a review of present and potential applications", Applied Thermal Engineering 23, 2003, pp. 913–935.

[25] G. Min and D. M. Rowe, "Recent Concepts in Thermoelectric Power Generation", 21st International Conference on Thermoelectronics, (2002), pp. 365-374.

[26] A. T. Josloff, H. S. Bailey, and D. N. Matteo, "SP100 system design and technology progress", American Inst. Of Physics Conf. Proc. 246, (1992), pp. 363-371.

[27] G. R. Schmidt, R. L. Wiley, R. L. Richardson, and R. R. Furlong, "NASA's Program for Radioisotope Power System Research and Development", American Institute of Physics Conf. Proc. 746, (2005), pp. 429-436.

[28] A. Allen, R. Haugeto, M. Kajor and M. Namazian, "Small Thermoelectric Generators", 21st International Conference on Thermoelectrics, (2002), pp. 424-426.

[29] Y. Yang, X. J. Wei and J. Liu, "Suitability of a thermoelectric power generator for implantable medical electronic devices", J. Phys. D: Appl. Phys. 40, (2007), pp. 5790–5800.

[30] R. W. Fritts, "Special Applications of Thermoelectric Generators", IEEE Transactions on Industry and General Applications Vol. IGA-3, No. 5, (1967), pp. 458-462.

[31] M. Kishi, H. Nemoto, T. Hamao, M. Yamamoto, S. Sudou, M. Mandai and S. Yamamoto, "Micro thermoelectric modules and their application to wristwatches as an energy source", 18th International Conference on Thermoelectrics, (1999), pp. 301-307.

[32] M. Niino, T. Ohshima and K. Matsubara, “Research Project on the Effective Use of Untapped Thermal Energy from Garbage Incineration etc.”, 16th International Conference on Thermoelectrics (1997), pp. 539-546.

[33] K. Nagao, A. Nagai, I. Fujii, T. Sakurai, M. Fujimoto, T. Furue, T. Hayashida, Y. Imaizumi, and T. Inoue, “Design of Thermoelectric Generation System Utilizing The Exhaust Gas of Internal-Combustion Power Plant”, 17th International Conference on Thermoelectrics, (1998), pp. 468-472.

[34] D. T. Morelli, “Potential Applications of Advanced Thermoelectrics in the Automobile Industry”, 15th International Conference on Thermoelectrics, (1996), pp. 383-386.

[35] J. C. Bass and R. L. Farley, “Examples of Power from Waste Heat for Gas Fields”, 16th International Conference on Thermoelectrics, (1997), pp. 547-550.

[36] P. Dubourdieu and G. Tribou, “Thermoelectric generator for underwater wellhead”, 16th International Conference on Thermoelectrics, (1997), pp. 603-606.

[37] R. E. Simons and R. C. Chu, “Application of Thermoelectric Cooling to Electronic Equipment: A Review and Analysis”, 16th IEEE Semi-Therm Symposium, (2000), pp. 1-9.

[38] R. Chein, G. Huang, “Thermoelectric cooler application in electronic cooling”, Applied Thermal Engineering 24, (2004), pp. 2207–2217.

[39] T. M. Tritt, “Thermoelectric Materials: Principles, Structure, Properties, and Applications”, Encyclopedia of Materials Science and Technology, (2002), pp. 1-11.

[40] G. Min and D. M. Rowe, “A novel principle allowing rapid and accurate measurement of a dimensionless figure of merit”, Meas. Sci. Technol. 12, (2001), pp. 1261-1262.

[41] K. Kontostavlakis, “Feasibility study of a novel technique for rapid and accurate measurement of thermoelectric figure of merit”, MSc. of Cardiff University (2002).

[42] D. M. Rowe, Gao Min, “Evaluation of thermoelectric modules for power generation”, Journal of Power Sources 73, (1998), pp. 193–198.

[43] A. F. Ioffe, “Semiconductor Thermoelements and Thermoelectric Cooling”, Infosearch Ltd., (1957).

[44] H. J. Goldsmid, “Conversion Efficiency and Figure-of-Merit”, CRC Handbook of Thermoelectrics edited by D. M. Rowe, CRC Press LLC, Boca Raton, (1995), pp. 19-25.

[45] H. J. Goldsmid, “Introduction to Thermoelectricity”, Materials Science Volume 121, (2009).

[46] B. Sherman, R. R. Heikes, and R. W. Ure, “Calculation of Efficiency of Thermoelectric Devices”, J. Appl. Phys. 31, (1960), pp. 1-16.

[47] L. Danielson, “Measurement of the Thermoelectric Properties of Bulk and Thin Film Materials”, Short courses: 5th International Conference on Thermoelectrics, (1996), pp. 1-26.

[48] S. Iwanaga, E. S. Toberer, A. LaLonde, and G. Jeffrey Snyder, “A high temperature apparatus for measurement of the Seebeck coefficient”, Review of Scientific Instruments 82, (2011), pp. 063905 (1-6).

[49] W. Gee and M. Green, “An improved hot-probe apparatus for the measurement of Seebeck Coefficient”, Journal of Physics E: Scientific Instruments Vol. 3, (1970), pp. 135-136.

[50] M. Fraser, “Apparatus for the rapid measurement of Seebeck coefficient”, Sci. Instrum., Vol. 39, (1962), pp. 227-228.

[51] H. J. Goldsmid, “A Simple Technique for determining the Seebeck coefficient of Thermoelectric materials”, J. Phys. E: Instrum. 19, (1986), pp. 921-922.

[52] C. N. Berglund and R. C. Beairsto, “An Automated Technique for accurate Measurement of Seebeck Coefficient”, The Review of Scientific Instruments Vol. 38, No. 1, (1967), pp. 66-68.

[53] L. E. J. Cowes, L. A. Dauncey, “Apparatus for the rapid scanning of the Seebeck coefficient of semiconductors”, J. Sci. Instrum., Vol. 39, (1962), pp. 16-18.

[54] F. Chen, J. C. Cooley, W. L. Hults, and J. L. Smith, “Low-frequency ac measurement of the Seebeck coefficient”, Review of Scientific Instruments Vol. 72 No. 11, (2001), pp. 4201-4206.

[55] T. Goto, J. H. Li, T. Hirai, Y. Maeda, R. Kato and A. Maesono, “Measurements of the Seebeck Coefficient of Thermoelectrics Materials by an AC Method”, International Journal of Thermophysics Vol. 18, No. 2, (1997), pp. 569-577.

[56] G. R. Caskey, D. J. Sellmyer, and L. G. Rubin, “A Technique for the Rapid Measurement of Thermoelectric Power”, Rev. Sci. Instrum. 40, (1969), pp. 1280-1282.

[57] C. Wood, D. Zoltan, and G. Stapfer, “Measurement of Seebeck coefficient using a light pulse”, Rev. Sci. Instrum. 56, (1985), pp. 719-722.

[58] J. Martin, T. Tritt, and C. Uher, “High temperature Seebeck coefficient metrology”, J. Appl. Phys. 108, (2010), p 121101(1-11).

[59] A. T. Burkov, A. Heinrich, P. P. Konstantinov, T. Nakama and K. Yagasaki, “Experimental set-up for thermopower and resistivity measurements at 100–1300 K”, Meas. Sci. Technol. 12, (2001), pp. 264–272.

[60] Z. Zhou and C. Uher, “Apparatus for Seebeck coefficient and electrical resistivity measurements of bulk thermoelectric materials at high temperature”, Review of Scientific Instruments 76, (2005), pp. 023901 (1-5).

[61] V. Ponnambalam, S. Lindsey, N. S. Hickman, and T. M. Tritt, “Sample probe to measure resistivity and thermopower in the temperature range of 300–1000 K”, Review of Scientific Instruments 77, (2006), pp. 073904 (1-5).

[62] C. Wood, A. Chmielewski and D. Zoltan, “Measurement of Seebeck Coeficcient using large thermal gradient”, Rev. Sci. Instrum. 59 (6), (1988), pp. 951-954.

[63] S. R. Sarath Kumar and S. Kasiviswanathan, “A hot probe setup for the measurement of Seebeck coefficient of thin wires and thin films using integral method”, Rev. Sci. Instrum. 79, (2008), pp. 024302 (1-4).

[64] H. J. Goldsmid, “Electronic Refrigeration”, Pion Publisher, 1985.

[65] Andrew P. Schuetze, Wayne Lewis, Chris Brown, and Wilhelmus J. Geerts, “A laboratory on the four-point probe technique”, Am. J. Phys. 72 (2), February (2004), pp. 149-153.

[66] Haldor Topsoe, “Geometric Factors in Four Point Resistivity Measurement”, 1968. http://www.fourpointprobes.com/haldor.html (access on 14 dec 2011).

[67] D. M. Rowe and C. M. Bhandari, “Modern Thermoelectrics”, Holt, Rinehart and Wiston Ltd., (1983).

[68] I. A. Nishida, “Measurement of Electrical Properties”, CRC Handbook of Thermoelectrics edited by D. M. Rowe, CRC Press LLC, Boca Raton, (1995), pp. 157-164.

[69] T. Dasgupta and A. M. Umarjia, “Apparatus to measure high-temperature thermal conductivity and thermoelectric power of small specimens”, Rev. Sci. Instrum. 76, (2005), pp. 094901 (1-5).

[70] A. D. Stuckes, “Measurement of thermal conductivity of semiconductors at high temperatures”, Br. J. Appl. Phys. 12, (1961), pp. 675-679.

[71] Thermal Conductivity - Different Methods for Measurement of Thermal Conductivity, http://www.azom.com/article.aspx?ArticleID=5615 (access on 1 Jan 2011).

[72] R. Taylor, “Measurement of thermal Properties”, CRC Handbook of Thermoelectrics edited by D. M. Rowe, CRC Press LLC, Boca Raton, (1995), pp. 165-180.

[73] B. Abeles, G. D. Cody, and D. S. Beers, "Apparatus for the Measurement of the Thermal Diffusivity of Solids at High Temperatures", J. Appl. Phys. 31, (1960), pp. 1585-1592.

[74] E Lopez-Baezatt, J de la Rubias and H J Goldsmid, "Angstorm's thermal diffusivity method for short sample", J. Phys. D: Appl. Phys. 20 (1987) pp. 1156-1158.

[75] T. C. Harman, "Special Techniques for Measurement of Thermoelectric Properties", J. Appl. Phys. 29, (1958), pp. 1373-1374.

[76] A. E. Bowley, L. E. J. Cowes, G. J. Williams and H. J. Goldsmid, "Measurement of the figure of merit of a thermoelectric Material", Journal of Scientlfic Instrument Vol. 38, (1961), pp. 433-435.

[77] A. Abrutin, I. Drabkin, V. Osvenski, "Corrections Used when Measuring Materials Thermoelectric Properties by Harman Method", Proc. 2nd Eur. Conf. on Thermoelectrics, Kraków, (2004).

[78] A. W. Penn, "The corrections used in the adiabatic measurement of thermal conductivity using the Peltier Effect", J. Sci. Instrum. 41, 1964, pp. 626-628.

[79] A. B. Putilin and E. A. Yuragov, "An Analysis of the Possibilities of Modern Methods Of Measuring The Efficiency Of Thermoelectric Elements And Their Realization", Measurement Techniques, Vol. 46, No. 12, (2003), pp. 1173-1179.

[80] Xianyu Ao, Johannes de Boor, and Volker Schmidt, "Radiation-Corrected Harman Method for Characterization of Thermoelectric Materials", Adv. Energy Mater. Vol. 1, (2011), pp. 1007–1011.

[81] H. Iwasaki and H. Hori, "Thermoelectric Property Measurements by the Improved Harman Method", 24th International Conference on Thermoelectrics, (2005), pp. 513-516.

[82] A. D. Downey and T. P. Hogan, "Characterization of thermoelectric elements and devices by impedance Spectroscopy", Review of Scientific Instruments 78, (2007), pp. 093904 (1-12).

[83] J. Symes and H. J. Goldsmid, "Measurement of the thermoelectric figure of merit using an oscilloscope", J. Sci. Instrum, Vol. 44, (1967), p. 551.

[84] G. Gromov, D. Kondratiev, A. Rogov, L. Yershova, "Z-meter: Easy-to-use Application and Theory", Proceedings. 6th European Workshop on Thermoelectricity of the European Thermoelectric Society Freiburg im Breisgau, September 20-21, (2001), pp. 1-8.

[85] V. Volodin, G. Gromov, D. Kondratiev, A. Ogryzko, A. Rogov, L. Yershova, "Z-metering Development", Journal of Thermoelectricity 3, (2002), p. 60-76.

[86] Woodbury, L. M. Levinson and R. S. Lewandowski, "Z-Meters", CRC Handbook of Thermoelectrics edited by D. M. Rowe", CRC Press LLC, Boca Raton, (1995), pp. 181-188.

[87] R. J. Buist, "A new Methodology for Testing Thermoelectric Materials and Devices", CRC Handbook of Thermoelectrics edited by D. M. Rowe", CRC Press LLC, Boca Raton, (1995), pp. 189-209.

[88] M. A. Korzhuev and E. S. Avilov, "Use of the Harman Technique for Figure of Merit Measurements of Cascade Thermoelectric Converters", Journal of Electronic Materials, Vol. 39, No. 9, (2010), pp. 1499-1503.

[89] U. Stöhrer, "Measurement of the transport properties of $FeSi_2$ and HMS by utilization of the Peltier effect in the temperature range 50-800°C", Meas. Sci. Technol. 5, (1994), pp. 440-446.

[90] S. Fujimoto, H. Kaibe, S. Sano and T. Kajiyani, "Development of transient Measurement method for Investigating Thermoelectric Properties in High Temperature Region", Japanese Journal of Applied Physics Vol. 45 No. 11, (2006), pp. 8805-8809.

[91] A. Jacquot, M. Jägle, J. König, D. G. Ebling and H. Böttner, "Theoretical Study of the Harman Method for Evaluating the Thermoelectric Performance of Materials and Components at High Temperature", 5th European Conference on Thermoelectrics , 2007, pp. 1-4.

[92] Y. S. Kang, S. Moriya, K. Kisara, M. Niino, Y. Noda, L. Chen and T. Sudo, "Evaluation of monolithic and segmented thermoelectric materials by using large-temperature-span apparatus", 16th International Conference on Thermoelectrics, (1997), pp. 390-393.

[93] Y.S. Kang, M. Niino, I. A. Nishida, .J. Yoshino, "Development and Evaluation of 3-Stage Segmented Thermoelectric Elements", 17th International Conference on Thermoelectrics (1998), pp. 429-432.

[94] E. Muller, J. U. Bruch, J. Schilz, "TE Generator Test Facility for Low Resistance Single Elements", 17th International Conference on Thermoelectrics, (1998), pp. 441-444.

[95] E. Muller, J. U. Bruch and J. Schilz, "Real Condition Test of Graded Thermoelectric Elements", Materials Science Forum Vols. 308-311, (1999), pp. 754-759.

[96] A. Muto, D. Kraemer, Q. Hao, Z. F. Ren, and G. Chen, "Thermoelectric properties and efficiency measurements under large temperature differences", Review of Scientific Instruments 80, (2009), pp. 093901 (1-7).

[97] G. Min and D. M. Rowe, "A novel principle allowing rapid and accurate measurement of a dimensionless figure of merit", Meas. Sci. Technol. 12 (2001), pp. 1261-1262.

[98] G. Min, "ZT Measurement under Large Temperature Difference", Journal of Electronic Material (2010), Vol. 39, No. 9, pp. 1782-1785.

[99] K. Kontostavlakis, "Feasibility study of a novel technique for rapid and accurate measurement of thermoelectric figure of merit", MSc. of Cardiff University (2002).

[100] G. Min, D. M. Rowe and K Kontostavlakis, "Thermoelectric figure-of-merit under large temperature differences", J. Phys. D: Appl. Phys. 37 (2004), pp. 1301-1304.

[101] G. Min and N Md Yatim, "Variable thermal resistor based on self powered Peltier effect", J. Phys. D: Appl. Phys., 41 (2008), pp. 1-3.

[102] D. M. Rowe, "General Principle and basic considerations", Thermoelectrics Handbook Macro to Nano (2006), pp. 1-10.

[103] Thermal Conductivity of some common Materials and Gases, http://www.engineeringtoolbox.com/thermal-conductivity-d_429.html (access on 6 Nov 2007).

[104] Iron Element Facts, http://www.chemicool.com/elements/iron.html (access on 6 Nov 2007).

[105] Platinum, http://en.wikipedia.org/wiki/Platinum (access on 10 May 2008)

[106] Y. C. Lan, D. Z. Wang, G. Chen, and Z. F. Ren, "Diffusion of nickel and tin in p-type $(Bi,Sb)_2Te_3$ and n-type $Bi_2(Te,Se)_3$ thermoelectric materials", Applied Physics Letters 92, (2008), pp. 101910 (1-3).

[107] D. Allred, "Thermoelectric element thermoelectric device and methods of manufacturing the same", UK Patent GB2171254B, (1988).

[108] S. Srivatsan, "Evaluation of Electrical Contact Resistance of Thermoelectric Junction", M.sc of Cardiff University (2008).

[109] Properties of thermoelectric materials SCTB Nord http://sctbnord.com/article_175.html (access on 15 June 2010).